University of Alberta

C-F Activation in Diphosphine-Bridged Binuclear Complexes of Rhodium & Iridium

by

Douglas Jason Anderson

A thesis
submitted to the Faculty of Graduate Studies and Research
in partial fulfillment of the requirements
for the degree of Doctor of Philosophy

Department of Chemistry

Edmonton, Alberta
Fall, 2007

Library and Archives Canada

Published Heritage Branch

395 Wellington Street
Ottawa ON K1A 0N4
Canada

Bibliothèque et Archives Canada

Direction du Patrimoine de l'édition

395, rue Wellington
Ottawa ON K1A 0N4
Canada

Your file Votre référence
ISBN: 978-0-494-32910-8
Our file Notre référence
ISBN: 978-0-494-32910-8

NOTICE:
The author has granted a non-exclusive license allowing Library and Archives Canada to reproduce, publish, archive, preserve, conserve, communicate to the public by telecommunication or on the Internet, loan, distribute and sell theses worldwide, for commercial or non-commercial purposes, in microform, paper, electronic and/or any other formats.

The author retains copyright ownership and moral rights in this thesis. Neither the thesis nor substantial extracts from it may be printed or otherwise reproduced without the author's permission.

AVIS:
L'auteur a accordé une licence non exclusive permettant à la Bibliothèque et Archives Canada de reproduire, publier, archiver, sauvegarder, conserver, transmettre au public par télécommunication ou par l'Internet, prêter, distribuer et vendre des thèses partout dans le monde, à des fins commerciales ou autres, sur support microforme, papier, électronique et/ou autres formats.

L'auteur conserve la propriété du droit d'auteur et des droits moraux qui protège cette thèse. Ni la thèse ni des extraits substantiels de celle-ci ne doivent être imprimés ou autrement reproduits sans son autorisation.

In compliance with the Canadian Privacy Act some supporting forms may have been removed from this thesis.

While these forms may be included in the document page count, their removal does not represent any loss of content from the thesis.

Conformément à la loi canadienne sur la protection de la vie privée, quelques formulaires secondaires ont été enlevés de cette thèse.

Bien que ces formulaires aient inclus dans la pagination, il n'y aura aucun contenu manquant.

Canada

"And all this science I don't understand
It's just my job five days a week"
'Rocket Man', Elton John, 1970

Abstract

Fluoride ion abstraction from the fluoroolefin-bridged adducts of $[Ir_2(CH_3)(CO)_2(dppm)_2][CF_3SO_3]$ (**1**; dppm = μ-$Ph_2PCH_2PPh_2$) (fluoroolefin = tetrafluoroethylene (**2**), trifluoroethylene (**3**), 1,1-difluoroethylene (**4**)) is achieved by the addition of trimethylsilyl triflate ($Me_3Si(CF_3SO_3)$). An isomer of **4**, containing a terminal (η^2-bound) olefin was unreactive to $Me_3Si(CF_3SO_3)$, establishing the cooperative activation in **4** by both metals. The bridging coordination of the fluorovinyl moiety in the resulting complexes $[Ir_2(CH_3)(CF_3SO_3)(CO)_2(\mu\text{-}\eta^1\text{:}\eta^2\text{-}C(F)=CXY)(dppm)_2][CF_3SO_3]_2$ (X = Y = F (**5**), X = F, Y = H (**7**), X = Y = H (**8**)) has been established on the basis of the coupling patterns in the NMR spectra involving the vinyl substituents. The trifluorovinyl-bridged species (**5**) rearranges to the η^1-trifluorovinyl product (**6**) at ambient temperature, accompanied by C-H activation of the methyl group, which has been confirmed by X-ray crystallography.

The reactivity comparison of μ-η^1:η^2-C_2F_3 *vs.* η^1-C_2F_3 groups has also been undertaken in compounds **5** and **6**, respectively, in which reaction with $Me_3Si(CF_3SO_3)$ showed that fluoride-ion abstraction from **5** occurs readily, yielding the difluorovinylidene product $[Ir_2(CH_3)(CF_3SO_3)(CO)_2(\mu\text{-}C=CF_2)(dppm)_2][CF_3SO_3]_2$ (**20**), while no reaction of **6** was observed. Facile fluoride removal from the *cis*-difluorovinyl- and 1-fluorovinyl-bridged species **7** and **8** is also

observed, resulting in the corresponding monofluorovinylidene- and vinylidene-bridged products $[Ir_2(CH_3)(CF_3SO_3)(CO)_2(\mu\text{-}C{=}CHX)(dppm)_2][CF_3SO_3]_2$ (X = F (**21**), H (**22**)).

Conversion of the fluorovinyl moieties into substituted fluoroolefins has been achieved in two ways: 1) reaction of the di- and trifluorovinyl complexes (**6** and **8**) with H_2 yields the corresponding olefins, *cis*-difluoroethylene and trifluoroethylene; and 2) the di- and monofluorovinyl species (**7** and **8**) react with CO over a 24-hour period to give *cis*-difluoropropene (along with its isomer 2,3-difluoropropene) and 2-fluoropropene, respectively.

In these studies we demonstrate facile C-F activation involving *both* types of fluorocarbyl groups in what is believed to be the first such study involving a closely related series of fluoroolefins and their derived fluorovinyl groups, and the first in which the cooperative activation by a pair of metals is observed.

Further C-F activation reactions, such as those described above, are proposed for systems employing the smaller, more basic alkyl-substituted diphosphine depm (*bis*(diethylphosphino)methane = $Et_2PCH_2PEt_2$). The preparation of the depm analogue of **1**, along with its dirhodium and mixed-metal analogues is also described herein.

Dedication

To my family

A mari usque ad mare

Acknowledgements

My graduate school experience has been enhanced by a variety of sources, in particular those with whom I have shared my academic life on a day-to-day basis. Dr. Martin Cowie (Marty) has been an exceptional supervisor and mentor, providing both guidance and insight throughout the research phase of my studies, along with indispensable, unending assistance during the preparation of this manuscript (Thanks for everything Boss!).

The Cowie group, both past and present, has always been full of colorful characters, who have made my experience at the U of A both enjoyable and successful. The giants on whose backs I've stood (research-wise) include past group members Dr. Jeffrey Torkelson, Dr. Frederick Antwi-Nsiah, and in particular Dr. Dusan Ristic Petrovic, who taught me many valuable techniques in organometallic synthesis and who initiated the depm chemistry which has since proven quite fruitful (Chapters 4 and 5). Other past members with whom I have shared my time include; Dr. Todd Graham (another early mentor, during a summer undergraduate research term), Dr. Steve Trepanier (for his endless insight into the human condition and 'Trepanier*isms*'), Dr. Bryan Rowsell (a true *b'y* at heart and my generous host at RDC), and Ms. Amala Chokshi (we shared this very strange 'dream' – be careful what you wish for). I've also been fortunate to work with some excellent post-doctoral fellows in our group; Dr. James Dennett (a fine British import and all-around good 'chap'), Dr. James 'Wiggy'

Wigginton (also from the U.K., yet perhaps more of a Canadian than even he knew) and Dr. Matthias Bierenstiel (a short but memorable visit). Current group members with whom I have shared many laughs (and CD_2Cl_2) include; Rahul Samant (fellow houseboat captain and ski-trip-planner to the stars), Kyle Wells (for his never-ending "awesome" adventures), and the new 'Calvies', Tiffany Ulmer, Lindsay Hounjet, Matt Zamora and in particular Mike Slaney, whose most capable assistance, in developing the mixed-metal depm chemistry (during a summer project), along with help tying up some 'loose ends' during the preparation of this manuscript, has been much appreciated. To all of you still 'in the trenches' I offer some words of encouragement and inspiration - *Ut sementem feceris, ita metes* - or as they say in (Red Deer) Alberta - *Git 'er done*. Good Luck.

None of the research accomplished in this thesis could have been achieved without the top-notch services available within the Chemistry department. In addition to being great guys in general, and relentless in extending an invitation to coffee, 'Camp X-ray', Dr. Bob McDonald and Dr. Mike Ferguson, have provided above-and-beyond efforts in solving the inevitably 'disordered' crystals that I was able to submit to them. The staff in the NMR lab have also been exceptional in their quality of service; Gertie Aarts, Lai Kong, and in particular Mark Miskolzie and Glen Bigam have facilitated the acquisition of much low-temperature data, critical to studies of this nature. Wayne Moffat in spectral services also deserves acknowledgment for his contributions to compound

characterization as does Angie Morales (a truly wonderful lady) in the mass spectrometry lab. Over the years I have also appreciated the great work done by the folks in the electronics shop (Ed, Al and Kim), the machine shop (Henry, Hubert, Randy, Paul, *et al*), the glass-blowers (Gerald and Todd), and chemistry stores (Tyler, Bernie, and Andrew). Administratively Jeanette Loiselle, the departmental secretary, has always been very helpful in knowing where to go and what to do, and when such questions pertained to graduate matters, both Ilona Baker, and her new replacement, Arlene Figley have also provided much assistance.

Personally I was able to derive inspiration for enduring the daily grind of grad school from my home life. Although from different perspectives, both of my parents have been extremely inspirational, showing me the benefits of hard work along with the potential rewards associated with both learning and teaching. Thank-you for both everything you have done for me. My extended family, both through blood and otherwise, has also provided much support and encouragement during my academic endeavors and I am grateful for them all. Finally, other than myself, nobody has felt the highs and lows of my graduate school experience more directly than my wife Mikaline. For her unending love and support during these times, I feel truly blessed, and look forward to the future we are building with one another - may we always be 'Lost Together'.

Table of Contents

Chapter 1	**Introduction**	1
	Objectives of this thesis	16
	References	17
Chapter 2	**C-F Activation in Fluoroolefin-Bridged Complexes**	22
2.1.	Introduction	22
2.2.	Experimental	27
2.2.1.	General Comments	27
2.2.2.	Preparation of Compounds	30
2.3.	Results and Compound Characterization	37
2.3.1.	Fluoroolefin-Bridged Complexes	37
2.3.2.	Reaction of Me_3SiOTf with Fluoroolefin-bridged Complexes	50
2.3.3	Reaction of Protic Acids with Fluoroolefiin-bridged Complexes	66
2.4.	Discussion	71
2.5.	Conclusions	81
2.6.	References	82

Chapter 3 **Reactivity of Fluorovinyl Complexes** 85

3.1. Introduction 85

3.2. Experimental 86

3.2.1. General Comments 86

3.2.2. Preparation of Compounds 87

3.3. Results and Compound Characterization 97

3.3.1. Reaction of Hydrogen with Fluorovinyl-containing Complexes 97

3.3.2. Reaction of Carbon Monoxide with Fluorovinyl-containing Complexes 113

3.3.3. Further Reaction of Me_3SiOTf with Fluoroolefin-Bridged Complexes 121

3.4. Discussion 125

3.5. Conclusions 136

3.6. References 138

Chapter 4 **Alkyl Analogues of $[Ir_2(CH_3)(CO)_2(dppm)_2][CF_3SO_3]$ (1)** 139

4.1. Introduction 139

4.2. Experimental 142

4.2.1. General Comments 142

4.2.2. Preparation of Compounds 146

4.3. Results and Compound Characterization 160

4.3.1. Diiridium Complexes 160

4.3.2. Dirhodium Complexes 174

4.3.3. Mixed Rhodium-Iridium Complexes 185

4.4. Discussion 196

4.5. Conclusions 205

4.6. References 206

Chapter 5 **Peripheral Reactivity Related to the DEPM Methyl Complexes of Iridium, Rhodium, and Rhodium/Iridium** 208

5.1. Introduction 208

5.2. Experimental 208

5.2.1. General Comments 208

5.2.2. Preparation of Compounds 212

5.3. Results and Discussion 217

5.3.1. Diiridium Complexes 217

5.3.2. Dirhodium Complexes 223

5.3.3. Mixed Rhodium-Iridium Complexes 230

5.4. Conclusions 232

5.5. References 233

Chapter 6 **Conclusions** 234

Appendix I Solvents and Drying Agents 239

List of Tables

Chapter 2

Table 2.1. NMR Data for the Fluoroolefin Compounds 28

Table 2.2. NMR Data for the Fluorovinyl Compounds 29

Table 2.3. Crystallographic Experimental Details $[Ir_2(\eta^1\text{-}CF{=}CF_2)(OTf)(CO)_2(\mu\text{-}CH_2)(\mu\text{-}H)(dppm)_2][CF_3SO_3]$ (**6**) 35

Table 2.4. Selected Interatomic Distances (Å) for $[Ir_2(CH_3)(CO)_2(\mu\text{–}C_2F_4)(dppm)_2]^+$ (**2**) 42

Table 2.5. Selected Interatomic Angles (deg) for $[Ir_2(CH_3)(CO)_2(\mu\text{–}C_2F_4)(dppm)_2]^+$ (**2**) 42

Table 2.6. Selected Interatomic Distances (Å) for $[Ir_2(CO)_2(C_2F_3)(OTf)(\mu\text{–}CH_2)(\mu\text{-}H)(dppm)_2]^+$ (**6**) 59

Table 2.7. Selected Interatomic Angles (deg) for $[Ir_2(CO)_2(C_2F_3)(OTf)(\mu\text{–}CH_2)(\mu\text{-}H)(dppm)_2]^+$ (**6**) 59

Table 2.8. Comparison of fluorovinyl coupling constants 79

Chapter 3

Table 3.1. NMR Data for the Compounds of the Hydrogenolysis Reactions 89

Table 3.2. NMR Data for the Compounds of the Carbon Monoxide Reactions 90

Table 3.3. NMR Data of the Fluorovinlylidene Complexes 91

Table 3.4. Crystallographic Experimental Details for $[Ir_2(H)_2(CO)_2(\mu\text{-}H)_2(dppm)_2][CF_3SO_3]_2$ 96

Table 3.5. Selected Interatomic Distances (Å) for $[Ir_2H_2(CO)_2(\mu\text{–}H)_2(dppm)_2]^{+2}$ 104

Table 3.6. Selected Interatomic Angles (deg) for $[Ir_2H_2(CO)_2(\mu\text{–}H)_2(dppm)_2]^{+2}$ 104

Chapter 4

Table 4.1. Spectroscopic data for the diiridium compounds 143

Table 4.2. Spectroscopic data for the dirhodium compounds 144

Table 4.3. Spectroscopic data for the rhodium-iridium compounds 145

Table 4.4. Crystallographic Experimental Details for Compounds **23, 28** and **33** the 'trans-depm' series. 154

Table 4.5. Crystallographic Experimental Details for $[Ir_2(H)(CO)_3(\mu\text{-}CH_2)(depm)_2][CF_3SO_3]$ (**26**) 157

Table 4.6. Crystallographic Experimental Details for $[RhIr(CH_3)(CO)_3(depm)_2][CF_3SO_3]$ (**36**) 158

Table 4.7. Selected Interatomic Distances (Å) for *trans*-$[Ir_2Cl_2(CO)_2(depm)_2]$ (**23**) 163

Table 4.8. Selected Interatomic Angles (deg) for *trans*-$[Ir_2Cl_2(CO)_2(depm)_2]$ (**23**) 164

Table 4.9. Selected Interatomic Distances (Å) for $[Ir_2(H)\text{-}(CO)_3(\mu\text{-}CH_2)(depm)_2]^+$ (**26**) 171

Table 4.10. Selected Interatomic Angles (deg) for $[Ir_2(H)(CO)_3(\mu\text{-}CH_2)(depm)_2]^+$ (**26**) 171

Table 4.11. Selected Interatomic Distances (Å) for *trans*-$[Rh_2Cl_2(CO)_2(depm)_2]$ (**28**) 178

Table 4.12. Selected Interatomic Angles (deg) for *trans*-$[Rh_2Cl_2(CO)_2(depm)_2]$ (**28**) 178

Table 4.13. Selected Interatomic Distances for (Å) *trans*-$[RhIrCl_2(CO)_2(depm)_2]$ (**33**) 187

Table 4.14. Selected Interatomic Angles (deg) for *trans*-$[RhIrCl_2(CO)_2(depm)_2]$ (**33**) 187

Table 4.15. Selected Interatomic Distances (Å) for $[RhIr(CH_3)(CO)_3(depm)_2]^+$ (**36**) 195

Table 4.16. Selected Interatomic Angles (deg) for $[RhIr(CH_3)(CO)_3(depm)_2]^+$ (**36**) 195

Chapter 5

Table 5.1. Spectroscopic data for the compounds 210

Table 5.2. Crystallographic Experimental Details for $[Rh_2(CO)_5(depm)2]^{2+}$ (**44**) 216

Table 5.3. Selected Interatomic Distances (Å) for $[Rh_2(CO)_5(depm)_2]^{2+}$ (**44**) 227

Table 5.4. Selected Interatomic Angles (deg) for $[Rh_2(CO)_5(depm)_2]^{2+}$ (**44**) 227

List of Figures

Chapter 1

Figure 1.1. *Bridging-olefin and bridging-vinyl arrangements in binuclear complexes* 4

Figure 1.2. *Bridging bis-dppm coordination geometries* 6

Figure 1.3. *Representation of olefin binding in transition metal complexes* 11

Chapter 2

Figure 2.1. *Dewar-Chatt-Duncanson model of metal-olefin bonding* 23

Figure 2.2. *View of the two disordered complex cations resolved from the disordered structure of* **2** 41

Figure 2.3. *Perspective view of* $[Ir_2(CH_3)(CO)_2(\mu\text{–}C_2F_4)(dppm)_2]^+$ 43

Figure 2.4. *Views of the cocrystallized cationic species* 55

Figure 2.5. *View of the equatorial planes of* $[Ir_2(CO)_2(C_2F_3)(OTf)\text{-}(\mu\text{–}CH_2)(\mu\text{–}H)(dppm)_2]^+$ and $[Ir_2(CO)_3(OTf)(\mu\text{–}CH_2)\text{-}(dppm)_2]^+$ 56

Figure 2.6. *Perspective view of the* $[Ir_2(CO)_2(C_2F_3)(OTf)(\mu\text{–}CH_2)\text{-}(\mu\text{–}H)(dppm)_2]^+$ 58

Figure 2.7. *Binuclear diphosphine framework of* **7**, *with bridging fluorovinyl group, illustrating inequivalence observed in phosphorus nuclei* 61

Chapter 3

Figure 3.1. *Proposed initial isomers resulting from hydrogen addition to* **6** 100

Figure 3.2. *Perspective view of the* $[Ir_2H_2(CO)_2(\mu\text{–}H)_2(dppm)_2]^{+2}$ *complex ion* 103

Figure 3.3. ^{19}F *NMR resonances for cis-difluoropropene* 111

Figure 3.4. ^{19}F *NMR resonances for 2,3-difluoropropene* 112

Figure 3.5. *Replacement of triflate by CO yielding the dicationic tricarbonyl species (***17** *and* **18***)* 132

Chapter 4

Figure 4.1. *Stick and space-filling representations of depm and dppm ligand systems* 141

Figure 4.2. *General structure of trans-*$[MM'_2Cl_2(CO)_2(depm)_2]$ *(M, M' = Rh, Ir)* 160

Figure 4.3. *Perspective view of one disordered molecule of trans-*$[Ir_2Cl_2(CO)_2(depm)_2]$ (**23**) 162

Figure 4.4. *Perspective view of the* $[Ir_2(H)(CO)_3(\mu\text{-}CH_2)(depm)_2]^+$ (**26**) *cation* 170

Figure 4.5. *Proposed structure of compound* **27**, $[Ir_2(CH_3)(CO)_2(depm)_2][CF_3SO_3]$ 173

Figure 4.6. *$^{31}P\{^1H\}$ NMR spectrum* $[Rh_2Cl_2(CO)_2(depm)_2]$ 175

Figure 4.7. *Perspective view of one of the disordered molecules of trans-*$[Rh_2Cl_2(CO)_2(depm)_2]$ (**28**) 177

Figure 4.8. *Proposed structure of* $[Rh_2(CO)_3(depm)_2]$ (**29**) 180

Figure 4.9. *Proposed structure of* $[Rh_2(CO)_4(depm)_2]$ (**30**) 181

Figure 4.10. *Proposed structure of* $[Rh_2(CH_3)(CO)_3(depm)_2]^+$ (**31**) 183

Figure 4.11. *Proposed structure of* $[Rh_2(CO)_2(\mu\text{-}CH_3CO)(depm)_2]^+$ (**32**) 185

Figure 4.12. *$^{31}P\{^1H\}$ NMR spectrum of* $[RhIr(CO)_3(depm)_2]$ (**34**) 188

Figure 4.13. *Proposed structure of* $[RhIr(CO)_3(depm)_2]$ (**34**) *together with its proposed fluxionality* 189

Figure 4.14. *Proposed structure of* $[RhIr(CH_3)(CO)_3(depm)_2]^+$ (**36**) 192

Figure 4.15. *Equatorial-plane view of* $[RhIr(CH_3)(CO)_3(depm)_2]^+$ 193

Figure 4.16. *Perspective view of the* $[RhIrMe(CO)_3(depm)_2]^+$ *cation* 194

Figure 4.17. *Proposed structure of compound* **37** 196

Figure 4.18. *General structure for trans-depm complexes* 198

Figure 4.19. *General structure for tricarbonyl depm complexes* 199

Figure 4.20. *General structure for tetracarbonyl depm complexes* 200

Figure 4.21. *C-H activation of imethyl ligand in diiridium compound* (**26**) 201

Figure 4.22. *Structure of methyl tricarbonyl mixed-metal complex* 202

Figure 4.23. *General structure proposed for* $[MIr(CH_3)(CO)_2depm_2]^+$ (M = Ir, Rh) *complexes* 205

Chapter 5

Figure 5.1. *A-frame structure in hydroxide-bridged dicarbonyl depm complexes* 218

Figure 5.2. *Proposed structure of hydride tricarbonyl depm complexes* 219

Figure 5.3. *Proposed structure of* $[Ir_2(H)(CO)_4(depm)_2]$-$[CF_3SO_3]$ (**40**) 221

Figure 5.4. *Proposed structure of* $[Rh_2(CO)_3(depm)_2]^{+2}$ (**43**) 224

Figure 5.5. *Structure of* $[Rh_2(CO)_5(depm)_2]^{+2}$ (**44**) 225

Figure 5.6. *Perspective view of* $[Rh_2(CO)_5(depm)_2]^{+2}$ (**44**) 226

Figure 5.7. *Proposed structure of* $[RhIr(CO)_3(\mu\text{-}H)(depm)_2]$-$[CF_3SO_3]$ (**48**) 232

List of Schemes

Chapter 1

Scheme 1.1. *Intramolecular C-H activation of a methyl ligand to give bridging-methylene hydride fragments* 7

Scheme 1.2. *Configurations resulting from different initial sites of attack on* **1** *by an incoming olefinic substrate* 8

Scheme 1.3. *Different bridging modes encountered in reaction of* **1** *with allene (R = H) and methylallene (R = CH_3)* 9

Chapter 2

Scheme 2.1. *CF_3 analogy for bridging-fluoroolefins.* 24

Scheme 2.2. *Fluoride abstraction from μ-C_2F_4* 25

Scheme 2.3. *Fluoroolefin-bridged complexes of* $[Ir_2(CH_3)(CO)_2(dppm)_2][OTf]$ (**1**) 25

Scheme 2.4. *Coordination of fluoroolefins in terminal and bridging modes* 37

Scheme 2.5. *Reactions of* **1** *with trifluoroethylene* 44

Scheme 2.6. *Reaction profile for the addition of 1,1-difluoroethylene to* **1** 47

Scheme 2.7. *C-F activation of bridging tetrafluoroethylene via addition of $Me_3Si(OTf)$* 51

Scheme 2.8. *Transformation from bridging* (**5**) *to terminal* (**6**) *trifluorovinyl complex* 53

Scheme 2.9. *C-F activation of bridging trifluoroethylene via addition of* $Me_3Si(OTf)$ 60

Scheme 2.10. *C-F activation of bridging difluoroethylene via addition of* $Me_3Si(OTf)$ 63

Scheme 2.11. *Transformation of compound* **8** *between 0 °C and ambient temperature* 65

Scheme 2.12. *C-F activation reaction of compound* **3** *with water* acting as the Lewis acid 68

Scheme 2.13. *C-F activation reaction of compound* **7** *with water* 70

Scheme 2.14. *Formation of 2-fluoropropene via reaction of compound* **4** *with water* 71

Scheme 2.15. *Sites of attack for substrate (L=olefin) addition to* **1** 72

Scheme 2.16. *Fluorovinyl products of fluoride abstraction from* compounds **2 - 4** 76

Scheme 2.17. *Reactivity comparison of* μ-$F_2C{=}CH_2$ *vs.* η^2-$F_2C{=}CH_2$ 77

Scheme 2.18. *Effect of trilfate ion displacement by hydroxide in difluorovinyl complex* 80

Chapter 3

Scheme 3.1. *Potential products from the removal of fluoride ion from fluorovinyl compounds* 86

Scheme 3.2. *Reaction of hydrogen with terminal trifluorovinyl compound* **6** 98

Scheme 3.3. *Reaction of hydrogen with bridging trifluorovinyl compound* **7** 105

Scheme 3.4. *Reductive elimination of hydrogen-substituted fluorolefins* 109

Scheme 3.5. *Addition of carbon monoxide (CO) to compounds* **5** *and* **6** 114

Scheme 3.6. *Reaction of compound* **7** *with CO* 117

Scheme 3.7. *Reaction of compound* **8** *with CO* 118

Scheme 3.8. *Reaction of compound* **9** *with CO* 120

Scheme 3.9. *C-F activation of bridging fluorovinyl complexes* 122

Scheme 3.10. *Reaction of H_2 with terminal and bridging fluorovinyl complexes* 126

Scheme 3.11. *Reaction of H_2 with compound* **6**, *resulting in two different proposed isomers,* **10** *and* **10a** 128

Scheme 3.12. *Proposed general mechanisms showing unobserved intermediates in the hydrogenolysis of the different isomers* (**10** *and* **10a**) resulting in *the production of* **11** 130

Scheme 3.13. *Replacement of triflate by CO yields* **15** *and triflic acid which then generates compound* **16** 133

Scheme 3.14. *Sequential C-F activation of fluoroolefin-bridged complexes to give bridging fluorovinyl and (fluoro)vinylidene compounds* 135

Scheme 3.15. *Reactivity comparison of* μ-η^1:η^2-C_2F_3 *vs.* η^1-C_2F_3 136

Chapter 4

Scheme 4.1. *Fluxionality of tricarbonyl complexes* 165

Scheme 4.2. *Fluxionality of tetracarbonyl complexes* 167

Scheme 4.3. *Reaction of* **24** *with MeOTf to generate* $[Ir_2(H)(CO)_3(\mu\text{-}CH_2)(depm)_2]^+$ (**26**) 168

Scheme 4.4. *Transformation of methyl tricarbonyl* (**31**) *to acyl dicarbonyl* (**32**) 203

Scheme 4.5. *Fluxionality proposed for* $[Ir_2(CH_3)(CO)_2depm_2]^+$ 204

Chapter 5

Scheme 5.1. *Mechanism proposed for fluxionality observed in the* $[MM'(CO)_3(\mu\text{-}H)(depm)_2][CF_3SO_3]$ 220

Scheme 5.2. *Reaction of CO with* $[Ir_2(H)(CO)_3(\mu\text{-}CH_2)\text{-}(depm)_2][CF_3SO_3]$ (**26**) 222

Scheme 5.3. *Generation of the hydroxide-bridged complex* (**45**) *via the addition of water to the dicationic tricarbonyl species* (**43**) 228

List of Abbreviations

s	sec
min	minute
h	hour
mL	milliliter
mg	milligram
mmol	millimole
ppm	parts per million
°	degrees
Å	Angstroms
Hz	Hertz
cm^{-1}	wavenumber
IR	infrared
NMR	Nuclear Magnetic Resonance
HRMS	High Resolution Mass Spectrometry
calcd	calculated
Et_2O	diethylether
THF	tetrahydrofuran
OTf	trfilate ion $(CF_3SO_3)^-$
dppm	*bis*(diphenylphosphino)methane ($Ph_2PCH_2PPh_2$)
depm	*bis*(diethylphosphino)methane ($Et_2PCH_2PEt_2$)
COD	1,5-cyclooctadiene (C_8H_{12})
TMNO	Trimethylamine-N-oxide
E^+	electrophile

Chapter 1

Introduction

At the heart of chemistry is effecting the transformation of one molecule into another, a process in which chemical bonds are broken and new bonds formed. One of the major challenges in effecting such transformations is the goal of achieving them in a selective manner. Related to this is the need to bring about the reaction under relatively mild conditions. Not only is the latter goal important economically, requiring less energy than transformations under extreme conditions, but mild reaction conditions also limit the reaction pathways available to those having sufficiently low activation energies, thereby introducing a level of selectivity. One effective way of achieving the above goals is through the use of metal centers to modulate the reactivity of substrate molecules.[1]

The activation of organic substrates by metal complexes is central to the subdiscipline of organometallic chemistry. This area of research, involving principles from both inorganic and organic chemistry, is primarily concerned with the interactions between metal ions and organic molecules, in particular those resulting in metal-carbon bond formation. Transition metal complexes in particular, are capable of facilitating many reactions involving organic substrates, both catalytically and stoichiometrically,[2] which would otherwise be inaccessible in their absence. One of the goals in organometallic chemistry is to develop catalysts that are able to effect the desired transformations efficiently, particularly when employing relatively expensive metals. Transition metals are currently used as catalysts in a great number of industrial processes, with a major application being the conversion of common chemical feedstocks into more useful products, through selective transformation of the target bonds. Many of these processes, such as hydrogenation,[3] hydroformylation[4] and polymerization[5] reactions, involve olefinic substrates, subsequently transforming them into other functionalities.

Most industrial processes employ heterogeneous catalysts, primarily due to their robust nature and ease of separation from products. In these catalytic processes substrates undergo metal-assisted transformations after being adsorbed onto a solid surface, and are subsequently released as the modified product. The heterogeneous aspect of this arrangement in which the catalyst, generally as a solid, is in a different phase from reactants and products, makes these systems generally difficult to study, thereby limiting our understanding of the mechanistic details of the reaction.[6] Furthermore, heterogeneous catalysts are not usually selective owing to the harsh conditions often necessary and to the presence of different catalytic sites on the catalyst surface that have different environments leading to a variety of transformations. Single-site catalysts, on the other hand, have a great advantage from the perspective of selectivity since the metal environment in each complex is identical, which in principle can effect the same transformation. Well-defined metal complexes also have the advantage that the metal reactivity can be "fine-tuned" by the appropriate choice of ligands from the vast and ever-expanding libraries of ligands. Not only can this feature of catalyst design influence the catalyst reactivity, often allowing reactions to be carried out under relatively mild conditions, but steric control can also be utilized, allowing an aspect of regioselectivity or even stereoselectivity to be realized. Examples of such steric control are the use of bulky phosphines in hydroformylation to favor the formation of linear over branched aldehydes,[7] and the use of complexes containing chiral ligands are now heavily used in asymmetric catalysis.[8] In addition, homogeneous transition metal complexes, which are more amenable to study by a variety of spectroscopic techniques, are often used as solution phase models of heterogeneous systems,[9] allowing a better understanding of the exact nature of the steps involved, and the roles of the metals, in the overall transformation.

Whereas the vast majority of studies involving substrate activation by transition metal complexes have utilized complexes containing a single metal center,[10] our interest in binuclear complexes is two-fold: first, we can use such systems as

better models for adjacent metal involvement in heterogeneous processes, and second, binuclear complexes can potentially offer access to transformations not readily available at single metal sites. Mononuclear systems, in which transformations occur at only one metal, are inherently limited to the interaction of only a single metal atom per substrate. Participation of more than one metal atom in the transformation process requires the presence of adjacent metals, within reasonable proximity, potentially allowing the two to react in a cooperative manner, as they might on a catalytic surface. Muetterties has proposed that the use of cluster compounds, made up of multiple metal atoms along with their supporting ligands, could amply mimic the conditions found on such a surface.[11] To this end, binuclear metal complexes represent the simplest system in which metal-metal cooperativity may be involved. In addition to serving as models for heterogeneous processes, bimetallic complexes also have potential applications, in their own right, in facilitating substrate transformations, both stoichiometrically and catalytically.[12] The use of such hetero- and homobinuclear complexes, in this capacity, is based on the concept that two metals together may function in a cooperative manner, promoting catalytic processes, not available to, or more efficiently than one metal alone. Such cooperativity may involve one or a combination of various processes, which may include, but are not limited to; simple ligand migration from one metal to the other, opening a vacant coordination site and thereby facilitating attack by an incoming substrate, or activation of a substrate bound at one metal by the adjacent metal center. In addition, adjacent metals have the potential to act as electron sinks or sources in facilitating transformations involving redox reactions, such as many of those found in nature. Many enzymes, catalyzing a wide variety of transformations, are complexes containing two or more metals; for example Nitrogenase (EC 1.18.6.1), the enzyme employed by some microorganisms to 'fix' nitrogen gas from the atmosphere, is a heterotetrameric protein containing molybdenum and iron in its active site, and is associated with another binuclear diiron protein during the 'nitrogen fixation' process.[13] These and many other metalloproteins may serve as inspiration for chemists who are interested in designing related

(binuclear) transition metal complexes that function cooperatively as catalysts for analogous transformations.

Metal-metal cooperativity is surely influenced by the different substrate-binding sites available to binuclear systems. Along with the coordination modes available to mononuclear complexes, additional modes of substrate binding are observed in binuclear complexes, in which substrates may bridge pairs of metals in a variety of ways (Figure 1.1). Such arrangements are otherwise inaccessible in their mononuclear counterparts. Intuitively, it seems clear that a substrate bridging a pair of metals should display reactivity that differs in some way from that observed when the substrate is terminally-bound to a single metal, and this is a concept that will be exploited within this thesis.

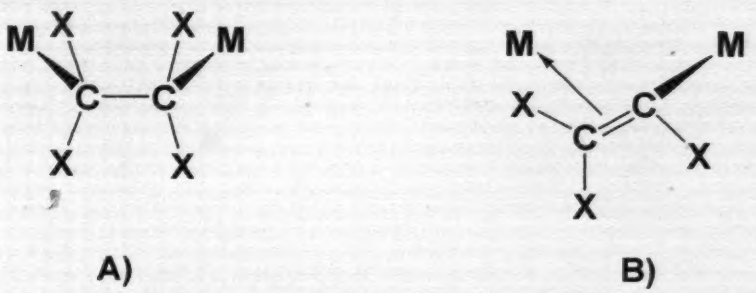

Figure 1.1. **A)** *Bridging-olefin and* **B)** *bridging-vinyl arrangements in binuclear complexes*

As illustrated, the bridging modes may either be symmetrical (Figure 1.1A) or unsymmetrical (Figure 1.1B). In the latter, the presence of two unsymmetrical adjacent metal centers, within a single complex, creates a situation in which the electron density may be polarized to one side, thus changing the propensity for particular reactivity at that metal. In this context, adjacent metals may act as ligand and/or electron "reservoirs" for one another during the stabilization of unique binding modes, and transformations arising from them. Changes in ligand binding mode, along with geometry and oxidation state that result from

such reactivity, would invariably have the potential to fragment the binuclear metal centers.

One of the challenges associated with effecting and studying cooperative activation of substrate molecules by adjacent metals lies in ensuring that the bimetallic framework remains intact during the reactions of interest. In order to achieve this, a robust framework, in the form of bridging ancillary ligands, is often used to hold the metals together. Many bridging ancillary ligands are known which maintain the binuclear (or higher) integrity of the complexes, while themselves remaining relatively inert.[14] In our studies, we have chosen a diphosphine-bridged framework in which the two metals are tethered together by a pair of diphosphine ligands, creating a stable, yet relatively flexible, scaffolding system. Such an arrangement allows considerable variation in the metal-metal distance and therefore in the degree of metal-metal interaction. One of the major advantages in the use of the diphosphine ligands, besides their ability to stabilize low-valent, late-metal complexes of interest to us, is the great utility of ^{31}P NMR spectroscopy for characterization of solution species.

The dppm ligand (dppm = *bis*(diphenylphosphino)methane = $Ph_2PCH_2PPh_2$) has been used extensively (within the Cowie group[15] and by others[16]) to bridge pairs of adjacent metals, with the usual stoichiometry being 1:1, that is, one diphosphine ligand per metal ($M_2(dppm)_2$). Its propensity to form bridging complexes is, in part, due to the unfavorable ring strain resulting upon chelation to one metal, compared to the relatively unstrained bridging arrangement. Under these conditions, the dppm ligand framework has shown the ability to take on a number of different orientations, with respect to one another, as illustrated in Figure 1.2.

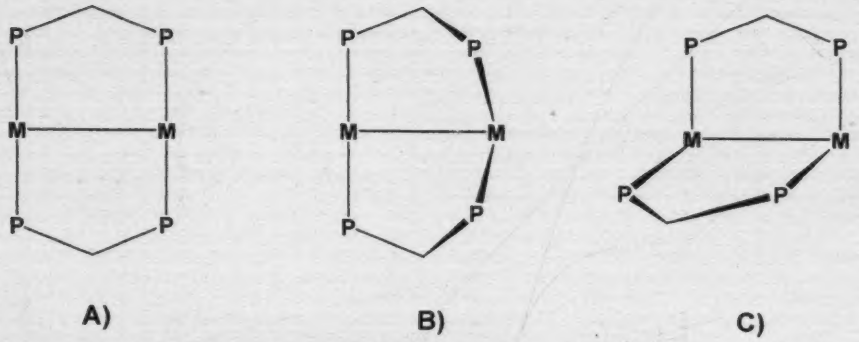

Figure 1.2. *Bridging bis-dppm coordination geometries*
A) *trans-trans* **B)** *cis-trans* **C)** *cis-cis*

Having the ligands in a *trans* arrangement at both metals, as they are often encountered, as shown in configuration Figure 1.2A, places the phosphines in an orientation that can be viewed as occupying the axial sites around the metal, while the equatorial sites are available for substrate and ancillary ligand coordination. The space in this region is largely influenced by the steric bulk of the substituents on the bridging diphosphine, in which "channels" are created in the equatorial plane depending on arrangement of the phenyl groups of dppm,[17] influencing the sites available for coordination by substrate molecules. The steric restriction, enforced by these relatively large groups, serves to limit the size and possibly the orientation of substrates that are able to access the metal centers, thereby potentially inhibiting otherwise favorable reactions. From this steric perspective smaller alkyl substituents on the diphosphine, such as methyl groups in the related dmpm (dmpm = $Me_2PCH_2PMe_2$), would be attractive alternatives to the phenyls of dppm,[16] allowing much easier substrate access to the metals. In addition, the increased phosphine basicity upon substituting phenyl by alkyl substituents can also clearly play a role in substrate activation.

Many binuclear compounds of rhodium and iridium have been prepared employing both the dmpm[19] and dppm[20] ligand systems, with the vast majority

being complexes of the latter. Like many of the related mononuclear species, such compounds have shown the remarkable ability to activate C-H bonds, under a variety of conditions.[21] A key difference in binuclear systems, compared to mononuclear complexes, is demonstrated in the intramolecular activation of alkyl ligands. Whereas in late-metal mononuclear species β-hydrogen elimination of alkyl ligands is common and α-hydrogen elimination is not, in the related binuclear complexes, in addition to the common β-hydrogen elimination pathway, α-hydrogen elimination can also be facile. The presence of another metal, adjacent to a methylated metal, renders the hydrogen in the α-position at this metal susceptible to pseudo-β-abstraction by the other (Scheme 1.1). Such an activation step can be envisioned as proceeding via an agostic interaction, as shown below.

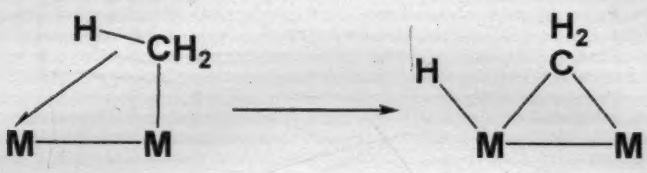

Scheme 1.1. *Intramolecular C-H activation of a methyl ligand to give bridging-methylene hydride fragments*

This reactivity has been well established for the diiridium complex, $[Ir_2(CH_3)(CO)_2(dppm)_2][CF_3SO_3]$ (**1**), in which a variety of incoming substrates have been shown to induce the intramolecular C-H activation of the component methyl ligand, leading to new methylene-bridged hydride complexes, $[Ir_2(L)(H)(CO)_2(\mu\text{-}CH_2)(dppm)_2][CF_3SO_3]$ (L = CO, PMe_3, C_2H_4).[22] Such a transformation could lead to alternate reactivity patterns involving alkyl groups, as has been observed via investigations of **1** with numerous unsaturated substrates, including olefins,[23] alkynes,[24] and cumulenes.[25]

Throughout these studies, a number of different combinations of substrate binding modes, in conjunction with the fate of the methyl ligand were encountered, as outlined in Scheme 1.2, in the reaction of **1** with olefin substrates. Whereas apparent attack at site **1** has resulted in activation of a C-H bond of the methyl ligand to give the methylene hydride, attack at site **2** generates a terminal olefin adduct in which the methyl group remains intact. In some cases olefin attack at site **3**, between the metals, can give rise to olefin-bridged species. One of our main interests in this chemistry was to establish the conditions under which attack at the various sites occurred and whether different transformations of the substrate would occur as a result of these different sites of attack and consequent coordination modes.

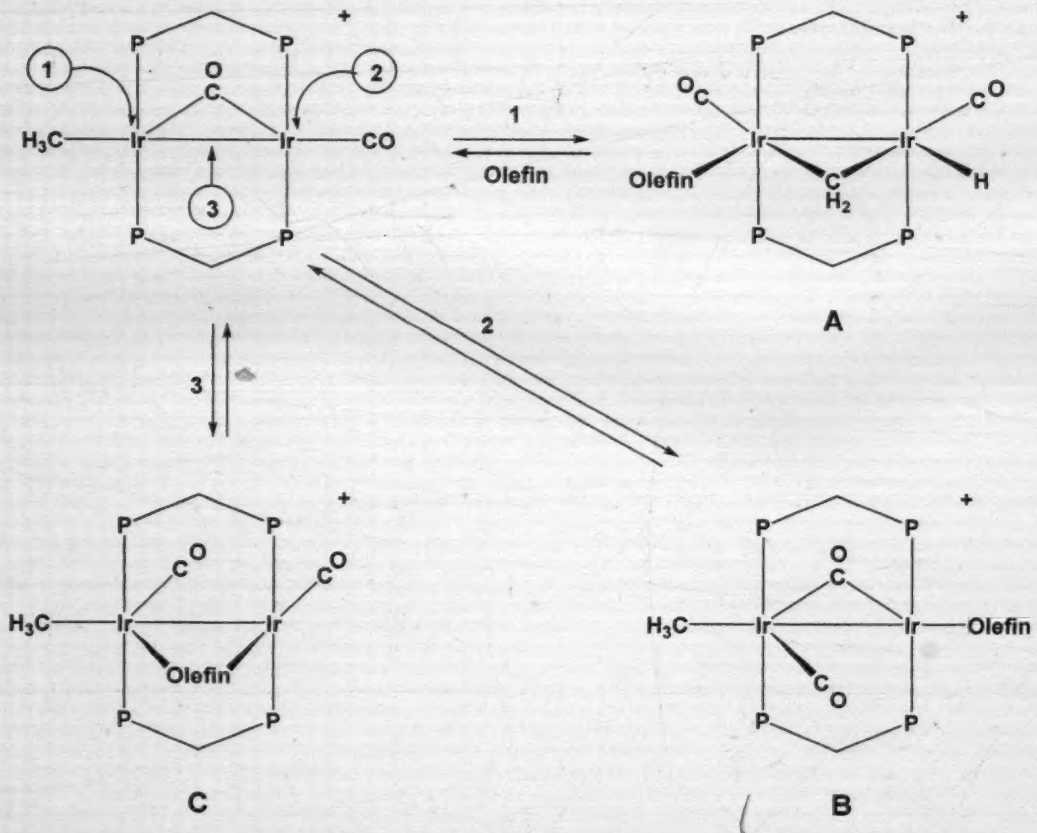

Scheme 1.2. *Configurations resulting from different initial sites of attack on* **1** *by an incoming olefinic substrate*

The relative stability of such complexes has been attributed, partly to the electronic properties of the incoming ligand, but to a large extent by the steric restrictions imposed by the bridging diphosphine substituents (*vide supra*). The different sites of attack, and the factors determining such, are probably best demonstrated in the reaction of **1** with a series of cumulenes.[25] For the less-bulky substrates, allene and methylallene, all three isomers, shown in Scheme 1.2, of the allene adducts were observed in turn. A product analogous to species **A** was found to be the kinetic product and was only observed at very low temperature. Upon warming, this species disappeared being first replaced by product **B** (resulting from attack at site **2**), while subsequent warming resulted in the disappearance of **B** and the concomitant appearance of **C**. In each case substrate coordination at a given site is reversible so the transformation of **A** to **B** and eventually to **C** is assumed to occur by substrate dissociation and subsequent attack at a more thermodynamically favored site. For these two allene substrates two bridging coordination modes (**C'** and **D**) were observed, as shown in Scheme 1.3, and interestingly subsequent transformations involving methyl migration to the allene followed by cleavage of a C-H bond in the new condensed substrate only occurred from the second bridging mode – an interesting example of adjacent metal involvement (cooperativity) at work in substrate activation.

C' **D**

Scheme 1.3. *Different bridging modes encountered in reaction of* **1** *with allene (R = H) and methylallene (R = CH_3)*

Steric and electronic influences in this chemistry were seen in the analogous reaction involving 1,1-dimethylallene and 1,1-difluoroallene, respectively. In the former case the larger steric bulk of the methyl substituents was assumed responsible for the inability of this group to occupy a bridging coordination site in which repulsions involving the dppm phenyl groups are presumably most severe. On the other hand, the difluoro-substituted allene was observed to favor the bridging site (**C'**) such that subsequent rearrangement to the second (reactive) bridging mode (**D**), as observed for allene and methylallene, did not occur. As a consequence, the subsequent migratory insertion and C-H activation steps were also not observed for this substrate. As noted, the subsequent reactivity observed for the substrate when bridging in structure **D** offered support to the idea that cooperative activation by adjacent metals can lead to reactivity not otherwise encountered.

In another example, complex **1** has also been shown to promote the sequential activation of two geminal C-H bonds of butadiene,[26] a transformation which has also been proposed to go through a bridging intermediate. Interestingly, ethylene, the smallest olefin investigated, was never observed in a bridging coordination site, and instead remained η^2-bound to a single metal center at ambient temperature, and as a consequence this substrate failed to display subsequent reactivity in this system.

The above studies were followed up with investigations on the binding of a series of fluoroethylenes with complex **1**.[27] Conceptually, coordination of the related fluorinated alkenes occurs via the same mechanism as that of the perprotio analogues, that is, through the C=C double bond. However, it is now widely recognized that the factors influencing the binding and subsequent activation of the C-F bonds are inherently different than those associated with C-H bond cleavage,[28] and thus one could reasonably expect different reactivity upon addition of fluoroolefin substrates to compound **1**. One of the biggest effects presumably arises from the difference in electronegativity between hydrogen and fluorine, with fluorine being the most electronegative of the elements.[29] As such,

increased fluorine substitution in ethylene leads to shorter C-F bond lengths and increased C-F bond strengths, with a concurrent shortening of the C=C double bond, relative to that of free ethylene.[30] The difference in electronegativity also manifests itself in the geometry encountered upon η^2-coordination of fluorinated olefins to a transition metal center. For instance, in tetrafluoroethylene complexes, the geometry at the olefinic carbon is substantially deformed from the sp^2-hybridization of the free olefin (Figure 1.3B), whereas a much smaller effect is generally encountered with ethylene or other perprotio-olefins (Figure 1.3A). The differences in olefin deformation can be rationalized on the basis of the Dewar-Chatt-Duncanson model[31] which is often invoked to describe the olefin-metal bond in η^2-olefin complexes. In this model, two synergic components of bonding, a σ-donation from the filled π orbital of the olefin along with back-donation from the metal, into the vacant π^* olefin orbital, are involved.

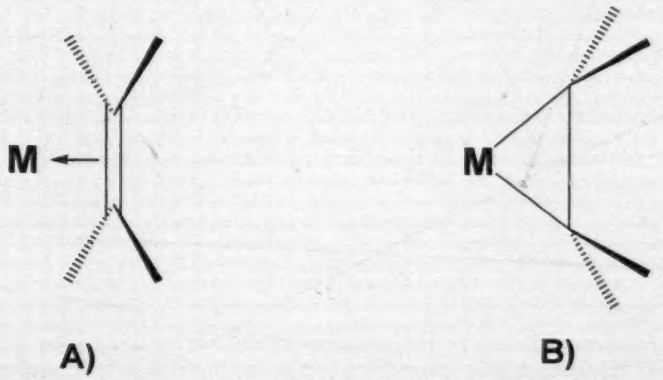

Figure 1.3. *Representation of olefin binding in transition metal complexes* **A)** *non-rehybridized extreme* **B)** *perfluorinated rehybridized extreme*

The rehybridization observed at carbon, upon fluorine substitution, is rationalized on the basis that increased back-donation from the metal, into the π^* antibonding orbital, is a consequence of the better electron withdrawing ability of the fluorine substituents. Using this simple electronic model, it would be predicted that increased fluorine substitution in olefins would lead to a strengthening of the

metal-olefin bond. However, this is not always the case. In our investigations, whereas ethylene was found to form a stable η^2-adduct at ambient temperature, both mono- and *cis*-difluoroethylene form only labile adducts, at low temperature, in spite of increasing fluorine substitution.[27] This decrease in metal-olefin bond strength has been attributed to a combination of the greater rehybridization energy necessary to deform the fluoroolefinic carbons to their sp^3 limits,[32] along with the associated steric repulsions associated with the larger fluorines. A similar decreasing trend in metal-olefin bond strengths with increasing fluorine substitution has previously been noted, and postulated to be due to the higher energy of the π^* orbitals in the fluorinated olefins, compared to that of ethylene, disfavouring the backbonding interaction with the occupied metal *d*-orbitals.[33]

Steric effects, between the lone pairs of electrons surrounding the fluorine atom in a fluorinated substrate and other atoms or groups in the complex, must also be considered in a discussion of differences between hydrogen- and fluorine-substituted olefins. While there is only a relatively small difference in the van der Waals radius of hydrogen and fluorine (1.2 Å and 1.5 Å, respectively),[34] certain restrictive circumstances are conceivable, like those created by the eight phenyl groups in dppm complexes (*vide supra*), in which slight differences in steric crowding may influence subsequent reactivity. This was presumably a factor for the tetrafluoroethylene complex observed in the above study,[27] in which prolonged reaction times were required, even at ambient temperature, to produce the bridging-olefin adduct, due to inhibited access of this substrate to the metals.

Although the trend in olefinic binding strength on proceeding from ethylene to monofluoroethylene to *cis*-difluoroethylene was not as expected (vide supra), subsequent increase in fluorine substitution did result in greater binding strengths. For example, relative stability of the olefin-bridged complexes increases on going from 1,1-difluoroethylene to trifluoroethylene to tetrafluoroethylene, resulting in the latter being the most stable fluoroolefin-bridged complex observed in these investigations. Having observed the effects of fluorine substitution on the resulting binding mode, we endeavored to probe

the differences in reactivity displayed by such species. On the basis of the C-H activation process previously observed in a bridging-allene complex (*vide supra*) we were particularly interested in establishing whether bridged fluoroolefins would display reactivity not seen (under comparable conditions) for terminal η^2-bound analogues.

The activation of otherwise unreactive bonds, such as carbon-hydrogen (C-H) and carbon-fluorine (C-F) bonds, using organometallic complexes, is an exciting area of current research.[35] The chemical and intellectual challenges associated with such processes, such as the activation of C-H bonds in saturated hydrocarbons, has undergone great advances in the past twenty years.[36]

The chemistry of fluorocarbon interconversion is a related area of research, with selective transformation of CFCs (chlorofluorocarbons) into hydrogen-substituted molecules being of particular interest.[37] From a synthetic viewpoint, C-F activation provides an alternate strategy to synthesize fluorocarbons; starting with a perfluorinated molecule and subsequently removing or substituting one of the fluorine atoms for another desired functional group, as opposed to the conventional method of incorporating fluorine into a hydrocarbon. Fluorinated hydrocarbons currently find uses in pharmaceutical and agricultural chemicals, as well as being extensively used as refrigerants, and as highly thermally stable, inert coatings.[38] Due to their typical inertness, and the associated long environmental life-times they possess,[39] their resistance to degradation is not only one of their useful properties, but because many of the chlorinated compounds are responsible for ozone depletion and/or are global warming gases, substantial problems arise in their destruction and disposal. Therefore selective transformations involving the activation of these bonds are desirable; not only to create new useful chemicals but also to transform existing ones into compounds having lower environmental impact.

The activation of C-F bonds by transition metal complexes has been well documented.[40, 41] Whereas the related C-H bond activation process primarily involves oxidative addition of the substrate to the metal center, C-F bond activation in fluorocarbons may be accomplished via a number of different routes, offering further complexity to their study. Six major intermolecular 'mechanisms' have been identified in these processes;[41] 1) oxidative addition, 2) M-C bond formation with HF elimination, 3) M-C bond formation with fluorosilane elimination, 4) hydrodefluorination with M-F bond formation, 5) nucleophilic attack and 6) photochemical defluorination. Many of these processes are more prevalent within particular classes of fluorocarbons; for example, while oxidative addition is seen primarily in reactions with fluoroaromatics (and is common only with group 10 transition metals, particularly nickel complexes), it is not observed in the activation of fluoroalkyl substrates. This is presumably a direct result of the differences in C-F bond strength, whereby the stronger fluoroalkyl C-F bond is harder to activate. Bond energies of the resultant products may also be an influencing factor, energetically driving the reaction forward. Such may be the case in processes 3, 4, and 5, above, wherein formation of the strong (~565 KJ/mol) H-F, Si-F and M-F bonds, respectively, increases the favorability of such reactions. Notably, *both* metal-fluoroalkyl *and* metal-fluoroaryl bonds are also stronger than their hydrocarbyl analogues,[42] resulting in significant differences in subsequent transformations (such as migrations, insertions, eliminations etc.) observed with these moieties.[43] The related intramolecular C-F activation processes are less well defined but again may be classed into six general mechanisms; 1) [1,2]-F shift, 2) [1,3]-F shift, 3) F^- abstraction induced by Lewis or Bronsted acid, 4) F^- abstraction with [1,2]-H/Me shift, 5) acid induced HF elimination and 6) reductive defluorination.

Whereas C-F activation and subsequent hydrodefluorination are more prevalent with polyfluorinated arenes,[44] there are relatively few reported examples of C-F activation and hydrodefluorination of fully or partially fluorinated olefins. Many strategies for effecting these transformations have been proposed, but only a small number provide for *selective* transformation of the substrate olefin, in the

production of the targeted, less fluorinated, product. Examples of such reactions have been reported in mononuclear complexes, employing both early and late transition metals (*vide infra*), and interestingly, many of the latter examples employ some variation of alkylphosphine moieties as ancillary ligands. One such system, $[RhH(PEt_3)_3]$, in the presence of hydrogen, displays the ability to activate and subsequently add hydrogen to, or "hydrodefluorinate" all of the olefinic fluorines of hexafluoropropene, resulting in the exclusive production of 1,1,1-trifluoropropane.[45] Under similar conditions, the same complex facilitated the conversion of (E)-1,2,3,3,3-pentafluoropropene into (Z)-1,3,3,3-tetrafluoropropene, wherein a fluorine atom has been substituted by a hydrogen and the resulting olefin released prior to hydrogenation of the unsaturated C=C bond. Whereas the above examples are presumed to be accompanied by HF elimination, a common pathway in this type of chemistry, another example using an early-transition metal hydride complex ($Cp^*_2ZrH_2$) found that the fluoroolefins undergo insertion into the metal-hydride bond, whereby a subsequent β-fluorine elimination step affords a new hydrogen-substituted fluoroolefin,[46] along with a metal bound fluoride.

Although postulated to be the initial step in the activation of fluoroaromatics, neither of the above processes reported any intermediates in which precoordination of the olefinic substrate was observed. Presumably the presence of an adjacent intramolecular hydride, in both cases, leads to rapid reactivity of any such species. Subsequent transformations in these systems appear to be selective for olefinic C-F bonds, and both show the potential for successive replacement of fluorine by hydrogen in polyfluoroolefins. However, while conversions such as these are highly desirable, reports of even more specific *regio*-selective hydrodefluorination reactions, are uncommon, and thus warrant further attention.

Objectives of this thesis

The first goal of this thesis was to expand the reactivity studies of $[Ir_2(CH_3)(CO)_2(dppm)_2][CF_3SO_3]$ (**1**), to include further investigations into the various binding modes encountered within a series of fluorinated ethylenes. With the knowledge that certain fluoroolefins form different coordination complexes with compound **1**, we also propose to explore the potential for C-F activation in such systems, comparing the differences in reactivity demonstrated for the various fluoroolefin binding modes. Upon accomplishing the initial activation, subsequent transformation of the resulting fluorocarbyl fragments will also be investigated in order to complete the cycle of converting a fluoroolefin into a less fluorinated product. It is thought that such fragments may be converted into less-fluorinated olefins through coupling with hydrogen via hydrogenolysis, or perhaps into larger fluorinated molecules (eg. fluoropropenes from fluoroethylenes) through methyl migration and subsequent elimination. The potential for multiple C-F bond activations, in order to effect multiple fluorine substitutions will also be explored.

Ultimately, we seek to obtain information that will lead us to develop new strategies for employing adjacent metals to promote selective C-F bond transformations. Our studies on the above selective C-F activation of fluoroethylene molecules will be described in Chapters 2 and 3 of this thesis.

Based on what we already know about the bond-activation tendencies of compound **1**, we anticipate that our studies in this area need to be expanded to allow better access of substrates to the metals, making substrate bulk less of a factor, and to facilitate many of the bond activation processes already noted earlier. To address this, we propose to substitute the phenyl groups in the dppm system by ethyl groups, to give *bis*(diethylphosphino)methane (depm=$Et_2PCH_2PEt_2$) analogues of **1**. Varying the R groups of the diphosphine moiety allows adjustment of the steric and electronic properties of the ligand, and thus may induce changes in the reactivity of the attached metal centers. By

switching to the depm analogues, a two-fold change towards reactivity is predicted; first, the smaller steric bulk should allow easier substrate access to the metals, and second, the more basic alkyl diphosphine ligands should favor oxidative addition processes at the metal centers. Although the chemistry of binuclear, dppm-bridged complexes is well developed, the analogous chemistry of depm is much less so. In the second part of this thesis (Chapters 4 and 5) we will seek to develop a series of complexes based upon the "MM'$(depm)_2$" framework (M,M' = Rh, Ir) which we anticipate being adapted for use in C-F and C-H bond activations. It is anticipated that studies involving the different metal combinations will shed light on the roles of the different metals in these activation processes and in subsequent derivatization of the substrates.

References

1. a) P. Knochel, A. Boudier, L.O. Bromm, E. Hupe, J.A. Varela, A. Rodriguez, C. Koradin, T. Bunlaksananusorn, H. Laaziri, F. Lhermitte, *Pure and Applied Chemistry* **2000**, 72(9), 1699-1703. b) B.M. Trost, *Org. Chem.* **1988**, 1(6), 415-35.
2. a) J.P. Collman, L.S. Hegedus, J.R. Norton, R. G. Finke, *Principles and Applications of Organotransition Metal Chemistry;* University Science Books, Mill Valley. CA, 1987. b) R.H. Crabtree, *The Organometallic Chemistry of the Transition Metals;* John Wiley and Sons, New York, 1988. c) A. Yamamoto, *Organotransition Metal Chemistry;* John Wiley and Sons, New York, 1987.
3. H.U. Blaser, C. Malan, B. Puqin, F. Spindler, H. Steiner, M. Struder, *Adv. Synth. Catal.* **2003**, *345*, 103-151.
4. a) M.L. Clarke, *Curr. Org. Chem.* **2005**, 9(7), 701-718. b) B. Breit, W. Seiche, *Synthesis*, **2001**, *1*, 1-36.

5. G.G. Hlatky, *Coord. Chem. Rev.* **2000**, *199*, 235-329.
6. a) R.K. Brown, J.M. Williams, A.J. Sivak, b) E.L. Muetterties, *Inorg. Chem.* **1980**, *19*, 370. c) F. Zaera, *Chem. Rev.* **1995**, *95*, 2651.
7. Z. Freixa, P.W.N.M. van Leeuwwen, *Dalton Trans.* **2003**, *10*, 1890-1901.
8. M. Tada, Y. Iwasawa, *Chem. Comm.*, **2006**, 27, 2833-2844.
9. a) J.D. Atwood, *Coord. Chem. Rev.* **1988**, *83*, 93. b) T.J. Marks, *Acc. Chem. Res.* **1992**, *25*, 57.
10. R.E. Douthwaite, *Ann. Rep. Prog. Chem. Sect. A,* **2004**, *100*, 385-406
11. E.L. Muetterties, *Science* **1977**, *196*, 839.
12. J.H. Sinfelt, *Bimetallic Catalysts: Discoveries, Concepts and Apllications*, Wiley, New York, 1983.
13. http://en.wikipedia.org/wiki/Nitrogenase, accessed July02,2007
14. F. A. Cotton, *Quart. Rev.* **1966**, *20*, 389.
15. M. Cowie, *Can. J. Chem.* **2005**, *83(8)*, 1043-1055 and references within.
16. See for example: a) A.L. Balch, *Homogeneous Catalysis with Metal Phosphine Complexes*, L.H. Pignolet, Ed., Plenum, New York, 1983, 167-213. b) A.L. Balch, *J. Am. Chem. Soc.* **1976**, *98*, 8049, c) C.P. Kubiak, C. Woodcock, R. Eisenebrg, *Inorg. Chem.* **1982**, *21*, 2219, d) R.J. Puddephatt, *Chem. Soc. Rev.* **1983**, *12*, 98. e) B. Chaudret, B. Delavaux, R. Poilblanc, *Coord. Chem. Rev.*, **1988**, *86*, 191.
17. D. Ristic-Petrovic, Ph. D. Thesis, University of Alberta, 2002.
18. a) L. Manojlovic-Muir, I. R. Jobe, B. J. Maya, R. J. Puddephatt, *J. Chem. Soc., Dalton Trans.* **1987**, 2117. b) J. Wu, P.E. Fanwick, C.P. Kubiak, *J. Am. Chem. Soc.* **1989**, *111*, 7812. c) M.A. Alvarez, M.E.Garcia, V. Riera, M.A. Ruis, L.R. Falvello, C. Bois, *Organometallics* **1997**, *16*, 354. d) W. Lin, S. R. Wilson, G. S. Girolami, *Organometallics* **1997**, *16*, 2987. e) M.H. Chisholm, K. Folting, K. S. Kramer, W.E. Streib, *Organometallics* **1997**, *119*, 5528. f) S.M. Reid, J.T.Mague, M.J. Fink, *J. Am.Chem. Soc.* **2001**, *123*, 4081. g) J.F. Hartwig, R.A. Andersen, R.G. Bergman, *Organometallics* **1991**, *10*, 1710.

19. See for example: a) J.A. Jenkins, J.P. Ennett, M. Cowie, *Organometallics* **1988**, *7*, 1845. b) J.A. Jenkins, M. Cowie, *Organometallics* **1992**, *11*, 2767. c) M.K. Reinking, Ph. D. Thesis, Purdue University, 1989. d) M.K. Reinking, P.E. Fanwick, C.P. Kubiak, *Angew. Chem. Intl. Ed. Eng.* **1989**, *28*, 1377. e) M.K. Reinking, J. Ni, P.E. Fanwick, C.P. Kubiak, *J. Am. Chem. Soc.* **1989**, *111*, 6459.

20. See for example: a) B.R. Sutherland, M. Cowie, *Inorg. Chem.* **1984**, *23*, 2324. b) B.R. Sutherland, M. Cowie, *Organometallics* **1985**, *4*, 1637-1648. c) C.P. Kubiak, C. Woodcock, R. Eisenberg, *Inorg. Chem.* **1982**, *21*, 2119. d) C. Woodcock, R. Eisenberg, *Inorg. Chem.* **1985**, *24*, 1285. e) F. Shafiq, K.W. Kramarz, R. Eisenberg, *Inorg. Chim. Acta.* **1993**, *213*, 111-119. f) J.T. Mague, J.P Mitchener, *Inorg. Chem.* **1969**, *8*, 119. g) S. Dwight, M. Cowie, *Inorg. Chem.* **1980**, *19*, 2500-2507.

21. a) A.A. Bengali, B.A. Arndtsen, P.M. Burger, R.H. Schultz, B.H. Weiller, K.R. Kyle, C.B. Moore, R.C. Bergman, *Pure and Appl. Chem.* **1995**, *67*, 281-8. b) R. Jimenez-Catano, M.B. Hall, *Organometallics* **1996**, *15*, 1889-97.

22. J.R. Torkelson, F.H. Antwi-Nsiah, R. McDonald, M. Cowie, J.G. Prius, K.J Jalkanen, R.L. DeKock, *J. Am. Chem. Soc.* **1999**, *121*, 3666.

23. J.R. Torkelson, Ph. D Thesis, University of Alberta, Edmonton, Alberta, 1998.

24. J.R. Torkelson, R. McDonald, M. Cowie, *J. Am. Chem. Soc.* **1998**, *120*, 4047-4048.

25. D. Ristic-Petrovic, D.J. Anderson, J.R Torkelson, R. McDonald, M. Cowie, *Organometallics* **2005**, *24*, 3711-3724.

26. D. Ristic-Petrovic, J.R. Torkelson, R.W. Hilts, R. McDonald, M. Cowie, *Organometallics* **2000**, *19*, 4432.

27. D. Ristic-Petrovic, D.J. Anderson, J.R. Torkelson, R. McDonald, M. Cowie, *Organometallics* **2003**, *22*, 4647-4657.

28. a) F. Colmenares, H. Torrens, *J. Phys. Chem.* **2005**, *109*(46), 10587-93. b) M. Reinhold, J.E. McGrady, R.N. Perutz, *J. Am. Chem. Soc.* **2004**, *126*, 5268-5276.

29. B. E. Smart, *The Chemistry of Functional Groups, Supplement D*, Chapter 14, eds. S. Patai and Z. Rappoport, John Wiley and Sons, Chichester, U.K., 1983.

30. a) C.R. Patrick, *Adv. Fluorine Chem.* **1961**, 2, 1. b) H.A. Bent, *Chem. Revs.*, **1961**, *61*, 275.

31. a) M.J.S. Dewar, *Bull. Soc. Chim. Fr.* **1951**, 18, C71. b) J. Chatt, L.A. Duncanson *J. Chem. Soc.* **1953**, 2939.

32. a) D. L. Cedeno, E. Weitz, *J. Phys. Chem.* **2001**, *105*, 8077-8085. b) D. L. Cedeno, E. Weitz, *J. Am. Chem. Soc.* **2001**, *123*, 12857. c) R.P Hughes, *Organometallics* **1993**, *12*, 4736. d) G.O. Spessard, G.L. Meissler, *Organometallic Chemistry,* Prentice Hall, New Jersey, 1997.

33. C.A. Tolman, *J. Am. Chem. Soc.* **1974**, *26*, 2780.

34. J.E. Huheey, E.A. Keiter, R.L. Keiter, *Inorganic Chemistry, Principles of Strucure and Reactivity*, Fourth Ed., Harper Collins, New York, 1993; 292.

35. a) W.D. Jones, *Inorg. Chem.*, **2005**, *44*, 4475-4484. b) R.H. Crabtree, *Dalton Trans.*, **2001**, *17*, 2437-2450. c) R.A. Gossage, G. van Koten, *Topics Organomet. Chem.* **1999**, *3*, 1. d) T.G. Richmond, in "Topics in Organometallic Chemistry: Activation of Unreactive Bonds and Organic Synthesis" Springer-Verlag, New York, 1999.

36. a) J.W. Herndon, *Coord. Chem. Rev.* **2007**, *252*, 1158-1258. b) F. Kakiuchi, N. Chatani, *Adv. Synth. Catal.*, **2003**, *345*, 1077-1101.

37. A.R. Ravishankara, S. Solomon, A.A. Turnipseed, R.F. Warren, *Science* **1993**, *259*, 194-199.

38. a) T. Hiyama, *Organofluorine Compounds*, Springer, Berlin 2000, b) *Organofluorine Chemistry: Principles and Commercial Applications*, eds. R.E. Banks, B.E. Smart and J.C. Tatlow, Plenum, New York, 1994.

39. A. McCulloch, *J. Fluor. Chem.* **2003**, *123*, 21-29

40. Relevant Reviews: a) J.L. Kiplinger, T.G. Richmond, C.E. Osterberg, *Chem. Rev.* **1994**, *94*, 373-431; b) J. Burdeniuc, B. Jedlicka, R.H. Crabtree, *Chem. Ber. Recl.* **1997**, *130*, 145-154; c) T.G. Richmond, *Topics Organomet. Chem.* **1999**, *3*, 243-269; d) T.G. Richmond, *Angew. Chem.* **2000**, *112*, 3378-3380; *Angew. Chem. Int. Ed.* **2000**, *39*, 3241-3244; e) T. Braun, R.N. Perutz, *Chem. Commun.* **2002,** 2749-2757; f) U. Mazurek, H. Schwartz, *Chem. Commun.* **2003**, 1321-1326; g) W. Jones, *Dalton Trans.* **2003**, 3991-3995; h) H. Torrens, *Coord. Chem. Rev.* **2005**, *249*, 1957-1985;

41. R.N. Perutz, T. Braun, *Comprehensive Organometallic Chemistry* III, Chapter 1.26, eds: R.H. Crabtree, D.M.P. Mingos, Elsevier, New York, 2007.

42. B. E. Smart, *The Chemistry of Functional Groups, Supplement D*, Chapter 14, eds. S. Patai and Z. Rappoport, John Wiley and Sons, Chichester, U.K. **1983**.

43. C.J. Bourgeois, R.P. Hughes, T.L. Husebo, J.M. Smith, I.M. Guzei, L.M. Liable-Sands, L.N. Zakharov, A.L. Rheingold, *Organometallics* **2005**, *24*, 6431-6439.

44. see for example: a) M. Aizenberg, D. Milstein, *Science* **1994**, *265*, 359-361. b) B.M. Kraft, W.D. Jones, *J. Organomet. Chem.* **2002**, *658*, 132-140. c) E. Clot, C. Megret, B.M. Kraft, O. Eisenstein, W.D. Jones, *J. Am. Chem. Soc.* **2004**, *126*, 5647-5653. d) M. Aizenberg, D. Milstein, *J. Am. Chem. Soc.* **1995**, *117*, 8674-8675.

45. D. Noveski, T. Braun, M. Schulte, B. Neumann, H-G. Stammler, *Dalton Trans.*, **2003**, 4075-4083.

46. W.D. Jones, *Dalton Trans.*, **2003**, 3991-3995.

Chapter 2

C-F Activation in Fluoroolefin-Bridged Complexes *

2.1. Introduction

In the past twenty years, substantial efforts have been focused on the activation of carbon-fluorine bonds in otherwise inert fluorocarbon molecules, mediated by transition-metal complexes.[1] This interest stems from a variety of perspectives, with one goal being the conversion of potentially harmful chlorofluorocarbon molecules (CFCs) into more industrially useful and environmentally benign compounds.[2] In addition, the functionalization of C-F bonds in precursor molecules could also lead to more direct routes to a wider variety of fluorinated products, which find commercial applications in pharmaceuticals, agri-chemicals and protective coatings.[3] C-F replacement by C-R (R = H, alkyl, aryl) in fluorinated starting materials offers an alternate strategy for the production of such compounds, rather than the conventional approach of introducing fluorine into non-fluorinated molecules. Selective hydrodefluorination of fully and partially fluorinated olefins to this end remains a challenge. The difficulty lies, for the most part, in breaking the carbon-fluorine bond – the strongest single bond involving carbon (485 KJ/mol),[4] although the electronegativity of, and the non-bonding pairs of electrons around fluorine also play a role.[5]

It has been demonstrated, however, that certain arrangements of fluorocarbons in transition metal complexes may render the C-F bond increasingly labile. For example, aliphatic C-F bonds, in fluoroalkyl groups bound in an α-position to late-transition metal centers, have been shown to be susceptible to activation, via fluoride ion abstraction, using both protic and Lewis acids.[6] We have attempted to adapt this concept to fluoroolefin substrates in which the fluoroolefin bridges a pair of iridium centers, as will be explained in what follows.

---

* A portion of this work has been published. J. Anderson, R. McDonald, M. Cowie. *Angew. Chim. Int. Ed.* **2007**, *46*, 3741.

Fluoroolefin binding at single metal centers has been thoroughly investigated. Using the standard Dewar-Chatt-Duncanson[7] model for ligand binding in organometallic complexes, the interaction may be viewed as a combination of σ-donation from the filled olefin π orbital into an empty d-orbital of σ-symmetry on the metal, and a concurrent (synergic) back-bonding from a filled d-π metal orbital into the C-C π^* orbital of the olefin, as diagrammed in Figure 2.1.

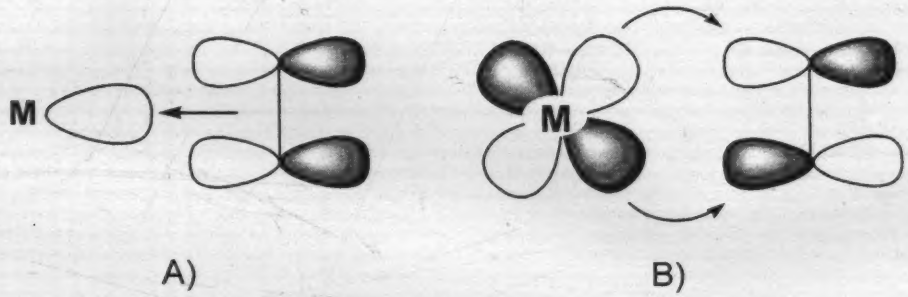

Figure 2.1. *Dewar-Chatt-Duncanson model of metal-olefin bonding:* **A)** *the σ-donor interaction* **B)** *the π-acceptor interaction*

Both interactions lead to strengthening of the M-olefin interaction and weakening of the olefinic C-C bond. The back-bonding component can be especially pronounced in fluoroolefins due to the electron-withdrawing nature of the constituent fluorine substituents, resulting in substantial lengthening of the olefinic carbon-carbon bond towards that of the single-bond extreme, accompanied by substantial rehybridization of the olefinic carbons towards the sp^3 limit. A very similar, although arguably more pronounced effect is encountered in binuclear compounds in which the fluoroolefin bridges the two metal centers, as shown in Scheme 2.1 for tetrafluroethylene. In the bridging arrangement, the bimetallic core can be considered as having added across the olefinic bond, generating a 1,2-dimetallated alkane, clearly defining the organic fragment as saturated. X-ray crystallographic characterization, by Cowie *et al.* on a tetrafluoroethylene-bridged species, $[Ir_2(CH_3)(CO)_3(\mu\text{-}C_2F_4)(dppm)_2][CF_3SO_3]$[8] and by Ibers, Poilblanc *et al.* on a di-iron system,

$[Fe_2(CO)_6(\mu\text{-}SCH_3)_2(\mu\text{-}C_2F_4)]$[9] have confirmed this binding picture in which both structures have shown essentially complete rehybridization of the olefinic carbons to the sp^3 limit, accompanied by lengthening of the olefinic C-C bond, to that of a single bond, with concomitant lengthening of the constituent C-F bonds.

This sp^3-like hybridization at the olefinic carbons of these fluoroolefins has fostered our proposal that these moieties can be considered as pseudo-fluoroalkyl groups, rendering them susceptible to C-F activation via electrophilic abstraction of fluoride ions, much like their mononuclear fluoroalkyl analogues, as diagrammed in Scheme 2.1.

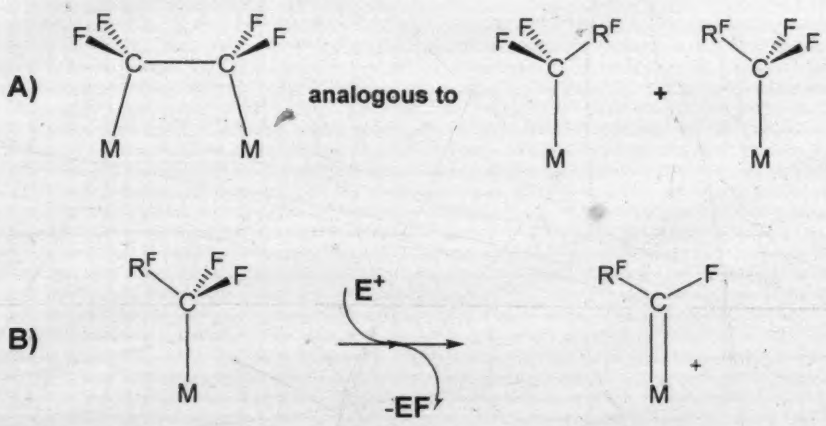

Scheme 2.1. **A)** *CF_3 analogy for bridging-fluoroolefins.* **B)** *Electrophilic fluoride abstraction in fluoroalkyl groups.*

Using this analogy, we might then anticipate that fluoride ion loss from a bridging fluoroolefin could yield either a bridging unit having carbene character at one end (Scheme 2.2(A)), analogous to that in mononuclear systems discussed above, or the isomeric vinyl-bridged species, as diagrammed in Scheme 2.2(B).

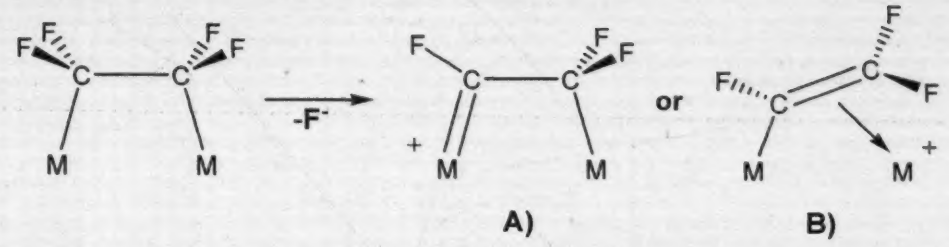

Scheme 2.2. *Fluoride abstraction from μ-C_2F_4 yielding either;* **A)** *fluorocarbene species, or* **B)** *fluorovinyl-bridged species.*

We have initially investigated the coordination modes of a series of fluoroolefins, based on fluorine substitution of the C_2 backbone of ethylene, with the diiridium compound $[Ir_2(CH_3)(CO)_2(dppm)_2][CF_3SO_3]$ (**1**).[8] It was discovered that only those fluoroolefins possessing a geminal C-F pair, such as tetrafluoroethylene, trifluoroethylene, and 1,1-difluoroethylene ultimately gave olefin-bridged species (Scheme 2.3), even in cases in which the terminal olefin binding mode was initially observed for these olefins (1,1-difluoroethylene, trifluoroethylene).[8]

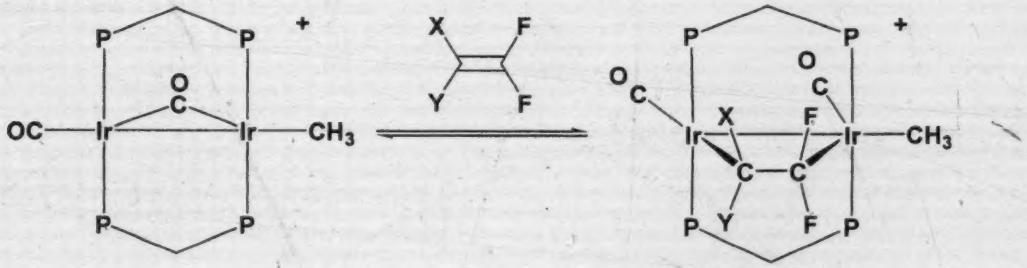

1

2 **X = F, Y = F**
3 **X = H, Y = F**
4 **X = H, Y = H**

Scheme 2.3. *Fluoroolefin-bridged complexes of* $[Ir_2(CH_3)(CO)_2(dppm)_2][CF_3SO_3]$ (**1**)

Using the aforementioned 'CF_3 analogy', we chose to employ these compounds in our studies on C-F bond activation of fluoroolefin-bridged complexes.

Trimethylsilyltrifluoromethylsulphonate, often referred to as trimethylsilyl triflate (Me_3SiOTf; OTf = CF_3SO_3), is a well established Lewis acid that is effective for fluoride ion abstraction, owing to the strong Si-F bond generated in the product Me_3SiF.[10] Furthermore, the ability of the triflate (OTf^-) anion to potentially coordinate to the metal can play an important role in stabilizing the resulting cationic complex. ^{19}F NMR spectroscopy is instrumental for characterizing the products in such reactions; Me_3SiF shows a characteristic splitting pattern at -159.9 ppm, in CD_2Cl_2, in the ^{19}F NMR spectrum, while the triflate counterion displays a slight (up to 4 ppm) down-field shift from the free counterion (-79 ppm) upon coordination to the metal center in these systems.[11] ^{19}F NMR spectroscopy is also essential for obtaining information on the remaining fluorine substituents on the resulting fluorocarbyl ligand.

In this chapter the coordination of fluoroolefins to **1** is further elucidated and attempts at fluoride ion removal from a number of fluoroolefin adducts will be investigated. Attempts to compare C-F bond activation of fluoroolefins bound in a bridging arrangement across two iridium centers with those coordinated terminally to a single metal will be discussed.

2.2. Experimental

2.2.1. General Comments. All solvents were dried (using appropriate drying agents, given in Appendix I), distilled before use and stored under dinitrogen. Deuterated solvents used for NMR experiments were freeze-pump-thaw degassed (three cycles) and stored under nitrogen or argon over molecular sieves. Reactions were carried out under argon using standard Schlenk techniques, and compounds that were obtained as solids were purified by recrystallization. Prepurified argon and nitrogen were purchased from Linde, carbon-13 enriched CO (99%) was supplied by Isotec Inc, certain fluoroolefins (fluoroethylene, Z-1,2-difluoroethylene, and 1,1-difluoroethylene) were supplied by Lancaster Synthesis; trifluoroethylene was supplied by SynQuest Fluorochemicals or prepared by a literature method,[12] tetrafluoroethylene was prepared by a literature method.[13] All purchased gases were used as received. All other reagents were obtained from Aldrich and were used as received (unless otherwise stated). The compound $[Ir_2(CH_3)(CO)(\mu\text{-}CO)(dppm)_2][CF_3SO_3]$ (**1**) was prepared as previously reported.[14]

Proton NMR spectra were recorded on Varian Unity 400 or 500 spectrometers, or on a Bruker AM400 spectrometer. Carbon-13 NMR spectra were recorded on Varian Unity 400 or Bruker AM300 spectrometers. Phosphorus-31 and fluorine-19 NMR spectra were recorded on Varian Unity 400 or Bruker AM400 spectrometers. Two-dimensional NMR experiments (COSY, NOESY and ^{13}C-^{1}H HMQC) were obtained on Varian Unity 400 or 500 spectrometers.

Spectral results for all compounds described in this Chapter are presented in Tables 2.1 – 2.2.

Table 2.1. NMR Data for the Fluoroolefin Compounds[a, b]

compounds[c]	$\delta(^{31}P\{^1H\})$[d]	$\delta(^1H)$[e, f]	$\delta(^{13}C\{^1H\})$[e]	$\delta(^{19}F)$[g]
$[Ir_2(CH_3)(CO)_2(\mu\text{-}CF_2{=}CF_2)(dppm)_2]^+$ (**2**)	17.0 (m, 2P), 5.0 (m, 2P)	3.89 (m, 4H), 0.41 (t, 3H, $^3J_{HP}$ = 6.0 Hz)	182 (b), 192 (b), -7.4	-80, -86
$[Ir_2(CH_3)(CO)_2(\mu\text{-}CF_2{=}CFH)(dppm)_2]^+$ (**3**)	14.9 (m, 2P), 5.1 (m, 2P)	5.9 (ddd, 1H), 3.97 (m, 1H), 3.92 (m, 2H), 3.56 (m, 1H), 0.36 (t, 3H, $^3J_{HP}$ = 6.0 Hz)	197 (b), 185 (b),	-53, -82, -194
$[Ir_2(H)(CO)_2(\eta^2\text{-}CF_2{=}CFH)(\mu\text{-}CH_2)(dppm)_2]^+$ (**3a**) [h]	-4.9 (m, 2P), -5.7 (m, 2P)	5.23(m, 2H), 5.02 (m, 2H), -12.7 (br, 1H)	195 (b), 188 (b)	-94, -97, -220
$[Ir_2(CH_3)(CO)_2(\mu\text{-}CF_2{=}CH_2)(dppm)_2]^+$ (**4**)	16.1 (m, 2P), 5.9 (m, 2P)	4.44 (m, 2H), 3.60 (m, 2H), 2.47 (m, 2H), 0.18 (t, 3H, $^3J_{HP}$ = 4.8 Hz)	197 (b), 186 (b), 44	-46
$[Ir_2(H)(CO)_2(\eta^2\text{-}CF_2{=}CH_2)(\mu\text{-}CH_2)(dppm)_2]^+$ (**4a**) [h]	-2.8, (m, 2P), -4.3 (m, 2P)	5.37(m, 2H), 5.11 (br, 2H), 3.28 (m, 2H), -12.4 (b, 1H), 0.08 (br, 2H)	191 (b)	-80
$[Ir_2(CH_3)(CO)_2(\eta^2\text{-}CF_2{=}CH_2)(dppm)_2]^+$ (**4b**) [h]	16.1 (m, 2P), 6.4 (m, 2P)	3.80 (m, 2H), 3.02 (m, 2H), 2.47 (m, 2H), 1.15 (t, 3H, $^3J_{HP}$ = 8.8 Hz), 0.37 (m, 2H)	211 (m), 202 (m)	-84

[a] NMR abbreviations: s = singlet, d = doublet, t = triplet, m = multiplet, b = broad. [b] NMR data in CD_2Cl_2 unless otherwise stated. [c] In all cases trifluoromethanesulfonate is the accompanying anion. [d] $^{31}P\{^1H\}$ chemical shifts are referenced vs. external 85% H_3PO_4 [e] ^1H and ^{13}C chemical shifts are referenced vs. external TMS. [f] Chemical shifts for the phenyl hydrogens are not given in the ^1H data. [g] ^{19}F chemical shifts referenced vs. $CFCl_3$. F-F and F-H coupling constants are reported in the Results section. [h] indicates low temperature data (see Results section)

Table 2.2. NMR Data for the Fluorovinyl Compounds[a, b]

compounds[c]	$\delta(^{31}P\{^1H\})$[d]	$\delta(^1H)$[e, f]	$\delta(^{13}C\{^1H\})$[e]	$\delta(^{19}F)$[g]
$[Ir_2(CH_3)(OTf)(CO)_2(\mu\text{-}\eta^1\text{:}\eta^2\text{-}CF{=}CF_2)(dppm)_2]^+$ (**5**)[h]	13.0 (t, 2P), -8.0 (t, 2P) ($^2J_{PP}$ = 24.0 Hz)	4.5 (b, 2H), 3.6 (b, 2H), 1.4 (q, 3H, $^3J_{HP}$ = 6.0 Hz)	161 (b), 178 (b), -18.6	-80, -120, -131 -76 (OTf)
$[Ir_2(\eta^1\text{-}CF{=}CF_2)(OTf)(CO)_2(\mu\text{-}H)(\mu\text{-}CH_2)(dppm)_2]^+$ (**6**)	-0.6 (m, 2P), -28.5 (m, 2P), ($^2J_{PP}$ = 26.0 Hz)	6.4 (q, $^3J_{HP}$ = 6.0 Hz, 2H), 5.0 (m, 4H), -12.2 (b, s, 1H)	164 (dt, ($^2J_{CP}$ = 11 Hz, $^4J_{CF}$ = 22 Hz), 166 (m), 38	-92, -121, -123 -76 (OTf)
$[Ir_2(CH_3)(OTf)(CO)_2(\mu\text{-}\eta^1\text{:}\eta^2\text{-}CF{=}CFH)(dppm)_2]^+$ (**7**)	9.0 (m, 1P), -2.5 (m, 2P), -19.0 (m, 1P)	6.1 (m, 1H), 6.0 (dd, 1H, $^2J_{HF}$ = 65 Hz, $^3J_{HF}$ = 10 Hz), 5.6 (m, 1H), 5.5 (m, 1H), 4.7 (m, 1H), 1.2 (t, 3H, $^3J_{HP}$ = 6.0 Hz)	165 (b), 172 (b), -23	-23, -171, -77 (OTf)
$[Ir_2(CH_3)(OTf)(CO)_2(\mu\text{-}\eta^1\text{:}\eta^2\text{-}CF{=}CH_2)(dppm)_2]^+$ (**8**)[h]	1.6 (dt, 2P, $^3J_{PF}$ = 45 Hz), -5.5 (t, 2P), ($^2J_{PP}$ = 18.5 Hz)	6.0 (d, 1H, $^2J_{HH}$ = 6 Hz), 5.4 (dd, 1H, $^2J_{HH}$ = 6 Hz, $^3J_{HF}$ = 14 Hz),), 4.3 (m, 2H), 3.1 (m, 2H), 0.2 (t, 3H, $^3J_{HP}$ = 6.0 Hz)	164 (d), 172 (t, $^2J_{CP}$ = 11 Hz)	-211, -78 (OTf)
$[Ir_2(CH_3)(CO)_2(\eta^1,\eta^1\text{-}C(F)\text{-}CH_2)(dppm)_2]^{+2}$ (**8a**)[h]	12.0 (d, 2P), -12.0 (br, 2P, $^2J_{PP}$ = 23.0 Hz)	5.5 (d, 2H, $^3J_{HF}$ = 13.4 Hz), 4.1 (m, 2H), 2.8 (m, 2H), 0.8 (br, 3H)	192 (b), 164 (b), -4.5	-48
$[Ir_2(CH_3)(\eta^1\text{-}CF{=}CFH)(CO)_2(\mu\text{-}OH)(dppm)_2]^+$ (**9**)	10.2 (b, 2P), -14.6 (t, 2P) ($^2J_{PP}$ = 9.0 Hz)	4.9 (dd, 1H, $^2J_{HF}$ = 80 Hz, $^3J_{HF}$ = 23 Hz), 4.5 (m, 2H), 3.1 (m, 2H), 3.6 (s, b, 1H), 0.6 (t, 3H, $^3J_{HP}$ = 8.0 Hz)	169 (b), 172 (b), -5	-93, -152

[a] NMR abbreviations: s = singlet, d = doublet, t = triplet, m = multiplet, b = broad. [b] NMR data in CD_2Cl_2 unless otherwise stated. [c] In all cases trifluoromethanesulfonate is the accompanying anion. [d] $^{31}P\{^1H\}$ chemical shifts are referenced vs. external 85% H_3PO_4 [e] ^1H and ^{13}C chemical shifts are referenced vs. external TMS. [f] Chemical shifts for the phenyl hydrogens are not given in the ^1H data. [g] ^{19}F chemical shifts referenced vs. $CFCl_3$. F-F and F-H coupling constants are reported in the Results section. [h] indicates low temperature data (see Results section)

2.2.2. Preparation of Compounds

(a) $[Ir_2(CH_3)(CO)_2(\mu\text{-}C_2F_4)(dppm)_2][CF_3SO_3]$ (2). A brick-red solution of $[Ir_2(CH_3)(CO)_2(dppm)_2][CF_3SO_3]$ (**1**) (50 mg, 0.037 mmol), dissolved in 5 mL of dichloromethane, was frozen using a liquid nitrogen bath. 2 mL of tetrafluoroethylene gas was transferred onto the frozen solution via a gas-tight syringe, and the mixture was allowed to warm to RT. After being stirred (closed) for 2 days, slow addition of 20 mL of pentane afforded a harvest gold colored powder. The product was washed twice with 10 mL of pentane, the supernatant decanted, and then the solid was dried briefly under a stream of argon and then *in vacuo* (87% yield). Anal. Calcd for $Ir_2SP_4F_7O_5C_{56}H_{47}$: C, 45.65; H, 3.22. Found C, 45.38; H, 3.02. IR ν_{CO} (Nujol mull cm^{-1}): 2020 vs, 2001, s.

(b) $[Ir_2(CH_3)(CO)_2(\mu\text{-}C_2F_3H)(dppm)_2][CF_3SO_3]$ (3). A brick-red solution of compound **1** (50 mg, 0.037 mmol), dissolved in 0.7 mL of CD_2Cl_2 in an NMR tube, was cooled to -78 °C using a dry ice/acetone bath. 2 mL of trifluoroethylene gas was transferred onto the solution via a gas-tight syringe, and the subsequent reaction was investigated via multinuclear NMR spectroscopy. At -80 °C, the $^{31}P\{^1H\}$ spectrum showed the presence of small amounts of compound **3a** (approximately 10%) along with the resonances for the starting material (**1**). At higher temperatures the resonances attributable to **3a** disappeared with a concomitant appearance of those of complex **3**. Upon holding the sample at -20 °C for 1 ½ h NMR spectroscopy showed quantitative conversion of **1** to compound **3**, which could be further reacted at this stage. This product was only characterized in solution, via NMR spectroscopy, since at higher temperatures (0 °C to room temperature) loss of substrate and subsequent regeneration of starting material occurred.

(c) **$[Ir_2(CH_3)(CO)_2(\mu\text{-}C_2F_2H_2)(dppm)_2][CF_3SO_3]$ (4).** A brick-red solution of compound **1** (50 mg, 0.037 mmol), dissolved in 0.7 mL of d_2-dichloromethane in an NMR tube, was cooled to -78 °C using a dry ice/acetone bath. 2 mL of 1,1-difluoroethylene gas was transferred onto the solution via a gas-tight syringe, and the subsequent reaction was investigated via multinuclear NMR spectroscopy. At -80 °C, the $^{31}P\{^1H\}$ spectrum generally showed three compounds, **1**, **4a**, and **4b**, in a ratio of *ca.* 2:1:2. Upon warming the solution from -80 °C to -30 °C the resonances attributable to **4a** disappeared with a concomitant increase in the relative ratio of complex **4b** to compound **1**. When the reaction was left at -20 °C over night the solution contained a 2:1:1 mixture of starting material (**1**), terminal-olefin complex (**4b**) $[Ir_2(CH_3)(CO)_2(\eta^2\text{-}CH_2{=}CF_2)(dppm)_2][CF_3SO_3]$ and bridging-olefin complex $[Ir_2(CH_3)(CO)_2(\mu\text{-}CH_2{=}CF_2)(dppm)_2][CF_3SO_3]$ (**4**), as determined by NMR spectroscopy. Through repeated temperature cycling from -40 °C to 0 °C we have been able to completely transform the starting material into products, and to increase the ratio of **4:4b** substantially (~5:1). Again, at temperatures above 0 °C olefin loss occurred yielding only starting material, thus these species have been characterized via their NMR spectroscopic profiles.

(d) **$[Ir_2(CH_3)(OTf)(CO)_2(\mu\text{-}\eta1{:}\eta2\text{-}C_2F_3)(dppm)_2][CF_3SO_3]$ (5).** 50 mg of compound **2** (0.034 mmol) was dissolved in 0.7 mL of CD_2Cl_2 and cooled to -20 °C. 30 µL of neat Me_3SiOTf was added, and the mixture left at this temperature for 1 ½ h, at which time NMR spectroscopy established that all of **2** had been converted to compound **5**. At temperatures above 0 °C compound **5** was found to be unstable and transformed into its isomer **6**, so isolated samples of **5** always contained substantial amounts of **6**, often with the latter as the dominant species. Characterization of **6** is described in part (e).

(e) **$[Ir_2(\eta 1\text{-}C_2F_3)(OTf)(CO)_2(\mu\text{-}CH_2)(\mu\text{-}H)(dppm)_2][CF_3SO_3]$ (6). Method a)** 50 mg of compound **2** (0.034 mmol) was dissolved in 7 mL of CH_2Cl_2 and cooled to -20 °C. 30 µL of Me_3SiOTf (0.166 mmol) was added dropwise and the mixture stirred while allowing it to warm to room temperature over a 3 h period. The resulting solution was reduced *in vacuo* to *ca.* 3 mL and 10 mL of pentane was added to precipitate a pale yellow microcrystalline compound **6**. Isolated samples of **6** generated via this method always contained some impurities, thus required recrystallization. **Method b)** 50 mg of compound **2** (0.034 mmol) was slurried into 7 mL of benzene. 30 µL of Me_3SiOTf was added dropwise and the mixture refluxed for 1h under argon. The resulting solution was cooled to induce the precipitation of a pale yellow microcrystalline powder. The clear yellow supernatant was decanted, the product was washed twice with 10 mL of pentane, and then dried briefly under a stream of argon and then *in vacuo*, giving 33 mg of spectroscopically pure compound **6** (68% yield). HRMS *m/z* calcd for $Ir_2P_4O_5C_{56}H_{47}F_6S$ $[M]^+$: 1453.1300. Found: 1453.1301. IR ν_{CO} (Nujol mull cm^{-1}): 2050 vs, 1998, s.

(f) **$[Ir_2(CH_3)(OTf)(CO)_2(\mu\text{-}\eta 1\text{:}\eta 2\text{-}C_2F_2H)(dppm)_2][CF_3SO_3]$ (7).** 10 µL of Me_3SiOTf was added dropwise to a 10 mL dichloromethane solution of compound **3** (50 mg, 0.034 mmol) that had been cooled to 0 °C. This mixture was subsequently stirred at this temperature for ½ h under argon. The resulting yellow-orange solution was warmed to room temperature, reduced *in vacuo* to *ca.* 5 mL, and Et_2O was added to precipitate a pale yellow microcrystalline compound **7**. The product was washed twice with 10 mL of Et_2O, the supernatant decanted, and then the solid was dried briefly under a stream of argon and then *in vacuo* (65% yield). HRMS *m/z* calcd for $Ir_2P_4O_5C_{56}H_{48}F_5S$ $[M]^+$: 1435.1395. Found: 1435.1391. IR ν_{CO} (Nujol mull cm^{-1}): 2053 vs, 2007, s.

(g) **$[Ir_2(CH_3)(OTf)(CO)_2(\mu\text{-}\eta1\text{:}\eta2\text{-}C_2FH_2)(dppm)_2][CF_3SO_3]$ (8).** To a 2:1 mixture of compounds **4** and **4b** in dichloromethane at -40 °C was added 30 μL of Me_3SiOTf dropwise. An immediate reaction with **4** produced a yellow-orange solution mixture of **8** and **4b**. Upon warming to 0 °C, compound **8** underwent rearrangement to give a proposed fluorocarbene complex $[Ir_2(CH_3)(CO)_2(\mu\text{-}\eta^1\text{:}\eta^1\text{-}C(F)\text{-}CH_2)(OTf)(dppm)_2][CF_3SO_3]$ (**8a**), which further transformed at ambient temperature to unidentified products, thus **8** and **8a** have only been characterized via NMR spectroscopy.

(h) **$[Ir_2(\eta1\text{-}C_2F_2H)(CH_3)(CO)_2(\mu\text{-}OH)(dppm)_2][CF_3SO_3]$ (9).** 0.5 mL of 1 molar KOH/H_2O was added dropwise to a THF solution of compound **3** (0.037 mmol) that had been cooled to 0 °C and stirred for 1½ h under argon. The resulting yellow orange solution was warmed to room temperature, stripped to dryness *in vacuo* and the residue extracted with 2 mL of benzene. The resulting solution was filtered through celite, and Et_2O (10 mL) was added to precipitate a bright yellow microcrystalline compound **9**. The product was washed twice with 10 mL of Et_2O, the supernatant decanted, and then the solid was dried briefly under a stream of argon and then *in vacuo* (74% yield). HRMS *m/z* calcd for $Ir_2P_4O_3C_{55}H_{49}F_2$ $[M]^+$: 1305.1858. Found: 1305.1853. Compound **9** could also be obtained through prolonged exposure of **7** to wet organic solvents.

X-ray Crystallographic Data Collection. Pale yellow crystals of **6**•$3CH_2Cl_2$ were obtained via slow diffusion of Et_2O into a CH_2Cl_2 solution of **6**. Crystallographic analysis has shown that **6** had cocrystallized with $[Ir_2(CF_3SO_3)(CO)_3(\mu\text{-}CH_2)(dppm)_2][CF_3SO_3]$ in 60:40 ratio. This latter compound has apparently resulted from loss of trifluoroethylene from the title species during crystallization, accompanied by scavenging of carbon monoxide from additional decomposition product(s) (*vide infra*).

Crystallographic data have been deposited with the Cambridge Crystallographic Data Centre under deposition number CCDC 620865, and may be retrieved free of charge via the World Wide Web at http://www.ccdc.cam.ac.uk/products/csd/request/.

Crystals of compound **2** were obtained via slow diffusion of diethylether into a saturated dichloromethane solution of the complex. In spite of starting with a pure sample of **2**, the crystals obtained were found to be composed of a disordered mixture of **2** and its carbonyl adduct $[Ir_2(CH_3)(CO)_3(\mu\text{-}CF_2{=}CF_2)(dppm)_2][CF_3SO_3]$ in an approximate 60:40 ratio (*vide infra*). Only a preliminary structure solution was attained on these species, owing to this disorder, thus no crystallographic experimental details are presented.

This and all other structure determinations in this thesis were determined by Dr. Robert (Bob) MacDonald and/or Dr. Mike Ferguson of the Departmental X-ray crystallography facility.

Table 2.3. Crystallographic Experimental Details for Disordered Crystal of $[Ir_2(\eta^1\text{-}CF{=}CF_2)(OTf)(CO)_2(\mu\text{-}CH_2)(\mu\text{-}H)(dppm)_2][CF_3SO_3]$ (**6**)

A. Crystal Data	
formula	$C_{59.6}H_{52.6}Cl_6F_{7.8}Ir_2O_{8.4}P_4S_2$
formula weight	1836.52
crystal dimensions (mm)	0.34 × 0.22 × 0.10
crystal system	orthorhombic
space group	$Pca2_1$ (No. 29)
unit cell parameters[a]	
a (Å)	24.274 (2)
b (Å)	11.933 (1)
c (Å)	23.325 (2)
V (Å^3)	6756 (1)
Z	4
ρ_{calcd} (g cm^{-3})	1.806
μ (mm^{-1})	4.403
B. Data Collection and Refinement Conditions	
diffractometer	Bruker PLATFORM/SMART 1000 CCD[b]
radiation (λ [Å])	graphite-monochromated Mo Kα (0.71073)
temperature (°C)	–80
scan type	ω scans (0.2°) (20 s exposures)
data collection 2θ limit (deg)	52.80
total data collected	47527 (-30 ≤ h ≤ 29, -14 ≤ k ≤ 14, -29 ≤ l ≤ 29)
independent reflections	13819 (R_{int} = 0.0513)
number of observed reflections (*NO*)	12270 [$F_o^2 \geq 2\sigma(F_o^2)$]
structure solution method	direct methods (*SHELXS–86*[c])
refinement method	full-matrix least-squares on F^2 (*SHELXL–93*[d,e])
absorption correction method	multi-scan (*SADABS*)
range of transmission factors	0.6672–0.3160
data/restraints/parameters	13819 [$F_o^2 \geq -3\sigma(F_o^2)$] / 22[f] / 478
Flack absolute structure parameter[g]	0.014 (6)
goodness-of-fit (S)[h]	1.006 [$F_o^2 \geq -3\sigma(F_o^2)$]
final R indices[i]	
R_1 [$F_o^2 \geq 2\sigma(F_o^2)$]	0.0348
wR_2 [$F_o^2 \geq -3\sigma(F_o^2)$]	0.0848
largest difference peak and hole	1.218 and –1.131 e Å^{-3}

[a]Obtained from least-squares refinement of 7350 reflections with 4.84° < 2θ < 52.58°.

[b]Programs for diffractometer operation, data collection, data reduction and absorption correction were those supplied by Bruker.

Table 2.3. Crystallographic Experimental Details (continued)

[c]Sheldrick, G. M. *Acta Crystallogr.* **1990**, *A46*, 467–473.

[d]Sheldrick, G. M. *SHELXL-93*. Program for crystal structure determination. University of Göttingen, Germany, 1993.

[e]Attempts to refine peaks of residual electron density as solvent dichloromethane carbon or chlorine atoms were unsuccessful. The data were corrected for disordered electron density through use of the SQUEEZE procedure (Sluis, P. van der; Spek, A. L. *Acta Crystallogr.* **1990**, *A46*, 194–201) as implemented in PLATON (Spek, A.L. *Acta Crystallogr.* **1990**, *A46*, C34. PLATON - a multipurpose crystallographic tool. Utrecht University, Utrecht, The Netherlands). A total solvent-accessible void volume of 1312.1 A^3 with a total electron count of 506 (consistent with twelve molecules of solvent dichloromethane, or three molecules per formula unit of the complex molecule) was found in the unit cell.

[f]Geometric restraints were applied as follows:

(i) The hydrido ligand H(1A) of the major (60%) conformer was not located, but its presence was established via spectroscopic methods. The Ir(1)–H(1A) and Ir(2)–H(1A) distances were fixed at 1.85 Å, and the Ir(1), Ir(2), C(3), and H(1A) atoms were constrained to be coplanar (i.e. by limiting to no more than 0.01 $Å^3$ the volume of the tetrahedron formed by these four atoms).

(ii) The F–C distances of the trifluorovinyl group of the major (60%) conformer were contrained to be equal but were allowed to refine. Distances involving the carbonyl group (C(4a)–O(4a)) of the minor (40%) conformer were fixed (d(Ir(1)–C(4a)) = 1.88 Å; d(C(4a)–O(4a)) = 1.13 Å; d(Ir(1)···O(4a)) = 3.01 Å).

(iii) The triflate ion was disordered in an 80:20 distribution of positions. Distances within the minor conformer were fixed: d(S(2B)–C(91B)) = 1.80 Å; d(S(2B)–O(91B)) = d(S(2B)–O(92B)) = d(S(2B)–O(93B)) = 1.45 Å; d(F(91B)–C(91B)) = d(F(92B)–C(91B)) = d(F(93B)–C(91B)) = 1.35 Å; d(F(91B)···F(92B)) = d(F(91B)···F(93B)) = d(F(92B)···F(93B)) = 2.20 Å; d(O(91B)···O(92B)) = d(O(91B)···O(93B)) = d(O(92B)···O(93B)) = 2.37 Å.

[g]Flack, H. D. *Acta Crystallogr.* **1983**, *A39*, 876–881; Flack, H. D.; Bernardinelli, G. *Acta Crystallogr.* **1999**, *A55*, 908–915; Flack, H. D.; Bernardinelli, G. *J. Appl. Cryst.* **2000**, *33*, 1143–1148. The Flack parameter will refine to a value near zero if the structure is in the correct configuration and will refine to a value near one for the inverted configuration.

[h]$S = [\Sigma w(F_o^2 - F_c^2)^2/(n-p)]^{1/2}$ (n = number of data; p = number of parameters varied; $w = [\sigma^2(F_o^2) + (0.0442P)^2]^{-1}$ where $P = [\mathrm{Max}(F_o^2, 0) + 2F_c^2]/3$).

[i]$R_1 = \Sigma||F_o| - |F_c||/\Sigma|F_o|$; $wR_2 = [\Sigma w(F_o^2 - F_c^2)^2/\Sigma w(F_o^4)]^{1/2}$.

2.3. Results and Compound Characterization

2.3.1. Fluoroolefin-Bridged Complexes

It has been previously established[8] that two distinct olefin binding modes are observed in the reactions of fluoro-substituted ethylenes with compound **1**, $[Ir_2(CH_3)(CO)_2(dppm)_2][CF_3SO_3]$. For fluoroolefins containing at least one pair of geminal fluorines, (i. e. tetrafluoroethylene, trifluoroethylene, and 1,1-difluoroethylene) relatively stable olefin-bridged complexes can be obtained (Scheme 2.4).

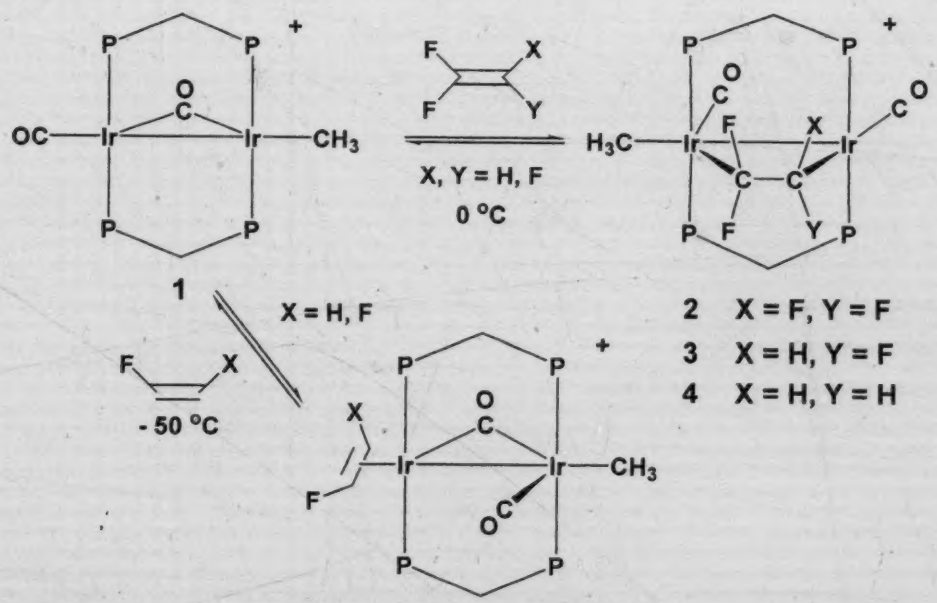

Scheme 2.4. *Coordination of fluoroolefins in terminal and bridging modes*

In both monofluoroethylene and cis-difluoroethylene, only the η^2-olefin binding mode, in which the olefin is bound to a single metal, was observed. Owing to the extreme lability of this latter group of olefin adducts, being observed only at temperatures of -50 °C or below, their reactivity has not been investigated. Furthermore, this class of compounds differs very little from the well known mononuclear analogues. Our interest in this study was to determine if the

bridging-olefin binding mode could give rise to unusual reactivity; for these reasons only the tetrafluoro-, trifluoro-, and 1,1-difluoroethylene products were investigated further.

As will become clear, in what follows, the three fluoroolefins investigated were sufficient to establish a role for binding olefin coordination in C-F activation that is not observed under comparable conditions for olefins bound to a single metal.

2.3.1.1. $[Ir_2(CH_3)(CO)_2(\mu\text{-}C_2F_4)(dppm)_2][CF_3SO_3]$ (2)

Tetrafluoroethylene forms the most stable bridged-adduct, namely, $[Ir_2(CH_3)(CO)_2(\mu\text{-}CF_2{=}CF_2)(dppm)_2][CF_3SO_3]$ (**2**), after prolonged exposure of compound **1** to the fluoroolefin gas in solution, over a period of two to three days. No evidence for any species containing a terminally bound η^2-tetrafluoroethylene unit was observed at any temperature between -80 °C and ambient. This product, as diagrammed in Scheme 2.4 (X=Y=F), is isolable at room temperature and the $^{31}P\{^1H\}$ NMR spectrum shows two resonances at 17.0 ppm and 5.0 ppm, having patterns typical of an AA'BB' spin system, consistent with two chemically inequivalent phosphorus environments. In the ^1H NMR spectrum the dppm methylene protons appear as a single broad multiplet at 3.89 ppm, integrating for four protons. Although the structure diagrammed for **2** should give rise to two different chemical environments for the methylene protons, and would therefore be expected to give rise to two resonances, we assume that the single resonance observed results from coincidental overlap of the two independent methylene signals; such observations are not unusual. The iridium-bound methyl group appears as a triplet at 0.41 ppm ($^3J_{HP}$ = 6.0 Hz), the protons of which couple equally to the pair of adjacent phosphorus nuclei at 5.0 ppm, suggesting that this methyl group and these phosphorus nuclei are bound to the same metal. A ^{13}C NMR spectrum of a $^{13}CH_3$-enriched sample of **2** is consistent with this assertion, with the associated methyl resonance at -7.4 ppm showing selective

^{31}P-decoupling upon irradiation of the high-field phosphorus resonance. Two inequivalent broad multiplet carbonyl resonances are also apparent in a ^{13}CO-enriched sample of **2**, appearing at 182 ppm and 192 ppm, with the former showing coupling to the same end of the diphosphine framework as the methyl group, and is therefore likely on the same metal, while the latter carbonyl shows coupling to the other set of ^{31}P nuclei. Although both carbonyls appear to be terminally bound to their respective metals, the slight downfield shift of these moieties, particularly of the latter, may be the result of a weak interaction with the adjacent metal, as has previously been observed.[15] More typically, higher field chemical shifts for exclusively terminal carbonyls will be shown in subsequent examples wherein the carbonyl is remote from the adjacent metal. As expected, the ^{19}F NMR spectrum shows two resonances, one for each end of the fluoroolefin ligand, at -80 ppm and -86 ppm, which appear as broad multiplets. Upon selective ^{31}P decoupling each resonance is shown to be coupled to different sets of phosphorus nuclei, which is consistent with the bridging arrangement of the fluoroolefin moiety as shown.

Crystals of compound **2** were obtained via slow diffusion of diethylether into a saturated dichloromethane solution of the complex, The crystals obtained were found to be composed of a disordered mixture of **2** and its carbonyl adduct $[Ir_2(CH_3)(CO)_3(\mu\text{-}CF_2{=}CF_2)(dppm)_2][CF_3SO_3]$ in an approximate 60:40 ratio (see Figure 2.2). The additional carbonyl in the tricarbonyl species has presumably resulted from the scavenging of CO by **2** from decomposition products. Stirring solutions of compound **2** for extended periods (*ca.* days) also resulted in the generation of this previously characterized species.[16] Although the disorder, in which the two species are superimposed, tends to mask the details of the structure, the gross structural arrangement is obvious; the symmetric, bridging assignment of the C_2F_4 group is clear, as is the rehybridization at the fluoroolefinic carbons towards that of their sp^3 limit. The resulting C-C bond length (1.563(7) Å; see Table 2.4) corresponds to a single C-C bond in an

alkane,[17] and the angles at these carbons (ranging from 101° to 116°; see Table 2.5) are indicative of sp^3 hybridization.

Although the parameters in this structure have to be viewed with some caution, owing to the disorder, it is encouraging that they agree very well with those obtained for a well behaved, ordered structure of the tricarbonyl analogue of **2**, $[Ir_2(CH_3)(CO)_3(\mu\text{-}CF_2{=}CF_2)(dppm)_2]^+$.[8] The fluoroolefin substrate is found to be symmetrically-bridged across the two iridium centers thereby creating a dimetallacyclobutane-like moiety in which each end of the organic portion resembles that of a perfluoroalkyl group (Figure 2.3). Interestingly, such an arrangement also leaves a conspicuously vacant coordination site in this complex, allowing terminal coordination of the third carbonyl ligand, as illustrated in the previous figure. Other related studies have also shown that this is the site occupied by the incoming phosphine ligand in the related PMe_3 adduct, $[Ir_2(CH_3)(CO)_2(PMe_3)(\mu\text{-}CF_2{=}CF_2)(dppm)_2]^+$.[16]

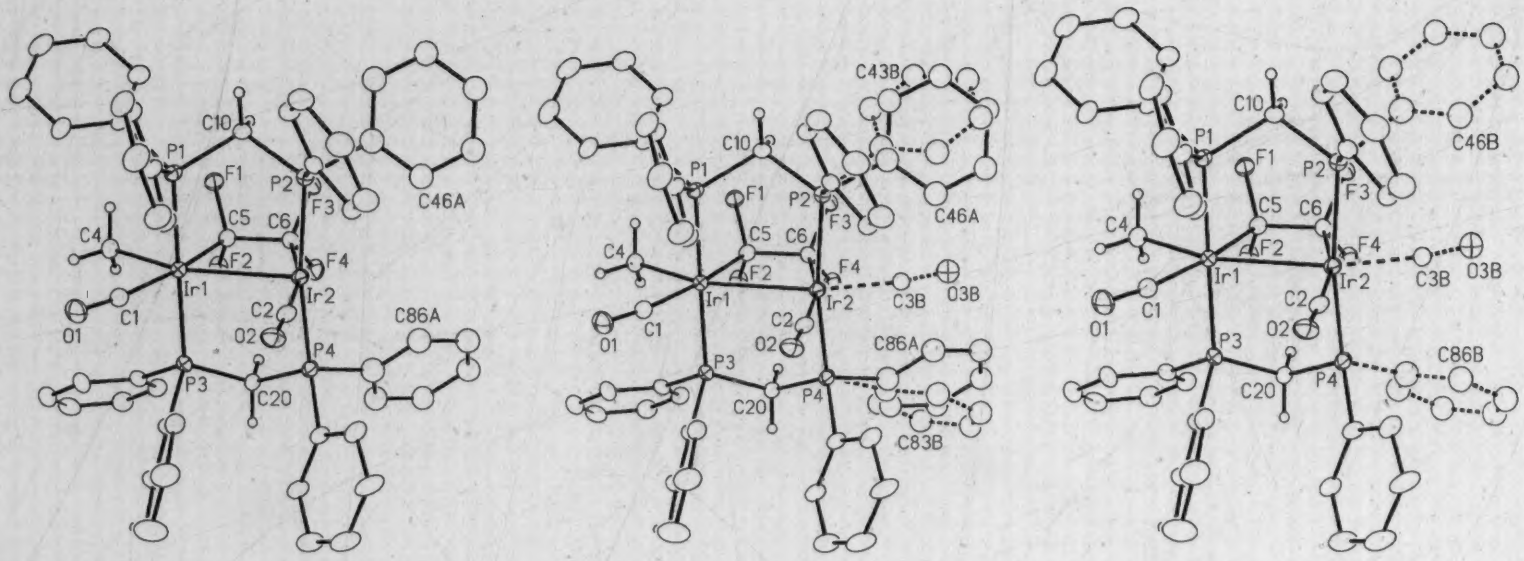

Figure 2.2. *View of the two disordered complex cations (left and right) resolved from the disordered structure of* **2**. *Solid bonds represent those present in the dicarbonyl cation of* **2** *and its carbonyl adduct, and in common with the tricarbonyl complex, while the dashed bonds are unique to the cation of the tricarbonyl complex. A superimposed image of both superimposed cations, as obtained from the electron density maps, is illustrated in the middle.*

Table 2.4. Selected Interatomic Distances (Å) for $[Ir_2(CH_3)(CO)_2(\mu\text{-}C_2F_4)(dppm)_2]^+$ (**2**)

Atom1	Atom2	Distance	Atom1	Atom2	Distance
Ir1	Ir2	2.8938(3)	P3	P4	3.0175(2)†
Ir1	P1	2.3552(1)	F1	C5	1.414(5)
Ir1	P3	2.3555(1)	F2	C5	1.403(6)
Ir1	C1	1.923(6)	F3	C6	1.392(6)
Ir1	C4	2.139(5)	F4	C6	1.396(6)
Ir1	C5	2.078(5)	O1	C1	1.115(6)
Ir2	P2	2.3528(1)	O2	C2	1.138(7)
Ir2	P4	2.3527(1)	C5	C6	1.563(7)
Ir2	C2	1.916(6)	P1	P2	3.0262(2)†
Ir2	C6	2.100(5)			

† Nonbonded distance

Table 2.5. Selected Interatomic Angles (deg) for $[Ir_2(CH_3)(CO)_2(\mu\text{-}C_2F_4)(dppm)_2]^+$ (**2**)

Atom1	Atom2	Atom3	Angle	Atom1	Atom2	Atom3	Angle
Ir2	Ir1	P1	89.45(3)	P2	Ir2	C2	92.6(2)
Ir2	Ir1	P3	89.20(3)	P2	Ir2	C6	88.4(2)
Ir2	Ir1	C1	118.88(1)	P4	Ir2	C2	92.5(2)
Ir2	Ir1	C4	154.97(1)	P4	Ir2	C6	88.7(2)
Ir2	Ir1	C5	70.8(1)	C2	Ir2	C6	164.8(2)
P1	Ir1	P3	176.39(5)	Ir1	C1	O1	167.5(5)
P1	Ir1	C1	88.7(2)	Ir2	C2	O2	175.0(5)
P1	Ir1	C4	90.9(2)	Ir1	C5	F1	113.4(3)
P1	Ir1	C5	91.6(2)	Ir1	C5	F2	113.8(3)
P3	Ir1	C1	89.1(2)	Ir1	C5	C6	110.4(3)
P3	Ir1	C4	91.8(2)	F1	C5	F2	101.5(4)
P3	Ir1	C5	91.1(2)	F1	C5	C6	108.2(4)
C1	Ir1	C4	86.1(2)	F2	C5	C6	109.1(4)
C1	Ir1	C5	170.3(2)	Ir2	C6	F3	116.3(3)
C4	Ir1	C5	84.2(2)	Ir2	C6	F4	116.0(3)
Ir1	Ir2	P2	93.66(3)	Ir2	C6	C5	106.7(3)
Ir1	Ir2	P4	93.67(3)	F3	C6	F4	101.5(4)
Ir1	Ir2	C2	92.7(2)	F3	C6	C5	108.0(4)
Ir1	Ir2	C6	72.0(1)	F4	C6	C5	107.9(4)
P2	Ir2	P4	170.84(5)				

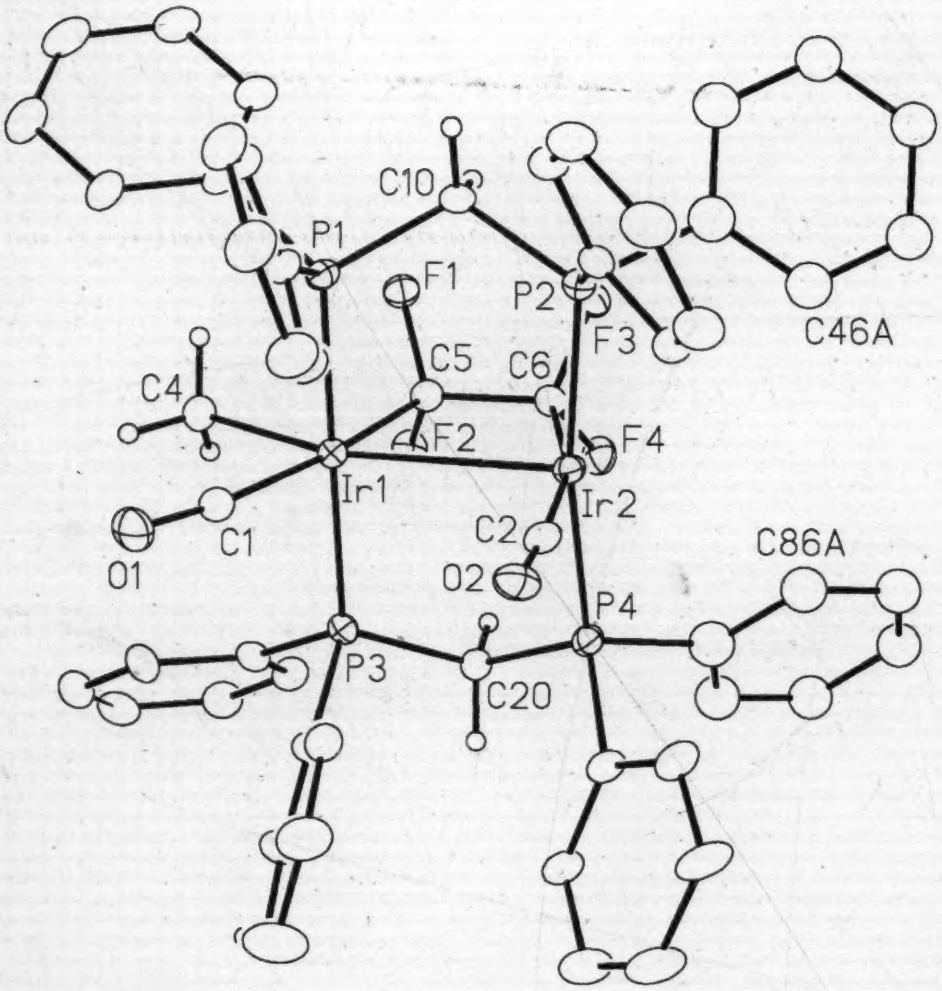

Figure 2.3. *Perspective view of the* $[Ir_2(CH_3)(CO)_2(\mu\text{–}C_2F_4)(dppm)_2]^+$ **(2)** *complex ion showing the atom labelling scheme. Non-hydrogen atoms are represented by Gaussian ellipsoids at the 20% probability level. The phenyl hydrogens have been omitted for clarity, while those on the methylene and methyl groups are shown artificially small.*

2.3.1.2. $[Ir_2(CH_3)(CO)_2(\mu\text{-}C_2F_3H)(dppm)_2][CF_3SO_3]$ (3)

Trifluoroethylene reacts with compound **1** at -80 °C, initially forming the adduct $[Ir_2(H)(\eta^2\text{-}CF_2{=}CFH)(CO)_2(\mu\text{-}CH_2)(dppm)_2][CF_3SO_3]$ (**3a**), in which the olefin is bound in an η^2-fashion to one metal, accompanied by C-H activation of the methyl group at the other metal, yielding bridging methylene and hydride fragments, as shown in Scheme 2.5.

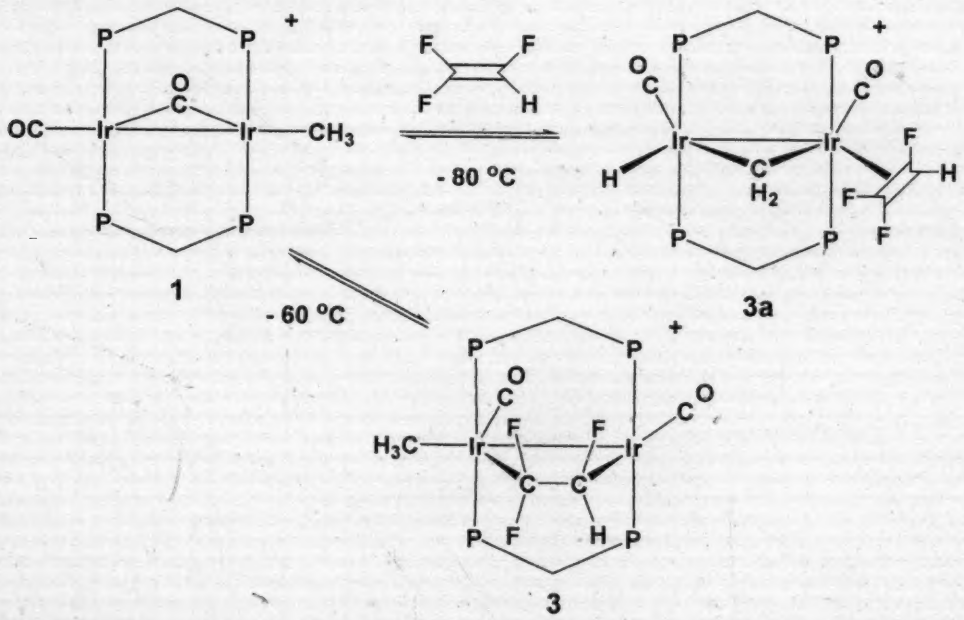

Scheme 2.5. *Reactions of **1** with trifluoroethylene to give complexes **3a** and **3***

Compound **3a** shows a $^{31}P\{^1H\}$ NMR spectrum, consistent with an AA'BB' spin system, with broad multiplet resonances at -4.9 ppm and -5.7 ppm. The ^1H NMR spectrum of this product displays the dppm methylene protons as typical multiplets at 5.23 ppm and 5.02 ppm, while the resonances for the metal-bridged methylene moiety and olefinic proton were unidentified. The hydride signal appears at -12.7 ppm as a broad resonance, with no resolvable decoupling upon broad band ^{31}P irradiation. The $^{13}C\{^1H\}$ NMR spectrum of a ^{13}CO-enriched sample of **3a** shows two broad carbonyl resonances, the first at 188 ppm, and

the second at 195 ppm, with both chemical shifts suggesting terminal arrangements. Again the chemical shifts for these carbonyls are consistent with the structure shown, in which both carbonyls are terminally bound in the vicinity between the respective adjacent metals. In a $^{13}CH_3$-enriched sample, the ^{13}C signal for the bridging methylene group appears at 44 ppm, a typical shift of these groups when in a bridging arrangement between the metals. The ^{19}F NMR spectrum shows three distinct signals; two mutually coupled doublets appearing at -94 ppm and -97 ppm, each displaying mutual $^2J_{FF}$ geminal coupling of 157 Hz, and the final fluorine resonance appearing upfield as a multiplet at -220 ppm. The proposed structure of **3a**, in which no rotation of the olefin is proposed, is based on the initial compounds produced in the analogous reactions of ethylene[8] and 1,1-difluoroethylene (*vide infra*) with compound **1** at -80 °C. Such products of methyl C-H activation, upon ligand addition to **1**, are well documented and have been previously established crystallographically in a PMe_3 adduct of **1**, $[Ir_2(H)(PMe_3)(CO)_2(\mu\text{-}CH_2)(dppm)_2][CF_3SO_3]$,[18] in which ligand attack at one metal results in C-H activation of the methyl ligand by the adjacent metal.

Warming of the sample to -60 °C or above, effects the irreversible conversion of complex **3a** to the compound $[Ir_2(CH_3)(CO)_2(\mu\text{-}CHF{=}CF_2)(dppm)_2][CF_3SO_3]$ (**3**), which was also observed in variable amounts at -80 °C.

Notably, no η^2-bound isomer, with the methyl group intact, was observed, as was the case with ethylene and 1,1-difluoroethylene (*vide infra*). The trifluoroethylene-bridged species (**3**) is significantly less stable than that of tetrafluoroethylene, yielding an unsymmetrically-bridged complex that persists only for a limited amount of time in ice-cooled solutions. At higher (ambient) temperatures compound **3** either loses the fluoroolefin substrate to regenerate starting material (**1**) and the free olefin, or reacts with adventitious water in the cooled solution to yield a C-F activated product (*vide infra*).

Held at 0 °C, the complex has been characterized using multinuclear NMR spectroscopy. The $^{31}P\{^1H\}$ NMR resonances of compound **3** appear as a pair of

multiplets at 14.9 ppm and 5.1 ppm, at very similar chemical shifts to that of the tetrafluoroethylene complex (**2**). Each multiplet is comprised of two closely spaced resonances, consistent with four inequivalent phosphorus nuclei. The ^{1}H NMR spectrum confirms the unsymmetrical nature of the substrate, with the resonances of the dppm protons appearing as independent broad multiplets at 3.97 ppm (1H), 3.92 ppm (2H), and 3.56 ppm (1H), with coincidental overlap of the middle two resonances. The iridium-bound methyl group appears as a triplet, integrating for three protons, at 0.36 ppm ($^{3}J_{HP}$ = 6.0 Hz), coupling equally to one pair of adjacent phosphorus nuclei. Selective phosphorus decoupling experiments have shown this moiety to be coupled to the ^{31}P nuclei giving rise to the resonances around 5.1 ppm in the ^{31}P NMR spectrum. The unique olefinic hydrogen appears as a weak, broad doublet of doublets of doublets at 5.9 ppm, at -60 °C in the ^{1}H NMR spectrum, showing distinct coupling to all three associated fluorines. In the original report of this compound, this resonance was not observed.[8] The ^{13}C NMR spectrum of a ^{13}CO-enriched sample of **3** shows two inequivalent terminal carbonyl resonances as broad multiplets at 185 ppm and 197 ppm, which are very similar to the terminal carbonyls of the tetrafluoroethylene-bridged product (**2**). The ^{19}F NMR spectrum shows three broad signals, at -53 ppm, -82 ppm and -194 ppm, all of which are shifted to low field from the free ligand, the corresponding resonances of which appear at -100 ppm, -126 ppm and -205 ppm, respectively. This shift to lower-field, with the geminal pair having moved the farthest, is consistent with rehybridization of the associated carbons toward sp^3, and suggestive of the addition of this group across the pair of metals. A similar, yet not nearly so pronounced, effect is also observed in the η^2-adduct (**3a**), however rehybridization is more clearly effected in the bridging complex (**3**), with a mutual coupling value of 253 Hz between the two lower-field resonances indicative of an sp^3 hybridized $-CF_2$ group.[18] Further supporting this arrangement, the $^{3}J_{FF}$ trans is significantly decreased, to 25 Hz, relative to that of the free the ligand, 115 Hz. Selective $^{19}F\{^{31}P\}$ decoupling NMR experiments have also shown the high-field resonance at -194 ppm is coupled to the resonance at 14.9 ppm in the ^{31}P NMR spectrum. This suggests that the

other, more-fluorinated end of the fluoroolefin, is bound to the metal associated with the methyl group.

2.3.1.3. $[Ir_2(CH_3)(CO)_2(\mu\text{-}C_2F_2H_2)(dppm)_2][CF_3SO_3]$ (4)

When a large excess of 1,1-difluoroethylene is passed through a solution of **1** (initially at at -78 °C), three different thermally unstable products are formed, as shown in Scheme 2.6, beginning with the C-H activated adduct $[Ir_2(H)(CO)_2(\eta^2\text{-}CF_2{=}CH_2)(\mu\text{-}CH_2)(dppm)_2][CF_3SO_3]$ (**4a**) observed between -80 °C and -60 °C. This product, in which the iridium-bound methyl of the starting complex **1** has undergone intramolecular C-H activation to form a hydride and a methylene ligand bridging the two metals, is analogous to that of the initial trifluoroethylene compound **3a**.

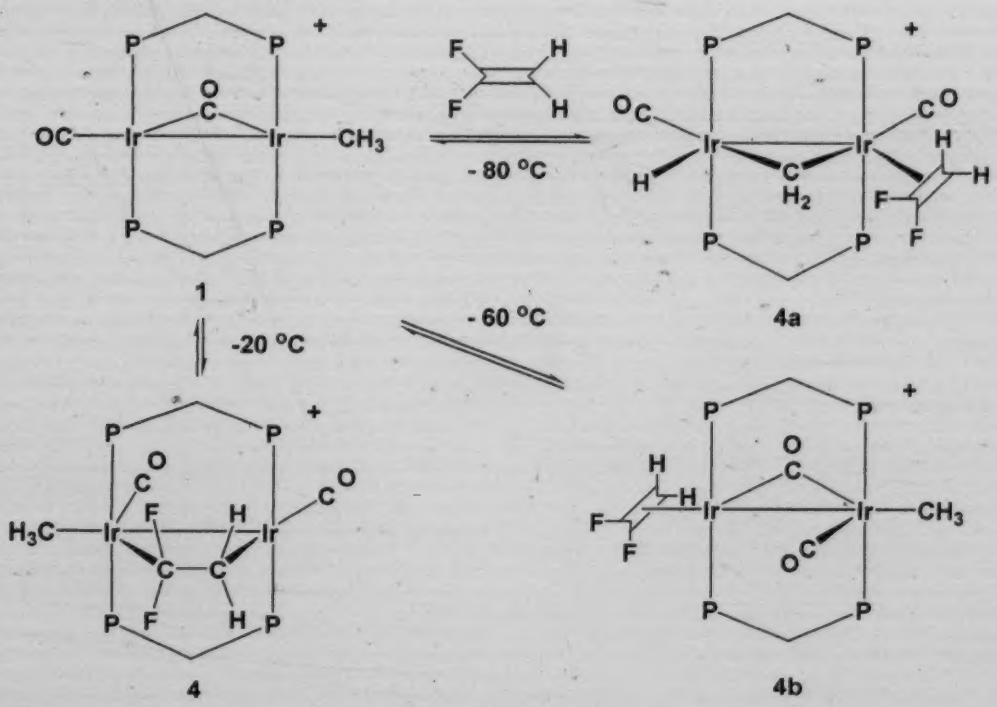

Scheme 2.6. *Reaction profile for the addition of 1,1-difluoroethylene to* ***1***

Compound **4a** is characterized in the $^{31}P\{^1H\}$ NMR spectrum by equal intensity broad multiplet resonances at -2.8 ppm and -4.3 ppm, again similar to those of the analogous η^2-bound ethylene and trifluoroethylene compounds. The proton NMR spectrum displays the typical dppm methylene resonances at 5.11 ppm and 3.28 ppm, along with a broad hydride signal at -12.4 ppm. A broad resonance at 5.37 ppm, integrating for two protons, is attributable to the bridging methylene group, while that of the coordinated 1,1-difluoroethylene appears as a broad resonance at 0.08 ppm, displaying the upfield chemical shift expected of a coordinated olefin.[19] In the ^{13}C NMR spectrum only a single very broad carbonyl resonance at 191 ppm could be attributed to **4a**, whereas a pair of signals would normally be expected, unless the carbonyl carbon resonances were coincidentally isochronous. The ^{19}F NMR spectrum shows a single broad peak at -80.4 ppm, shifted only slightly downfield from the free olefin at -82.2 ppm.

Warming the solution above -60 °C causes the signals of compound **4a** to disappear, being replaced by those of a new compound $[Ir_2(CH_3)(CO)_2(\eta^2\text{-}CH_2{=}CF_2)(dppm)_2][CF_3SO_3]$ (**4b**), the $^{31}P\{^1H\}$ NMR resonances of which appear as a pair of multiplets at 16.1 ppm and 6.4 ppm, consistent with an AA'BB' spin system. The ^1H NMR spectrum shows the reformed iridium-bound methyl group as a triplet at 1.15 ppm ($^3J_{HP}$ = 8.8 Hz), the protons of which couple equally to the adjacent pair of phosphorus nuclei at 6.4 ppm. The dppm methylene protons appear as two independent broad multiplets at 3.80 ppm and 3.02 ppm, integrating for two protons each, while the methylene signal of the coordinated difluoroethylene ligand shows resolved coupling, appearing as a virtual quintet at 0.37 ppm, which upon broadband ^{31}P-decoupling collapses to an apparent triplet ($^3J_{HF}$ = 9.2 Hz). The pair of olefinic fluorines appear as one broad resonance in the ^{19}F NMR spectrum at -83.7 ppm, shifted slightly upfield, in this case, from the free olefin at -82.2 ppm. In the ^{13}C NMR spectrum of a ^{13}CO-enriched sample of **4b**, two broad multiplet carbonyl resonances are apparent at 211 ppm and 202 ppm, strongly suggesting some type of bridging or semi-bridging arrangement in these moieties. However, another explanation is plausible, in which exchange

between terminal and bridged carbonyls is rapid on the NMR timescale so that the signals observed have chemical shifts that represent the average of those of the terminal and bridging groups. In spite of this exchange, two signals are still observed because the average environment of each is different, which suggests that the olefin is not undergoing rapid rotation at the metal. Such an exchange was previously proposed for the related ethylene adduct $[Ir_2(CH_3)(\eta^2\text{-}C_2H_4)(\mu\text{-}CO)_2(dppm)_2][CF_3SO_3]$,[20] for which the chemical shift of the single averaged carbonyl resonance is quite similar (204 ppm). In this case, the ethylene adduct was observable at higher temperature, at which IR spectra could be obtained; this spectrum showed distinct bands corresponding to a terminal and a bridging carbonyl. In the present case, we were unable to obtain an IR spectrum at low temperature, nonetheless, a fluxional process, in which there is exchange between the terminal and bridging carbonyls, is proposed. Although not observed for trifluoro- and tetrafluoroethylene adducts, this type of binding has also been observed in all of the other fluoroethylenes we have investigated.

Above -20 °C there is slow conversion (*ca.* 50% in 18 h at -20 °C) to a third species $[Ir_2(CH_3)(CO)_2(\mu\text{-}CH_2{=}CF_2)(dppm)_2][CF_3SO_3]$ (**4**) which transforms back to starting material and free olefin at temperatures above 0 °C. The $^{31}P\{^1H\}$ NMR resonances of compound **4** appear as a pair of multiplets at 16.1 ppm and 5.9 ppm, at very similar chemical shifts to those of the terminal isomer, observed at 16.4 ppm and 6.4 ppm. In the ^1H NMR spectrum, the dppm methylene protons appear as broad multiplets at 4.44 ppm and 3.60 ppm, integrating for two protons each, while the iridium-bound methyl group appears as a triplet, integrating for three protons, at 0.18 ppm ($^3J_{HP}$ = 4.8 Hz), coupling equally to the pair of phosphorus nuclei at 5.9 ppm. The olefinic protons appear as a multiplet at 2.47 ppm, and show some decoupling upon selective ^{31}P irradiation of the corresponding phosphorus nuclei at 16.1 ppm. A ^{13}CO-enriched sample of **4** shows two inequivalent terminal carbonyl resonances in the ^{13}C NMR spectrum, displayed as multiplets at 197 ppm and 186 ppm, similar to those of the other fluoroolefin-bridged compounds, **2** and **3**. In the ^{19}F NMR spectrum the

difluoromethylene group of **4**, appears as a multiplet at -46 ppm, and also displays ^{31}P coupling, collapsing to a triplet upon selective irradiation of the ^{31}P resonance at 5.9 ppm. This directly suggests that the methyl group and fluorinated end of the olefin share the same metal, shown in the orientation displayed in Scheme 2.6, and is the opposite orientation originally suggested for this compound,[9] before the ^{31}P decoupling information was available.

Through repeated temperature cycling from -40 °C to 0 °C we have been able to increase the ratio of **4:4b** to as high as 5:1, however we have not succeeded in obtaining a pure sample of **4** on its own, without contamination by **4b**. The lack of any resolvable exchange between the two isomers, in the associated spin saturation transfer NMR experiment suggests that either the exchange process occurs outside of the timescale resolvable by NMR spectroscopy, or that the isomers are not interconverting directly (See Scheme 2.6).

2.3.2. Reaction of Me_3SiOTf with Fluoroolefin-Bridged Complexes

In keeping with our proposed analogy of bridging fluoroolefins and fluoroalkyl groups, we sought to explore the activation of the C-F bonds in the fluoroolefin-bridged complexes, via the addition of the Lewis acid trimethylsilyl triflate ($Me_3Si(CF_3SO_3)$). Furthermore, the availability of the bridged and terminal isomers (**4** and **4b**) under identical conditions, should allow a comparison of the reactivity of the two coordination modes.

2.3.2.1. $[Ir_2(CH_3)(OTf)(CO)_2(\mu\text{-}\eta1\text{:}\eta2\text{-}C_2F_3)(dppm)_2][CF_3SO_3]$ (5)

Reaction of $[Ir_2(CH_3)(CO)_2(\mu\text{-}C_2F_4)(dppm)_2][CF_3SO_3]$ (**2**) with $Me_3Si(CF_3SO_3)$ at -20 °C results in an immediate reaction as demonstrated by the appearance of a new set of resonances in the $^{31}P\{^1H\}$ NMR spectrum corresponding to the trifluorovinyl compound $[Ir_2(CH_3)(OTf)(CO)_2(\mu\text{-}\eta^1\text{:}\eta^2\text{-}CF{=}CF_2)(dppm)_2][CF_3SO_3]$ (**5**) (see Scheme 2.7).

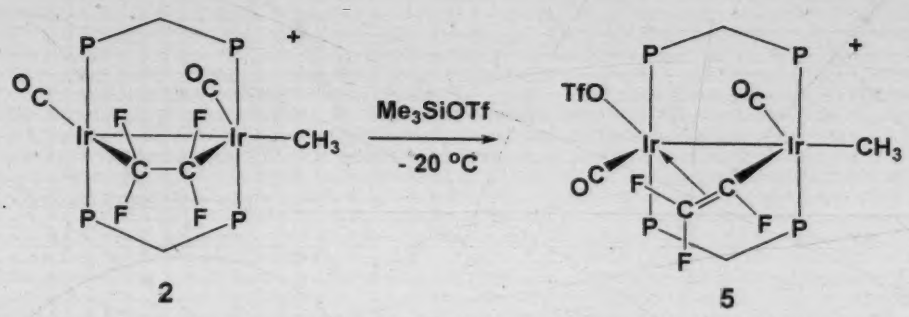

2 5

Scheme 2.7. *C-F activation of bridging tetrafluoroethylene via addition of $Me_3Si(OTf)$*

The instability of this species at temperatures above 0 °C has limited our characterization of this product to NMR methods in solution. In the $^{31}P\{^1H\}$ NMR spectrum a pair of pseudo-triplets appear at 13.0 ppm and -8.0 ppm, corresponding to compound **5**. Whereas an ABCD type spin system is predicted for the arrangement illustrated in Scheme 2.7, the presence of only two resonances, suggests that there is coincidental overlap of pairs of the signals corresponding to the four inequivalent phosphorus nuclei. The mutual coupling of 24 Hz between these resonances is typical of diphosphines which are arranged in a trans orientation at each metal. The ^1H NMR spectrum shows the dppm methylene protons as a pair of doublets of multiplets, integrating for two protons each, at 4.5 ppm and 3.6 ppm and displaying the characteristic 14 Hz coupling to phosphorus. The iridium-bound methyl group appears as a pseudo-quartet (over-lapping doublet of triplets) at 1.4 ppm ($^3J_{HP}$ = 6.0 Hz, $^5J_{HF}$ = 6.0 Hz). Selective ^{31}P decoupling experiments indicate that these protons are coupled approximately equally to one pair of phosphorus nuclei at -8.0 ppm, presumably those adjacent to the methyl group, along with a unique long-range coupling to a single fluorine at -120 ppm. This coupling pattern strongly suggests that the methyl group is bound to one metal adjacent to the α-carbon of the resulting trifluorovinyl group. The $^{13}C\{^1H\}$ NMR spectrum of a ^{13}CO-enriched sample of **5** shows two broad multiplet carbonyl resonances at 161 ppm and 178 ppm. The lower-field shift of the latter suggests that this carbonyl approaches the second

metal, possibly even interacting with it weakly in a semi-bridging arrangement, while the high-field shift is typical for such arrangements in which the carbonyl lies in a position remote from the adjacent metal.[15] This arrangement is confirmed through the $^{13}C\{^{1}H, ^{31}P\}$ NMR spectrum in which the terminal carbonyl at 161 ppm shows coupling only to the pair of phosphorus nuclei on the non-methylated metal (13.0 ppm), while the down-field signal at 178 ppm shows partial coupling to both sets of phosphines, with a stronger interaction displayed with those opposite of the higher-field signal (-8.0 ppm). Interestingly both carbonyls are also coupled to a single fluorine atom in the complex; the lower-field carbonyl is coupled (13 Hz) through the σ bond, while the higher-field carbonyl resonance is coupled (7 Hz) through the π interaction to the fluorine on the α carbon (-131 ppm). This unique observation helps to establish the bridging orientation of the perfluorovinyl moiety. The $^{13}CH_3$-enriched methyl group displays a broad high-field doublet at -19 ppm, arising from another long-range coupling to a single fluorine ($^{4}J_{CF}$ = 13.0 Hz) at -120 ppm.

The resulting trifluorovinyl group of **5** appears in the ^{19}F NMR spectrum as three new signals, at -80 ppm, -120 ppm and -131 ppm, consistent with the chemical shifts expected for a trifluorovinyl moiety. The two lower-field resonances (-80 ppm and -120 ppm) show mutual coupling of 85 Hz, which is consistent with the geminal coupling of an sp^2 hybridized $-CF_2$ group.[21] Coupling of the two higher-field resonances (-120 ppm and -131 ppm) is 100 Hz, which suggests a trans arrangement of these two fluorines; however, the lower than usual coupling value implies some loss of s-character between them, possibly resulting from partial rehybridization of the olefinic carbons upon π coordination to the second metal. Finally, the cis orientation of the remaining pair is confirmed through their mutual coupling of 20 Hz, which is also diminished relative to that of a terminal arrangement, establishing the presence of a bridging perfluorovinyl moiety in the molecule. Other diagnostic couplings between the fluorine atoms and other active nuclei in the $^{13}CH_3/^{13}CO$-labelled compound have confirmed the assignment of the orientation of the perfluorovinyl group as bridging (*vide supra*). Also in the ^{19}F NMR spectrum, the Me_3SiF generated in the above transformation

of **2** to **5** appears as a characteristic signal at -159.9 ppm, along with two clearly spaced signals at -76 ppm and -79 ppm, corresponding to the coordinated and free triflate anions, respectively.

Complex **5** is unstable at temperatures above 0 °C, rearranging via C-H activation of the methyl group, followed by triflic acid loss and subsequent addition of the proton and triflate ions, generating the compound $[Ir_2(\eta^1\text{-}CF{=}CF_2)(OTf)(CO)_2(\mu\text{-}CH_2)(\mu\text{-}H)(dppm)_2][CF_3SO_3]$ (**6**) which is stable and isolable at room temperature (see Scheme 2.8). We have not yet established the detailed mechanism of this rearrangement, which gives rise to hydride and methylene groups on opposite faces of the complex; however, it seems to occur by a deprotonation/reprotonation sequence as evidenced by the observation of free triflic acid at intermediate times, appearing at 12 ppm in the ^{1}H NMR spectrum.

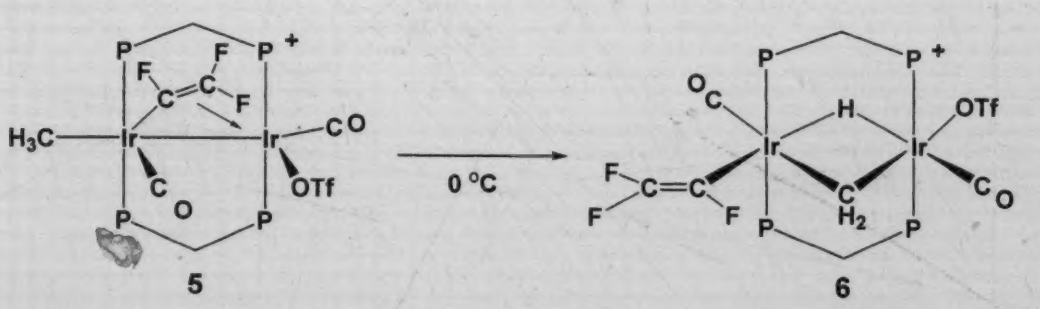

Scheme 2.8. *Transformation from bridging (**5**) to terminal (**6**) trifluorovinyl complex*

The $^{31}P\{^1H\}$ NMR spectrum of compound **6** consists of a pair of mutually coupled ($^2J_{PP}$ = 26 Hz) multiplets at -0.6 ppm and -28.5 ppm, as expected for a species having two different metal environments. In the ^{1}H NMR spectrum, compound **6** shows the dppm methylene protons as a broad multiplet, integrating for four protons, at 5.0 ppm, while the bridging methylene group appears as a doublet of quintets at 6.4 ppm ($^3J_{HP}$ = 6.0 Hz, $^3J_{HH}$ = 6.0 Hz), indicating that there is equal coupling to all phosphorus nuclei along with an additional coupling to a single

hydride. Although the coupling with the methylene protons was confirmed by a gCOSY NMR experiment, the hydride resonance appears at -12.2 ppm as a broad unresolved singlet, masking the 6.0 Hz coupling observed in the methylene group signal. A ^{13}CO-enriched sample of **6** shows two carbonyl resonances in the $^{13}C\{^1H\}$ NMR spectrum; the first is a doublet of triplets ($^2J_{CP}$ = 11 Hz, $^4J_{CF}$ = 22 Hz) at 164 ppm while the second is a multiplet at 166 ppm. Both high-field chemical shifts suggest terminal arrangements, in which the carbonyls do not approach the adjacent metal. The IR spectrum confirms this assertion with ν(CO) values of 2050 and 1998 cm^{-1}, respectively. In the $^{13}C\{^1H, ^{31}P\}$ NMR spectrum the carbonyl at 164 ppm loses its coupling to the pair of phosphorus nuclei at -28.5 ppm, leaving only a doublet due to coupling to a single fluorine. In a $^{13}CH_3$-enriched sample, the ^{13}C signal for the bridging methylene group appears at 37.9 ppm, a typical resonance of these groups, offering further support for the bridging arrangement of this moiety.

Again the ^{19}F NMR spectrum shows the characteristic signals and couplings of a perfluorovinyl group; however now the orientation is clearly terminal. Three new signals, all doublets of doublets, appear at -92 ppm, -121 ppm and -123 ppm. The two lower field signals (-92 ppm and -121 ppm) again show mutual geminal coupling of 85 Hz, while the two higher-field signals (-121 ppm and -123 ppm) display the normal 115 Hz coupling of two fluorine atoms in a trans arrangement. The remaining pair also show mutual cis coupling of 37 Hz to one another. Another sharp singlet, in addition to that seen at -79 ppm for the free triflate counterion, is also observed in the ^{19}F NMR spectrum at -76 ppm which is consistent with a coordinated triflate ion. The structure proposed above and shown in Scheme 2.8 has been confirmed by an X-ray structure determination, as shown in Figure 2.6. It should first be pointed out that the structure is disordered with sample crystals actually containing two different compounds superimposed in the average structure (see Figures 2.4 and 2.5).

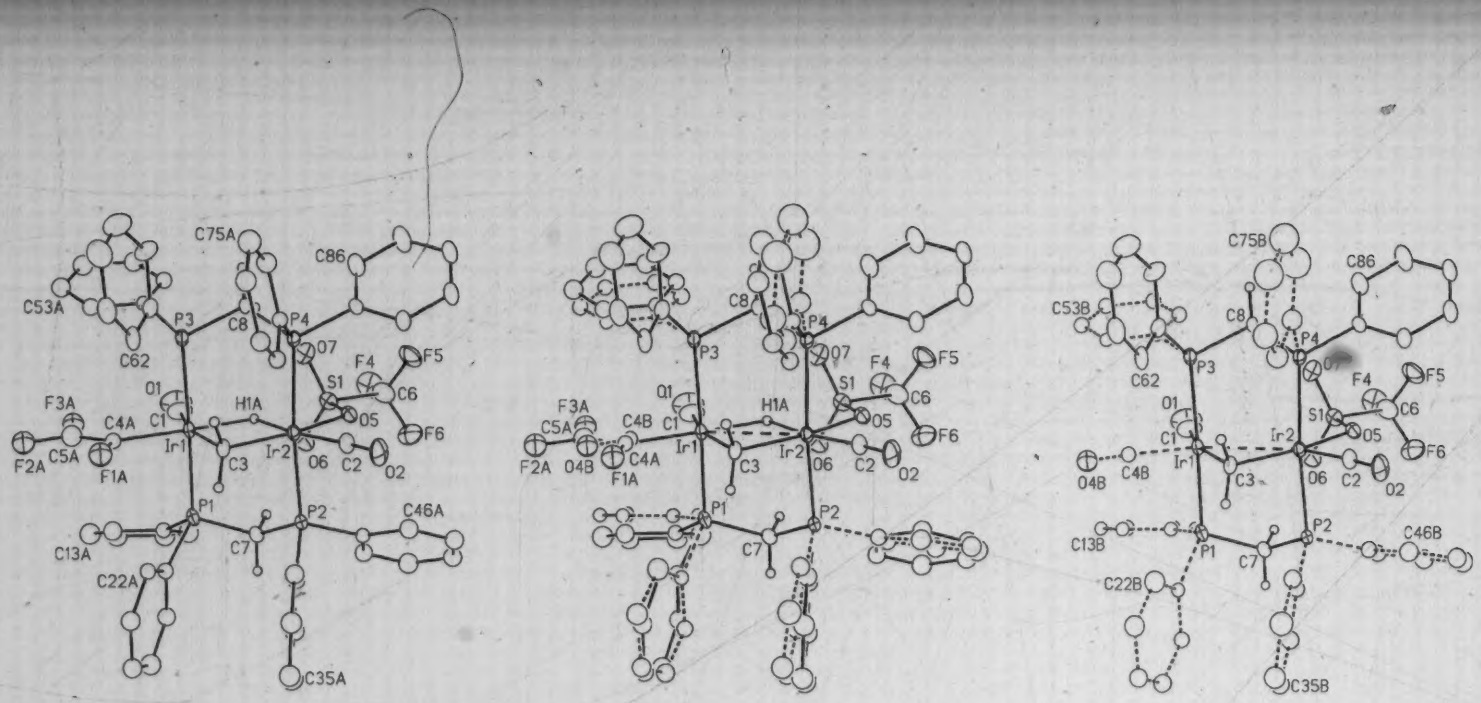

Figure 2.4. *Views of the cocrystallized cationic species. (a) (left)* $[Ir_2(\eta^1\text{-}CF{=}CF_2)(OTf)(CO)_2(\mu\text{-}CH_2)(\mu\text{-}H)(dppm)_2]^+$ **(6)** *(60%). (b) (center) The two cationic species superimposed as they occur in the structure. (c) (right)* $[Ir_2(CO)_3(OTf)(\mu\text{–}CH_2)(dppm)_2]^+$ *(40%). Solid bonds are those for compound* **6** *and for bonds that are in common with the impurity. Dashed bonds represent groups in the impurity.*

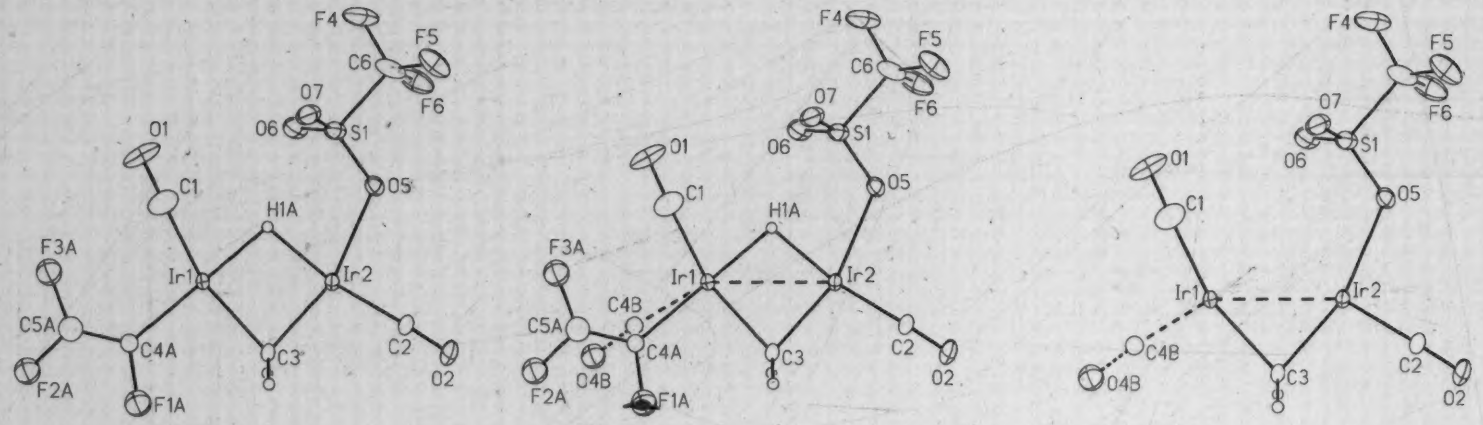

Figure 2.5. *View of the equatorial plane (dppm ligands omitted). (a) (left)* $[Ir_2(\eta^1\text{-}CF{=}CF_2)(OTf)(CO)_2(\mu\text{-}CH_2)(\mu\text{-}H)(dppm)_2]^+$ *(60%). (b) (center) The two cationic species superimposed as they occur in the structure. (c) (right)* $[Ir_2(CO)_3(OTf)(\mu\text{–}CH_2)(dppm)_2]^+$

It is presumed that the $[Ir_2(CO)_3(OTf)(\mu\text{–}CH_2)(dppm)_2][CF_3SO_3]$ complex that is present as the "other" molecule in the disordered structure, has resulted from the reductive elimination of the trifluorovinyl and hydride moiety yielding trifluoroethylene, accompanied by addition of a CO ligand, which was presumably scavenged from decomposition products.

Owing to the above disorder some uncertainty is expected in the structural parameters. Unfortunately, the superposition of the additional carbonyl of the impurity and the trifluorovinyl group of compound **6**, leads to poor determination of the exact position of the disordered atoms, resulting in weakly defined structural parameters for this group. Nonetheless, the η^1-binding and orientation of this group are unambiguous, and the structure proposed, based on spectral evidence and shown in Scheme 2.8, is clearly confirmed (see Figure 2.6). The η^1-trifluorovinyl group on one metal and a carbonyl at the other metal are on the same face of the complex, and cis to the bridging methylene group, which is opposite to the second carbonyl moiety at the first metal and the coordinated triflate anion at the other. Although the hydride ligand in **6** was not located in the X-ray study, its bridging position is supported by the NMR data and from the absence of any alternate coordination site in the complex. It has therefore been placed in an idealized position, symmetrically bridging the metals.

Selected bond lengths and angles are given in Tables 2.6 and 2.7, respectively.

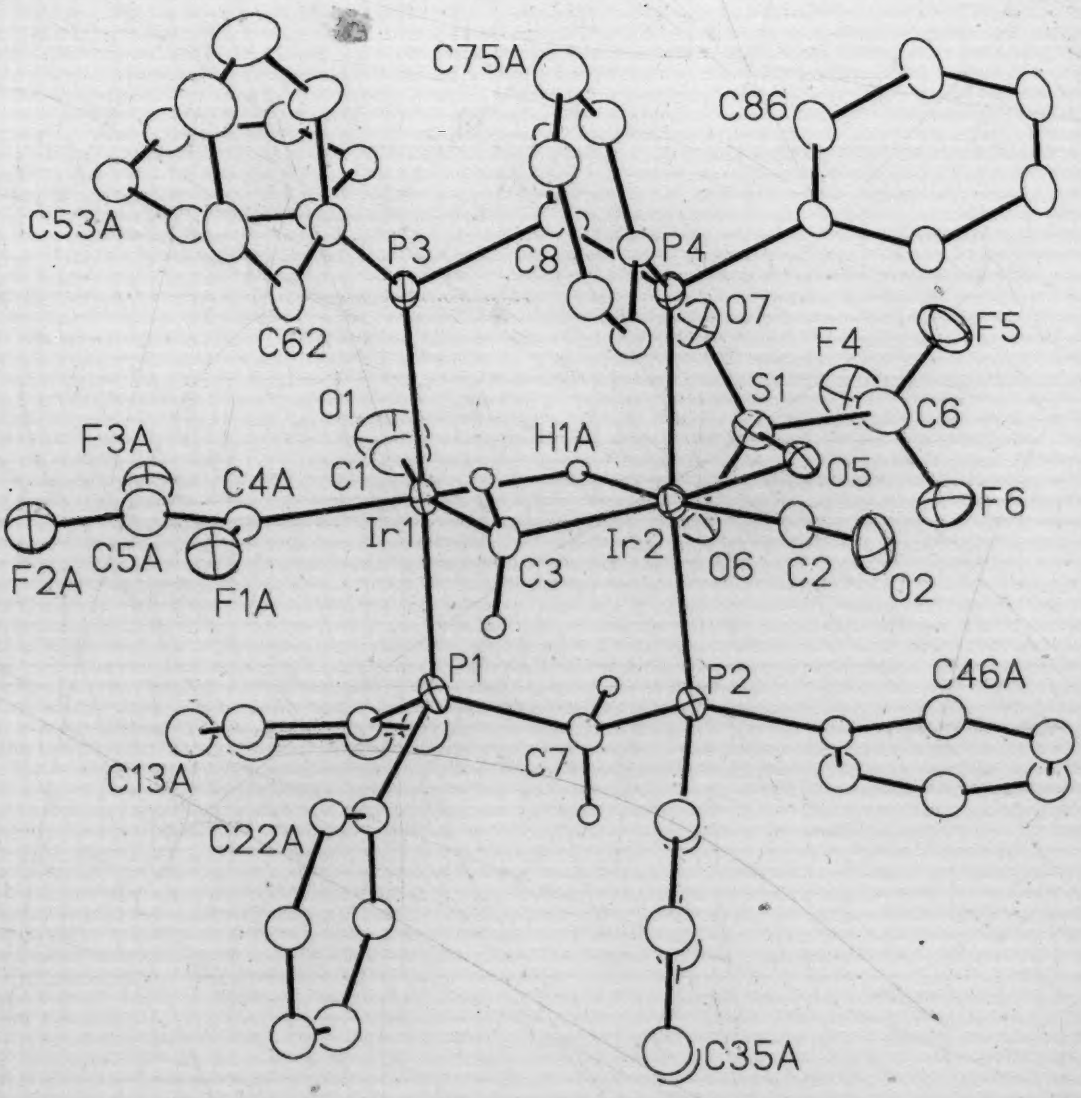

Figure 2.6. *Perspective view of the* $[Ir_2(CO)_2(C_2F_3)(OTf)(\mu\text{–}CH_2)(\mu\text{-}H)(dppm)_2]^+$ **(6)** *complex ion showing the atom labelling scheme. Non-hydrogen atoms are represented by Gaussian ellipsoids at the 20% probability level. The phenyl hydrogens have been omitted for clarity. Other hydrogens are drawn artificially small.*

Table 2.6. Selected Interatomic Distances (Å) for $[Ir_2(CO)_2(C_2F_3)(OTf)(\mu\text{–}CH_2)(\mu\text{-}H)(dppm)_2]^+$ **(6)**

Atom1	Atom2	Distance	Atom1	Atom2	Distance
Ir(1)	P(1)	2.358(2)	Ir(2)	H(1A)	1.85†
Ir(1)	P(3)	2.370(2)	F(2A)	C(5A)	1.310(8)‡
Ir(1)	C(1)	1.91(1)	F(3A)	C(5A)	1.309(8)‡
Ir(1)	C(3)	2.105(6)	F(4)	C(6)	1.32(1)
Ir(1)	C(4A)	2.08(1)	F(5)	C(6)	1.30(1)
Ir(1)	H(1A)	1.85†	F(6)	C(6)	1.35(1)
Ir(2)	P(2)	2.359(2)	O(1)	C(1)	1.13(1)
Ir(2)	P(4)	2.358(2)	O(2)	C(2)	1.126(8)
Ir(2)	O(5)	2.263(4)	O(4A)	C(4A)	1.13†
Ir(2)	C(2)	1.852(6)			
Ir(2)	C(3)	2.079(6)			

During refinement, †distance fixed, ‡distances constrained to be equal.

Table 2.7. Selected Interatomic Angles (deg) for $[Ir_2(CO)_2(C_2F_3)(OTf)(\mu\text{–}CH_2)(\mu\text{-}H)(dppm)_2]^+$ **(6)**

Atom1	Atom2	Atom3	Angle	Atom1	Atom2	Atom3	Angle
P(1)	Ir(1)	P(3)	174.75(7)	P(2)	Ir(2)	C(3)	91.4(2)
P(1)	Ir(1)	C(1)	88.7(3)	P(4)	Ir(2)	O(5)	86.8(1)
P(1)	Ir(1)	C(3)	91.9(2)	P(4)	Ir(2)	C(2)	89.4(2)
P(1)	Ir(1)	C(4A)	89.9(6)	P(4)	Ir(2)	C(3)	94.7(2)
P(3)	Ir(1)	C(1)	86.3(3)	O(5)	Ir(2)	C(2)	95.8(2)
P(3)	Ir(1)	C(3)	93.3(2)	O(5)	Ir(2)	C(3)	161.5(2)
P(3)	Ir(1)	C(4A)	88.9(6)	C(2)	Ir(2)	C(3)	102.7(3)
C(1)	Ir(1)	C(3)	163.9(4)	Ir(2)	O(5)	S(1)	119.9(2)
C(1)	Ir(1)	C(4A)	92.8(5)	Ir(1)	C(1)	O(1)	176(1)
C(3)	Ir(1)	C(4A)	103.3(4)	Ir(2)	C(2)	O(2)	176.7(7)
P(2)	Ir(2)	P(4)	173.79(6)	Ir(1)	C(3)	Ir(2)	86.0(2)
P(2)	Ir(2)	O(5)	87.1(1)	Ir(1)	C(4A)	O(4A)	173.9(8)
P(2)	Ir(2)	C(2)	90.2(2)	F(2A)	C(5A)	F(3A)	112(1)

2.3.2.2. $[Ir_2(CH_3)(OTf)(CO)_2(\mu\text{-}\eta 1{:}\eta 2\text{-}C_2F_2H)(dppm)_2][CF_3SO_3]$ (7)

C-F bond activation is similarly achieved employing the bridging trifluoroethylene complex **3** in reaction with $Me_3Si(CF_3SO_3)$ at -20°C, yielding the targeted product $[Ir_2(CH_3)(OTf)(CO)_2(\mu\text{-}\eta^1{:}\eta^2\text{-}CF{=}CFH)(dppm)_2][CF_3SO_3]$ (**7**), as outlined in Scheme 2.9. This product, containing a *cis*-1,2-difluorovinyl moiety is stable at ambient temperature and can be isolated and characterized.

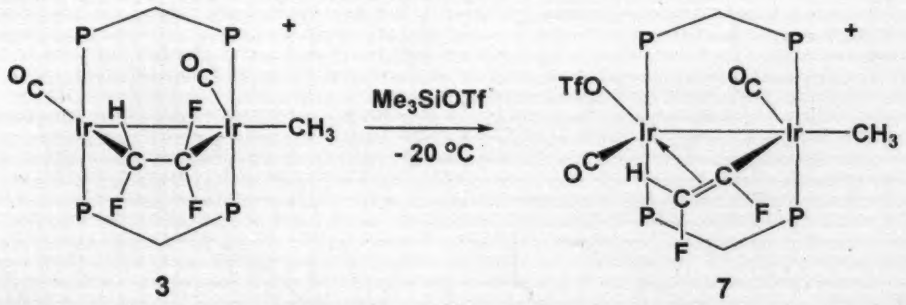

3 **7**

Scheme 2.9. *C-F activation of bridging trifluoroethylene via addition of $Me_3Si(OTf)$*

The $^{31}P\{^1H\}$ NMR spectrum of **7** reveals a characteristic ABCD spin pattern indicating four inequivalent phosphorus atom environments. Signals are observed at 9.0 ppm (1P), -2.5 ppm (2P) and -19.0 ppm (1P), each being a complex multiplet showing some mutual coupling to its neighbors. Two distinct magnitudes of $^2J_{PP}$ couplings are apparent, with the smaller more typical $^2J_{PP}$ couplings due to the phosphorus-phosphorus coupling within each diphosphine ligand, the ^{31}P nuclei of which are rendered inequivalent by the chemical inequivalence of each metal. The much larger splitting is due to coupling between nonequivalent phosphorus atoms oriented in a trans arrangment across each metal, indicative of a lack of top/bottom symmetry (see Figure 2.7).

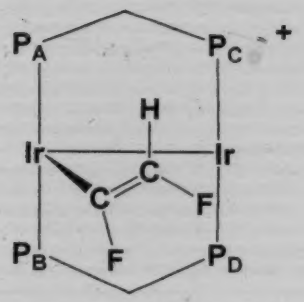

7

Figure 2.7. *Binuclear diphosphine framework of* **7**, *with bridging fluorovinyl group, illustrating inequivalence observed in phosphorus nuclei*

Accidental superposition of the signals from two inequivalent phosphorus nuclei accounts for the larger integration of the central resonance in the $^{31}P\{^{1}H\}$ NMR spectrum. In the ^{1}H NMR spectrum the dppm methylene protons appear as four separate multiplets (dt) at 6.1 ppm (1H), 5.6 ppm (1H), 5.5 ppm (1H) and 4.7 ppm (1H) with characteristic 14 Hz coupling to phosphorus. The appearance of four resonances is consistent with the absence of top/bottom and front/back symmetry in the product. The iridium-bound methyl group appears as a triplet at 1.2 ppm ($^{3}J_{PH}$ = 6.0 Hz), displaying equal coupling to the adjacent two independent phosphorus nuclei, while the vinylic proton is identifiable by its distinct splitting pattern, which appears as a multiplet (dddd) at 6.0 ppm showing all anticipated couplings. The first and most prominent coupling is the diagnostic hydrogen-fluorine coupling ($^{2}J_{HF}$), with a value of 65 Hz consistent with the geminal coupling of an sp^2 hybridized –C(H)F group.[22] The smaller coupling ($^{3}J_{HF}$ = 10 Hz) is suggestive, albeit a lower value than usual, with the H and the other F atom being in a trans arrangement across the vinylic center. These couplings are consistent with those seen in the ^{19}F NMR spectrum (*vide infra*). Selective $^{1}H\{^{31}P\}$ decoupling experiments have established that two of the couplings apparent in the ^{1}H NMR resonance of the fluorovinyl moiety are due to the neighboring phosphorus atoms. The first coupling is small (5 Hz) and corresponds to a cis arrangment between the vinylic proton and one phosphorus

atom, whereas the other larger coupling ($^3J_{HP}$=18 Hz) is consistent with a trans orientation between the vinylic proton and the opposite phosphorus atom. This difference in coupling constants further indicates a loss of top/bottom symmetry, and suggests that the vinyl moiety is positioned in a η^1:η^2- bridging arrangement across the bimetallic core.

The $^{13}C\{^1H\}$ NMR spectrum of a ^{13}CO-enriched sample of **7** shows two independent carbonyl resonances, both multiplets at 165 ppm and 172 ppm. Although similar in nature to those of compound **5**, both carbonyl ligands in **7** are presumed to be terminal, each showing coupling to different sides of the diphosphorus framework, with no detectable semi-bridging interaction. Consistent with that assertion, the IR spectrum shows the carbonyl stretches at 2053 cm^{-1} and 2007 cm^{-1}, respectively.

In the ^{19}F NMR spectrum there are three characteristic signals along with that of the triflate counterion at -79 ppm. The first is a sharp singlet at -77 ppm, integrating for three fluorines, and is assigned to the coordinated triflate ion. The other two signals consist of complex doublets displaying fluorine-phosphorus, fluorine-proton, and fluorine-fluorine coupling. The fluorine-proton coupling is consistent with that described above, with the higher field signal corresponding to the geminal partner to the proton. This signal shows mutual coupling of 35 Hz to the other fluorine, consistent with a *cis* arrangement of these atoms across the vinylic center. Selective $^{19}F\{^{31}P\}$ decoupling experiments have established that both fluorine atoms couple to ^{31}P nuclei on different ends of the framework; however, only peak sharpening was observable and the actual magnitudes of the coupling were undeterminable. Interestingly, diminished ^{19}F-^{19}F coupling through the unsaturated component of the vinyl center, compared to those of a terminal η^1-fluorovinyl moiety (see Discussion section), again establishes this as a bridging vinyl species.

2.3.2.3. $[Ir_2(CH_3)(OTf)(CO)_2(\mu\text{-}\eta1\text{:}\eta2\text{-}C_2FH_2)(dppm)_2][CF_3SO_3]$ (8)

As noted earlier in the chapter, the 1,1-difluoroethylene-bridged compound **4** is always found in conjunction with its isomer, compound **4b**, which contains a terminally bound olefinic unit. Through repeated temperature cycling, we have been able to affect the ratio of **4:4b**, obtaining up to a 5:1 mixture, optimally. Typically, however, the initial ratio of the bridging μ-$C_2F_2H_2$ (**4**) complex to its terminal η^2-$C_2F_2H_2$ (**4b**) isomer, at -40 °C in solution, is 2:1, allowing us to compare the difference in reactivity of these two species.

The subsequent reaction of such a mixture with $Me_3Si(CF_3SO_3)$ at -20 °C results in the C-F activation of complex **4**, as demonstrated by the disappearance of its associated signals and the concomitant appearance of a new set of resonances in the $^{31}P\{^1H\}$ NMR spectrum, corresponding to the compound $[Ir_2(CH_3)(OTf)(CO)_2(\mu\text{-}\eta^1\text{:}\eta^2\text{-}CF{=}CH_2)(dppm)_2][CF_3SO_3]$ (**8**), as outlined in Scheme 2.10.

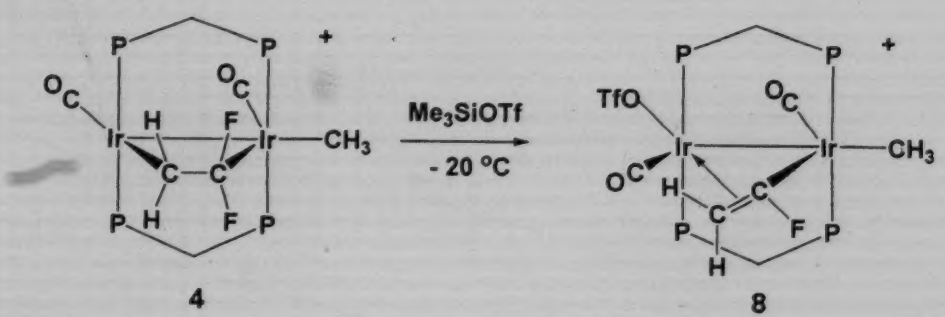

4 8

Scheme 2.10. *C-F activation of bridging difluoroethylene via addition of $Me_3Si(OTf)$*

Interestingly, the species (**4b**) containing the η^2-bound olefin remains unchanged and shows only liberation of the free olefin when the temperature is raised above 0 °C. Furthermore, the instability of species **8** at temperatures above 0 °C has limited our characterization of this product to solution NMR at lower temperature.

The $^{31}P\{^1H\}$ NMR spectrum of compound **8** shows two mutually coupled pseudo-triplets ($^2J_{PP}$ = 18.5 Hz) at 1.6 ppm and -5.5 ppm, with the lower field signal

showing an additional splitting of 45 Hz ($^3J_{PF}$). In the ^1H NMR spectrum the dppm methylene protons appear as typical multiplets at 3.1 ppm and 4.3 ppm, integrating for two protons each, with typical 14 Hz coupling to phosphorus. Again, as was the case with compound **5**, the ^{31}P and ^1H NMR data, involving the dppm methylene protons, are simpler than anticipated showing *apparent* top/bottom symmetry within the molecule. This clearly cannot be the case and must be due to accidental degeneracy of the NMR signals. The resonance for the iridium-bound methyl group, in the ^1H NMR spectrum, is a triplet at 0.2 ppm ($^3J_{PH}$ = 5.6 Hz), displaying coupling to the two adjacent phosphorus nuclei at -5.5 ppm. The vinylic protons are identifiable by their characteristic coupling pattern, in which they appear as mutually coupled doublets at 6.04 ppm and a 5.40 ppm, with the latter having a single additional splitting of 14 Hz ($^3J_{HF}$), due to its trans arrangement with the fluorine across the vinylic center. A gCOSY NMR experiment also confirms the correlation between the geminal pair of vinylic protons. In a ^{13}CO-enriched sample of **8**, two carbonyl resonances appear in the $^{13}C\{^1H\}$ NMR spectrum; the first is a broad doublet ($^3J_{CF}$ = 58 Hz) at 164 ppm while the second is a triplet ($^2J_{CP}$ = 11 Hz) at 172 ppm. Both shifts are very similar to those of compound **7**, and again suggest terminal binding of these groups. The low-field carbonyl shows coupling to the diphosphine ends associated with the methylated metal at -5.5 ppm in the ^{31}P NMR spectrum, while the high-field carbonyl is coupled to the other side of the diphosphine framework (1.5 ppm). The ^{13}C-methyl signal, in a $^{13}CH_3$-enriched sample of **8**, appears as a broad singlet at 4.8 ppm.

In the ^{19}F NMR spectrum, the single fluorovinyl resonance at -211 ppm, appears as a triplet, displaying the same 45 Hz coupling to phosphorus as observed in the $^{31}P\{^1H\}$ NMR spectrum of compound **8**. Selective decoupling confirms this relationship, although interestingly, this coupling is not to the set of phosphorus nuclei adjacent to the σ-vinyl moiety, but is to the ^{31}P nuclei that are bound to the metal which interacts with the fluorovinyl group via the π-interaction. Furthermore, in the ^{13}CO–labelled complex, this fluorine also displays a strong coupling to a carbonyl that correlates to the distal set of ^{31}P nuclei, as seen with

compound **5**. This further suggests the perfluorovinyl group allows coupling through the π-component when the moiety is in a bridged orientation. ^{19}F NMR spectroscopy also confirms the coordinated triflate counterion at -78 ppm and again shows Me_3SiF as a product of the reaction with a characteristic splitting pattern at -159.9 ppm.

At temperatures higher than 0 °C, compound **8** transforms into the related fluorocarbene (see Scheme 2.2A) complex $[Ir_2(CH_3)(CO)_2(\mu\text{-}\eta^1\text{:}\eta^1\text{-}C(F)\text{-}CH_2)(dppm)_2][CF_3SO_3]_2$ (**8a**), in which the $\mu\text{-}\eta^1\text{:}\eta^2$-bridging fluorovinyl moiety has isomerized into a new conformation (Scheme 2.11).

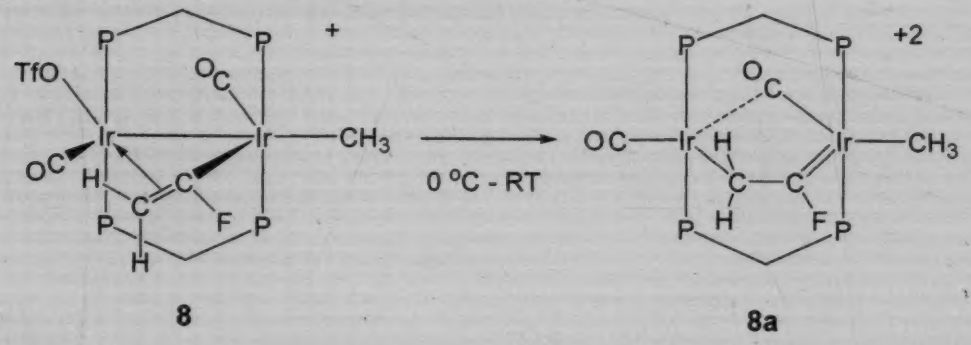

8 **8a**

Scheme 2.11. *Transformation of compound **8** between 0 °C and ambient temperature*

The $^{31}P\{^1H\}$ NMR resonances of **8a** appear as pair of pseudo-triplets in the spectrum at 12.0 ppm and -12.0 ppm, showing mutual coupling of 23 Hz. The ^1H NMR spectrum shows the pair of geminal protons as a doublet at 5.5 ppm, showing coupling ($^3J_{HF}$ = 13.4 Hz) to the adjacent fluorine. For a monofluorovinyl group, as in **8**, we expect two inequivalent proton resonances, showing different *cis* and *trans* couplings to the unique fluorine, whereas in the carbene formulation the protons are equivalent, and thus display a single resonance. The ^{19}F NMR spectrum of compound **8a** shows only one signal attributable to the vinylic fluorine, appearing at -48 ppm, the chemical shift of which closer to that of a

fluorocarbene, than of a monoflorovinyl complex.[23] The complementary $^3J_{HF}$ coupling (13.4 Hz) is also apparent in this signal, which is displayed as a triplet.

In the ^{1}H NMR spectrum of this product, the dppm methylene protons appear as typical multiplets at 4.1 ppm and 2.8 ppm, while the iridium-bound methyl group protons give a broad resonance at 0.8 ppm, integrating for three protons. A ^{13}CH-enriched sample of **8a** shows the ^{13}C-methyl carbon as a broad singlet at -4.5 ppm, along with two different carbonyl resonances apparent at 192 ppm and at 164 ppm. Selective ^{31}P decoupling experiments indicate that the lower-field carbonyl signal is coupled to both sides of the diphosphine framework, suggesting that it coordinated in a bridging arrangement, while the other carbonyl is terminally bound.

This complex undergoes further transformation at ambient temperature to unidentified products, thus has only been characterized spectroscopically, leaving its structural assignment as tentative.

2.3.3. Reaction of Protic Acids with Fluoroolefin-bridged Complexes

2.3.3.1. Reaction of HOTf with Fluoroolefin-bridged Complexes

When triflic acid was added in place of Me_3SiOTf in NMR-scale versions of the reactions described above for compounds **2**, **3**, and **4**, the identical C-F activation products (**5**, **7**, and **8**) were observed spectroscopically to be the major products. However, numerous other unidentified products were also apparent, presumably due to the potential for direct protonation by triflic acid to the metallic centers, or the subsequent reactivity of the generated HF from the C-F activation process. With the Lewis acid addition typically being performed on compounds that were generated *in situ* at lower temperatures, we preferred the more selective transformations afforded by the Me_3SiOTf, thus chose not to further investigate the less reliable pathways associated with the protic acid.

2.3.3.2. Reaction of H_2O with Fluoroolefin-bridged Complexes

Water has also been shown to be a suitable acid for facilitating C-F activation in these systems. Although no reaction is seen with water and any of the tetrafluoroethylene complexes or their derivatives, some interesting transformations are effected via the addition of water to the bridging trifluoro- (**3**) and difluoroethylene (**4**) complexes, as described in what follows.

2.3.3.2.1. $[Ir_2(CH_3)(CO)_2(\mu\text{-}C_2F_3H)(dppm)_2][CF_3SO_3]$ (3)

Upon exposure to water, complex **3** displays an immediate reaction, established initially via low temperature spectroscopic studies. During the course of the reaction, evidence for an intermediate containing an intermolecular hydrogen-bonded interaction between the water and a C-F bond of the bridging fluoroolefin (H-O···H···F···C~; Scheme 2.12), is apparent in both the ^1H and ^{19}F NMR spectra. The complementary appearance of two new signals in the ^{31}P NMR spectrum, both triplets at 1.5 ppm and -14.4 ppm, is consistent with this intermediate species. The intermediate H···F moiety is proposed on the basis of the mutual proton fluorine coupling constant ($^1J_{HF}$) observed in two distinct signals: a high-field doublet with 450 Hz coupling appearing at -196 ppm in the ^{19}F spectrum, and a broad doublet at 8.93 ppm in the ^1H spectrum which also shows the same $^1J_{HF}$ coupling. Hydrogen-bonded HF coupling constants have been shown to decrease by as much as 20% from experimental gas values (530 Hz),[24] which is in line with the value observed, and consistent with a previously reported iridium complex of this nature.[25]

The reaction gives products consistent with such a transformation and although the resultant free HF product is not observed spectroscopically, we assume rapid exchange with water broadens the anticipated resonance. The generated HF may also react with the glass, although 'etching' of the glass was not observed.

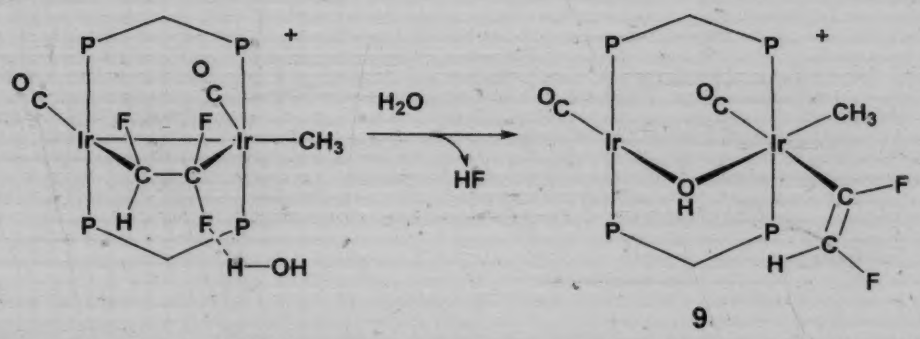

Scheme 2.12. *C-F Activation reaction with water acting as the Lewis acid*

Upon warming the sample to -20 °C, a new difluorovinyl product $[Ir_2(CH_3)(CO)_2(\eta^1\text{-}CF{=}CFH)(OH)(dppm)_2][CF_3SO_3]$ (**9**) is generated. Compound **9** is stable at ambient temperature and thus may be isolated and characterized. The $^{31}P\{^1H\}$ NMR spectrum shows two relatively broad, mutually coupled pseudo-triplets ($^2J_{PP}$ = 9.0 Hz) at 10.2 ppm and -14.6 ppm, consistent with two sets of inequivalent phosphines. The ^1H NMR spectrum shows the dppm methylene protons as two doublets of multiplets, integrating for two protons each, at 4.5 ppm and 3.1 ppm, displaying the characteristic 14 Hz coupling to phosphorus. The iridium-bound methyl group appears as a triplet, integrating for three protons, at 0.6 ppm ($^3J_{HP}$ = 8.0 Hz). Selective ^{31}P decoupling experiments indicate that these protons are coupled equally to one pair of phosphorus nuclei at -14.6 ppm, which strongly suggests that the methyl group is bound to a single metal. The vinylic proton is identifiable by its characteristic splitting pattern, which appears as a doublet of doublets (dd) at 4.9 ppm with all of the coupling resolvable. The first and most prominent coupling is the $^2J_{HF}$, with a value of 80 Hz consistent with the geminal coupling of an sp^2 hybridized –C(H)F group. The smaller coupling ($^3J_{HF}$ = 23 Hz) is consistent with the H and the other F atom being in a trans arrangement across the vinylic center. These couplings are reflected in those seen in the ^{19}F NMR spectrum and imply a terminal arrangement of this moiety. The hydroxide group proton signal is displayed as a broad signal at 3.6 ppm which shows some sharpening upon ^{31}P decoupling,

however no definitive realtionship to either side of the diphosphine framework was resolved by selective ^{31}P decoupling experiments. Nevertheless, the hydroxide group is proposed to occupy a bridging position, based on geometrical considerations, and the stability of the resulting square planar Ir(I), and octahedral Ir(III) metal centers. The $^{13}C\{^{1}H\}$ NMR spectrum of a ^{13}CO-enriched sample of **9** shows two independent terminal carbonyl resonances, both multiplets at 169 ppm and 172 ppm. The $^{13}CH_3$-enriched methyl group displays a broad singlet at -5 ppm.

In the ^{19}F NMR spectrum there are two characteristic signals together with that of the triflate counterion at -79 ppm, in a 1:1:3 ratio. Both minor resonances consist of complex doublets displaying fluorine-phosphorus, fluorine-proton, and fluorine-fluorine coupling. The fluorine-proton coupling is consistent with that described above, with the higher field signal (-152 ppm) corresponding to the geminal partner of the proton. This signal shows mutual coupling of 10 Hz to the other fluorine (-93 ppm) indicative of a cis arrangement of these atoms across the vinylic double bond. In addition, the coupling through the π component of the vinyl center is not diminished relative to other terminal fluorovinyl complexes (vide infra), helping to establish this as a terminal fluorovinyl species.

This species may also be generated from the analogous difluorovinyl complex **7**. Over time in wet organic solvents, movement of the difluorovinyl group from the bridging to a terminal position is seen in compound **7**, via HOTf loss with the hydroxide counterion filling the vacant coordination site generating compound **9**. The tendency of the hydroxide ligand is to bridge the two metal centers, as illustrated in Scheme 2.13, which puts the fluorovinyl and methyl ligands in ideal an arrangement for reductive elimination; however, even under refluxing conditions, this process is not observed.

This species (**9**) may also be generated more cleanly and efficiently through the addition of aqueous KOH to either compound **3** or **7** (see Experimental section).

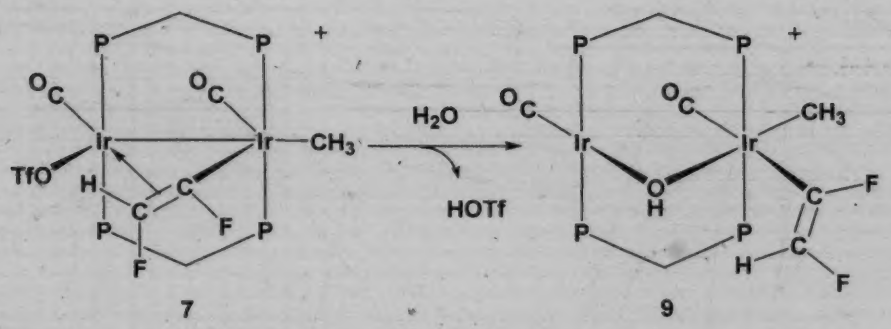

7 9

Scheme 2.13. *C-F activation reaction of compound* **7** *with water*

2.3.3.2.2. $[Ir_2(CH_3)(CO)_2(\mu\text{-}C_2F_2H_2)(dppm)_2][CF_3SO_3]$ (4)

Low temperature spectroscopic studies on compound **4** also reveal that it too is reactive upon exposure to water. Although the initial evidence for an intermolecular hydrogen bonded interaction (H-O···H···F···C~) is not observed, we again propose that the complex reacts similarly, leading to C-F activation and loss of H-F.

In this case, however, subsequent coordination of the hydroxy counterion occurs in conjunction with the reductive elimination of the methyl and fluorovinyl moiety to give 2-fluoropropene as a free gas, which has been identified in the ^{19}F NMR spectrum by comparison to reported spectral data.[18,26] The coordinated hydroxyl group takes a bridging position generating the previously characterized complex, $[Ir_2(CO)_2(\mu\text{-}OH)(dppm)_2][CF_3SO_3]$.[27] Other than the latter reductive elimination step, the C-F activation process in this reaction, may be viewed mechanistically as analogous to the trifluoroethylene activation (2.3.3.2.1) (see Scheme 2.14).

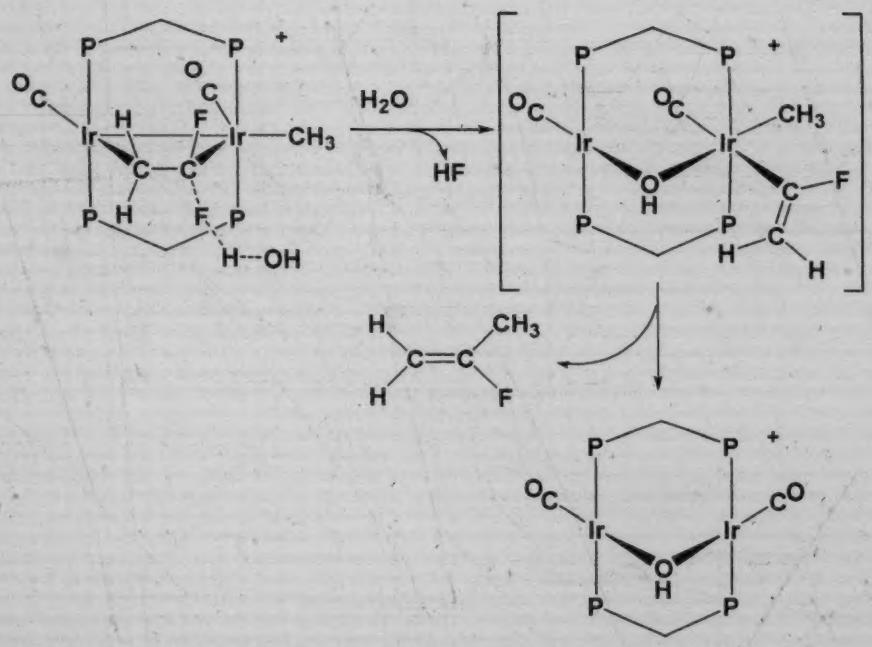

Scheme 2.14. *Formation of 2-fluoropropene via reaction of compound **4** with water*

2.4. Discussion

a) Fluoroolefin binding

As noted in Chapter 1, a number of isomers can be observed in the reactions of compound **1** with olefins, as demonstrated in the reactions of **1** with allenes.[28] In general, the kinetic product observed at low temperatures results from substrate addition adjacent to the methyl group (site '**a**' as shown in Scheme 2.15), leading to C-H activation of this group to give the methylene-bridged hydride.

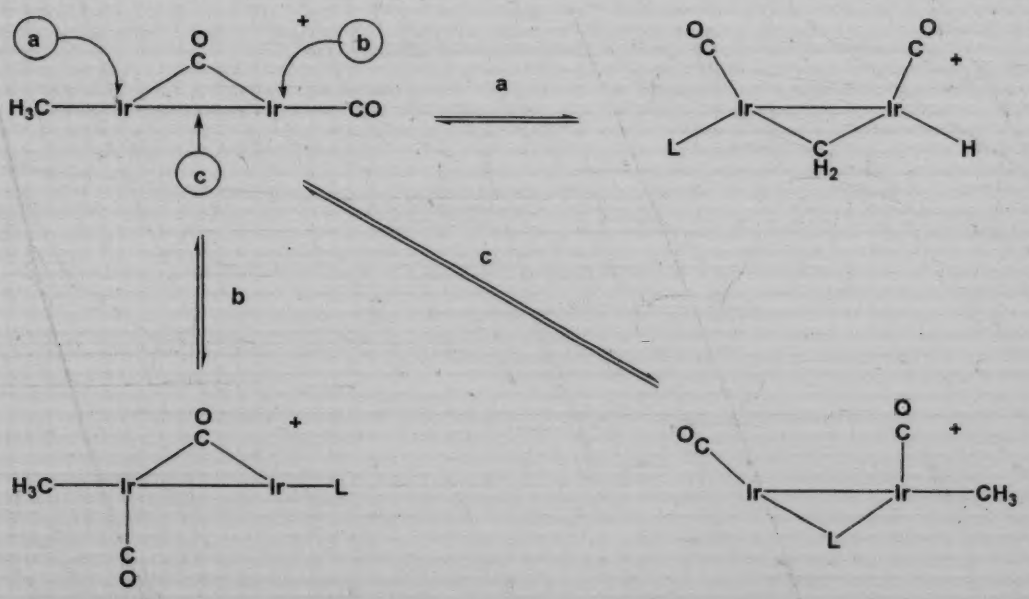

Scheme 2.15. *Sites of attack for substrate (L=olefin) addition to* **1**. *Note: the dppm ligands above and below the plane have been omitted.*

At intermediate temperatures the next favored product, when observed, results from attack at site '**b**' and has the olefin substrate terminally coordinated at one metal with the intact methyl group in the *trans* position at the adjacent metal. At even higher temperatures, species '**b**' often disappears in favor of the substrate-bridged product, which can arise by a number of routes, but can be generated through coordination in the vicinity of both metals, approximated as site '**c**'. In the case of allenes, not all three products are observed for all allenes studied, presumably owing to steric and/or electronic factors which either disfavor a given isomer for steric reasons or favor an isomer for electronic reasons. With ethylene,[8] only the first two isomers were observed, with no evidence of an ethylene-bridged complex observed.

Reactions of compound **1** with fluoroolefins proceed much like those encountered with allenes, as described above. In these cases, however, the only fluoroolefin to give all three isomers (**a**, **b** and **c**), shown in Scheme 2.15, is 1,1-difluoroethylene. We assume, as was the case for several of the allenes,[28] that

the kinetic products in these reactions are the ones in which the substrates have better access to the metal center. Often, however, the olefins in these kinetic products also have the lowest binding energy, so that upon warming these isomers give way to those having the higher binding energy. For monofluoroethylene and *cis*-difluoroethylene, only weakly bound terminal adducts (isomer '**b**') were observed, and in both cases the olefin adduct is extremely labile, displaying olefin loss at temperatures greater than -50 °C and -40 °C, respectively. Presumably the binding energy for isomer '**a**' of these complexes is so low that even at -80 °C it is not observed. Interestingly, the binding of these fluoroolefins, compared to ethylene itself, is not in line with our expectations, on the basis of the Dewar-Chatt-Duncanson model of olefin binding. We would have expected that the electron withdrawing substituents would have given rise to better π back-donation and stronger binding than ethylene, the same isomer of which persists at ambient temperature. Possibly the olefins in these isomers are functioning primarily as σ-donors, for which electronegative substituents disfavor coordination, however because these are already low valent, electron rich systems, this explanation seems unlikely. Alternatively, the increased repulsion owing to the fluorine lone pairs outweighs any increase in electronic stabilization afforded by the fluorine substituents. Additionally, it has also been suggested that the net attractive energy gained in these systems is offset by the substantial cost in deformation energy associated with the change in geometry upon rehybridization.[29]

Although there is no obvious trend in binding ability on moving from ethylene to monofluoroethylene to cis-difluoroethylene, the move to 1,1 difluoroethylene does give rise to improved binding energies with the first isomer (**a**) persisting to -40 °C and the thermodynamically favored product, in which the olefin binds in a bridging manner, persisting to 0 °C. Following this trend the bridging trifluoroethylene is stable for hours at 0 °C, and the tetrafluoroethylene analogue is stable at ambient temperatures for extended periods. For trifluoroethylene, isomer (**a**) is obtained briefly at -80 °C, but even at this temperature the bridging mode (**c**) competes effectively, and is the only species observed at higher

temperatures. No other isomer, other than (**c**) is observed for tetrafluoroethylene.

The propensity of the more highly substituted fluoroolefins to attain the bridging coordination mode can be rationalized in terms of Bent's rule.[30] First, the electronegative substituents should favor rehybridization from sp^2 to sp^3 that occurs in the bridging site, resulting in an increase in p-character in the C-F bonds. Second, the tendency towards increased p-character in these bonds will result in greater s-character in the adjacent metal-carbon bonds, increasing the strength of these interactions. The increased strength of metal-carbon bonds in fluoroalkyl groups is well documented.[5]

Notably, only if a geminal difluoro-moiety is present in the fluoroolefin does the substrate bridge the two metals, as observed with the complexes $[Ir_2(CH_3)(CO)_2(\mu\text{-olefin})(dppm)_2][CF_3SO_3]$ (olefin = C_2F_4 (**2**), C_2F_3H (**3**), 1,1-$C_2F_2H_2$ (**4**)). It is proposed that coordination in the bridging position may be viewed as an addition across the fluoroolefin double bond, a process which has been determined to more exothermic, in such systems, than that of the reaction involving the analogous hydrocarbon.[31] In such cases, the increased stability has been related to the presence of a geminal-difluoro group, which has been postulated to destabilize the π-bond, through its increased draw of p-character from the olefinic carbon.[32] It is not surprising then, that greater fluorine substitution on the olefinic backbone tends to lead to a more stable bridging adduct, as seen in the increasing stability trend on going from 1,1-difluoroethylene to tetrafluoroethylene.

The orientation of the bridging fluoroolefins, not relevant in the symmetrical tetrafluoroethylene adduct, was established for the unsymmetrical bridging fluoroolefins as being in the opposite orientation from that previously reported.[8] The initial report had proposed an olefin orientation on the basis of steric arguments, which would favor the bulkier, more substituted end of the fluoroolefin at the less substituted metal, i.e. the one remote from the methyl group.

However, spectral data acquired from selective ^{31}P heteronuclear NMR decoupling experiments, suggest that the opposite is true, with the pair of fluorines being positioned at the end adjacent to the methyl group, putting these two moieties on the same metal. We assume that this orientation may be electronically favored, with the electron-donating methyl group, relative to the positive charge on the opposite metal, favoring binding of the more electron withdrawing, more highly fluorinated end of the olefin at this metal. This orientation is further supported by the ensuing reactions with Me_3SiOTf and the configuration of the resulting C-F activated products (**5**, **7**, and **8**).

b) C-F Activation

Our strategy for effecting the activation of olefinic C-F bonds was based on the premise that olefins bound in the bridging site between a pair of metals should undergo greater rehybridization of the olefinic carbons towards their sp^3 limit than observed when bound in an η^2-fashion to a single metal, owing to interaction of the olefin with two metals instead of just one. Substantial rehybridization has been confirmed in the structures of C_2F_4-bridged diiron and the above diiridium compounds in which the olefinic C-C bond lengths (1.534(7), 1.563(7) and 1.54(3) Å, respectively) have lengthened to that of a single bond, while the angles at these carbons are also consistent with sp^3 hybridization. We suggested that in such a geometry the bridging fluoroolefin can be viewed as analogous to two fluoroalkyl groups. The well-established lability of such α-fluorines towards fluoride abstraction and the above analogy suggested to us that bridging fluoroolefins should also be susceptible to fluoride ion abstraction.

In keeping with this proposal, fluoride-ion abstraction from the bridging fluoroolefin ligands in compounds **2-4**, to give the respective fluorovinyl products (**5-8**), was readily achieved by the addition of either trimethylsilyl triflate (Me_3SiOTF) or protic acids (H_2O and HOTf) (see Scheme 2.16).

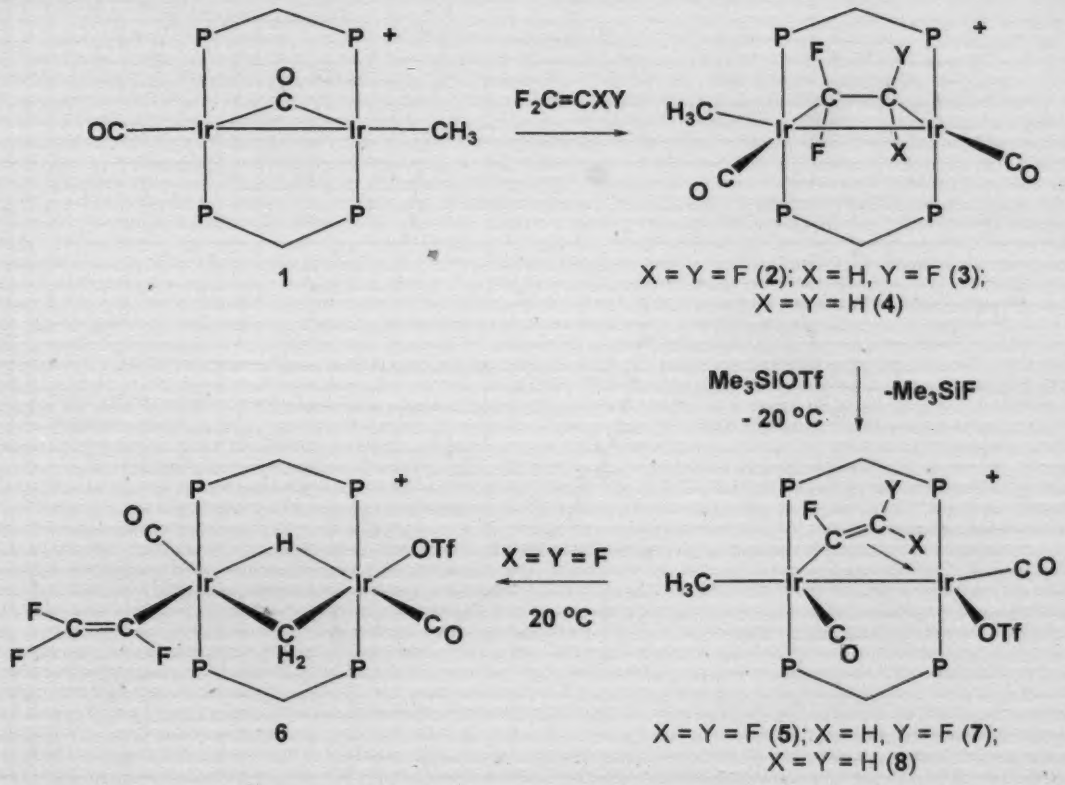

Scheme 2.16. *Fluorovinyl products of fluoride abstraction from compounds* **2-4**

For the tetrafluoro- and trifluoroethylene complexes, which exist primarily as bridged compounds at conveniently accessible temperatures, the absence of the η^2-bound isomer does not allow a comparison of the reactivity involving these two olefin binding modes and the unambiguous determination of whether metal-metal cooperativity involved is in the activation process. However, in the case of 1,1-difluoroethylene, both bridging (**4**) *and* terminal isomers (**4b**) can be present simultaneously, allowing a direct comparison of the reactivity of both types of species to be made (Scheme 2.17).

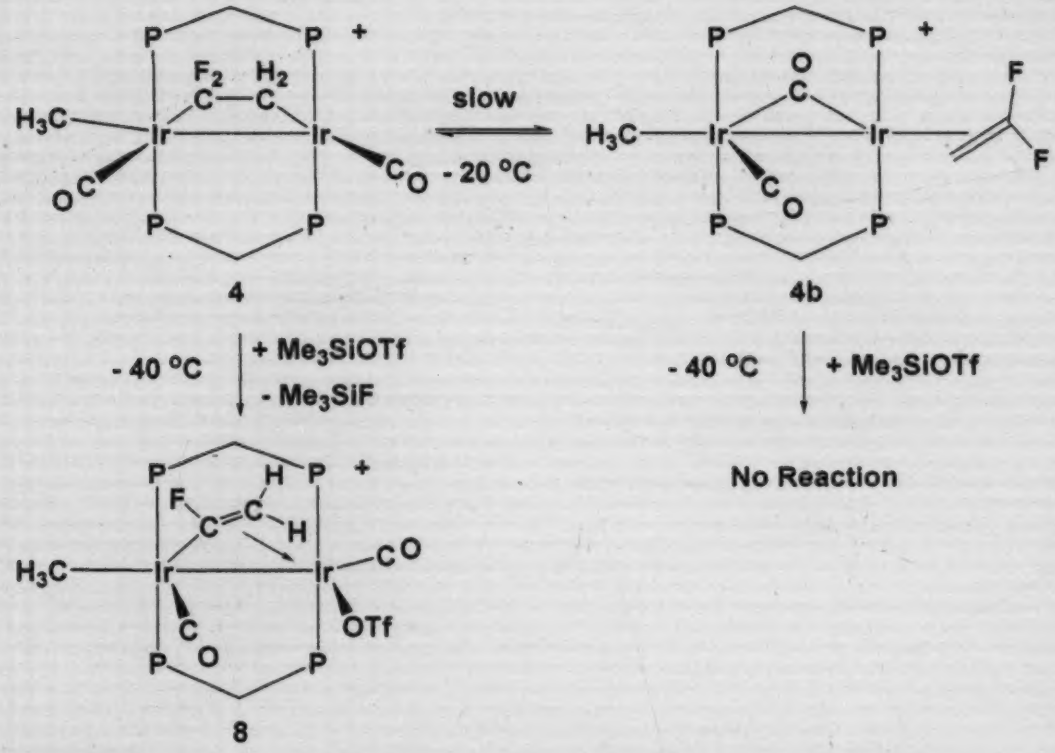

Scheme 2.17. *Reactivity comparison of μ-$F_2C{=}CH_2$ vs. η^2-$F_2C{=}CH_2$*

Reaction of a mixture of **4** and **4b** with Me_3SiOTf results in C-F activation in compound **4**, to give the fluorovinyl product **8**, whereas compound **4b**, containing a terminal olefin, is unreactive. The fact that the reaction is only effected on the bridging isomer (**4**) is the first clear documentation of the increased reactivity of the μ-olefin binding mode and the cooperative involvement of the pair of metals in the activation of C-F bonds in binuclear systems. In a previous case involving C-F activation of a bridging tetrafluoroethylene ligand, it was proposed that fluoride ion loss yielded an unobserved σ-π bonded trifluorovinyl intermediate, which then rearranged to give a bridging perfluoroethylidene (μ-$C(F)CF_3$) complex.[33] Another study proposed the existence of such a group on the basis of IR studies.[34] However, the study described in this chapter appears to be the best supporting evidence for the existence of such bridging fluorovinyl ligands. Our experiments have shown, in all cases that the initial products of C-F

activation in these systems are indeed the bridging fluorovinyl complexes (**5**, **7**, and **8**).

Unfortunately we have been unable to obtain suitable single crystals of any of the fluorovinyl-bridged complexes, and thus have had to rely upon spectral characterization of these species. The differentiation between terminal and bridging fluorovinyl groups was made on the basis of the different NMR coupling patterns observed between the fluorovinyl substituents in the proposed bridging and terminal geometries. For example, fluorine-fluorine coupling constants for the terminal η^1-trifluorovinyl group in compound **6** ($^3J_{trans}$=115 Hz, $^2J_{gem}$=90 Hz, $^3J_{cis}$=40 Hz) are consistent with previous determinations and are all greater than the respective values for the bridging group proposed in the otherwise isomeric compound **5** (100 Hz, 85 Hz, 20 Hz). A summary of these comparisons is presented in Table 2.8.

In all cases, the *trans* coupling ($(^3J_{FF})_{trans}$ and $(^3J_{HF})_{trans}$) observed in the fluorovinyl groups investigated, are lower in the bridging case than in the terminal one, a trend that has been previously established for perprotio vinyl moieties.[35] Although not general among all fluorovinyl comparisons, the $(^2J_{FH})_{gem}$ values in bridging difluorovinyl and the $(^2J_{FF})_{gem}$ and $(^3J_{FF})_{cis}$ are also often lower in the bridging geometry. We assume that this decrease in coupling is due to a loss of orbital overlap, along with decreased nuclear penetration, created by rehybridization of the component carbon; on going from an sp^2 hybrid, with a higher degree of s-character, to an sp^3 hybridized moiety, containing a lower component of s-character. Further corroboration of the above coupling constant data was also found in the spin-spin coupling observed between the fluorine on the α-carbon with other NMR active nuclei in the complex. While the terminal binding mode of the fluorovinyl group resulted only in spin-spin coupling between this fluorine and other nuclei attached to the same metal, the bridging fluorovinyl group gave rise to coupling with nuclei on **both** metals, further supporting its bridging arrangement across the binuclear core.

Table 2.8. Comparison of ^{19}F-^{19}F and ^{19}F-^{1}H coupling constants for bridging and terminal fluorovinyl compounds

Fluorovinyl	Orientation	Coupling (Hz) $^3J_{trans}$	$^2J_{geminal}$	$^3J_{cis}$	Trend in going from terminal to bridging
$-C_2F_3$ [a]	η^1-	115	90	40	$^3J_{trans}$ $^3J_{cis}$ and $^2J_{gem}$ decrease
	μ -	100	85	20	
$-C_2F_2H$ [a]	η^1-	23	80	10	$^3J_{trans}$ and $^2J_{gem}$ decrease
	μ -	10	65	35	
$-C_2FH_2$	η^1- [b]	12-34	<5	1-8	$^3J_{trans}$ decreases
	μ - [a]	13	~6	0	
$-C_2H_3$ [b]	η^1-	17	1.5	10	$^3J_{trans}$ decreases
	μ-	11	1.5	7	

a) values acquired from experimental data (see Results Section)
b) values obtained from literature references[35] (reported as ranges where variable)

In characterizing the initial products of C-F activation from bridging fluoroolefins, some interesting observations can be made regarding the regioselectivity of fluoride abstraction. First, this process always appears to occur from the end of the fluoroolefin adjacent to the methyl ligand. Using the simplified concept that the lability of the α-fluorine in fluoroalkyl groups results from back donation from the metal into C-F σ^* orbitals, the greater donor ability of the methyl group could account for this trend. Second, in the case of fluoride abstraction from the trifluoroethylene-bridged species only the *cis*-difluorovinyl isomer is observed, when in principle both *cis* and *trans* should be possible. This is consistent with the well established 'cis effect', in which the *cis* isomer is thermodynamically favored over the *trans* isomer, for vicinally substituted ethylenes with electronegative atoms.[36]

While it may not be as surprising that MeSiOTf, a strong fluorophile, succeeded in abstracting a fluoride ion from all fluoroolefin-bridged species, even the related protic acid, triflic acid, was able to effect this transformation. More interesting yet was the relatively clean fluoride ion abstraction that was effected via the addition of water to the bridging trifluoro- and difluoroethylene complexes. In the case of trifluoroethylene, the product is the hydroxide analogue of the triflate product, which differs from the latter owing to a minor rearrangement that has occurred (Scheme 2.18).

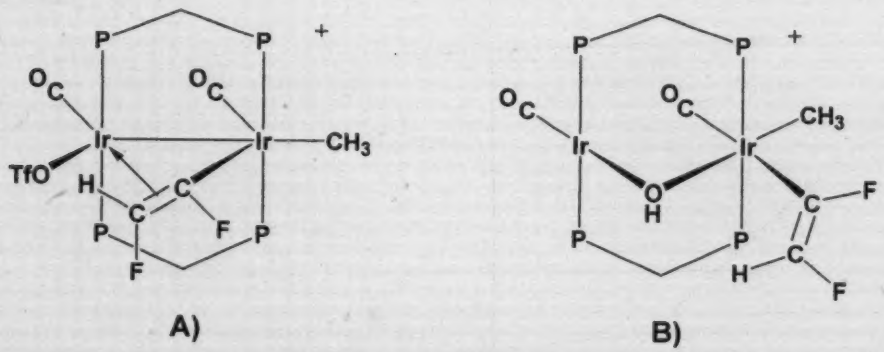

Scheme 2.18. *Effect of trilfate ion displacement by hydroxide in difluorovinyl complex* **A)** *difluorovinyl-bridged* **B)** *terminal difluorovinyl*

We propose that the hydroxide, being a superior bridging group to either the triflate or difluorovinyl groups, displaces the latter from the bridging site, generating an isolable η^1-trifluorovinyl methyl compound. This is clearly related to the triflate complex (**A**) via a partial "merry-go-round" motion of the ligands, in the equatorial plane, that brings OH^- to the bridging site accompanied by movement of the fluorovinyl group to a terminal position.

While the analogous reaction with the 1,1-difluoroethylene-bridged complex presumably operates via a similar mechanism, yielding a monofluorovinyl intermediate, assumed to have a geometry like that of (**B**), in this case, further reactivity is observed, with the generation of 2-fluoropropene, via reductive

elimination of the methyl moiety and fluorovinyl fragments, leaving the previously characterized hydroxy-bridged compound, $[Ir_2(CO)_2(\mu\text{-}OH)(dppm)_2][CF_3SO_3]$.[27] The failure of the related difluorovinyl complex to undergo reductive elimination of cis-difluoropropene, even upon heating, is of some surprise, however this may be the result of a stronger metal-carbon bond attributable to the presence of the second fluorine atom on the adjacent vinylic carbon.

2.5. Conclusions

We have clearly established a role played by adjacent metals in the activation of fluoroolefins. It was found that only those fluoroolefins possessing a geminal difluoro group formed bridging-fluoroolefin complexes, in which the substrate is bound in a bridging position, between the two metals. Only in these bridging-fluoroolefin complexes were we able to effect C-F bond activation via fluoride-ion abstraction. No fluoride abstraction is seen in the terminally bound fluoroolefin complex studied, suggesting that activation is promoted via the bridging arrangement, and is due to metal-metal cooperativity at work in the system. These abstractions are regioselective and only a single fluorovinyl isomer is observed in the three cases studied (1,1-difluoroethylene, trifluoroethylene, and tetrafluoroethylene), resulting from the abstraction of fluoride ions from the carbon of the bridged-fluoroolefin that is adjacent to the iridium-bound methyl group. We have also established ^{19}F coupling parameters, allowing the characterization of the resulting fluorovinyl orientation as either bridging *vs.* terminal, and will subsequently compare the reactivity differences between the two different binding modes. In the next chapter we propose to investigate the propensity for further C-F activation in the newly generated fluorovinyl complexes, and to further explore their reactivity potential.

2.6. References

1) Relevant Reviews: a) J.L. Kiplinger, T.G. Richmond, C.E. Osterberg, *Chem. Rev.* **1994**, *94*, 373-431; b) J. Burdeniuc, B. Jedlicka, R.H. Crabtree, *Chem. Ber. Recl.* **1997**, *130*, 145-154; c) T.G. Richmond, *Topics Organomet. Chem.* **1999**, *3*, 243-269; d) T.G. Richmond, *Angew. Chem.* **2000**, *112*, 3378-3380; *Angew. Chem. Int. Ed.* **2000**, *39*, 3241-3244; e) T. Braun, R.N. Perutz, *Chem. Commun.* **2002,** 2749-2757; f) U. Mazurek, H. Schwartz, *Chem. Commun.* **2003**, 1321-1326; g) W. Jones, *Dalton Trans.* **2003**, 3991-3995; h) H. Torrens, *Coord. Chem. Rev.* **2005**, *249*, 1957-1985; i) R.N. Perutz, T. Braun, *Comprehensive Organometallic Chemistry* III, Chapter 1.26, eds: R.H. Crabtree, D.M.P. Mingos, Elsevier, New York, 2007.

2) A.R. Ravishankara, S. Solomon, A.A. Turnipseed, R.F. Warren, *Science* **1993**, *259*, 194-199.

3) a) T. Hiyama, *Organofluorine Compounds*, Springer, Berlin, 2000. b) *Organofluorine Chemistry: Principles and Commercial Applications*, eds. R.E. Banks, B.E. Smart and J.C. Tatlow, Plenum, New York, 1994.

4) D.A. Dixon, B.E. Smart, P.J. Krusic, N.J. Matsuzawa, *Fluorine Chem.* **1995**, *72*, 209-214.

5) B. E. Smart, *The Chemistry of Functional Groups, Supplement D*, Chapter 14, eds. S. Patai and Z. Rappoport, John Wiley and Sons, Chichester, U.K. 1983.

6) a) S.A. Garratt, R.P. Hughes, I. Kovacik, A.J. Ward, S. Willemsen, D. Zhang, *J. Am. Chem. Soc.* **2005**, *127*, 15585-15594. b) A.K. Burrell, G.R. Clark, C.E.F. Rickard, W.R. Roper, *J. Organomet. Chem.* **1994**, *482*, 261-269. c) R.P. Hughes, R.B. Laritchev, J. Yuan, J.A. Golen, A.N. Rucker, A.L. Rheingold, *J. Am. Chem. Soc.* **2005**, *127*, 15020-15021.

7) a) M.J.S. Dewar, *Bull. Soc. Chim. Fr.* **1951**,*18*, C71. b) J. Chatt, L.A. Duncanson, *J. Chem. Soc.* **1953**, 2939.

8) D. Ristic-Petrovic, D.J. Anderson, J.R Torkelson, R. McDonald, M. Cowie, *Organometallics* **2003**, *22*, 4647-4657.

9) J.J. Bonnet, R. Mathieu, R. Poilblanc, J.A. Ibers, *J. Am. Chem. Soc.* **1979**, *101*, 7487-7496.

10) A. C. Cooper, J. C. Huffman, K. G. Caulton *Inorg. Chim. Acta.* **1998**, *5*, 261-272.

11) A. Svetlanova-Larsen, J. L. Hubbard, *Inorg. Chem.* **1996**, *33*, 3073-3076 and references cited therein.

12) R.N. Haszeldine, B.R. Steele, *J. Chem. Soc.* **1957**, 2800-2806.

13) J.D. Lazerte, L.J. Hals, T.S. Reid, G.H. Smith. *J. Am. Chem. Soc.* **1953**, *75*, 4525-4528.

14) J.R. Torkelson, F.H. Antwi-Nsiah, R. McDonald, M. Cowie, J.G. Pruis, K.J. Jalkanen, R.L. DeKock, *J. Am. Chem. Soc.* **1999**, *121*, 3666-3683.

15) D.S.A. George, R. W. Hilts, R. McDonald, M. Cowie, *Inorg. Chim. Acta.* **2000**, *300*, 353-358.

16) J. R. Torkelson, Ph. D Thesis, University of Alberta, Edmonton, Alberta, 1998.

17) H. A. Bent, *Chem. Rev.* **1961**, *61*, 275.

18) C. H. Dungan, J. R. Van Wazer, *Compilation of reported ^{19}F NMR chemical shifts, 1951 to mid-1967*, Wiley-Interscience, New York, 1970.

19) C. Elsenbroich, A. Salzer, *Organometallics: A Concise Introduction*, VCH, Weinheim, Germany, **1989**, 298.

20) F. Antwi-Nsiah, M. Cowie. *Organometallics* **1992**, *11*, 3157.

21) a) A. K. Brisdon, I. R. Crossley, R. G. Pritchard, J. E. Warren, *Inorg. Chem.* **2002**, *41*, 4748-4755. b) D. Ristic-Petrovic, M. Wang, R. McDonald, M. Cowie. *Organometallics* **2002**, *21*, 5172-5181; and references cited therein.

22) H. C. Clark, J. H. Tsai, *Inorg. Chem.* **1966**, *5*, 1407-1415.

23) D. Huang, P.R. Koren, K. Folting, E.R. Davidson, K.G. Caulton, *J. Am. Chem. Soc.* **2000**, *122*, 8916-8931.

24) W. Schulze; K. Seppelt, *Inorg. Chem.* **1988**, *27*, 3872-3873.

25) B.P. Patel, R.H. Crabtree, *J. Am. Chem. Soc.* **1996,** *118,* 13105-13106.

26) M. Y. DeWolf, J. D. Baldeschwieler, *J. Molec. Spec.* **1964**, *13*, 344-359.

27) B.R. Sutherland, Ph. D Thesis, University of Alberta, Edmonton, Alberta, 1984. B.R. Sutherland, M. Cowie, *Organometallics* **1985**, *4*, 1637-1648.

28) D. Ristic-Petrovic, D.J. Anderson, J.R Torkelson, R. McDonald, M. Cowie, *Organometallics* **2005**, *24*, 3711-3724.

29) D. L. Cedeno, E. Weitz, *J. Phys. Chem.* **2001**, *105*, 8077-8085.

30) J.E. Huheey, E.A. Keiter, R.L. Keiter, *Inorganic Chemistry, Principles of Structure and Reactivity*, 4th ed.; Harper Collins, New York, 1993.

31) J. R. Lacher, H.A. Skinner, *J. Chem. Soc.* A. **1968**, 1034.

32) P.D. Bartlett, R.C. Wheland, *J. Am. Chem. Soc.* **1972,** *94,* 2145-2146.

33) J.J. Bonnet, R. Mathieu, R. Poilblanc, J.A. Ibers, *J. Am. Chem. Soc.* **1979,** *101,* 7487-7496.

34) H. C. Clark, J. H. Tsai, *Inorg. Chem.* **1966**, *5*, 1407-1415.

35) a) A. N. Nesmeyanov, M. I. Rybinskaya, L. V. Rybin, V. S. Kaganovich, P. V. Petrovskii, *J. Organomet. Chem.* **1971**, *31*, 257-267. b) H.C Clark, W.S. Tsang, *J. Am. Chem. Soc.* **1967,** *89,* 533-539. c) A.M. Ihrig, S.L. Smith, *J. Am. Chem. Soc.* **1972,** *94,* 34-41.

36) R.C. Bingham, *J. Am. Chem. Soc.* **1976,** *98,* 535.

Chapter 3

Reactivity of Fluorovinyl Complexes *

3.1. Introduction

In Chapter 2 the transformation of fluoroolefins that bridged two metal centers into the corresponding fluorovinyl products was described, and the unique reactivity of these bridging fluoroolefins over the terminally bound analogues was demonstrated. In this chapter we set out to study the reactivity of these fluorovinyl groups and to determine if the bridging and terminal coordination modes of these groups also give rise to reactivity differences.

One of the principal goals of these investigations was to transform fluoroolefins into derivative olefins through substitution of one or more fluorines by either a hydrogen atom or a methyl group. Having effected the first step - the regioselective removal of a fluoride ion from the olefin - it remained to generate the new olefin. This may be accomplished by either of two ways; through hydrogenolysis of the iridium-fluorovinyl bond, eliminating the hydrogen-substituted fluoroolefin, or by reductive elimination of the adjacent fluorovinyl and methyl ligands generating the corresponding fluoropropene.

A second goal of this chapter was to effect subsequent fluoride removal from the fluorovinyl groups, which would constitute removal of a second fluoride from the precursor fluoroolefin-bridged complexes. Two questions were obvious in this second fluoride abstraction: (1) which carbon-fluorine bond would be activated in this process, and (2) would a bridging fluorovinyl group be more prone to fluoride ion abstraction than a terminally bound group? Removal of the remaining α-fluorine on the fluorovinyl group would yield the corresponding vinylidene product while removal of a β-fluorine would yield a fluoroalkyne, as shown for the trifluorovinyl group in Scheme 3.1.

---

* A portion of this work has been published. J. Anderson, R. McDonald, M. Cowie. *Angew. Chim. Int. Ed.* **2007**, *46*, 3741.

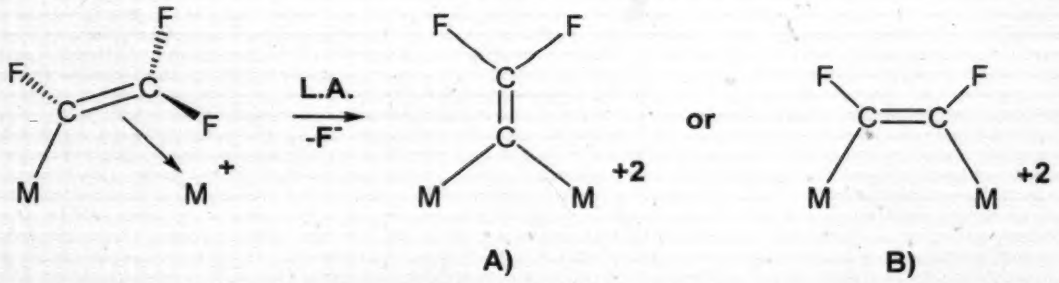

Scheme 3.1. *Potential products from the removal of fluoride ion from fluorovinyl compound generating:* **A)** *fluorovinylidene or* **B)** *fluoroalkyne groups*

Subsequent hydrogenolysis of these products would generate geminal and cis-substituted olefins, respectively, expanding the degree and variation of accessible fluoroolefin derivatives.

In this chapter, our preliminary studies on the reactivity of the fluorovinyl compounds are reported, with emphasis on hydrogenolysis of the remaining fluorovinyl fragment, and on carbon-carbon bond formation reactions, towards the substitution of one or more fluorine substituents by hydrogen or methyl groups.

3.2. Experimental

3.2.1. General Comments. All solvents were dried (using appropriate drying agents), distilled before use and stored under dinitrogen. Deuterated solvents used for NMR experiments were freeze-pump-thaw degassed (three cycles) and stored under nitrogen or argon over molecular sieves. Reactions were carried out under argon using standard Schlenk techniques, and compounds that were obtained as solids were purified by recrystallization. Prepurified argon, nitrogen and hydrogen gases were purchased from Linde, and carbon-13 enriched CO (99%) was supplied by Isotec Inc. All purchased gases were used as received.

All other reagents were obtained from Aldrich and were used as received (unless otherwise stated). Compounds **5-8** were prepared as previously reported in Chapter 2. The compound $[Ir_2(CH_3)(CO)(\mu\text{-}CO)(dppm)_2][CF_3SO_3]$ (**1**) was prepared as previously reported,[1] with the perdeuteromethyl analogue, **1-d_3**, being prepared by the reaction of methyl-d_3 trifluoromethanesulfonate with $[Ir_2(CO)_3(dppm)_2]$.

Proton NMR spectra were recorded on Varian Unity 400, 500 or 600 spectrometers, or on a Bruker AM400 spectrometer. Carbon-13 NMR spectra were recorded on Varian Unity 400 or Bruker AM300 spectrometers. Phosphorus and fluorine NMR spectra were recorded on Varian Unity 400 or Bruker AM400 spectrometers. Two-dimensional NMR experiments (COSY, ROESY, TOCSY and ^{13}C-^{1}H HMQC) were obtained on Varian Unity 400 or 500 spectrometers.

3.2.2. Preparation of Compounds

3.2.2.1. Addition of Hydrogen to Fluorovinyl Complexes

In a typical experiment, 50 mg (~0.033 mmol) of the appropriate fluorovinyl complex, was dissolved in 0.7 mL of CD_2Cl_2 in an NMR tube at -78 °C. To this solution was slowly added a stoichiometric excess, between 3 and 5 equivalents, of gaseous hydrogen by means of a gas-tight syringe. NMR spectra (^{31}P, ^{1}H, ^{13}C and ^{19}F) were recorded from -80 °C to ambient temperature in 20 °C intervals. NMR spectroscopy has been used in the characterization of all observable transient intermediates (**10** and **12, 13**) from the reaction of hydrogen with the tri- and difluorovinyl complexes (**6** and **7**, respectively), as is described in the following Results section. The relative instability of the monofluorovinyl compound **8** at temperatures above 0 °C, along with our inability to isolate a pure sample, has prevented its investigation under these conditions. The subsequent isolable products (**11** and **14**, respectively) along with the final metal-containing

product in both instances, the previously isolated tetrahydride complex $[Ir_2(H)_2(CO)_2(\mu\text{-}H)_2(dppm)_2]^{+2}$,[2] have been further characterized, the latter by X-ray crystallography (*vide infra*). Identification of the fluoroolefin products generated was established by spectral comparison to the known compounds.[3]

The complete spectral results for all compounds observed are summarized in Tables 3.1 – 3.3.

(a) $[Ir_2(\eta 1\text{-}C_2F_3)(H)(CO)_2(\mu\text{-}H)_2(dppm)_2][CF_3SO_3]_2$ (11). Compound **6**, $[Ir_2(\eta^1\text{-}CF{=}CF_2)(OTf)(CO)_2(\mu\text{-}CH_2)(\mu\text{-}H)(dppm)_2][CF_3SO_3]$, (50 mg, 0.031 mmol) was dissolved in 5 mL of dichloromethane at -78 °C, and hydrogen gas was passed through the solution for 30 s at a rate of approximately 0.1 mL / s. As the pale yellow solution was warmed to ambient temperature and stirred closed for 3 h, a lightening of the solution became apparent. 10 mL of Et_2O was added to precipitate a very pale yellow, barely off-white, microcrystalline powder. The product was washed twice with 10 mL of Et_2O, the supernatant decanted, and then the solid was dried briefly under a stream of argon and then *in vacuo* giving 28 mg of spectroscopically pure compound **11** (67% yield). HRMS *m/z* calcd for $Ir_2P_4O_2C_{54}H_{46}F_3$ $[M\text{-}H^+]^+$: 1293.1654. Found: 1293.1656. **Low temperature reaction profile**: When this reaction was monitored spectroscopically, at 0 °C, a set of resonances was apparent in the ^{31}P NMR spectrum, corresponding to the intermediate compound $[Ir_2(\eta^1\text{-}CF{=}CF_2)(H)(CO)_2(\mu\text{-}CH_2)(\mu\text{-}H)(dppm)_2][CF_3SO_3]_2$ (**10**), which upon subsequent cooling to -80 °C, displayed additional resonances attributable to the isomer **10a** (see Results section for a full discussion of the NMR spectra).

Table 3.1. NMR Data for the Compounds of the Hydrogenolysis Reactions [a, b]

compounds[c]	$\delta(^{31}P\{^1H\})$[d]	$\delta(^1H)$[e,f]	$\delta(^{13}C\{^1H\})$[e]	$\delta(^{19}F)$[g]
$[Ir_2(\eta^1\text{-}CF{=}CF_2)(H)(CO)_2(\mu\text{-}CH_2)(\mu\text{-}H)(dppm)_2]^+$ (**10**)	-5.8 (t, $^2J_{PP}$ = 26 Hz, 2P), -13.5 (m, br, 2P)	5.3 (q, 2H, $^3J_{HP}$ = 6.0 Hz), 4.3 (m, 2H), 3.5 (m, 2H), -12 (b, s, 1H), -15 (b, s, 1H)	165 (m), 169 (dt, $^2J_{CP}$ = 18 Hz), 38	-97, -122, -132
$[Ir_2(\eta^1\text{-}CF{=}CF_2)(H)(CO)_2(\mu\text{-}CH_2)(\mu\text{-}H)(dppm)_2]^+$ (**10a**)		See Results section		
$[Ir_2(\eta^1\text{-}CF{=}CF_2)(H)_3(CO)_2(dppm)_2]^{+2}$ (**11**)	-0.0 (t, 2P), -10.0 (t, 2P), ($^2J_{PP}$ = 22 Hz)	5.7 (m, 2H), 5.3 (m, 2H), -10.4 (b, m, 1H), -16.9 (b, s, 1H), -21.6 (m, 1H)	162 (s), 166 (m)	-97, -122, -125
$[Ir_2(CH_3)(H)(CO)_2(\mu\text{-}\eta^1{:}\eta^2\text{-}CF{=}CFH)(dppm)_2]^+$ (**12**)	18.0 (m, 1P), 9.0 (m, 1P), -2.0 (m, 1P), -6.0 (m, 1P)	6.4 (m, 2H), 4.9 (dd, 1H, $^2J_{HF}$ = 63 Hz, $^3J_{HF}$ = 15 Hz), 4.2 (m, 2H), 3.6 (m, 2H), 3.2 (m, 2H), 1.0 (t, 3H, $^3J_{HP}$ = 5.0 Hz), -7.0 (dt, $^2J_{HP}$ = 14.0 Hz, $^3J_{HH}$ = 6.0 Hz, 1H)	175 (b), 179 (b), -21	-60, -173
$[Ir_2(CH_3)(H)_2(CO)_2(\mu\text{-}\eta^1{:}\eta^2\text{-}CF{=}CFH)(dppm)_2]^{+2}$ (**13**)	-13.0 (m, 2P), -15.0 (m, 2P)	5.3 (m, 2H), 4.1 (m, 2H), 0.9 (t, 3H, $^3J_{HP}$ = 5.5 Hz), -11 (t, $^2J_{HP}$ = 12.0 Hz, 1H), -14 (b, s, 1H)	160 (b), 168 (b), -18	-87, -144
$[Ir_2(H)_3(\eta^1\text{-}CF{=}CHF)(CO)_2(dppm)_2]^{+2}$ (**14**)	-2.7 (m, 4P)	5.4 (dd, 1H, $^2J_{FH}$ = 76 Hz, $^3J_{FH}$ = 22 Hz), 4.9 (m, 2H), 4.7 (m, 2H), -10.4 (b, s, 1H), -14.2 (b, s, 1H), -18.2 (b, s, 1H)	159 (b), 166 (b)	-97, -147

[a] NMR abbreviations: s = singlet, d = doublet, t = triplet, m = multiplet, b = broad. [b] NMR data CD_2Cl_2 unless otherwise stated. [c] In all cases trifluoromethanesulfonate is the accompanying anion. [d] $^{31}P\{^1H\}$ chemical shifts are referenced vs. external 85% H_3PO_4 [e] ^1H and ^{13}C chemical shifts are referenced vs. external TMS. [f] Chemical shifts for the phenyl hydrogens are not given in the ^1H data. [g] ^{19}F chemical shifts referenced vs. $CFCl_3$. F-F and F-H coupling constants are reported in the Results section. [k] indicates low temperature data (see Results section)

Table 3.2. NMR Data for the Compounds of the Carbon Monoxide Reactions [a, b]

compounds[c]	$\delta(^{31}P\{^1H\})$[d]	$\delta(^1H)$[e,f]	$\delta(^{13}C\{^1H\})$[e,f]	$\delta(^{19}F)$[g]
$[Ir_2(\eta^1\text{-}CF{=}CF_2)(CO)_3(\mu\text{-}CH_2)(dppm)_2]^+$ (**15**) [k]	-13.0 (b, d, 4P)	6.2 (d, 2H, $^1J_{HC}$ = 148 Hz), 5.6 (m, 2H), 3.8 (m, b, 2H)	158 (b), 162 (b), 184 (b), 50	-95, -122, -125
$[Ir_2(\eta^1\text{-}CF{=}CF_2)(CO)_3(\mu\text{-}H)(\mu\text{-}CH_2)(dppm)_2]^{+2}$ (**16**)	-19.6 (b, s, 4P)	6.0 (q, 2H, $^3J_{HP}$ = 8.0 Hz), 5.0 (m, 2H), 4.5 (m, b, 2H) -14.6 (s, b, 1H)	156 (s), 157 (s), 165 (m), 44	-95, -119
$[Ir_2(CH_3)(CO)_3(\mu\text{-}\eta^1{:}\eta^2\text{-}CF{=}CHF)(dppm)_2]^{+2}$ (**17**)	4.0 (m, 1P), 7.4 (m, 1P), -9.4 (m, 1P), -18.2 (m, 1P)	6.6 (dd, 1H, $^2J_{FH}$ = 64 Hz, $^3J_{FH}$ = 15 Hz), 6.4 (m, 1H), 5.1 (m, 1H), 4.4 (m, 1H), 3.7 (m, 1H), 1.1 (t, b, 3H, $^3J_{HP}$ = 5 Hz)	159 (b), 168 (b), 173 (b), -13	-54, -158
$[Ir_2(CH_3)(CO)_3(\mu\text{-}\eta^1{:}\eta^1\text{-}CF\text{-}CH_2)(dppm)_2]^{+2}$ (**18**)	2.7 (t, $^2J_{PP}$ = 26 Hz, 2P), 16 (t, 2P)	6.3 (dd, 2H, $^2J_{FH}$ = 13.4 Hz), 5.73 (m, 2H), 5.37 m, 2H), 0.4 (t, 3H, $^3J_{HP}$ = 6.6 Hz)	159 (m), 169 (b), 175 (b), -26	-20 (b)
$[Ir_2(\eta^1\text{-}CF{=}CHF)(CO)_4(dppm)_2]^+$ (**19**)	-10.4 (t, $^2J_{PP}$ = 28 Hz, 2P), -17.7 (t, 2P)	3.9 (dd, 2H, $^2J_{FH}$ = 80 Hz, $^3J_{FH}$ = 23 Hz), 4.3 (m, 2H), 3.3 (m, 2H)	194 (b), 178 (t, $^2J_{CP}$ = 10 Hz)	-92 -135

[a] NMR abbreviations: s = singlet, d = doublet, t = triplet, m = multiplet, b = broad. [b] NMR data CD_2Cl_2 unless otherwise stated. [c] In all cases trifluoromethanesulfonate is the accompanying anion. [d] $^{31}P\{^1H\}$ chemical shifts are referenced vs. external 85% H_3PO_4 [e] ^1H and ^{13}C chemical shifts are referenced vs. external TMS. [f] Chemical shifts for the phenyl hydrogens are not given in the ^1H data. [g] ^{19}F chemical shifts referenced vs. $CFCl_3$. F-F and F-H coupling constants are reported in the Results section. [k] indicates low temperature data (see Results section)

Table 3.3. NMR Data of the Fluorovinlylidene Complexes[a, b]

compounds[c]	$\delta(^{31}P\{^1H\})$[d]	$\delta(^1H)$[e,f]	$\delta(^{13}C\{^1H\})$[e]	$\delta(^{19}F)$[g]
$[Ir_2(CH_3)(OTf)(CO)_2(\mu\text{-}C{=}CF_2)(dppm)_2]^{+2}$ (**20**)	-6.2 (t, 2P), -20.6 (t, 2P) ($^2J_{PP}$ = 21.0 Hz)	4.1 (m, 2H), 2.8 (m, 2H), 1.95 (t, 3H, $^3J_{HP}$ = 6.0 Hz)	151 (b), 174 (b), 38	-69, -86, -76 (OTf)
$[Ir_2(CH_3)(OTf)(CO)_2(\mu\text{-}C{=}CFH)(dppm)_2]^{+2}$ (**21**)	-5.0 (t, 2P), -21.0 (t, 2P) ($^2J_{PP}$ = 23.0 Hz)	8.6 (d, 1H, $^2J_{HF}$ = 90 Hz), 4.3 (m, 2H), 2.8 (m, 2H), 2.15 (t, 3H, $^3J_{HP}$ = 9.0 Hz)	153 (b), 176 (b), 41	-107, -76 (OTf)
$[Ir_2(CH_3)(OTf)(CO)_2(\mu\text{-}C{=}CH_2)(dppm)_2]^{+2}$ (**22**)	-10.0 (t, 2P), -20.0 (t, 2P, ($^2J_{PP}$ = 17.0 Hz)	6.01 (s, 1H), 5.99 (s, 1H), 4.1 (m, 2H), 2.9 (m, 2H), 1.35 (t, 3H, $^3J_{HP}$ = 4.9 Hz)	164 (b), 170 (b), 0.2	-77 (OTf)

[a] NMR abbreviations: s = singlet, d = doublet, t = triplet, m = multiplet, b = broad. [b] NMR data CD_2Cl_2 unless otherwise stated. [c] In all cases trifluoromethanesulfonate is the accompanying anion. [d] $^{31}P\{^1H\}$ chemical shifts are referenced vs. external 85% H_3PO_4 [e] ^1H and ^{13}C chemical shifts are referenced vs. external TMS. [f] Chemical shifts for the phenyl hydrogens are not given in the ^1H data [g] ^{19}F chemical shifts referenced vs. $CFCl_3$. F-F and F-H coupling constants are reported in the Results section.

(b) **$[Ir_2(\eta 1\text{-}C_2F_2H)(H)(CO)_2(\mu\text{-}H)_2(dppm)_2][CF_3SO_3]_2$ (14).** Compound **7**, $[Ir_2(CH_3)(OTf)(CO)_2(\mu\text{-}\eta^1\text{:}\eta^2\text{-}CF{=}CFH)(dppm)_2][CF_3SO_3]$, (50 mg, 0.032 mmol) was dissolved in 5 mL of CH_2Cl_2 at -78 °C, and hydrogen gas passed through the solution at a rate of approximately 0.1 mL / s for 30 s, whereupon the mixture was allowed to warm gradually. After the resulting pale yellow solution was stirred closed, at room temperature for 3 h, the solution was back-filled with argon and 10 mL of Et_2O was added to precipitate a pale, off-white microcrystalline compound **14**. The product was washed twice with 10 mL of Et_2O, the supernatant decanted, and then the solid was dried briefly under a stream of argon and then *in vacuo* (70% yield). HRMS *m/z* calcd for $Ir_2P_4O_2C_{54}H_{47}F_2$ $[M\text{-}H^+]^+$: 1256.2852. Found: 1256.2854. **Low temperature reaction profile**: At 0 °C, when this reaction was monitored by NMR spectroscopy, a new set of resonances were displayed in the ^{31}P NMR spectrum, corresponding to the compound $[Ir_2(CH_3)(H)(CO)_2(\mu\text{-}\eta^1\text{:}\eta^2\text{-}CF{=}CFH)(dppm)_2][CF_3SO_3]$ (**12**). At temperatures above 0 °C, this species subsequently transformed into the next spectroscopically observed intermediate, $[Ir_2(H)_2(CH_3)(CO)_2(\mu\text{-}\eta^1\text{:}\eta^2\text{-}CF{=}CFH)(dppm)_2][CF_3SO_3]_2$ (**13**) (see Results section for a full discussion of the NMR spectra).

3.2.2.2. Addition of Carbon Monoxide to Fluorovinyl Complexes

(c) **$[Ir_2(\eta 1\text{-}C_2F_3)(CO)_3(\mu\text{-}CH_2)(\mu\text{-}H)(dppm)_2][CF_3SO_3]_2$ (16).** Compound **6** (50 mg, 0.031 mmol) was dissolved in 10 mL of dichloromethane, at -20 °C, and CO was passed through the solution for 30 s at a rate of 0.1 mL / s, giving a distinct darkening of the yellow solution. The resulting mixture was allowed to warm to room temperature, while stirring for ½ h under CO. The yellow solution was then reduced *in vacuo* to *ca.* 5 mL

and Et_2O was added to precipitate a pale yellow microcrystalline compound **16**. The product was washed twice with 10 mL of Et_2O, the supernatant decanted, and the solid was dried briefly under a stream of argon and then *in vacuo* (89% yield). Compound **16** could also be produced by the reaction of one equivalent of Me_3SiOTf with $[Ir_2(CH_3)(CO)_3(\mu\text{-}C_2F_4)(dppm)_2][CF_3SO_3]$ (the tricarbonyl analogue of compound **2** – see chapter 2). Anal. Calcd. for $Ir_2S_2P_4F_9O_9C_{58}H_{47}$: C, 42.65; H, 2.90. Found: C, 42.95; H, 3.16%. **Low temperature reaction profile**: When the reaction was investigated by NMR spectroscopy, the appearance a new set of resonances in the $^{31}P\{^1H\}$ NMR spectrum is apparent at -20 °C corresponding to the new tricarbonyl compound $[Ir_2(\eta^1\text{-}CF{=}CF_2)(CO)_3(\mu\text{-}CH_2)(dppm)_2][CF_3SO_3]$ **(15)** (see Results section for a full discussion of the NMR spectra).

(d) **$[Ir_2(CH_3)(CO)_3(\mu\text{-}\eta1{:}\eta2\text{-}C_2F_2H)(dppm)_2][CF_3SO_3]_2$ (17).** 50 mg of compound **7** (0.032 mmol) was dissolved in 10 mL of CH_2Cl_2 and CO was passed through the solution for 30 s at a rate of 0.1 mL / s. The resulting yellow solution was stirred for ½ h, reduced *in vacuo* to *ca.* 5 mL and Et_2O was added to precipitate a pale yellow microcrystalline compound **17**. The product was washed twice with 10 mL of Et_2O, the supernatant decanted, and then the solid was dried briefly under a stream of argon and then *in vacuo* giving 38 mg of spectroscopically pure compound (74% yield). MS: *m/z* 644.1 $(M\text{-}CO)^{+2}$ If compound **17** was left under an atmosphere of CO overnight a subsequent elimination of *cis*-difluoropropene (along with its isomer 2,3-difluoropropene) ensued, leaving behind, exclusively, the previously characterized compound $[Ir_2(CO)_5(dppm)_2][CF_3SO_3]_2$.[4]

(e) **$[Ir_2(CH_3)(CO)_3(\mu\text{-}\eta1{:}\eta1\text{-}CFCH_2)(dppm)_2][CF_3SO_3]_2$ (18).** To a 1:1 mixture of **8,** $[Ir_2(CH_3)(OTf)(CO)_2(\mu\text{-}\eta^1{:}\eta^2\text{-}C_2FH_2)(dppm)_2][CF_3SO_3]$, and **4a,** $[Ir_2(CH_3)(CO)_2(\eta^2\text{-}CH_2{=}CF_2)(dppm)_2][CF_3SO_3]$, in 0.7 mL of CD_2Cl_2 in

an NMR tube at -40 °C, was added 3 mL of CO via a gas-tight syringe. As the temperature was raised to 0 °C, the orange solution turned yellow coinciding with the reaction of CO with **8** to produce compound **18**, along with the regeneration of **1** (from **4a**) which subsequently reacted with CO to give the previously characterized $[Ir_2(CH_3)(CO)_4(dppm)_2][CF_3SO_3]$.[5] Left overnight under an atmosphere of CO, compound **8** showed quantitative conversion by NMR spectroscopy, to $[Ir_2(CO)_5(dppm)_2]^{+2}$, as above, with the concurrent liberation of 2-fluoropropene.

(f) **$[Ir_2(\eta 1\text{-}C_2F_2H)(CO)_4(dppm)_2][CF_3SO_3]$ (19).** Compound **9** $[Ir_2(CH_3)(\eta^1\text{-}CF=CFH)(CO)_2(\mu\text{-}OH)(dppm)_2][CF_3SO_3]$ (50 mg, 0.030 mmol) was dissolved in 2 mL of THF and stirred overnight at ambient temperature, under a static atmosphere of CO. After 18 h, a precipitate was visible, and the accompanying solution was slightly brighter yellow in color than the precursor. The supernatant was decanted, the residual yellow solid was washed twice with 10 mL of Et_2O, and dried briefly under a stream of argon and then *in vacuo* giving 32 mg of spectroscopically pure compound **19** (72% yield). Anal. Calcd. for $Ir_2SP_4F_5O_7C_{57}H_{45}$: C, 46.34; H, 3.07. Found: C, 46.12; H, 3.39%.

3.2.2.3. Addition of Me_3SiOTf to Fluorovinyl Complexes

(g) **$[Ir_2(CH_3)(OTf)(CO)_2(\mu\text{-}C=CF_2)(dppm)_2][CF_3SO_3]_2$ (20).** 30 µL of neat Me_3SiOTf (0.155 mmol) was added dropwise to a solution of compound **5**, $[Ir_2(CH_3)(OTf)(CO)_2(\mu\text{-}\eta^1\text{:}\eta^2\text{-}CF=CF_2)(dppm)_2][CF_3SO_3]$ (50 mg, 0.031 mmol), generated in 7 mL of CH_2Cl_2, and the mixture stirred at room temperature for 1 ½ h. The resulting yellow solution was reduced *in vacuo* to dryness and extracted into 5 mL of benzene. 20 mL of pentane was added to precipitate a pale yellow microcrystalline compound **20**. The product was washed twice with 10 mL of pentane,

the supernatant decanted, and then the solid was dried briefly under a stream of argon and then *in vacuo* (63% yield). Anal. Calcd. for $Ir_2S_3P_4F_{11}O_{11}C_{58}H_{47}$: C, 40.19; H, 2.73. Found: C, 40.40; H, 3.15%.

(h) **$[Ir_2(CH_3)(OTf)(CO)_2(\mu\text{-}C{=}CFH)(dppm)_2][CF_3SO_3]_2$ (21).** Compound **7**, $[Ir_2(CH_3)(OTf)(CO)_2(\mu\text{-}\eta^1{:}\eta^2\text{-}CF{=}CFH)(dppm)_2][CF_3SO_3]$ (50 mg, 0.032 mmol), was dissolved in 7 mL of CH_2Cl_2, to which was added dropwise 30 µL of Me_3SiOTf, and the mixture stirred at room temperature for 1 ½ h. The resulting yellow solution was reduced *in vacuo* to *ca.* 3 mL followed by the addition of 10 mL of pentane, resulting in the precipitation of a pale yellow microcrystalline compound **21**. The product was washed twice with 10 mL of pentane, the supernatant decanted, and then the solid was dried briefly under a stream of argon and then *in vacuo* (61% yield). Anal. Calcd. for $Ir_2S_3P_4F_{10}O_{11}C_{58}H_{48}$: C, 40.61; H, 2.82. Found: C, 40.28; H, 3.18%.

(i) **$[Ir_2(CH_3)(OTf)(CO)_2(\mu\text{-}C{=}CH_2)(dppm)_2][CF_3SO_3]_2$ (22).** 30 µL of Me_3SiOTf was added dropwise to a 1:1 NMR-scale sample (~50 mg of initial precursor) of a mix of compounds **8** and **4a** (*vide supra*) and the mixture left at 0 °C for 1 h. During this time the reaction was monitored spectroscopically, showing the appearance of signals corresponding to compound **22**, along with those of compound **1** (from **4a**) and **8a** (see Chapter 2). Due to its instability at higher temperatures, and subsequent rearrangement to undetermined products, compound **22** has only been spectroscopically characterized at 0 °C.

X-ray Crystallographic Data Collection. Pale yellow crystals of $[Ir_2(H)_2(CO)_2(\mu\text{-}H)_2(dppm)_2][CF_3SO_3]_2$ were obtained via slow diffusion of pentane into a CH_2Cl_2 solution of compound **11** under hydrogen. Crystallographic data are summarized in Table 3.4. The hydrogen atoms (except for hydrido ligand (*vide*

infra)) were generated from geometries of their attached carbon atoms and were assigned thermal parameters of 20% greater than those of the attached carbons. The position of one terminal hydrido ligand was fixed at 1.70 Å during refinement of the positions for the bridging hydrides. The resulting symmetrical structure has an inversion center between the two metals, with each face having a terminal hydride on one metal, a bridging hydride between the two, and a terminal carbonyl on the other metal center.

Table 3.4. Crystallographic Experimental Details for $[Ir_2(H)_2(CO)_2(\mu\text{-}H)_2(dppm)_2][CF_3SO_3]_2$

A. Crystal Data	
formula	$C_{54}H_{48}F_6Ir_2O_8P_4S_2$
formula weight	1511.32
crystal dimensions (mm)	0.58 × 0.32 × 0.22
crystal system	monoclinic
space group	$P2_1/n$ (an alternate setting of $P2_1/c$ [No. 14])
unit cell parameters[a]	
a (Å)	10.8474 (9)
b (Å)	21.306 (2)
c (Å)	12.482 (1)
β (deg)	109.410 (1)
V (Å^3)	2720.9 (4)
Z	2
ρ_{calcd} (g cm^{-3})	1.845
μ (mm^{-1})	5.155
B. Data Collection and Refinement Conditions	
diffractometer	Bruker PLATFORM/SMART 1000 CCD[b]
radiation (λ [Å])	graphite-monochromated Mo Kα (0.71073)
temperature (°C)	–80
scan type	ω scans (0.3°) (15 s exposures)
data collection 2θ limit (deg)	52.84
total data collected	19967 ($-13 \le h \le 13$, $-26 \le k \le 26$, $-15 \le l \le 15$)
independent reflections	5578 (R_{int} = 0.0273)
number of observed reflections (*NO*)	4920 [$F_o^2 \ge 2\sigma(F_o^2)$]
structure solution method	direct methods (*SHELXS–86*[c])

Table 3.4. Crystallographic Experimental Details (continued)

refinement method	full-matrix least-squares on F^2(*SHELXL93*[d])
absorption correction method	multi-scan (*SADABS*)
range of transmission factors	0.3968–0.1540
data/restraints/parameters	5578 [$F_o^2 \geq -3\sigma(F_o^2)$] / 1[e] / 351
goodness-of-fit (*S*)[f]	1.082 [$F_o^2 \geq -3\sigma(F_o^2)$]
final *R* indices[g]	
R_1 [$F_o^2 \geq 2\sigma(F_o^2)$]	0.0236
wR_2 [$F_o^2 \geq -3\sigma(F_o^2)$]	0.0587
largest difference peak and hole	2.564 and –0.548 e Å^{-3}

[a]Obtained from least-squares refinement of 7453 reflections with $4.32° < 2\theta < 52.78°$.

[b]Programs for diffractometer operation, data collection, data reduction and absorption correction were those supplied by Bruker.

[c]Sheldrick, G. M. *Acta Crystallogr.* **1990**, *A46*, 467–473.

[d]Sheldrick, G. M. *SHELXL-93*. Program for crystal structure determination. University of Göttingen, Germany, 1993.

[e]The Ir–H(1) distance was refined with a fixed value (1.70 Å).

[f]$S = [\Sigma w(F_o^2 - F_c^2)^2/(n-p)]^{1/2}$ (n = number of data; p = number of parameters varied; $w = [\sigma^2(F_o^2) + (0.0345P)^2 + 1.0808P]^{-1}$ where $P = [\text{Max}(F_o^2, 0) + 2F_c^2]/3$).

[g]$R_1 = \Sigma||F_o| - |F_c||/\Sigma|F_o|$; $wR_2 = [\Sigma w(F_o^2 - F_c^2)^2/\Sigma w(F_o^4)]^{1/2}$.

3.3. Results and Compound Characterization

3.3.1. Reaction of Fluorovinyl-containing Complexes with Hydrogen

3.3.1.1. $[Ir_2(\eta 1\text{-}C_2F_3)(OTf)(CO)_2(\mu\text{-}CH_2)(\mu\text{-}H)(dppm)_2][CF_3SO_3]$ (6)

Upon addition of hydrogen to compound **6** at 0 °C, a reaction occurs as demonstrated by the slow disappearance of the $^{31}P\{^1H\}$ NMR resonances of compound **6**, and the concomitant appearance of a new set of signals corresponding to the compound $[Ir_2(\eta^1\text{-}CF{=}CF_2)(H)(CO)_2(\mu\text{-}CH_2)(\mu\text{-}H)(dppm)_2][CF_3SO_3]$ **(10)**, as shown in Scheme 3.2.

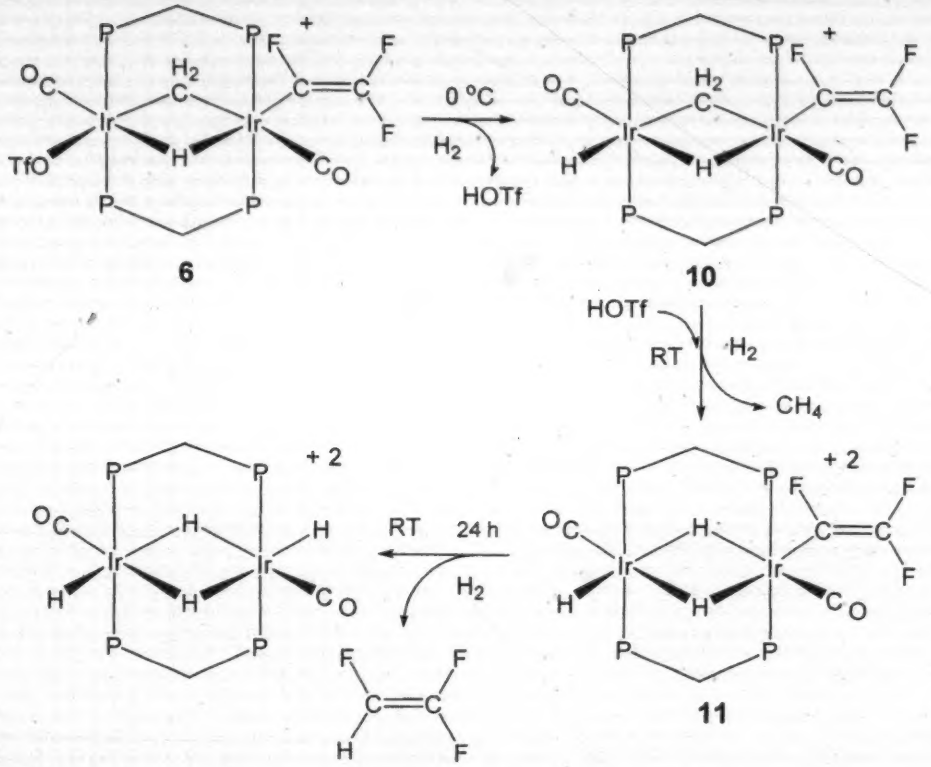

Scheme 3.2. *Reaction of hydrogen with terminal trifluorovinyl compound* ***6***

At 0 °C, this new compound is represented by a pair of pseudo-triplets in the $^{31}P\{^{1}H\}$ NMR spectrum at -5.8 ppm and -13.5 ppm consistent with an AA'BB' spin system, displaying mutual coupling of 26 Hz ($^{2}J_{PP}$). Notably, the latter resonance is much broader than the former at this temperature. In the ^{1}H NMR spectrum, a broad single peak at 12 ppm indicates the presence of triflic acid, which is presumably produced via deprotonation of a dihydrogen ligand,[6] in an unobserved molecular hydrogen adduct, resulting effectively in hydride exchange for the displaced triflate ion. The dppm methylene resonances appear as broad multiplets at 4.3 ppm and 3.5 ppm, while the bridging methylene group appears as a broad quintet at 5.3 ppm ($^{3}J_{HP}$ = 6.0 Hz), displaying equal coupling to all four phosphorus nuclei. The two hydride signals, integrating as one proton each, appear at -12.0 and -15.0 ppm, as broad unresolved singlets.

In the $^{13}C\{^1H\}$ NMR spectrum, two distinct carbonyl resonances are apparent in a ^{13}CO-enriched sample; the first is a broad singlet at 165 ppm, while the second is a doublet of triplets ($^2J_{CP}$ = 9 Hz, $^4J_{CF}$ = 17 Hz) at 169 ppm. Both chemical shifts are very similar to those of compound **6**, again suggesting terminal arrangements. Selective decoupling experiments show that each carbonyl is coupled to different ends of the diphosphine framework, indicating that they are bound to different metals; the high-field carbonyl is coupled to the ^{31}P atoms resonating at -13.5 ppm and the lower-field carbonyl to those at -5.8 ppm. The higher-field carbonyl displays coupling to the same set of ^{31}P nuclei as the higher-field hydride, indicating that these two moieties share the same metal, and are probably in a mutually *trans* arrangement. The ^{13}C-enriched methylene carbon in the product, derived from the $^{13}CH_3$-methyl-enriched precursor, appears as a broad resonance at 38 ppm, the shift of which is consistent with the bridging arrangement of this group.

Notably, the typical down-field resonance associated with the coordinated triflate moiety is absent from the ^{19}F NMR spectrum, which displays the free triflate ion at -79 ppm along with three sets of broad signals appearing at -97 ppm, -122 ppm, and at -132 ppm, corresponding to the trifluorovinyl group. The coupling in these ^{19}F resonances is unresolvable at 0 °C group, but upon cooling this species such information was obtained (*vide infra*).

When cooled to -60 °C, some interesting changes take place in the NMR spectroscopy of compound **10**. In the $^{31}P\{^1H\}$ NMR spectrum, at this temperature, the lower-field resonance remains unchanged, while the higher-field, broad resonance, is resolved into two closely spaced signals, appearing in a 60:40 ratio at -12.4 ppm and -14.2 ppm respectively. Such resolution is also apparent in the hydride signals displayed in the ^1H NMR spectrum, both of which resolve into pairs of signals having the same relative intensities as those of the higher-field phosphines (60:40). The lower-field hydride signal now appears as two closely spaced doublets of triplets ($^2J_{CC}$=28 Hz, $^2J_{CP}$=9 Hz), centered around -12.0 ppm, both of which show coupling to only one side of the diphosphine

framework (-5.8 ppm). Although the other, higher-field signals (-14.9 ppm) remain broad, they do show peak sharpening upon selective decoupling of both sets of phosphorus nuclei. In the ^{19}F NMR spectrum, two distinct sets of doublets of doublets are shown, again in a 60:40 ratio, displaying typical fluorine-fluorine couplings of terminal fluorovinyl groups (see Chapter 2). The first set appears at -97 ppm , -122 ppm and -132 ppm, with the two lower-field resonances showing mutual $^2J_{FF}$ geminal coupling of 90 Hz, while the two higher-field resonances display mutual $^3J_{FF}$ trans coupling of 108 Hz. Characteristic $^3J_{FF}$ cis coupling of 35 Hz is also observed between the resonances at -97 ppm and -132 ppm, confirming the terminal arrangement of the trifluorovinyl moiety. The second set of resolved signals appear at similar chemical shifts to those of the first, resonating at -99 ppm, -126 ppm and -135 ppm, displaying the same type of coupling patterns; ($^3J_{FF}$) trans = 113 Hz, ($^3J_{FF}$) cis = 32 Hz, ($^2J_{FF}$) gem = 90 Hz.

Based on these low temperature NMR data for compound **10**, we propose that two isomers, **10** and **10a**, as shown in the following Figure 3.1, result from the addition of hydrogen to the precursor compound **6**.

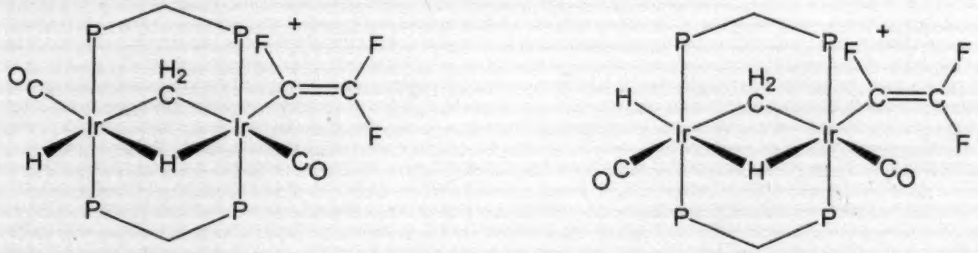

Figure 3.1. *Proposed initial isomers resulting from hydrogen addition to* ***6***

Presumably, these isomers are being produced via a molecular H_2 adduct with a subsequent deprotonation/reprotonation mechanism leading to the observation of two isomers. Since only a single isomeric product is observed in the subsequent reaction, as will be discussed later, we propose that only one of these leads to a productive pathway, or both share a common productive isomer.

Upon warming this mixture of isomers to 0 °C, a further reaction with hydrogen occurs as evidenced in the $^{31}P\{^1H\}$ NMR spectrum by the gradual appearance of a new set of signals at 0.0 ppm and -10.0 ppm, due to compound **11**, along with the concomitant disappearance of the signals due to **10** and **10a**. Interestingly, subsequent reaction of both isomers of **10** generates a single product (**11**). In the ^1H NMR spectrum, along with the disappearance of triflic acid, three distinct hydrides appear in the high-field region, each integrating for a single hydrogen; the first is as a broad multiplet at -10.4 ppm, the next is a broad singlet at -16.9 ppm, and the final appears as a multiplet (virtual septet) splitting pattern at -21.6 ppm. Broad-band and selective $^1H\{^{31}P\}$ experiments demonstrate that the high-field hydride is coupled only to the two adjacent ^{31}P nuclei (0.0 ppm) on one iridium, while the other two show partial coupling to both sides of the diphosphine framework. Methane is also evident as a product of this reaction, as seen in the ^1H NMR spectrum. The $^{13}C\{^1H\}$ NMR spectrum of a ^{13}CO-enriched sample shows two terminal carbonyl resonances as broad multiplets at 162 ppm and 166 ppm. In the ^{19}F NMR spectrum the three anticipated signals appear for the terminal fluorovinyl moiety. The first appears as a doublet of doublets at -97 ppm showing characteristic geminal and cis couplings ($^2J_{FF}$ = 85 Hz, $^3J_{FF}$ = 40 Hz). The second geminal fluorine displays a doublet of doublets at -122 ppm, with mutual coupling of 85 Hz to the first fluorine, and a larger (115 Hz) coupling with the final high-field signal consistent with a trans arrangement between these two ^{19}F nuclei. The final signal at -125 ppm is a resolvable doublet of doublets of doublets ($^3J_{FF}$ = 115 Hz, $^3J_{FF}$ = 40 Hz, $^3J_{FH}$ = 22 Hz). Again, this fluorine shows cis-coupling to the low-field ^{19}F nucleus, in addition to the trans-coupling discussed, however an additional coupling is also apparent due to coupling of this fluorine to the neighboring hydride (-10.4 ppm).

Notably, when the perdeuteromethyl complex is employed as the starting material for this reaction, giving the bridging CD_2 and bridging deuteride groups in $[Ir_2(\eta^1\text{-}CF{=}CF_2)(CF_3SO_3)(CO)_2(\mu\text{-}CD_2)(\mu\text{-}D)(dppm)_2][CF_3SO_3]$ (**6-*d*$_3$**), CD_2H_2 is observed exclusively upon reaction with H_2, with the deuteride ligand remaining

in its bridging position, showing no signs of exchange with any adjacent hydride groups. This suggests that the methylene and hydride groups, that originate from C-H activation of the methyl ligand, do not recombine prior to elimination, presumably because of their placement on opposite sides of the bimetallic core, as shown in the crystal structure of **6** (Chapter 2).

The trihydride species (**11**) may be isolated at this stage, or left in solution to react further with hydrogen gas. Left overnight under an atmosphere of H_2, complete conversion of **11** to the previously characterized[2] $[Ir_2(H)_2(CO)_2(\mu\text{-}H)_2(dppm)_2][CF_3SO_3]_2$ occurs. This reaction involves hydrogenolysis of the trifluorovinyl moiety yielding trifluoroethylene, as observed in the ^{19}F NMR spectrum by characteristic signals at -100 pp, -126 ppm, and -205 ppm. Colorless crystals of $[Ir_2(H)_2(CO)_2(\mu\text{-}H)_2(dppm)_2][CF_3SO_3]_2$, suitable for X-ray diffraction were obtained *via* slow diffusion of *n*-pentane into a dichloromethane solution of the complex. The general structure shows two terminal hydrides, one on each metal and two bridging hydride ligands occupying the region between the bimetallic core. Each metal also has one carbonyl ligand, both of which are arranged on opposite sides of the iridium-phosphorus framework. A representation of this tetrahydride product is shown in Figure 3.2, with relevant structural parameters appearing in Tables 3.5 and 3.6.

Although the structure of this tetrahydride was rather clear on the basis of its spectral parameters, the X-ray structure confirms this and offers structural insight into the nature of the preceding hydride intermediates; in particular, it unambiguously establishes that the mutually trans arrangement of the carbonyls at the adjacent metals.

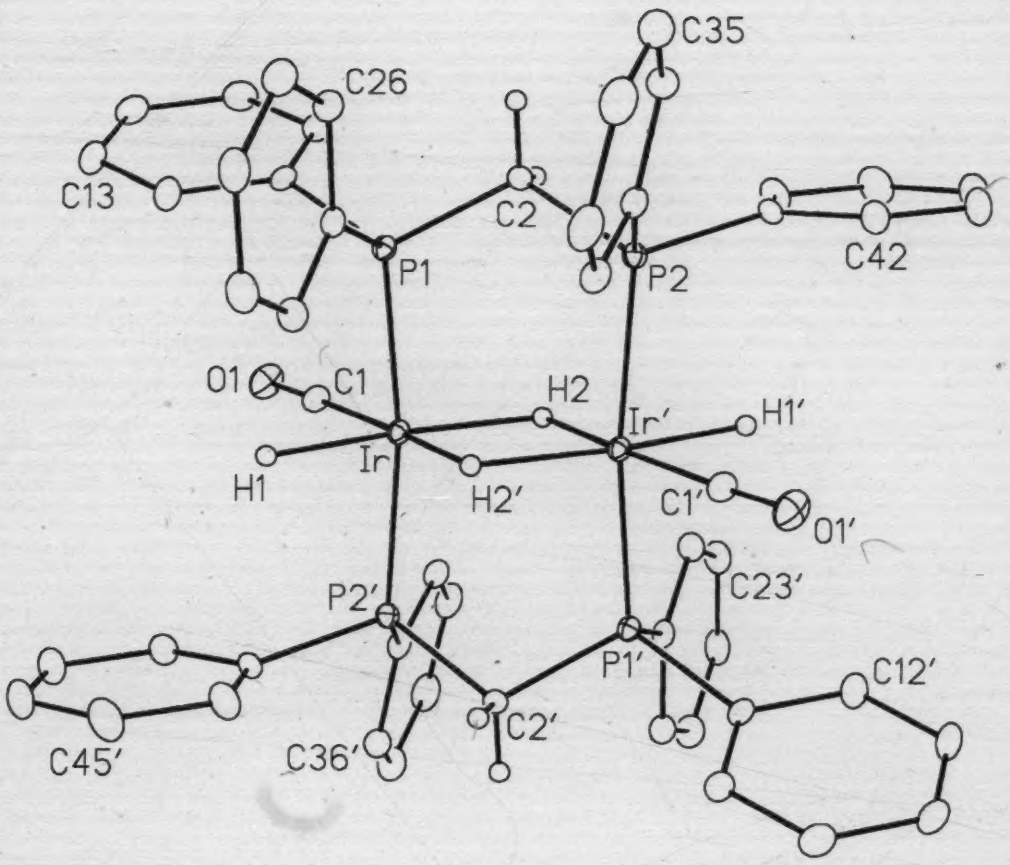

Figure 3.2. *Perspective view of the* $[Ir_2H_2(CO)_2(\mu\text{–}H)_2(dppm)_2]^{+2}$ *complex ion showing the atom labelling scheme. Non-hydrogen atoms are represented by Gaussian ellipsoids at the 20% probability level. Hydrogen atoms are shown with arbitrarily small thermal parameters except for phenyl hydrogens, which are not shown. Primed atoms are related to unprimed ones via the crystallographic inversion center at the midpoint between the pair of iridium atoms.*

Table 3.5. Selected Interatomic Distances (Å) for $[Ir_2H_2(CO)_2(\mu\text{–}H)_2(dppm)_2]^{+2}$

Atom1	Atom2	Distance	Atom1	Atom2	Distance
Ir	Ir'	2.7368(3)	Ir	C(1)	1.893(3)
Ir	P(1)	2.3338(8)	P(1)	P(2)	2.961(1)[b]
Ir	P(2')	2.3448(8)	P(1)	C(2)	1.829(3)
Ir	H(1)	1.70[a]	P(2)	C(2)	1.828(3)
Ir	H(2)	1.85(4)	O(1)	C(1)	1.125(4)
Ir	H(2')	1.75(4)			

Primed atoms are related to unprimed via the crystallographic inversion center (0, 0, 0). [a]Distance fixed during refinement. [b]Nonbonded distance.

Table 3.6. Selected Interatomic Angles (deg) for $[Ir_2H_2(CO)_2(\mu\text{–}H)_2(dppm)_2]^{+2}$

Atom1	Atom2	Atom3	Angle	Atom1	Atom2	Atom3	Angle
Ir'	Ir	P(1)	91.54(2)	Ir	C(1)	O(1)	177.4(3)
Ir'	Ir	P(2')	93.47(2)	P(1)	C(2)	P(2)	108.11(6)
Ir'	Ir	C(1)	142.82(1)	H(1)	Ir	H(2')	94(2)
Ir'	Ir	H(1)	136(2)	H(2)	Ir	H(2')	81(2)
Ir'	Ir	H(2)	39(1)	P(1)	Ir	H(2')	88(1)
Ir'	Ir	H(2')	42(1)	P(2')	Ir	C(1)	90.4(1)
P(1)	Ir	P(2')	170.30(3)	C(1)	Ir	H(2)	103(1)
P(1)	Ir	C(1)	90.6(1)	C(1)	Ir	H(2')	175(1)
P(1)	Ir	H(1)	88(2)	H(1)	Ir	H(2)	174(2)
P(1)	Ir	H(2)	94(1)	H(1)	Ir	H(2')	94(2)
C(1)	Ir	H(2')	175(1)	H(2)	Ir	H(2')	81(2)
H(1)	Ir	H(2)	174(2)	P(2')	Ir	H(1)	82(2)
Ir	P(1)	C(2)	111.03(1)	P(2')	Ir	H(2)	95(1)
Ir'	P(2)	C(2)	112.50(1)	P(2')	Ir	H(2')	90(1)

Primed atoms are related to unprimed via the crystallographic inversion center (0, 0, 0).

3.3.1.2. $[Ir_2(CH_3)(OTf)(CO)_2(\mu\text{-}\eta1\text{:}\eta2\text{-}C_2F_2H)(dppm)_2][CF_3SO_3]$ (7)

The addition of hydrogen to compound **7** at 0 °C gives an immediate reaction as demonstrated by the replacement of the $^{31}P\{^1H\}$ NMR resonances of **7** by a complicated new set of signals, due to $[Ir_2(CH_3)(H)(CO)_2(\mu\text{-}\eta^1\text{:}\eta^2\text{-}CF{=}CFH)(dppm)_2]^+$ (**12**), along with the appearance of a broad single peak at 12 ppm in the ^1H NMR spectrum, indicative of triflic acid (See Scheme 3.3).

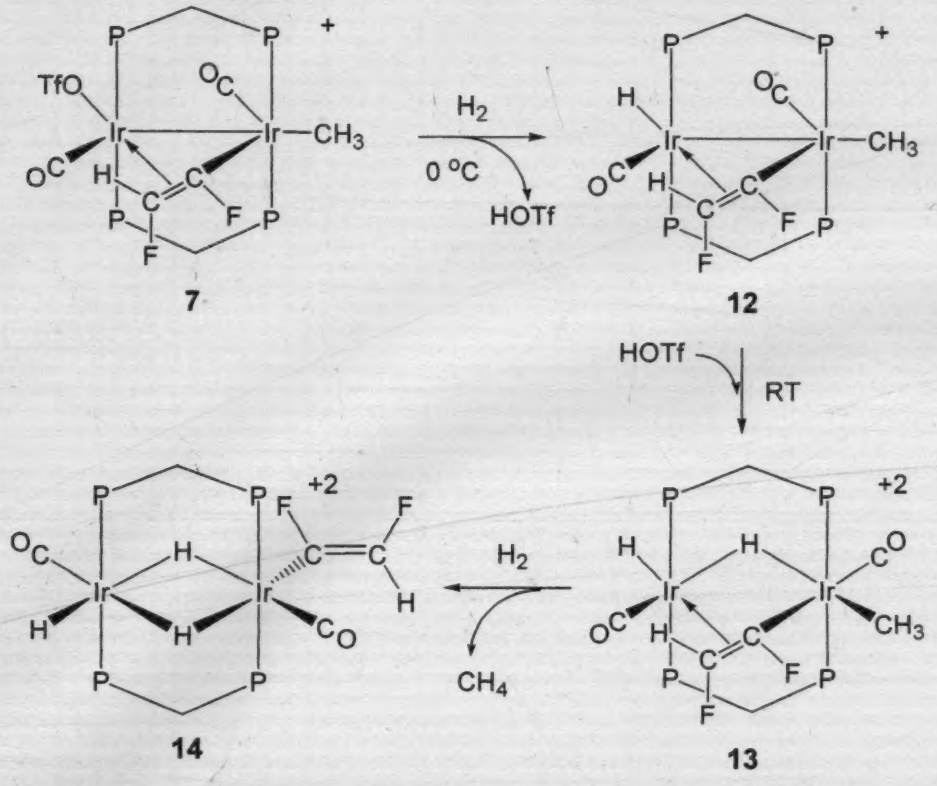

Scheme 3.3. *Reaction of hydrogen with bridging trifluorovinyl compound* **7**

The new compound **(12)** displays an ABCD splitting pattern in the $^{31}P\{^1H\}$ NMR spectrum, displaying complicated multiplets at 18.0 ppm, 9.0 ppm, -2.0 ppm and -6.0 ppm, indicating chemically inequivalent environments for all of the phosphorus atoms. Although no evidence was observed for an initial molecular

H_2 adduct, the presence of triflic acid in the reaction mixture is again presumed to be the result of the deprotonation of such a complex, by the displaced triflate ion, as was postulated in the generation of compound **10** (*vide supra*), and supported by the appearance of a hydride signal in the ^1H NMR spectrum. The new hydride resonance appears at -7.0 ppm as a pseudo doublet of triplets, showing 6 Hz coupling each to the two adjacent non-equivalent phosphorus atoms (-2 ppm and 18 ppm) and coupling to the proton of the bridging vinylic group. The ^1H NMR spectrum also shows the dppm methylene protons as independent multiplets at 6.4 ppm, 4.2 ppm, 3.6 ppm and 3.2 ppm, all integrating for one proton each, while the methyl moiety appears as a pseudo-triplet at 1.0 ppm ($^3J_{HP}$ = 5.0 Hz), showing selective decoupling upon irradiation of the two ^{31}P resonances corresponding to one side of the diphosphine framework (-6 ppm and 9 ppm). The vinylic proton appears as a multiplet at 4.9 ppm, displaying two major resolvable couplings, the largest of which is the $^2J_{HF}$, with a value of 63 Hz, consistent with the geminal coupling of an sp^2 hybridized –C(H)F group[7] (see Chapter 2). The smaller coupling ($^3J_{HF}$ = 15 Hz) confirms that this hydrogen is in a trans arrangement across the vinylic center to the other fluorine, consistent with that seen in the ^{19}F NMR spectrum (*vide infra*). Selective decoupling $^1H\{^{31}P\}$ experiments also indicate that the vinylic proton is coupled to the same two phosphorus nuclei as is the hydride; displaying 4 Hz coupling to the phosphorus at 18.4 ppm and 18 Hz coupling to the phosphorus at -2.0 ppm. Presumably, the larger coupling indicates a pseudo-trans arrangement between the vinylic hydrogen and one of the neighboring phosphorus atoms, while the smaller coupling is due to the corresponding *cis* arrangement with the other. The final coupling is to the hydride (*vide supra*), again suggesting a bridging orientation of this moiety. The $^{13}C\{^1H\}$ NMR spectrum of a ^{13}CO- and $^{13}CH_3$-enriched sample shows two terminal carbonyl resonances at 175 ppm and 179 ppm, while the methyl carbon is a broad singlet at -21 ppm.

In the ^{19}F NMR spectrum of compound **12** there are two signals displaying typical vinyl fluorine-fluorine and fluorine-hydrogen coupling. The first is a doublet of doublets at -60 ppm ($^3J_{FF}$ = 30 Hz, $^3J_{FH}$ = 15 Hz). The next consists of a doublet

of doublet of doublets at -173 ppm, with mutual coupling of 30 Hz to the first fluorine suggesting a cis relationship between the two, and the larger coupling ($^2J_{FH}$ = 63 Hz) to the hydrogen consistent with their geminal arrangement. The latter resonance also displays coupling to phosphorus, and selective decoupling $^{19}F\{^{31}P\}$ experiments show coupling between it and the two adjacent phosphorus coupled to its geminal proton. Such coupling was evident in compound **7** and is again presumed to be indicative of the bridging orientation of the fluorovinyl moiety.

As the temperature is raised to ambient a new set of broad multiplets in the $^{31}P\{^1H\}$ spectrum, appearing at -13.0 ppm and -15.0 ppm, begin to grow at the expense of compound **12**, with concomitant disappearance of the triflic acid resonance in the ^1H NMR spectrum. These data suggest that protonation of **12** by triflic acid occurs, yielding the compound $[Ir_2(H)_2(CH_3)(CO)_2(\mu\text{-}\eta^1\text{:}\eta^2\text{-}CF{=}CFH)(dppm)_2]^{+2}$ (**13**). The ^1H NMR spectrum now shows two new distinct hydrides present in the high-field region; the first appears as a triplet at -11.0 ppm, with $^2J_{HP}$ coupling of 12.0 Hz, to one side of the diphosphine framework, while the other gives a broad, unresolved singlet at -14.4 ppm, that sharpens under broad-band ^{31}P-decoupling. The methyl moiety shows a triplet at 0.9 ppm ($^3J_{HP}$ = 5.5 Hz) in the ^1H NMR spectrum suggesting terminal coordination, and is coupled to the set of ^{31}P nuclei opposite to that of the lower-field hydride. Unfortunately, the vinylic proton was not identified in the ^1H NMR spectrum, possibly being obscured by the dppm phenyl resonances. In a $^{13}CH_3$-enriched sample the methyl carbon resonance is seen in the ^{13}C NMR spectrum at -18 ppm as a broad singlet. A ^{13}CO-enriched sample of **13** shows two independent broad carbonyl resonances at 160 ppm and 168 ppm, suggesting terminal arrangements for these moieties.

In the ^{19}F NMR spectrum the two fluorines appear as a broad multiplet at -87 ppm and a doublet of doublets at -144 ppm. The latter displays two diagnostic couplings ($^2J_{FH}$ = 69, $^3J_{FF}$ = 26 Hz) with the 26 Hz coupling consistent with a cis relationship between the two fluorine atoms, and the larger coupling to the

hydrogen, consistent with their geminal arrangement. The decreased values in both couplings across the π-center, relative to those encountered in a purely terminal arrangement, again suggests that the vinyl moiety may remain in a bridged orientation.

Left under an atmosphere of hydrogen, at ambient temperature, for a prolonged period of time, a subsequent reaction ensues as demonstrated by the gradual appearance of a new broad signal in the $^{31}P\{^1H\}$ NMR spectrum, corresponding to $[Ir_2(\eta^1\text{-}CF{=}CHF)(H)_3(CO)_2(dppm)_2][CF_3SO_3]_2$ **(14)**. This product displays a single complex pattern at approximately -2.7 ppm in the $^{31}P\{^1H\}$ NMR spectrum, with both sides of the phosphorus framework presumably overlapping coincidentally. As observed in the reaction of the trifluorovinyl compound (**7**) with hydrogen, methane is also evident as a product of this reaction in the ^1H NMR spectrum. In this case, however, reactions starting with ***7-d₃***, $[Ir_2(CD_3)(OTf)(CO)_2(\mu\text{-}\eta^1{:}\eta^2\text{-}CF{=}CFH)(dppm)_2][CF_3SO_3]$, lead to the liberation of CD_3H, observed as a doublet ($^2J_{HD}$ = 2 Hz) at 0.2 ppm in the ^2H NMR spectrum. These deuterium (^2H NMR) experiments show that the methyl moiety remains intact throughout the course of the reaction of compound **7** with hydrogen, and is eliminated together with one hydrogen atom, supplied by H_2, as methane. Subsequent addition of hydrogen generates compound **14**, which displays three distinct hydride resonances in the high-field region of the ^1H NMR spectrum, very similar to those of **11**. One hydride appears as a broad multiplet at -10.4 ppm, another is a broad singlet at -14.2 ppm, while the final high-field hydride gives a multiplet splitting pattern at -18.2 ppm. While selective $^1H\ \{^{31}P\}$ decoupling experiments were not possible, due to the overlapping nature of the ^{31}P signals, all hydrides did show partial decoupling upon broad-band irradiation; in particular the high field resonance, which decoupled into a resolvable doublet, displays what is presumably trans coupling to an adjacent bridging hydride ($^2J_{HH}$ = 7 Hz).

The vinylic proton resonance (a doublet of doublets at 5.4 ppm) was identified via its complementary coupling to two characteristic signals in the ^{19}F NMR spectrum, which display typical vinyl fluorine-fluorine and fluorine-hydrogen

coupling. The first is a broad doublet at -97 ppm ($^3J_{HF}$ = 22 Hz), while the next is a broad doublet at -147 ppm ($^2J_{HF}$ = 76 Hz). The larger coupling to to the vinylic proton, in the latter signal, is consistent with their geminal relationship, while the 22 Hz coupling, in the former, is indicative of their *trans* relationship. While the ^{19}F-^{19}F *cis* coupling was not resolvable due to the broadness of the resonances, the values of both observed coupling constants ($^2J_{HF}$ and $^3J_{HF}$) suggests the vinyl moiety is now oriented in a terminal position.

In the ^{13}C NMR spectrum, a ^{13}CO-enriched sample of **14** shows two broad resonances at 159 ppm and 166 ppm, suggesting terminal orientations for both carbonyl groups.

When a sample of **14** is left overnight under an atmosphere of H_2 complete conversion to the previously characterized $[Ir_2(H)_2(CO)_2(\mu\text{-}H)_2(dppm)_2][CF_3SO_3]_2$ (*vide supra*) is observed due to hydrogenolysis of the difluorovinyl moiety and subsequent elimination of *cis*-difluoroethylene (Scheme 3.4) as seen in the ^{19}F NMR spectrum by its resonance at -164 ppm, identifiable through to its reported literature value[3] or comparison to that of an authentic sample.

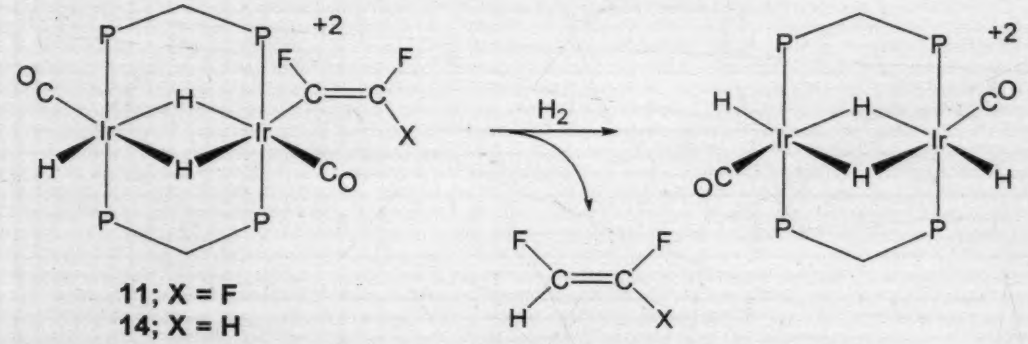

11; X = F
14; X = H

Scheme 3.4. *Reductive elimination of hydrogen-substituted fluorolefins*

Small amounts (*ca.* 10%) of *cis*-difluoropropene (along with the isomer 2,3-difluoropropene (*vide infra*)) are also evident when the reaction of compound **7** with hydrogen is left in a sealed vessel, at ambient temperature, overnight. This

presumably is the result of reductive elimination of the methyl and fluorovinyl groups from compound **13**, however the aforementioned experiments show spectroscopically that methane liberation is preferred over this C-C bond forming process.

No spectral data were available in the literature for *cis*-difluoropropene, thus the identity of this fluoroolefin, along with that of a second observed isomer, 2,3-difluoropropene, is based upon two distinct sets of resonances observed in the ^{19}F NMR, along with their complementary sets of signals in the ^{1}H NMR spectrum, as described below. Notably, the 2,3-difluoropropene is found in a 2:1 ratio to the *cis*-difluoropropene, and is presumed to result from a metal-assisted isomerization of the latter.

The first set of ^{19}F resonances, in the ^{19}F NMR spectrum, appear as complex multiplets at approximately -167.0 ppm and -130.4 ppm, displaying mutual cis-coupling of the ^{19}F nuclei ($^{3}J_{FF}$ = 10 Hz) (see Figure 3.3).

The lower-field signal (-130.4 ppm, Figure 3.3B) also shows additional coupling to the adjacent methyl group protons ($^{3}J_{HF}$ = 17 Hz), as well as a trans-coupling to the olefinic proton ($^{3}J_{HF}$ = 17 Hz), which is observed in the complementary proton signal (*vide infra*). Notably, an additional coupling to the ^{13}C nucleus in the labelled methyl moiety (~10 Hz) is also apparent in this signal, causing a slightly more complex pattern than otherwise expected. Other resolvable couplings in the higher-field multiplet (-167.0 ppm, Figure 3.3A) include a geminal coupling to hydrogen ($^{2}J_{HF}$ = 74 Hz), along with a long-range coupling to the methyl group protons ($^{4}J_{HF}$ = 5 Hz). These data suggest that this pair of ^{19}F resonances correspond to the *cis*-fluoropropene, the formation of which is rationalized on the basis of reductive elimination from the methyl/vinyl complex (**13**). In the ^{1}H NMR spectrum, the olefinic proton signal appears as a doublet of doublets at 6.3 ppm, with values consistent with both the cis- and trans- coupling observed in the ^{19}F NMR experiments. The methyl protons resonate in the region typical for such a group (1.85 ppm), and appear as a doublet of doublets,

displaying the coupling to both fluorine atoms, as described above. In a $^{13}CH_3$-labelled sample this methyl resonance is further split, showing 129 Hz coupling to the attached ^{13}C-nucleus.

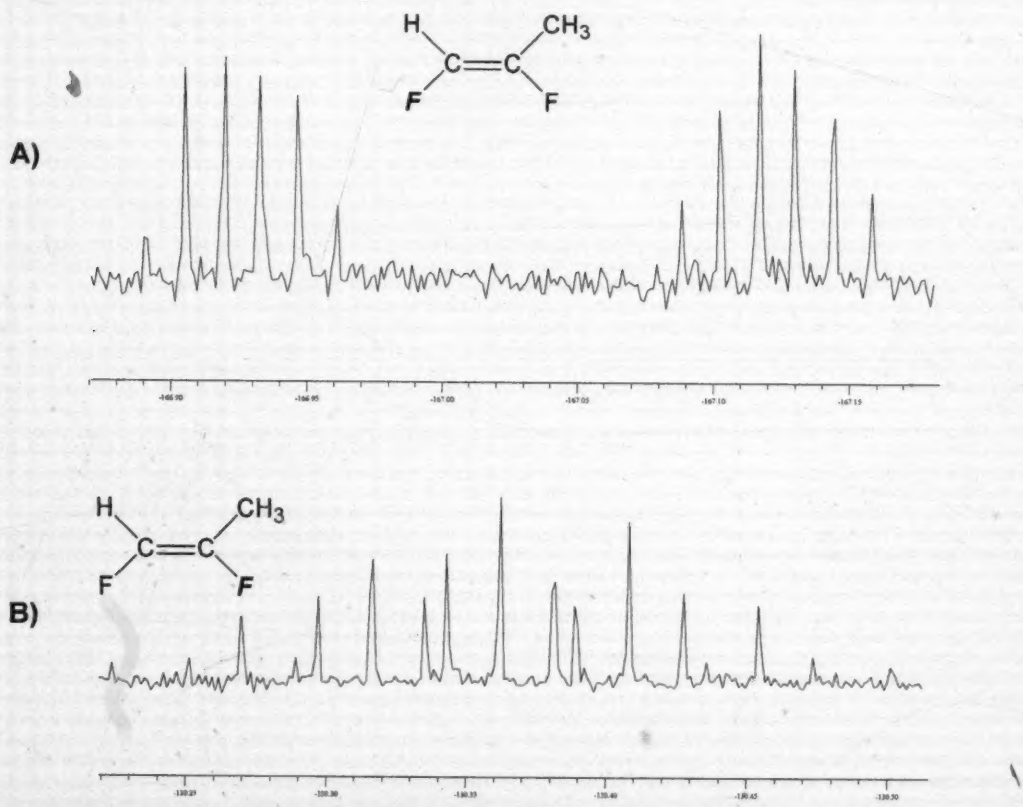

Figure 3.3. *^{19}F NMR resonances for cis-difluoropropene*

Interestingly, an isomer of the *cis*-difluoropropene was also identified in the reaction mixture, corresponding to 2,3-difluoropropene. In this isomer, in which the methyl group in **7** was $^{13}CH_3$-enriched, two downfield resonances are observed in the ^1H NMR spectrum at 4.7 ppm and 4.9 ppm, both showing distinct ^{13}C-coupling of 162 Hz, the increased coupling value and chemical shift of which suggest they are bound to an sp^2 carbon. Both signals appear as doublets of doublets of doublets, with the remaining coupling (other than that to carbon)

being attributable to mutual geminal coupling of 3 Hz, along with a larger (47 Hz) coupling in the higher-field resonance, and a smaller (15 Hz) coupling in the lower-field signal. These latter couplings are to the ^{19}F nucleus on the adjacent carbon, with the larger coupling value corresponding to a trans-arrangement, while the smaller value is consistent with cis-coupling. These data suggest that the *cis*-difluoropropene has undergone, what is effectively, a 1-3 hydride shift, leaving behind an CH_2 center, adjacent to one fluorine atom which remains on an sp^2-carbon, and creating a sp^3-fluoromethyl center (CFH_2) on the distal carbon. The protons on this moiety resonate downfield at 4.8 ppm and appear as a doublet of doublets, showing 45 Hz coupling to the fluorine nucleus on the same

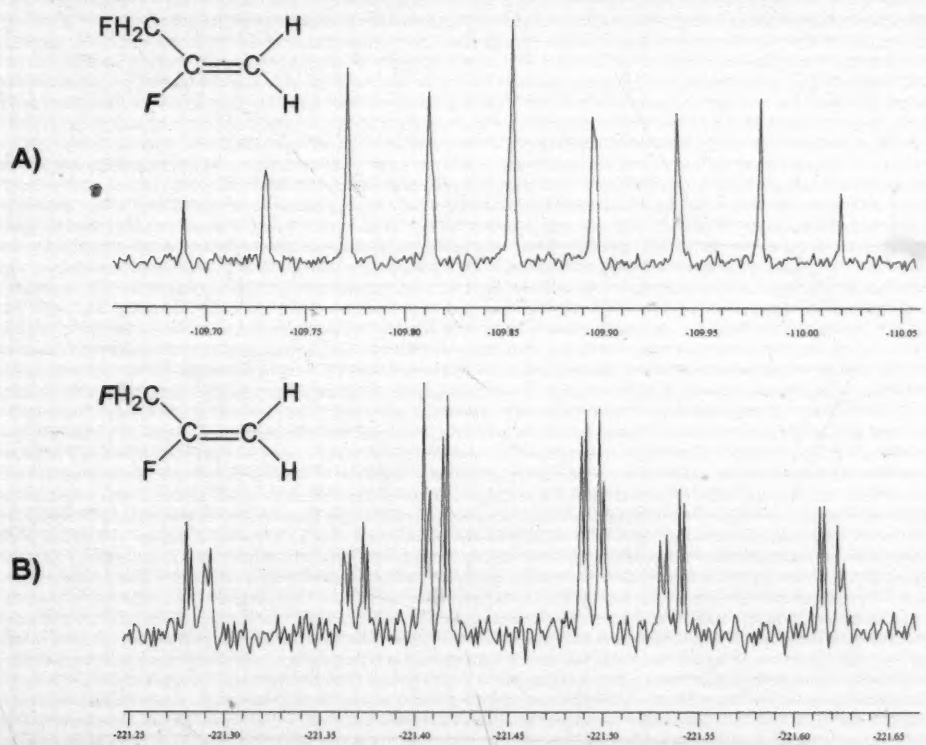

Figure 3.4. *^{19}F NMR resonances for 2,3-difluoropropene*

carbon along with 15 Hz coupling to the adjacent olefinic fluorine. In the ^{19}F NMR spectrum (Figure 3.4), the ^{19}F resonances of 2,3-difluoropropene appear as

complex multiplets at approximately -109.9 ppm and -221.5 ppm, displaying mutual coupling of 30 Hz.

The lower-field ^{19}F NMR signal (-109.9 ppm, Figure 3.4A) shows additional coupling to the adjacent fluoromethyl group protons ($^3J_{HF}$ = 15 Hz), as well as *cis*-coupling to one olefinic proton ($^3J_{FF}$ = 15 Hz), and *trans*-coupling to the other olefinic proton ($^3J_{FF}$ = 47 Hz), all of which are observed in the complementary proton signals (*vide supra*). The higher-field resonance (-221.5 ppm, Figure 3.4B) also displays the complementary ($^2J_{FH}$) coupling to the adjacent methyl proton nuclei (45 Hz) consistent with its position on the fluoroalkyl moiety.[8] This latter resonance also displays some finer splitting patterns due to coupling between the ^{19}F nucleus and the distal ^{13}C-labelled methylene carbon (6 Hz), along with long-range $^4J_{FH}$ coupling (1.5 Hz) to the hydrogen atom in the trans position to the fluoroalkyl moiety.

3.3.2. Reaction of Fluorovinyl Complexes with Carbon Monoxide

3.3.2.1. $[Ir_2(\eta 1\text{-}C_2F_3)(CO)_3(\mu\text{-}CH_2)(dppm)_2][CF_3SO_3]_2$ (15)

Upon addition of carbon monoxide to compound **5** at -20 °C, an immediate reaction occurs as demonstrated by the appearance of new overlapping multiplets in the $^{31}P\{^1H\}$ NMR spectrum at -13.0 ppm, corresponding to the new tricarbonyl compound $[Ir_2(\eta^1\text{-}CF{=}CF_2)(CO)_3(\mu\text{-}CH_2)(dppm)_2][CF_3SO_3]$ **(15)** (see Scheme 3.6).

Triflic acid also appears as a product of this reaction, as observed by the low-field resonance at 12 ppm, in the ^1H NMR spectrum, and is proposed to be produced via deprotonation of the presumed hydride intermediate that is generated in the intramolecular C-H activation of the methyl group. This process is similar to that observed upon simply warming compound **5**, and is proposed to be induced at this temperature by CO displacement of the coordinated triflate ion,

which results in a "merry-go-round" rearrangement of equatorial ligands leading to methyl group activation.

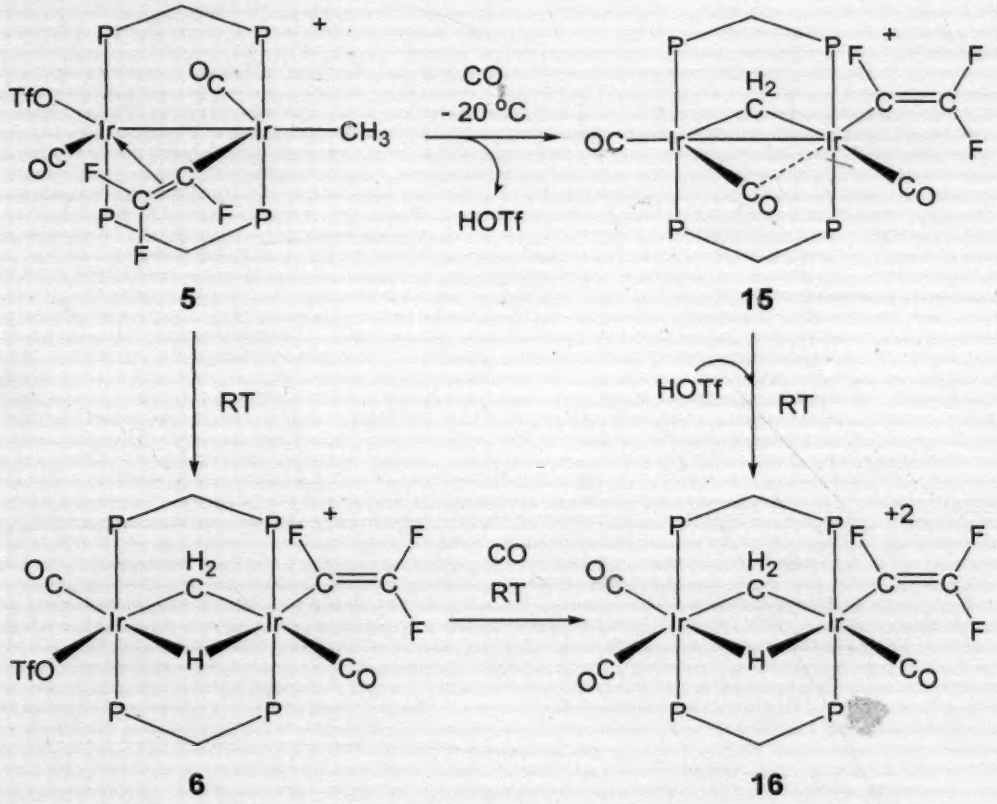

Scheme 3.6. *Addition of carbon monoxide (CO) to compounds **5** and **6***

In the ^{1}H NMR spectrum, the dppm methylene protons appear as normal multiplets, at 5.6 ppm and 3.8 ppm, while the bridging methylene ligand appears as a broad multiplet at 6.2 ppm, with coupling to all phosphorus nuclei. The ^{13}C methylene signal in a $^{13}CH_2$-enriched sample of **15** appears at 50 ppm in the $^{13}C\{^{1}H\}$ NMR spectrum, while in a ^{13}CO-enriched sample, three distinct carbonyl resonances are apparent at 158 ppm, 162 ppm, and 184 ppm. No selective decoupling information was attainable, however the chemical shifts and information gained from the subsequent rearrangement to compound **16** (*vide infra*), suggest that there are two terminal and one semi-bridging carbonyl. In the

^{19}F NMR spectrum there are three characteristic signals, consistent with a perfluorovinyl group, at -95 ppm, -122 ppm, and -125 ppm. The high-field resonance is a doublet of doublets ($^3J_{FF}$ = 115 Hz, $^3J_{FF}$ = 40 Hz), showing 115 Hz coupling to the high-field signal, with which it shares a trans arrangement, and 40 Hz cis-coupling to the other fluorine. The two lower-field resonances display mutual coupling of 90 Hz, indicative of a geminal relationship between the two respective fluorines. All coupling constants (J_{FF}) suggest the fluorovinyl moiety has moved into a terminal position upon addition of a CO ligand which also presumably displaces the coordinated triflate anion, as evidenced by a disappearance of the down-field resonance associated with it, in the ^{19}F NMR spectrum of the reaction.

Upon warming to room temperature, **15** is subsequently transformed, presumably via reaction with the HOTf generated, to give compound **16**, which is also produced, more directly, by the addition of CO to compound **6** (Scheme 3.6). The spectroscopic characterization of **16** is described below.

3.3.2.2. $[Ir_2(\eta 1\text{-}C_2F_3)(CO)_3(\mu\text{-}H)(\mu\text{-}CH_2)(dppm)_2][CF_3SO_3]_2$ (16)

Addition of carbon monoxide to compound **6** at ambient temperature, gives an immediate reaction as demonstrated by the disappearance of resonances of **6** and the concomitant appearance of a new broad signal, at -19.6 ppm in the $^{31}P\{^1H\}$ NMR spectrum, corresponding to the compound $[Ir_2(\eta^1\text{-}CF{=}CF_2)(CO)_3(\mu\text{-}H)(\mu\text{-}CH_2)(dppm)_2][CF_3SO_3]_2$ **(16)**, as previously described in the reaction of **5** with CO. The ^1H NMR spectrum shows the dppm methylene protons of **16** as normal multiplets at 5.0 ppm and 4.5 ppm. The hydride appears at -14.6 ppm as a broad singlet, integrating for one proton, while the bridging methylene group appears as a quintet at 6.0 ppm ($^3J_{HP}$ = 8.0 Hz), indicating essentially equivalent coupling to all phosphorus nuclei. A $^{13}CH_3$-enriched sample also shows the ^{13}C methylene signal at 44 ppm in the $^{13}C\{^1H\}$ NMR spectrum, consistent with the bridging nature of this moiety, and the ^1H NMR spectrum of this sample shows

the additional coupling ($^1J_{HC}$ = 146 Hz) between the methylene protons and the ^{13}C nucleus. The $^{13}C\{^1H\}$ NMR spectrum of a ^{13}CO-enriched sample of **16** shows three distinct carbonyl resonances, which appear as two broad singlets at 156 ppm, and 157 ppm and a broad multiplet at 165 ppm, all consistent with carbonyls arranged in terminal positions. The IR spectrum confirms this assertion with values of 2036 cm^{-1}, 1996 cm^{-1} and 1958 cm^{-1}, respectively for the carbonyl stretches. Unfortunately, selective $^{13}C\{^{31}P,^1H\}$ decoupling experiments are again not possible, owing to the overlap of the ^{31}P signals. In the ^{19}F NMR spectrum there are only two sets of signals in a 2:1 ratio, rather than the three expected for a perfluorovinyl moiety. The first, at -119 ppm, appears as a multiplet, corresponding to the two fluorine atoms oriented in a trans position to one another, whose signals are accidentally overlapping, while the second appears as a broad resonance at -95 ppm, corresponding to the other fluorine on the β-carbon. The breadth of these signals presumably masks the expected ^{19}F-^{19}F coupling.

3.3.2.3. - $[Ir_2(CH_3)(CO)_3(\mu\text{-}\eta1\text{:}\eta2\text{-}C_2F_2H)(dppm)_2][CF_3SO_3]_2$ (17)

Upon addition of carbon monoxide to compound **7** at ambient temperature, an immediate reaction occurs as demonstrated by the disappearance of its $^{31}P\{^1H\}$ NMR resonances and the corresponding appearance of a new set of signals due to the tricarbonyl compound $[Ir_2(CH_3)(CO)_3(\mu\text{-}\eta^1\text{:}\eta^2\text{-}CF{=}CFH)(dppm)_2][CF_3SO_3]_2$ **(17)**, as shown in Scheme 3.6. Compound **17** is an isolable species and has been characterized by NMR and IR spectroscopy, and by elemental analysis.

The $^{31}P\{^1H\}$ NMR spectrum of compound **17** reveals an ABCD spin system pattern, indicative of four inequivalent phosphorus atom environments, like that of the precursor. Signals are present at 7.4 ppm, 4.0 ppm, -9.4 ppm and -18.2 ppm, each being a complex multiplet showing some mutual coupling similar to that of the precursor compound **7** (see Chapter 2). Its ^1H NMR spectrum shows

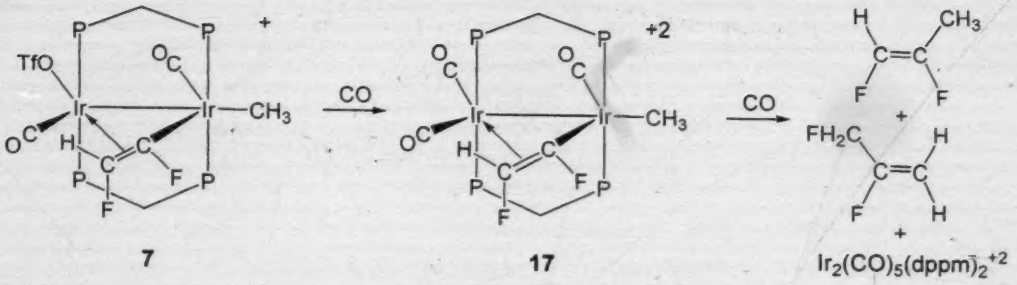

Scheme 3.6. *Reaction of compound* ***7*** *with CO*

the dppm methylene protons as typical multiplets at 6.4 ppm, 5.1 ppm, 4.4 ppm and 3.7 ppm, all integerating for one proton each. The iridium-bound methyl group appears as a broad triplet at 1.1 ppm, suggesting that it is terminally-bound. The vinylic proton, at 6.6 ppm, is identifiable by its multiplet splitting pattern, with two of the resolvable couplings being diagnostic of hydrogen-fluorine coupling; the first and most prominent is the $^2J_{HF}$, with a value of 64 Hz, which is consistent with the geminal coupling of an sp^2 hybridized-C(H)F group.[9] The smaller coupling ($^3J_{HF}$ = 15 Hz) confirms that the H and other F atom are in a trans arrangement across the vinylic center. These couplings are reflected in the ^{19}F NMR spectrum (*vide infra*), and their values suggest that the fluorovinyl moiety remains in a bridging orientation. The ^{13}C NMR spectrum of a ^{13}CO-enriched sample of **17** shows three independent carbonyl resonances at 159 ppm, 168 ppm and 173 ppm, and a singlet at -13 ppm corresponding to the methyl carbon. In the ^{19}F NMR spectrum there are two characteristic signals displaying fluorine-proton and fluorine-fluorine coupling, the values of which again suggest a bridging orientation of the fluorovinyl moiety. The first is a broad unresolved signal at -54 ppm, whereas the other is a higher field signal at -158 ppm displaying fluorine-proton coupling ($^2J_{HF}$= 64 Hz) that is consistent with it being the geminal partner to the proton described above. This signal also shows coupling of 31 Hz to the other fluorine, indicative of a cis arrangement of these atoms across the vinylic center. Presumably this species maintains the bridging

orientation during this transformation, whereas the trifluorovinyl complex (**5**) did not, due to the slight decrease in steric demands of the *cis*-difluorovinyl moiety.

Subsequently, when a sample of **17** is left overnight, under an atmosphere of CO, it completely converts to the previously characterized $[Ir_2(CO)_5(dppm)_2][CF_3SO_3]_2$ by reductive elimination of the mutually adjacent methyl and difluorovinyl groups to give *cis*-difluoropropene (and its isomer 2,3-difluoropropene), identified by their characteristic resonances (*vide supra*) observed in the ^{19}F and ^{1}H NMR spectra.

3.3.2.4. $[Ir_2(CH_3)(CO)_3(\mu\text{-}\eta1\text{:}\eta1\text{-}C_2FH_2)(dppm)_2][CF_3SO_3]_2$ (18).

Upon addition of carbon monoxide gas to compound **8** at -40.0 °C, a slow reaction occurs as demonstrated by the disappearance of the $^{31}P\{^{1}H\}$ NMR resonances of **8** and the concomitant appearance of a new pair of pseudo-triplets in the spectrum at 2.7 ppm and -16.0 ppm, corresponding to compound **18,** $[Ir_2(CH_3)(CO)_3(\mu\text{-}\eta^1\text{:}\eta^1\text{-}CF\text{-}CH_2)(dppm)_2][CF_3SO_3]_2$.

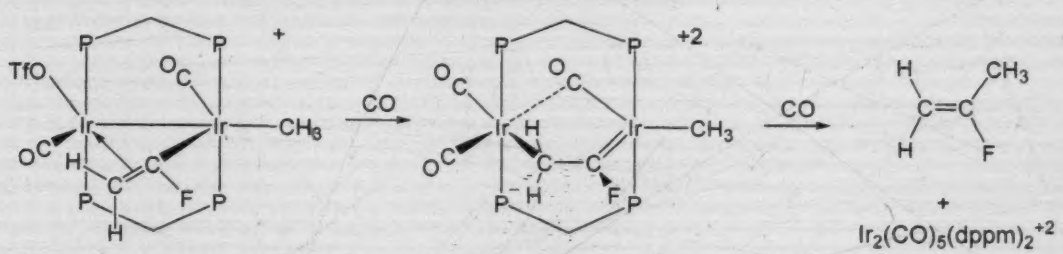

8 **18**

Scheme 3.7. *Reaction of compound **8** with CO*

The spectral data for **18** are not consistent with a fluorovinyl product, as is discussed below, but are more reminiscent of those observed for the related compound **8a** (see Chapter 2) in which a fluorocarbene structure is proposed. The ^{1}H NMR spectrum shows the pair of protons in the fluorocarbyl ligand as a

doublet, integrating for two protons at 6.3 ppm, with $^3J_{HF}$ of 13.4 Hz to the adjacent fluorine. For a monofluorovinyl group, as in **8**, we would have expected two inequivalent proton resonances, showing different cis and trans couplings to the unique fluorine. The ^{19}F NMR spectrum of compound **18** shows only a broad signal attributable to the lone fluorine, appearing at -20 ppm, the chemical shift of which is similar to other reported fluorocarbenes,[10] and quite different from that of monofluorovinyl complexes in which a much higher-field shift is observed. Due to the breadth of this signal, coupling information, particularly to the methylene protons was unresolvable.

In the ^1H NMR spectrum of this product, the iridium-bound methyl appears as a triplet at 0.4 ppm ($^3J_{PH}$ = 6.6 Hz), indicating that it is terminally-bound, with selective ^{31}P decoupling experiments revealing that it is coupled to the two phosphorus nuclei at -16.0 ppm. A ^{13}C-enriched sample of **18** shows the ^{13}C methyl carbon as a broad singlet at -26 ppm, while three different carbonyl resonances are apparent, as expected. The first is a broad multiplet at 159 ppm, the second at 169 ppm, and the final at 175 ppm. Selective ^{31}P decoupling experiments indicate that there are two terminal and one bridging carbonyl, with the latter corresponding to the shift at 169 ppm, showing unresolved coupling to both sets of the diphosphines, and the other two resonances showing coupling only to the phosphorus resonance at 2.7 ppm. This is an atypical result. Whereas the lower-field resonance would usually correspond to the bridging carbonyl, in this case, the anomalous high-field chemical shift of the semi-bridging carbonyl may be influenced by the adjacent fluorocarbene moiety.

When a sample of **18** is left overnight under an atmosphere of CO complete conversion to the previously characterized $[Ir_2(CO)_5(dppm)_2][CF_3SO_3]_2$[4] is observed. This reaction involves reductive elimination of 2-fluoropropene via coupling of the adjacent methyl and fluorovinyl groups, as seen in the ^{19}F NMR spectrum, and characterized by comparison to known spectral data.

3.3.2.5. $[Ir_2(\eta 1\text{-}C_2F_2H)(CO)_4(dppm)_2][CF_3SO_3]$ (19).

Addition of carbon monoxide to the hydroxide-bridged species $[Ir_2(CH_3)(\eta^1\text{-}CF{=}CFH)(CO)_2(\mu\text{-}OH)(dppm)_2][CF_3SO_3]$ (**9**) at ambient temperature, results in the slow disappearance of resonances of **9** and the simultaneous appearance of a new set of signals, at -10.4 ppm and -17.7 ppm in the $^{31}P\{^1H\}$ NMR spectrum, corresponding to the difluorovinyl compound $[Ir_2(\eta^1\text{-}CF{=}CHF)(CO)_4(dppm)_2][CF_3SO_3]$ **(19)**, as shown in Scheme 3.8.

Both ^{31}P resonances of compound **19** show mutual coupling of 28 Hz, and are consistent with an AA'BB' spin system. The ^1H NMR spectrum shows the dppm methylene protons as normal multiplets at 4.3 ppm and 3.3 ppm, with the typical 14 Hz coupling to phosphorus. The vinylic proton resonance appears at 3.9 ppm as a doublet of doublets, as would be expected for the difluorovinyl group, with the most prominent coupling to the geminal fluorine ($^2J_{HF}$ = 80 Hz), and the smaller coupling ($^3J_{HF}$ = 23 Hz) to the fluorine atom in the trans position. These

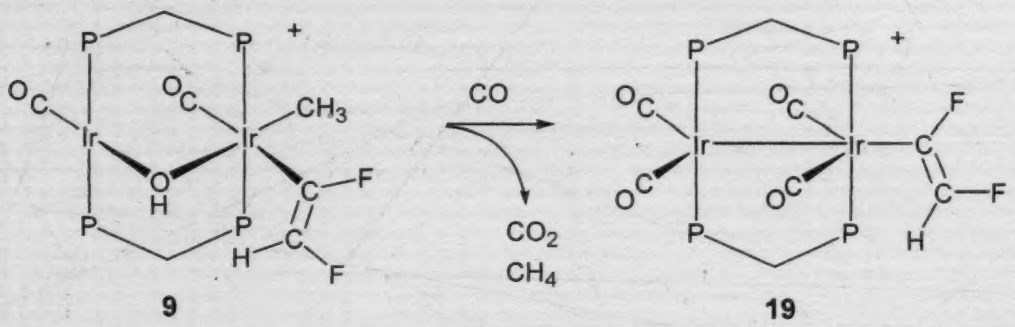

9 **19**

Scheme 3.8. *Reaction of compound **9** with CO*

couplings are consistent with those observed in the ^{19}F NMR spectrum (*vide infra*), and their values suggest that the fluorovinyl moiety remains in a terminal position. A $^{13}CH_3$-enriched sample shows that the methyl group has been lost as methane, as observed in the $^{13}C\{^1H\}$ NMR spectrum, presumably from reductive elimination with a hydride, generated in a water-gas-shift-like reaction, in which the addition of CO to the precursor hydroxide species yields carbon dioxide and

the hydride ligand. The $^{13}C\{^1H\}$ NMR spectrum of a ^{13}CO-enriched sample of **19** shows only two distinct carbonyl resonances, which appear as a broad singlet at 194 ppm, and a triplet at 178 ppm. Selective $^{13}C\{^1H, ^{31}P\}$ decoupling experiments have shown that the higher-field carbonyl resonance is coupled to the ^{31}P nuclei resonating at -10.4 ppm, while the lower-field signal only shows slight sharpening under broad-band decoupling conditions. It is assumed that each resonance is attributable to two equivalent carbonyl groups, with assignment of the high-field resonances due to terminal carbonyls, sharing one metal, while the low-field carbonyls are proposed to be terminally bound, but occupying positions approaching the adjacent metal. The IR spectrum of **19** shows only terminal carbonyl stretches (2043 cm^{-1}, and 2005 cm^{-1}) seemingly ruling out a formal semi-bridging arrangement. In the ^{19}F NMR spectrum there are two sets of signals corresponding to the difluorovinyl moiety. The first is a broad doublet at -92 ppm, with 23 Hz trans coupling to the proton, which places this fluorine atom on the α-carbon, while the other signal is also a doublet ($^3J_{HF}$= 80 Hz) appearing at -135 ppm, consistent with the fluorine on the β-carbon, geminal to the proton. A second, smaller coupling is evident in the higher-field resonance (~8 Hz) and is presumed to be the *cis*-coupling between the two fluorine atoms across the vinylic center. Both resolved $^2J_{HF}$ coupling values suggest that the difluorovinyl group is now in a terminal position on one metal.

3.3.3. Further Reaction of Me_3SiOTf with Fluorovinyl-bridged Complexes

3.3.3.1. $[Ir_2(CH_3)(OTf)(CO)_2(\mu\text{-}C{=}CF_2)(dppm)_2][CF_3SO_3]_2$ (20)

Reaction of $[Ir_2(CH_3)(OTf)(CO)_2(\mu\text{-}\eta^1{:}\eta^2\text{-}CF{=}CF_2)(dppm)_2][CF_3SO_3]$ (**5**) with a five-fold excess of $Me_3Si(CF_3SO_3)$ at -20 °C results in the formation of a new product as demonstrated by the appearance of a new pair of pseudo-triplets in the $^{31}P\{^1H\}$ NMR spectrum at -6.2 ppm and -20.6 ppm, corresponding to the compound $[Ir_2(CH_3)(OTf)(CO)_2(\mu\text{-}C_2F_2)(dppm)_2][CF_3SO_3]_2$ (**20**). The new product

results from the removal of a fluoride ion from the precursor (**5**), as shown for all fluorovinyl species in the following Scheme 3.9. Alternately, these reactions can be viewed as removal of a second fluoride from the respective fluoroolefin precursors (**2 – 4**).

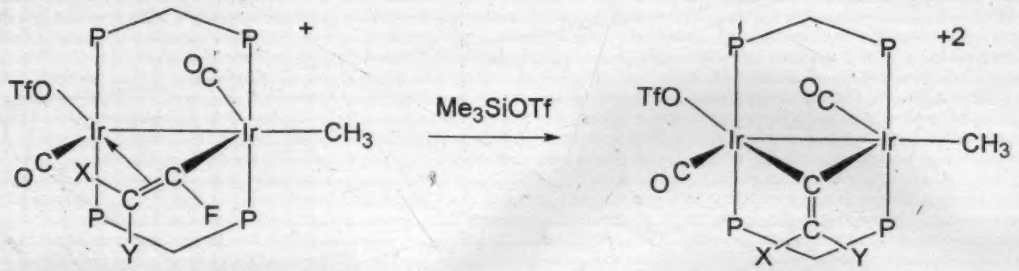

5; X = F, Y = F
7; X = H, Y = F
8; X = H, Y = H

20; X = F, Y = F
21; X = H, Y = F
22; X = H, Y = H

Scheme 3.9. *C-F activation of bridging fluorovinyl complexes*

In the resulting difluorovinylidene compound (**20**) mutual coupling of 21 Hz between the $^{31}P\{^{1}H\}$ NMR resonances is consistent with an AA'BB' spin system, suggesting that both ends of the pair of diphosphines are in different chemical environments. In the ^{1}H NMR spectrum, the dppm methylene protons occur as two doublets of multiplets, integrating for two protons each, at 4.1 ppm and 2.8 ppm, displaying the typical 14 Hz coupling to phosphorus. The iridium-bound methyl group appears as a triplet, integrating for three protons, at 1.9 ppm ($^{3}J_{HP}$ = 6.0 Hz). Selective ^{31}P decoupling experiments indicate that these protons are coupled equally to the pair of phosphorus nuclei resonating at -6.2 ppm, which strongly suggests that the methyl group is bound to a single metal. The ^{13}C NMR spectrum of a ^{13}CO-enriched sample of **20** shows two broad multiplet carbonyl resonances at 151 ppm and 174 ppm. The lower-field shift of the latter suggests that this carbonyl approaches the second metal, possibly even interacting with it weakly in a semi-bridging arrangement. This arrangement is confirmed through the $^{13}C\{^{1}H, ^{31}P\}$ NMR spectrum in which the terminal carbonyl at 151 ppm shows coupling only to the pair of phosphorus nuclei on the non-methylated metal

(-20.6 ppm), while the down-field signal at 174 ppm shows coupling to both sets of phosphines, displaying a stronger interaction with the pair of phosphorus nuclei resonating at -6.2 ppm. The ^{13}C-enriched methyl group displays a broad, relatively low-field singlet at 38 ppm, which is at significantly lower field than the other methyl species presumably due to the higher charge on the complex.

The difluorovinylidene group appears in the ^{19}F NMR spectrum as two new doublet signals, at -69 ppm and -86 ppm, with mutual coupling of 97 Hz, consistent with the geminal coupling seen in a previously crystallographically established di-iron complex.[11] Again, in the ^{19}F NMR spectrum a resonance appears for the coordinated triflate ion, at -76 ppm, along with that of the triflate counterions at -79 ppm, and a characteristic signal at -159.9 ppm corresponding to the Me_3SiF that is generated in the above transformation.

3.3.3.2. $[Ir_2(CH_3)(OTf)(CO)_2(\mu\text{-}C{=}C(H)F)(dppm)_2][CF_3SO_3]_2$ (21)

Reaction of compound **7**, $[Ir_2(CH_3)(OTf)(CO)_2(\mu\text{-}\eta^1{:}\eta^2\text{-}CF{=}CFH)(dppm)_2][CF_3SO_3]$, with excess $Me_3Si(CF_3SO_3)$ also results in an additional C-F activation reaction. The appearance of a new pair of pseudo-triplets in the $^{31}P\{^1H\}$ NMR spectrum at -5.0 ppm and -21.0 ppm, corresponds to the compound $[Ir_2(CH_3)(OTf)(CO)_2(\mu\text{-}C_2FH)(dppm)_2][CF_3SO_3]_2$ (**21**). The chemical shifts, and mutual coupling of 23 Hz between these signals is very similar to those encountered in compound **20**.

The ^1H NMR spectrum shows the iridium-bound methyl group as a triplet, integrating for three protons, again at the relatively low-field chemical shift of 2.15 ppm ($^3J_{HP}$ = 9.0 Hz). Selective ^{31}P decoupling experiments indicate that these protons couple to the pair of phosphorus nuclei resonating at -5.0 ppm, strongly suggesting that the methyl group is bound only to the associated metal. The chemical shift of the vinylidene proton, which appears as a broad doublet, was determined to be 8.6 ppm showing coupling to fluorine (*vide infra*). The $^{13}C\{^1H\}$ NMR spectrum of a ^{13}CO-enriched sample of **21** shows two broad multiplet

carbonyl resonances at 153 ppm and 176 ppm. Whereas the high-field carbonyl shows coupling only to the pair of phosphorus nuclei on the non-methylated metal (-21.0 ppm), and is therefore presumably terminally bound to this end, the lower-field carbonyl shows coupling to both sets of diphosphine resonances, the larger of which is to the pair of phosphorus nuclei resonating at -5.0 ppm, suggesting a semi-bridging arrangement with the adjacent metal. The ^{13}C-enriched methyl group displays a broad, relatively low-field singlet at 41 ppm, which again, much like compound **20,** is shifted downfield due to the higher positive charge on the complex. The monofluorovinylidene group appears in the ^{19}F NMR spectrum as a new doublet at -107 ppm, with a $^{2}J_{HF}$ coupling of 85 Hz, which is on the order with that seen in both the analogous difluorovinylidene compound (~100 Hz) and related fluorovinyl complexes that display geminal H-F coupling ($^{2}J_{HF}$). Other relevant signals in the ^{19}F NMR spectrum show the coordinated triflate ion, at -76 ppm, along with that of the free triflate counterions at -79 ppm, in a 1:2 ratio, respectively, and the characteristic Me_3SiF signal at -159.9 ppm.

3.3.3.3. $[Ir_2(CH_3)(OTf)(CO)_2(\mu\text{-}C{=}CH_2)(dppm)_2][CF_3SO_3]_2$ (22)

Reaction of compound **8**, $[Ir_2(CH_3)(OTf)(CO)_2(\mu\text{-}C_2FH_2)(dppm)_2][CF_3SO_3]$, with excess $Me_3Si(CF_3SO_3)$ at -20 °C also results in an additional C-F activation reaction as demonstrated by the appearance of a new set of signals in the $^{31}P\{^{1}H\}$ NMR spectrum at -10.0 ppm and -20.0 ppm, corresponding to the compound $[Ir_2(CH_3)(OTf)(CO)_2(\mu\text{-}C_2H_2)(dppm)_2][CF_3SO_3]_2$ (**22**). The instability of this species at temperatures above 0 °C has limited our characterization of this product to solution NMR at this temperature.

In the ^{1}H NMR spectrum the dppm methylene protons appear as usual and the iridium-bound methyl group appears as a broad triplet, integrating for three protons, at 1.35 ppm ($^{3}J_{HP}$ = 4.9 Hz). Selective ^{31}P decoupling experiments indicate that these protons are coupled to one pair of phosphorus nuclei at -20

ppm, which strongly suggests that the methyl group is bound to a single metal. The vinylidene protons appear as two relatively broad singlets, which integrate for one proton each, at 5.99 ppm and 6.01 ppm. The lack of resolvable coupling between the pair of vinylidene protons is typical for such an arrangement. The $^{13}C\{^1H\}$ NMR spectrum of a ^{13}CO enriched sample of **22** shows two broad multiplet carbonyl resonances at 164 ppm and 170 ppm, both of which show coupling to different sets of phosphines, with the latter ^{13}CO resonance (170 ppm) sharpening upon irradiation of the higher-field phosphorus signal. This is in contrast to the fluorinated vinylidene compounds (**20** and **21**), in which one carbonyl showed some degree of semi-bridging character to the adjacent metal. The ^{13}C-methyl signal of a $^{13}CH_3$ enriched sample of **22** also appears in contrast with that of the fluorinated vinylidene compounds, showing a more typical, high-field, broad singlet at 0.2 ppm.

There is again evidence for the coordinated triflate ion, at -77 ppm in the ^{19}F NMR spectrum, along with that of the free triflate counterions at -79 ppm. The Me_3SiF that is generated in the above transformation of **8** to **22** also appears as a characteristic signal at -159.9 ppm in the ^{19}F NMR spectrum.

3.4. Discussion

As noted in the Introduction, we set out, in this chapter, to investigate the reactivity of fluorovinyl ligands. Primarily we sought to eliminate this moiety together with either a hydrogen or a methyl group, thereby completing the cycle of substituting a fluorine in the precursor fluoroolefin by a H or CH_3.

a) Hydrogenolysis

The first process has been successfully achieved through hydrogenolysis of the fluorovinyl complexes, with a number of intermediates being observed leading to the formation of the fluoroolefin product. Addition of hydrogen to samples of both compound **6**, containing a terminally bound trifluorovinyl group, and compound **7**,

containing a bridging cis-difluorovinyl group, has resulted in the transformation of the bound fluorovinyl moiety into its liberated hydrogen-substituted olefin, trifluoroethylene and *cis*-difluoroethylene, respectively. Two different mechanisms, involving similar elementary steps, appear to be occurring for these transformations, as demonstrated by the various intermediates encountered in each route.

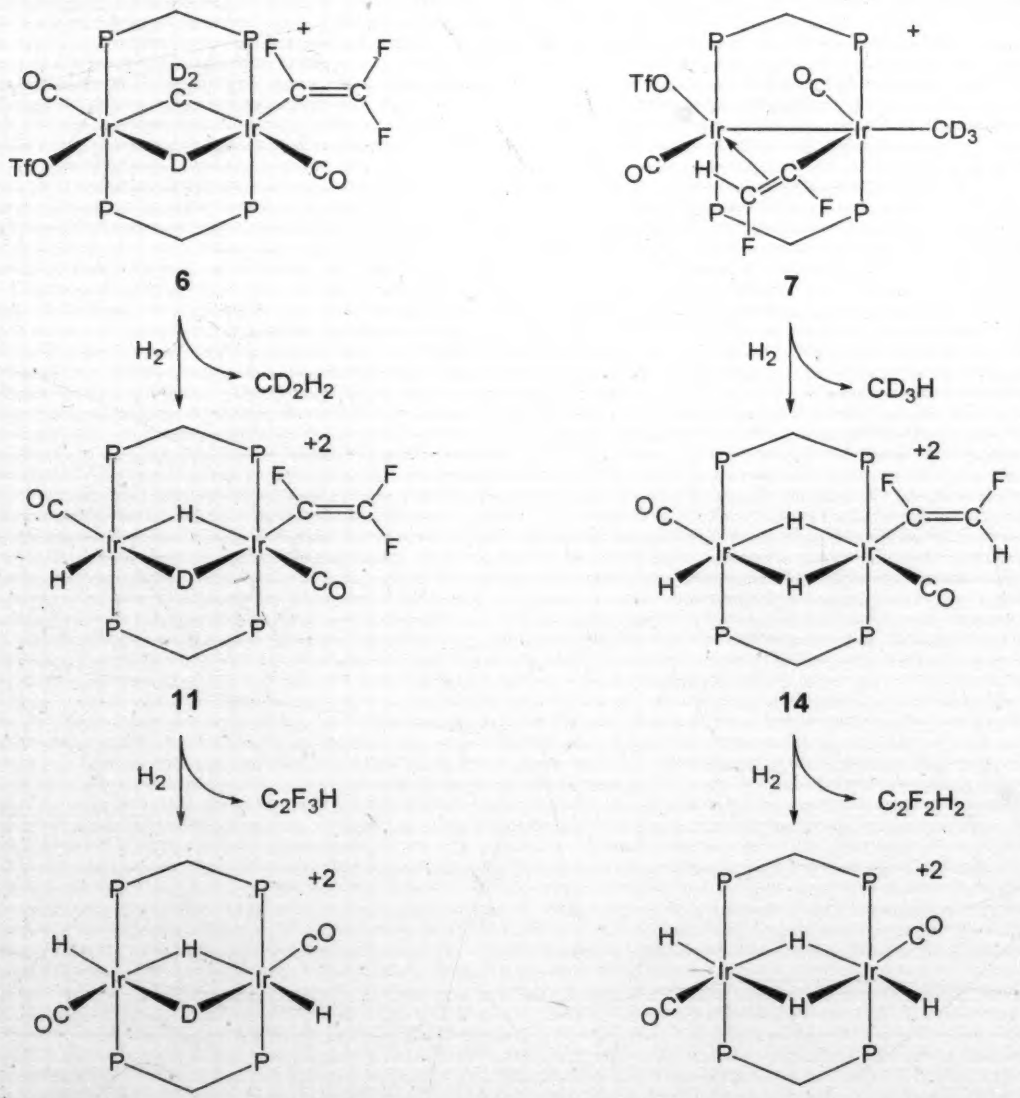

Scheme 3.10. *Reaction of H_2 with terminal and bridging fluorovinyl complexes*

Labelling studies in which the methyl ligand in the precursor was deuterium labelled show that **6** yields CD_2H_2 upon reaction with hydrogen, while **7** yields CD_3H. These labelling results are clearly a consequence of the d_3-methyl group having been cleaved into D and CD_2 fragments in **6**, while it remains intact in **7** (see Scheme 3.10).

On the basis that the D and CD_2 fragments in **6** occupy different faces of the complex, it is not surprising that their recombination does not occur upon reaction with H_2, and in this case hydrogenolysis of the μ-CD_2 group occurs, rather than hydrogenolysis of the original CD_3 group. It is also notable that the deuteride ligand in compound **6** is not in a position adjacent to the trifluorovinyl moiety, precluding the direct elimination of these two groups, and subsequently the deuterium label remains in the site bridging the metals throughout the process. Interestingly, there is no net difference in reactivity observed in the processes involving either μ-vinyl and η^1-vinyl moieties, wherein both reactions with H_2 lead to the respective substituted fluoroolefin. However, it is notable that, the fluorovinyl moiety is bound in a terminal position prior to subsequent elimination.

While the reaction of **7** with H_2 has not been studied in detail, the reaction of **6** has been investigated at low temperatures by NMR spectroscopy. Although not observed spectroscopically, in either instance, the first step in both processes is proposed to involve the displacement of the triflate ion by H_2, resulting in a weakly-bound molecular hydrogen adduct. Such complexes have been shown to render one of the component hydrogen atoms relatively acidic,[6] thereby allowing deprotonation via the displaced triflate ion, yielding triflic acid, which was observed spectroscopically. At this stage two isomers of the deprotonated dihydride intermediate are observed (**10** and **10a**), presumably resulting from the intermediacy of two isomeric H_2 adducts, as shown in Scheme 3.11.

It is assumed that the two isomers result from the weakly-bound nature of the putative molecular hydrogen ligands, leading to their facile dissociation, followed

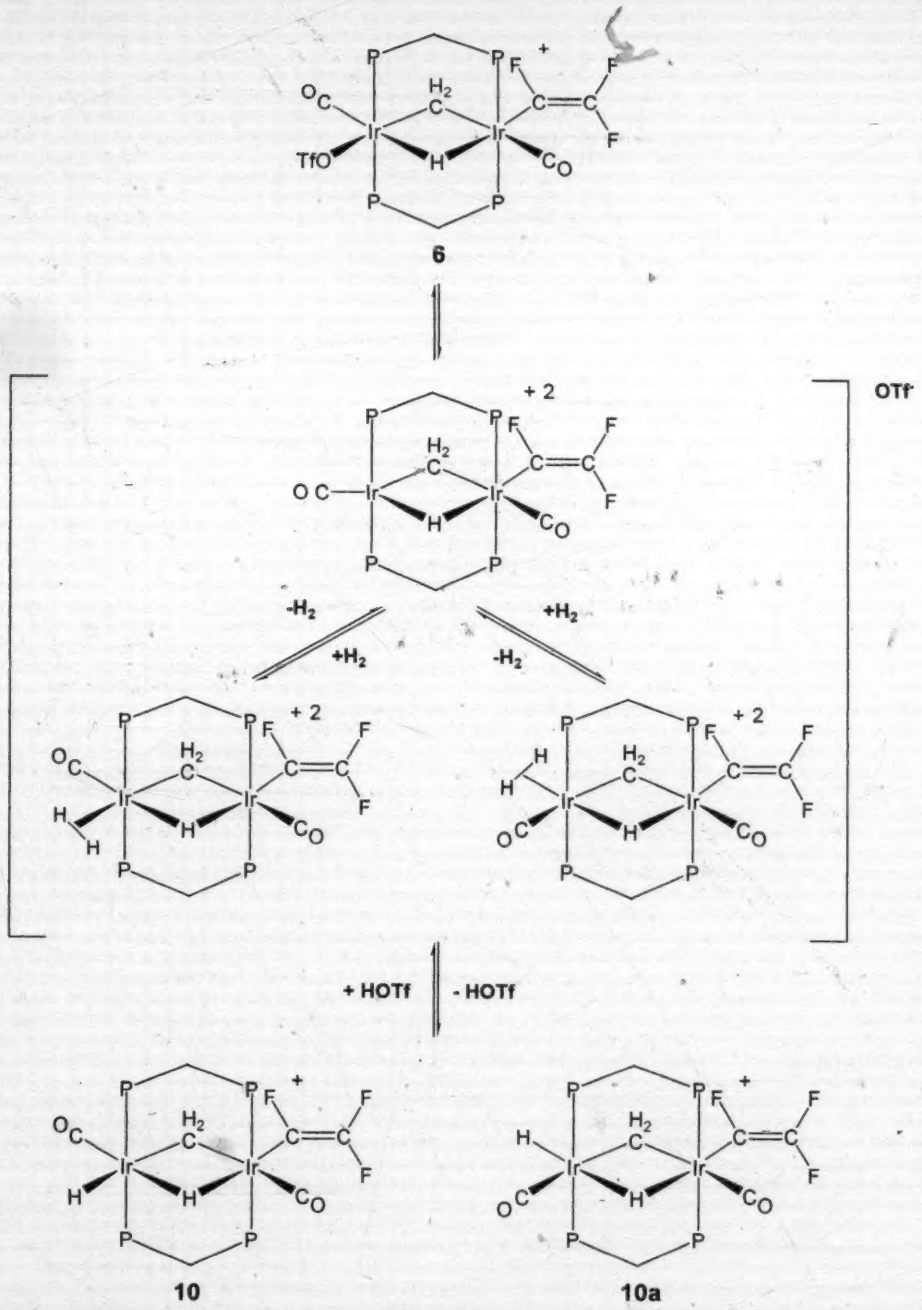

Scheme 3.11. *Reaction of H_2 with compound* **6**, *resulting in two different proposed isomers,* **10** *and* **10a**

by recoordination in the other site adjacent to the carbonyl. In this proposed mechanism, subsequent deprotonation via the triflate ion, as discussed above, leads to the generation of isomers **10** and **10a**.

Although there are two precursor isomers, the next step in this process results in a single observed product (**11**), in conjunction with the production of methane, and the consumption of triflic acid. This convergence to a single product may either be due to the presence of a unique productive pathway, combined with the facile conversion of **10** and **10a**, as noted above, or perhaps through an intermediate common to both. In either case the conversion of **10** and **10a** to **11** requires reprotonation and reaction with H_2, although we have no evidence to indicate the order of the steps. However, we can suggest a couple of pathways (see Scheme 3.12). If methane elimination from isomer **10** is to occur its reaction with H_2 does not seem feasible, since this species is coordinatively saturated. Furthermore, the combination of the bridging methylene group with the hydride ligands also does not seem feasible because these are not adjacent, but are on opposite faces of the complex. We might suggest in this case that protonation could occur next to give a dicationic methyl intermediate **A**, which can now react with H_2 to yield **B**, which upon methane loss could generate **11**. In the case of **10a**, migration of the hydride adjacent to the methylene group could yield the methyl intermediate **C** which upon reaction with H_2 might yield the trihydride **D** followed by methane loss, movement of the terminal hydride to the bridging site vacated by the methylene group, and protonation to yield **11**. Why protonation adjacent to either μ-H groups does not occur to give two isomers of **11** is not clear.

For the two H_2-addition steps in these suggested pathways we have indicated two subtly different mechanisms (Scheme 3.12). Intermediate **B** is suggested to be an H_2 complex, since oxidative addition at a pair of Ir(3+) centers, possessing an overall 2+ charge seems less likely. That being the case methane elimination could occur via a σ-complex-assisted metathesis (σ-CAM) mechanism.[12] The result of H_2 attack on intermediate **C**, on the other hand, could proceed via an

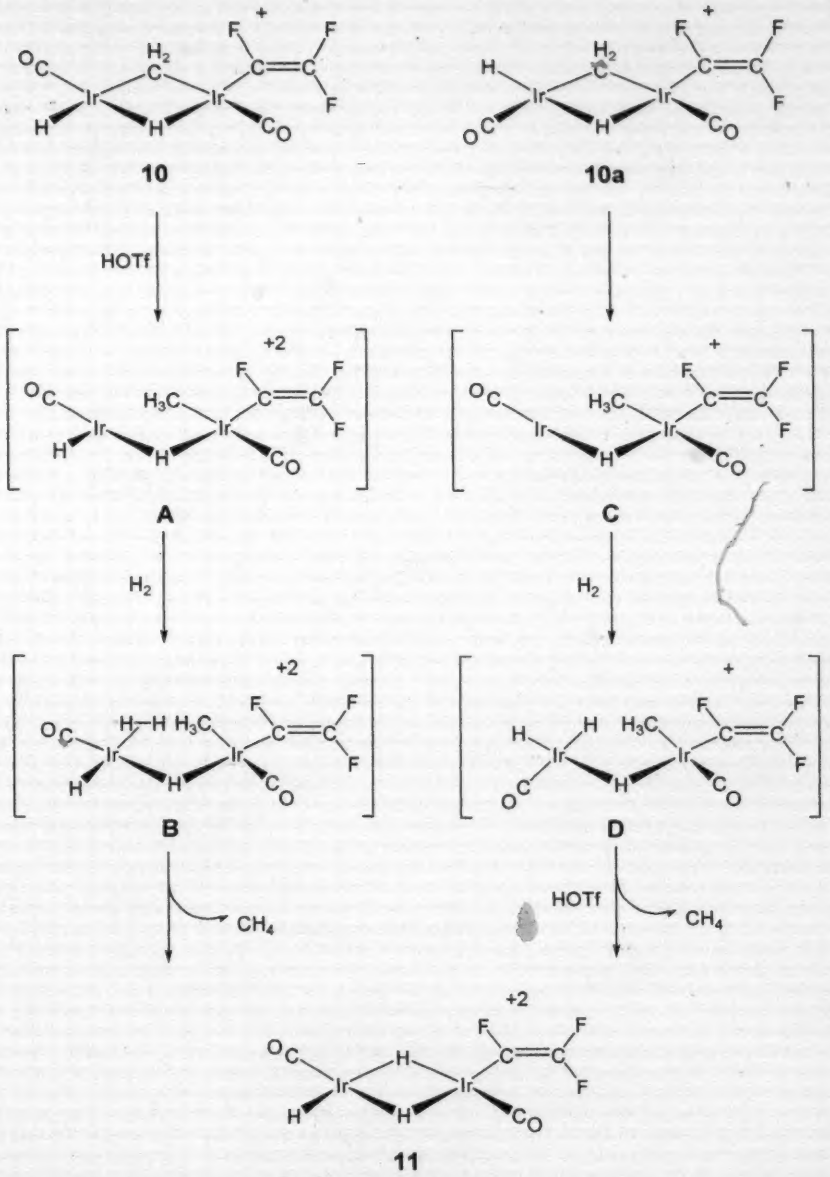

Scheme 3.12. *Proposed general mechanisms, showing unobserved intermediates, in the hydrogenolysis of the different isomers* (**10** *and* **10a**) *resulting in the production of* **11**. *Dppm ligands are omitted.*

oxidative addition step at the Ir(+1) center, with methane loss occurring through a reductive elimination step. It is to be emphasized that both pathways are merely suggestions.

Further mechanistic studies of these reactions are required, at even lower temperatures, to determine whether proposed intermediates, particularly the molecular H_2 adducts, can be observed under these conditions. In addition, the low temperature reaction of hydrogen with compounds **5** (the trifluorovinyl analogue of **7** and the precursor to **6**) and **7** should also be investigated.

Whatever the mechanism in generating CD_2H_2 from **6** and CD_3H from **7**, subsequent steps involving hydrogenolysis of the fluorovinyl groups in **11** and **14**, respectively, are presumably the same, since these intermediates have very analogous structures. This step is proposed to involve the slow reductive elimination of the corresponding fluoroolefin, followed by oxidative addition of H_2, to generate the identical diiridium tetrahydride complex in both cases, which has been characterized crystallographically.

b) Fluoropropene elimination

Another stated goal of these investigations was the reductive elimination of the fluorovinyl and methyl groups, leading to fluoropropene formation. As will be recalled, such a process had been observed earlier in the reaction of the 1,1-difluoroethylene-bridged species (**4**) with water. We had wondered whether the reaction might be more general and might be observed for the other fluorovinyl complexes. In order to favor the elimination process, it was reasoned that replacement of the anionic triflate in compounds **5 – 8** by a neutral ligand would yield a dicationic species, which should be more prone to reductive elimination. Furthermore, if the neutral ligand were also a strong π-acceptor, further lowering the electron density on the metals, reductive elimination might be even more favorable.

Reaction of the difluorovinyl and monofluorovinyl-bridged species, **7** and **8**, with CO gives the anticipated replacement of triflate by CO, readily yielding the targeted dicationic tricarbonyl species (**17** and **18**, respectively) (Figure 3.5).

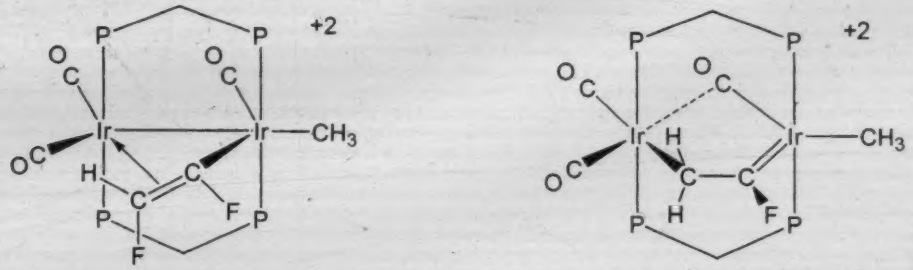

17 **18**

Figure 3.5. *Replacement of triflate by CO (from* **7** *and* **8**, *respectively) yielding the dicationic tricarbonyl species* ***17*** *and* ***18***

These two complexes have a notable difference in the bridging modes of their respective fluorocarbyl moieties; whereas the difluorovinyl group remains in a μ-η^1:η^2 bridging arrangement in compound **17**, the monofluorovinyl group of **8** has rearranged in **18**, to a μ-η^1:η^1 fluorocarbene group (see Scheme 2.2A, Chapter 2). In spite of these differences reductive elimination of the appropriate fluoropropene was subsequently observed in both species, through prolonged exposure to CO. However in the case of the *cis*-difluorovinyl species, some isomerization of the *cis*-difluoropropene to 2,3-difluoropropene also occurred. Although the mechanism of this rearrangement is unknown, the isomerization product should be favored over the initial product having one electronegative fluorine on a carbon of lower s-character (sp^3 *vs* sp^2).

In the case of the trifluorovinyl-bridged compound (**5**), reaction with CO again results in triflate displacement by CO, as shown earlier in Scheme 3.6. However in this case 1,1,2-trifluoropropene is not observed; instead movement of the vinyl moiety from the bridging site to a terminal position, is accompanied by C-H activation of the methyl group. The resulting putative dicationic hydride

intermediate is apparently acidic, with deprotonation by the triflate anion leading to compound **15**, followed by reprotonation at the more basic bridging position producing compound **16** (see Scheme 3.13).

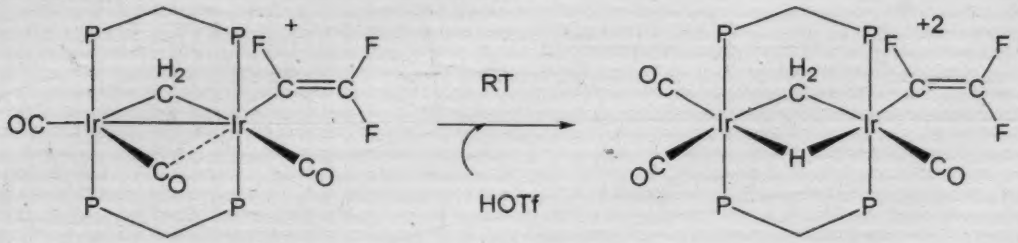

15 **16**

Scheme 3.13. *Replacement of triflate by CO (from* **5***) yields* **15** *and triflic acid, which upon reprotonation generates compound* **16**

In this product (**16**) the hydride occupies a site on the opposite face of the bimetallic core from the methylene and perfluorovinyl moieties, as was observed in the transformation of compound **5** to **6**. Such an arrangement makes facile methyl reformation less favorable, thereby inhibiting subsequent reductive coupling pathways to give 1,1,2-trifluoropropene, or direct reductive elimination of the hydride with the fluorovinyl group to produce trifluoroethylene. Although migration of the trifluorovinyl group to the methylene group could occur, paralleling a transformation championed by Maitlis and coworkers as a key step in the Fischer-Tropsch chemistry,[13] no reactivity of this type is seen with the perfluorovinyl complexes under these conditions. This is consistent with the well documented lower tendency of perfluorocarbyl fragments to undergo migratory insertion reactions, compared to their perprotio analogues.[14]

Such an argument also rationalizes the slower reductive elimination of the *cis*-difluoropropene from **17**, compared to that of the 2-fluoropropene from **18**. Presumably, the greater number of fluorine substituents gives rise to a stronger Ir-fluorovinyl bond, although we would have thought that fluorine substitution at the β-carbon would have much less influence on the Ir-C bond than substitution

at the α-carbon. Such an argument of increased Ir-C bond strength with increasing fluorine substitution, would also explain the observation in Chapter 2 of facile elimination of 2-fluoropropene from the reaction of compound **4** with water.

The addition of carbon monoxide to the hydroxide compound (**9**) was investigated to see if reductive elimination could similarly be promoted between the terminally bound difluorovinyl ligand and the adjacent methyl group. However, the presence of the hydroxide group, led to "water-gas-shift-related" chemistry in which facile conversion of the hydroxide-bridged complex into a putative hydrido-bridged species leads to reductive elimination of methane and formation of a tetracarbonyl complex (**19**), containing a terminally bound difllluorovinyl group. Deuterium labelling of the hydroxide group shows that this proton ends up in the eliminated methane (CDH_3), and no further insertion or coupling reactions were observed with this species.

c) Additional C-F activation

A secondary goal of this study was to effect additional fluoride ion removal, leading ultimately to substitution of two fluorines in the precursor fluoroolefins. In the species in which the fluorovinyl moiety remains in the bridge (**5**, **7**, and **8**), a second C-F activation has been achieved at the α-carbon (see Scheme 3.14). Upon treatment with excess $Me_3Si(CF_3SO_3)$ these compounds are subsequently transformed into the respective bridging difluorovinylidene, monofluorovinylidene, and vinylidene complexes (**20**, **21**, **22**). Although bridging fluorovinylidenes are not common, the nature of these moieties was established via comparison of their NMR spectroscopy data to that of the few previously established analogous complexes in the literature (*vide supra*).

The fact that further C-F activation has only been achieved in complexes in which the fluorovinyl moiety remains in the bridge, is in excellent agreement with our proposal that activation involves both metals working cooperatively. Evidence for this phenomenon was best illustrated by comparison of reactivity between

isomers **5** and **6**. Reaction of compound **5** with trimethylsilyl triflate at -20 °C results in the abstraction of a fluoride ion from the same α-carbon as before, with subsequent additional coordination of this carbon to the other metal generating a new bridging difluorovinylidene complex (**20**). Once compound **5** has rearranged

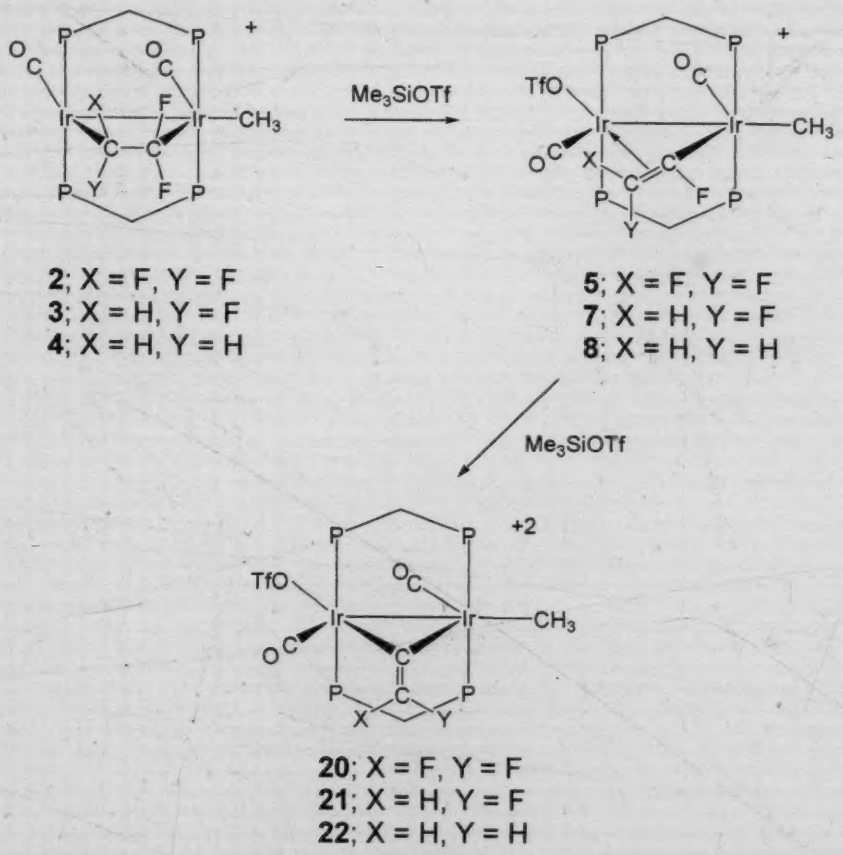

2; X = F, Y = F
3; X = H, Y = F
4; X = H, Y = H

5; X = F, Y = F
7; X = H, Y = F
8; X = H, Y = H

20; X = F, Y = F
21; X = H, Y = F
22; X = H, Y = H

Scheme 3.14. *Sequential C-F activation of fluoroolefin-bridged complexes to give bridging fluorovinyl and (fluoro)vinylidene compounds*

to **6**, no further reaction with trimethylsilyl triflate is effected with the fluorovinyl group in the terminal position (Scheme 3.15).

Having generated the fluorovinylidene complexes, **20** and **21**, hydrogenolysis would in principle yield the corresponding olefins, in which a pair of geminal

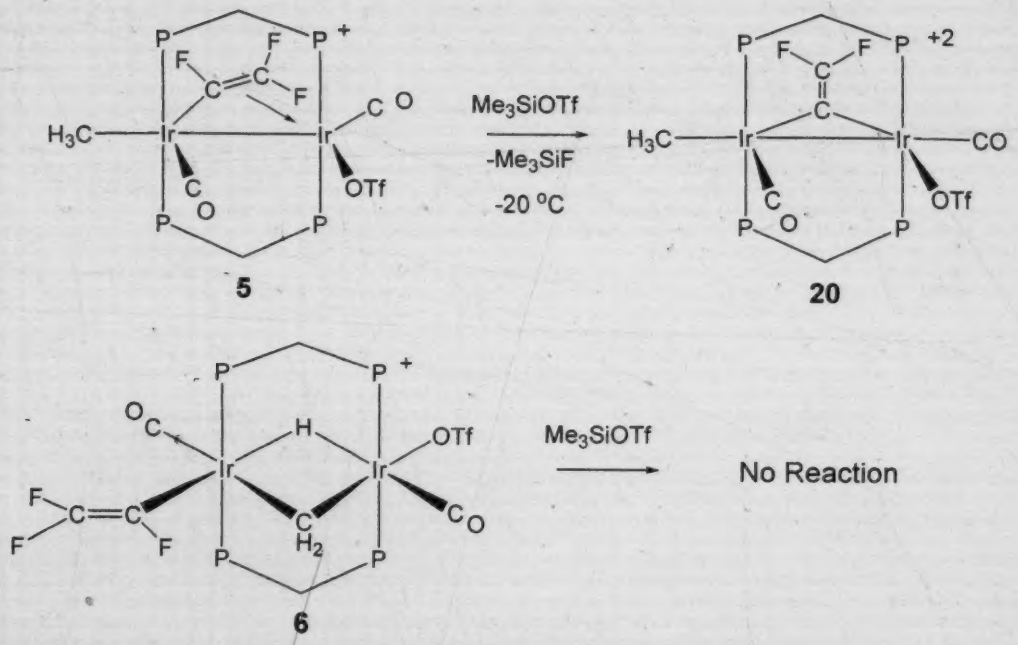

Scheme 3.15. *Reactivity comparison of μ-η¹:η²-C_2F_3 vs. η¹-C_2F_3*

fluorines had been replaced by hydrogens. This would result (in the case of **20** for example) in the conversion of tetrafluoroethylene into 1,1-difluoroethylene. However, these fluoroethylidene species were remarkably unreactive towards the addition of hydrogen, presumably due to their high positive charge (+2). In addition, their reaction with CO gave rise to the expected displacement of triflate by CO, but no migratory insertion of the methyl and vinylidene ligands was observed. Although not investigated in this study, the reaction of the fluorovinylidene and vinylidene products with nucleophiles should be explored.

3.5. Conclusions

We have accomplished all three of our goals related to the reactivity of the fluorovinyl groups that were generated through C-F activation of fluoroolefins.

First, through hydrogenolysis of trifluorovinyl and cis-difluorovinyl complexes we generated the respective trifluoroethylene and cis-difluoroethylene. As a result we have successfully converted tetrafluoroethylene into the former and trifluoroethylene into the latter, through a sequence of C-F activation and hydrogenolysis. Second, we effected the reductive elimination of the methyl and fluorovinyl groups (*cis*-difluorovinyl and 1-fluorovinyl) generating *cis*-1,2-difluoropropene and 2-fluoropropene. This has resulted in the ultimate conversion of trifluoroethylene and 1,1-difluoroethylene into the above respective fluoropropenes by substitution of the appropriate fluorine by a methyl group. Our third goal, the C-F activation within a bridging fluorovinyl group yielded the corresponding difluoro, monofluorovinylidene and vinylidene groups. However, these bridging vinylidene groups have proven to be unreactive so our ultimate goal in this part – to substitute two fluorines in a fluoroolefin with either H or CH_3 – has not yet been realized. Nevertheless we were again able to demonstrate that pairs of metals could act cooperatively in the activation of C-F bonds, since this second activation step occurred only with bridging fluorovinyl groups; terminal fluorovinyls were unreactive.

The dppm-bridged system used in these studies has two drawbacks. First, the bulky phenyl substituents have limited the reactivity by limiting substrate access to the metals. As an example, the largest fluoroolefin investigated, tetrafluoroethylene, reacted very sluggishly, requiring days for completion. We anticipate that smaller ancillary ligands are needed to allow easier access to the metals. The second drawback is the relatively slow rate of the subsequent elimination reactions (either reductive elimination or hydrogenolysis). Here the strength of the iridium-fluorovinyl bond may be at issue. If we can effect the C-F activation step on more labile rhodium, subsequent steps may prove to be faster. To do this we will move to a smaller, more basic diphosphine, to facilitate olefin binding to this metal.

We anticipate achieving both of these objectives with *bis*(diethylphosphino)methane (depm) in which the phenyl groups of dppm are

replaced by ethyl substituents. In the next chapter we will seek to develop a series of depm precursors analogous to compound **1** using the Rh_2, Rh/Ir and Ir_2 metal combinations for ultimate studies in C-F activation.

3.6. References

1. J.R. Torkelson, F.H. Antwi-Nsiah, R. McDonald, M. Cowie, J.G. Prius, K.J. Jalkanen, R.L. DeKock, *J. Am. Chem. Soc.* **1999**, *121*, 3666.
2. R. McDonald, B.R. Sutherland, M. Cowie, *Inorg. Chem.* **1987**, *26*, 3333-3339.
3. C. H. Dungan, J. R. Van Wazer, *Compilation of reported ^{19}F NMR chemical shifts, 1951 to mid-1967*, Wiley-Interscience, New York, 1970.
4. B.R. Sutherland, M. Cowie, *Organometallics* **1985**, *4*, 1637-1648.
5. J. R. Torkelson, Ph. D. Thesis, University of Alberta, 1998.
6. R. H. Morris, *Inorg. Chem.* **1992**, *31*, 1471-1478.
7. H. C. Clark, J. H. Tsai, *Inorg. Chem.* **1966**, *5*, 1407-1415.
8. D.D. Elleman, L.C. Brown, D. Williams, *J. Molec. Spec.* **1961**, *7*, 307-321.
9. D. Huang, P.R. Koren, K. Folting, E.R. Davidson, K.G. Caulton, *J. Am. Chem. Soc.* **2000**, *122*, 8916-8931.
10. M. Fujiwara, J. Ichikawa, T. Okauchi and T. Minami, *Tetrahedron Lett*, **1999**, *40*, 7621-7265.
11. W. Schulze, K. Seppelt, *Inorg. Chem.* **1988**, *27*, 3872-3873.
12. R.N. Perutz, S. Sabo-Etienne, *Angew. Chem. Int. Ed.* **2007**, *46*, 2578-2592.
13. H.C Long, M.L. Turner, P. Fornasiero, J. Kaspar, M. Graziani, P.M. Maitlis, *J. Catal.* **1997**, 172-179.
14. a) T.G. Richmond, *Topics Organomet. Chem.* **1999**, *3*, 243-269; b) R.N. Perutz, T. Braun, *Comprehensive Organometallic Chemistry* III, Chapter 1.26, eds: R.H. Crabtree, D.M.P. Mingos, Elsevier, New York, 2007.

Chapter 4

Towards Alkyl-diphosphine (DEPM) Analogues of $[Ir_2(CH_3)(CO)_2(dppm)_2][CF_3SO_3]$ (1) Involving Diiridium, Dirhodium, and Rhodium/Iridium Centers

4.1. Introduction

In the previous chapters, it was shown that compound **1**, $[Ir_2(CH_3)(CO)_2(dppm)_2][CF_3SO_3]$, displayed a quite remarkable ability to effect the regioselective activation of C-F bonds, in both a series of fluoroolefins and the derived series of fluorovinyl ligands. It was also demonstrated that the pair of metals acted cooperatively in such a way that C-F activation was only effected when the substrates bridged the metals. The above complex (**1**) has also demonstrated a wealth of interesting chemistry, involving C-H bond activation and C-C bond formation, with a variety of unsaturated substrate molecules,[1,2] and again, cooperative activation has been proposed for at least some of these substrates.

Two problems in the above chemistry have been identified. First, coordination of the substrate prior to activation has been inhibited (except for the smallest substrates) presumably through repulsive interactions between the substrate and the bulky phenyl substituents of the dppm ligands. This was observed, for example, for tetrafluoroethylene, the reaction of which took several days, at ambient temperature, and was also observed with 1,3-butadiene, the adduct of which was only observed at temperatures below *ca.* -50 °C.[2] Second, a number of oxidative addition reactions, leading to the activation of selected bonds (usually C-H bonds) were often slow at ambient temperatures (see Chapter 3).

One potential solution to these problems is the replacement of the phenyl groups on the diphosphine ligands by smaller alkyl substituents such as methyl or ethyl groups. The smaller size of these substituents should facilitate substrate access to the metals and the greater basicity of the alkyl diphosphine over the aryl

analogues should favor oxidative addition reactions. We also reasoned that although the C-F activation reactions noted in earlier chapters did not involve oxidative addition, these too might benefit, through stabilization of dicationic intermediates and products that resulted from fluoride ion abstraction, by the better donor alkyl phosphines. We had also hoped that the more basic diphosphine would lead to reactivity of the rhodium-containing analogues of **1**, which had proven to be unreactive towards C-H and C-F bond activation in the case of dppm complexes and for which the olefin adducts were often not observed. The incorporation of the more labile rhodium might be beneficial in promoting the elimination of modified fluoroolefins.

The initial target of our studies on binuclear alkyl diphosphine-bridged species was the dmpm analogue of compound **1**, $[Ir_2(CH_3)(CO)_2(dmpm)_2][CF_3SO_3]$ (dmpm = *bis*(dimethylphosphino)methane = $Me_2PCH_2PMe_2$) which had been previously reported,[3] but for which the subsequent reactivity had apparently never been pursued. However, extensive attempts to synthesize this compound, by myself and independently by a fellow graduate student,[4] via either the published route or by other seemingly rational routes, led to failure, leaving us with the impression that the original report of this species was either in error or that the reported compound had been obtained serendipitously. We therefore switched our emphasis to the analogous depm species (*depm* = *bis*(diethylphosphino)methane = $Et_2PCH_2PEt_2$), anticipating that the slightly larger ethyl substituents (*cf.* methyl) might help to stabilize the targeted complexes.

Depm possesses very similar electron-donating properties to those of dmpm,[5] and while it is more bulky than dmpm, it remains less sterically demanding than dppm, as seen by comparison of their Tolman cone angles (132 ° *vs.* 145 °),[6] and as shown in the space-filling representation in Figure 4.1.

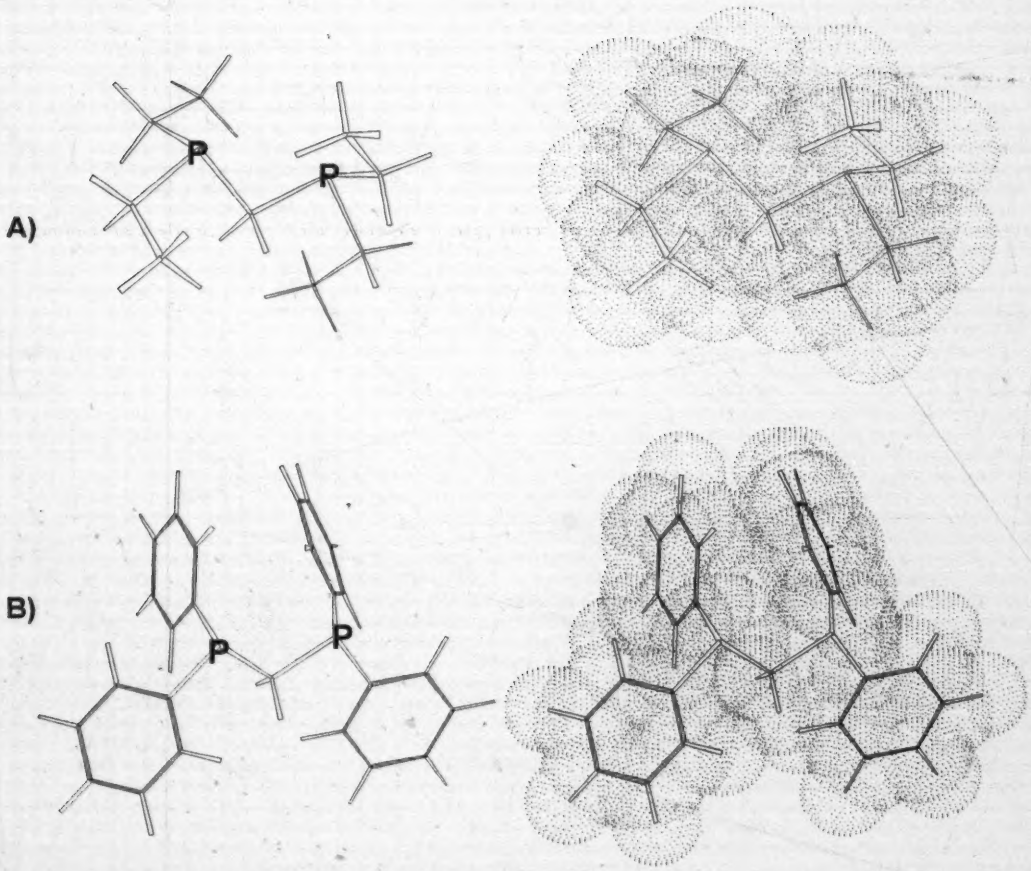

Figure 4.1. *Stick and space-filling representations of;* **A)** *depm vs.* **B)** *dppm ligand systems*

In this chapter the studies on the synthesis of the depm analogue of compound **1**, namely $[Ir_2(CH_3)(CO)_2(depm)_2][CF_3SO_3]$, and also of the dirhodium and mixed rhodium/iridium analogues $[RhM(CH_3)(CO)_2(depm)_2][CF_3SO_3]$ (M = Rh, Ir), are outlined along with a description of the chemistry leading to these targets. It was initially hoped that a comparison of the reactivity between these closely related species might be undertaken, especially with regards to the C-F bond activation chemistry. However, these reactions remain for future investigation.

4.2. Experimental

4.2.1. General Comments. All solvents were dried (using appropriate drying agents), distilled before use and stored under dinitrogen. Deuterated solvents used for NMR experiments were freeze-pump-thaw degassed (three cycles) and stored under nitrogen or argon over molecular sieves. Reactions were carried out under argon using standard Schlenk techniques, and compounds that were used as solids were purified by recrystallization. Prepurified argon and nitrogen were purchased from Linde, carbon-13 enriched CO (99%) was supplied by Isotec Inc. All purchased gases were used as received. The *bis*(diethylphosphino)methane (depm) ligand was prepared by a variation of a literature method,[7] along with $[IrCl(COD)]_2$, $[Ir(Cl)(CO)(PPh_3)]_2$, $[RhCl(COD)]_2$, and $[RhCl(CO)_2]_2$, which were all prepared as previously described.[8, 9, 10, 11] All other reagents were obtained from Aldrich and were used as received (unless otherwise stated).

Proton NMR spectra were recorded on Varian Unity 400, 500 or 600 spectrometers, or on a Bruker AM400 spectrometer. Carbon-13 NMR spectra were recorded on Varian Unity 400 or Bruker AM300 spectrometers. Phosphorus-31 and fluorine-19 NMR spectra were recorded on Varian Unity 400 or Bruker AM400 spectrometers. Two-dimensional NMR experiments (COSY, ROESY, TOCSY and ^{13}C-^{1}H HMQC) were obtained on Varian Unity 400 or 500 spectrometers.

Spectroscopic parameters for all compounds appearing in this chapter are given in Tables 4.1 - 4.3.

Table 4.1. Spectroscopic data for the diiridium compounds

Compound	$\delta(^{31}P\{^1H\})^c$	$\delta(^1H)^d$	$\delta(^{13}C\{^1H\})^d$	IR, cm^{-1} [g,j]
trans-$[Ir_2Cl_2(CO)_2(depm)_2]$ (**23**)	8.28 (s)	2.52 (q, 4H), 2.23 (m, 16H), 1.20 (m, 24H)	168 (s)	1937 (s)
$[Ir_2(CO)_3(depm)_2]$ [i] (**24**)	-11.0 (s, br) (8.9, -28.0) [k]	3.13 (q, 4H), 1.95 (m, 16H), 1.09 (m, 24H)	185 (s, br) (194 (s, br), 189 (s, br), 180 (s)) [k]	1983 (s), 1964 (vs), 1952 (s), 1758 (m, br)
$[Ir_2(CO)_4(depm)_2]$ [i] (**25**)	-31.4 (s, br) (-19.6, -41.1) [k]	2.71 (q, 4H), 1.75 (m, 16H), 0.85(m, 24H)	190 (s, br) (195 (s, br), 194 (s, br), 192 (s), 181 (s)) [k]	2013 (m), 1997 (s), 1937 (s), 1780 (w, br)
$[Ir_2(H)(CO)_3(\mu\text{-}CH_2)(depm)_2][CF_3SO_3]$ (**26**)	-8.9 (m, br), -19.5 (m, br) (-7.5 (t, $^2J_{PP}$ = 32 Hz), -18.9 (t, br)) [k]	3.95 (br, 2H), 2.75 (dm, 4H), 2.10 (m, 16H), 1.10 (m, 24H), -12.4 (t, $^2J_{PH}$ = 16 Hz)	177 (s, br) 47 (m) (180.2 (m, br), 178.7 (dt, $^2J_{CP}$ = 19 Hz), 166.3 (dt, $^2J_{CP}$ = 12 Hz)) [k]	1990 (w), 1965 (s), 1932 (vs)
$[Ir_2(CH_3)(CO)_2(depm)_2][CF_3SO_3]$ (**27**)	23.2 (s)	2.80 (m, 2H), 2.30 (m, 2H), 2.10 (m, 16H), 1.20 (m, 24H), 0.57 (t, 3H, $^3J_{PH}$ = 4 Hz)	168 (br) 180 (br) 19.5	n/a

Notes: [a] NMR abbreviations: s = singlet, d = doublet, t = triplet, q = quintet, m = multiplet, br = broad. [b] NMR data in CD_2Cl_2 unless otherwise stated. [c] $^{31}P\{^1H\}$ chemical shifts are referenced vs. external 85% H_3PO_4 [d] ^1H and ^{13}C chemical shifts are referenced vs. external TMS [e] $\nu(CO)$ [f] Nujol. [g] CH_2Cl_2 [h] C_6H_6 [i] C_6D_6 [j] IR abbreviations: s = strong, m = medium, w = weak [k] indicates low temperature data (see Reslts section)

Table 4.2. Spectroscopic data for the dirhodium compounds

compound	$\delta(^{31}P\{^1H\})^c$	$\delta(^1H)^d$	$\delta(^{13}C\{^1H\})^d$	IR, cm^{-1} [g, j]
trans-$[Rh_2Cl_2(CO)_2(depm)_2]$ (**28**)	17.9 (dm, $^1J_{RhP}$ = 117 Hz)	2.37 (q, 4H), 2.06 (m, 16H), 1.20 (m, 24H)	189 (d, $^1J_{CRh}$ = 75 Hz)	1950 (s)
$[Rh_2(CO)_3(depm)_2]$ [i] (**29**)	15.1 (d, $^1J_{RhP}$ = 138 Hz) (22.5, 8.5) [k]	2.17 (q, 4H), 1.64 (m, 16H), 1.04 (m, 24H)	199 (s, br) (209 (dt, br, $^1J_{CRh}$ = 77 Hz, $^2J_{CP}$ = 32 Hz), 207 (d, br), 183 (d)) [k]	1952 (s), 1934 (vs), 1863 (s)
$[Rh_2(CO)_4(depm)_2]$ [i] (**30**)	12.4 (d, $^1J_{RhP}$ = 133 Hz) (24.3, -1.3) [k]	2.60 (q, 4H), 1.75 (m, 16H), 1.10 5(m, 24H)	204 (s, br, 3C), 214 (dt, $^1J_{CRh}$ = 90 Hz, $^2J_{CP}$ = 30 Hz) [k]	n/a
$[Rh_2(CH_3)(CO)_3(depm)_2][CF_3SO_3]$ (**31**)	35.6 (m, br) (37.3 (dm, $^1J_{RhP}$ = 110 Hz)) [k]	2.35 (q, 4H), 2.60 (m, 16H), 1.15 (m, 24H), 0.63 (q, 3H, $^3J_{HRh}$ = 4 Hz)	214 (t, $^2J_{PC}$ = 33 Hz, 2C), 199 (s, 1C), -0.3 (s)	n/a
$[Rh_2(CH_3CO)(CO)_2(depm)_2][CF_3SO_3]$ (**32**)	22.5 (m, br), 17.2 (m ,br) (21.5 (dm, $^1J_{RhP}$ = 120 Hz), 15.6 (dm, $^1J_{RhP}$ = 139 Hz, $^2J_{PP}$ = 19 Hz)) [k]	2.55 (dm, 4H), 2.42 (s, 3H), 2.20 (m, 16H), 1.20 (m, 24H)	320 (m, br, 1C), 200 (m, 1C), 194 (d, $^1J_{CRh}$ = 76 Hz), 44 (s)	n/a

Notes: [a] NMR abbreviations: s = singlet, d = doublet, t = triplet, q = quintet, m = multiplet, br = broad. [b] NMR data in CD_2Cl_2 unless otherwise stated. [c] $^{31}P\{^1H\}$ chemical shifts are referenced vs. external 85% H_3PO_4 [d] ^1H and ^{13}C chemical shifts are referenced vs. external TMS [e] $\nu(CO)$ [f] Nujol. [g] CH_2Cl_2 [h] C_6H_6 [i] C_6D_6 [j] IR abbreviations: s = strong, m = medium, w = weak [k] indicates low temperature data (see Results section)

Table 4.3. Spectroscopic data for the rhodium-iridium compounds

compound	$\delta(^{31}P\{^1H\})^c$	$\delta(^1H)^d$	$\delta(^{13}C\{^1H\})^d$	IR, cm^{-1} [g,j]
trans-$[RhIrCl_2(CO)_2(depm)_2]$ (**33**)	18.0 (dt, $^1J_{RhP}$ = 118 Hz), 9.6 (t, $^2J_{PP}$ = 64 Hz)	2.42 (q, 4H), 2.15 (m, 16H), 1.15 (m, 24H)	190 (br) 172(s)	1943 (vs), 1934 (s)
$[RhIr(CO)_3(depm)_2]$ [i] (**34**)	17.4 (dt, $^1J_{RhP}$ = 124 Hz), -28.8 (t, $^2J_{PP}$ = 64 Hz) (18.8, -30.5) [k]	3.00 (m, 4H), 1.95 (m, 16H), 0.90 (m, 24H)	189 (s, br, 2C), 186 (d, 1C, $^2J_{CRh}$ = 70 Hz) (191(s, br), 188 (s, br), 186 (d)) [k]	1995 (sh,m), 1959 (s), 1795 (w)
$[RhIr(CO)_4(depm)_2]$ [i] (**35**)	31.5 (dt, $^1J_{RhP}$ = 110 Hz), -3.3 (t, $^2J_{PP}$ = 54 Hz)	2.42 (m, 4H), 1.70 (m, 16H), 1.10 (m, 24H)		n/a
$[RhIr(CH_3)(CO)_3(depm)_2][CF_3SO_3]$ (**36**)	33.0 (dt, $^1J_{RhP}$ = 110 Hz), -10.5 (t, $^2J_{PP}$ = 42 Hz)	3.00 (m, 4H), 2.10 (m, 16H), 1.20 (m, 24H), 0.2 (t, 3H, $^3J_{PH}$ = 6 Hz)	185 (s, 2C) 183.6 (dt, 1C, $^2J_{CRh}$ = 71 Hz, $^2J_{CP}$ = 22 Hz) -35.0 (s)	1792 (w), 1967 (s), 2003 (s)
$[RhIr(CH_3)(CO)_2(depm)_2][CF_3SO_3]$ (**37**)	22.5 (dt, $^1J_{RhP}$ = 111 Hz), 19.8 (t, $^2J_{PP}$ = 47 Hz)	2.7 (m, 2H), 2.4 (m, 2H), 2.05 (m, 16H), 1.2 (m, 24 H), 0.58 (t, 3H, $^3J_{PH}$ = 9 Hz)	182.7 (t, 1C, $^3J_{CP}$ = 7 Hz) 176.6 (dt, 1C, $^2J_{RhC}$ = 73 Hz, $^2J_{CP}$ = 17 Hz) 9.9 (s)	n/a

Notes: [a] NMR abbreviations: s = singlet, d = doublet, t = triplet, q = quintet, m = multiplet, br = broad. [b] NMR data in CD_2Cl_2 unless otherwise stated. [c] $^{31}P\{^1H\}$ chemical shifts are referenced vs. external 85% H_3PO_4 [d] ^1H and ^{13}C chemical shifts are referenced vs. external TMS [e] $\nu(CO)$ [f] Nujol. [g] CH_2Cl_2 [h] C_6H_6 [i] C_6D_6 [j] IR abbreviations: s = strong, m = medium, w = weak [k] indicates low temperature data (see Results section)

4.2.2. Preparation of Compounds

(a) **[Ir(CO)(depm)$_2$][Cl].** To a solution of Vaska's complex, [Ir(Cl)(CO)(PPh$_3$)]$_2$ (250 mg, 0.320 mmol) in 25 mL of THF was added, via cannula, 150 μL (0.66 mmol) of *bis*(diethylphosphino)methane (depm), causing the solution to change from yellow to red-purple. The solution was stirred for 1 h and then was reduced *in vacuo* to *ca.* 10 mL and pentane (40 mL) was added to precipitate a light mauve colored solid. The product was isolated, washed twice with pentane (2x10 mL), dried briefly under a stream of argon, and then *in vacuo*, to give spectroscopically pure [Ir(CO)(depm)$_2$][Cl] in typically good yields.

(b) ***trans*-[Ir$_2$Cl$_2$(CO)$_2$(depm)$_2$] (23).** To a solution of [Ir(Cl)(COD)]$_2$ (200 mg, 0.30 mmol) in 25 mL of dichloromethane was quickly added, via cannula, 100 μL (0.60 mmol) of *bis*(diethylphosphino)methane (depm) in 5 mL of dichloromethane, causing the solution to change from orange/red to yellow/orange. The solution was stirred for 15 min and then stirred under a slow CO purge for 5 min. The CO was replaced by an argon purge and the solution set to reflux for ½ h. Reducing the solution to dryness *in vacuo* left an oily orange residue which was redissolved into 25 mL of tetrahydrofuran (THF). This solution was set to reflux again for 1½ h, with a continuing argon purge, resulting in a notable color change to dark red/purple. The solution was reduced *in vacuo* to *ca.* 10 mL and Et$_2$O (40 mL) was added to precipitate a deep red-purple solid, which was isolated, washed twice with Et$_2$O (2x10 mL), dried briefly under a stream of argon, and then *in vacuo* to yield 150 mg (60 %) of compound **23**. HRMS *m/z* calcd for Ir$_2$P$_4$O$_2$C$_{20}$H$_{44}$Cl: 860.3804. Found: 860.3805.

(c) **$[Ir_2(CO)_3(depm)_2]$ (24).** 100 mg (0.090 mmol) of compound **23** was dissolved into 10 mL of THF giving a turbid, deep scarlet-purple solution. This was placed under an atmosphere of CO resulting in a series of color changes, through red, and finally to clear orange. The addition of *ca.*2.5 mL of 1 M KOH/H_2O yielded a dark orange solution which was stirred (closed under CO) at room temperature for ½ h. At this point the solution was stripped to dryness *in vacuo*, extracted (3x) with 10mL of benzene and filtered through celite. The resulting solution was refluxed with an argon purge for 2 h after which time it could be carried forward as such, or stripped again to dryness to give 75 mg (98 %) of spectroscopically pure compound **24**, as a dark brown-orange oil. HRMS *m/z* calcd for $Ir_2P_4O_3C_{21}H_{44}$: 852.9381.

(d) **$[Ir_2(CO)_4(depm)_2]$ (25).** $[Ir_2(CO)_3(depm)_2]$ (**24**) (50 mg, 0.058 mmol) was dissolved in 10 mL of benzene and stirred under a dynamic atmosphere of CO for ½ h, causing the color to change from orange to bright yellow. Removal of the solvent at this point resulted in an oily, dark yellow-orange residue containing a mixture of compounds **24** and **25** in variable proportions, as gauged by NMR spectroscopy, revealing the susceptibility of compound **25** to CO loss. The lability of this carbonyl has limited the characterization of compound **25** to NMR spectroscopy (see Results section).

(e) **$[Ir_2(H)(CO)_3(\mu\text{-}CH_2)(depm)_2][CF_3SO_3]$ (26).** 11 μL (1.00 mmol) of neat methyltrifluoromethanesulphonate (MeOTf) was slowly added drop-wise to a solution of $[Ir_2(CO)_3(depm)_2]$ (**24**) (75 mg, 0.088 mmol) in 15 mL of benzene. The resulting turbid, dark orange mixture was stirred for 1 h whereupon it was reduced *in vacuo* to *ca.* 2 mL, and pentane (10

mL) was added dropwise to precipitate a resinous yellow-orange solid. This solid was further washed with pentane (2 x 10 mL) and dried *in vacuo* giving 80 mg of pale orange powder (89 % yield). HRMS *m/z* calcd for $Ir_2P_4O_3C_{22}H_{47}$: 867.9729. Found: 867.9732.

(f) **$[Ir_2(CH_3)(CO)_2(depm)_2][CF_3SO_3]$ (27).** To a solution of $[Ir_2(H)(CO)_3(\mu\text{-}CH_2)(depm)_2][CF_3SO_3]$ (**26**) (55 mg, 0.63 mmol) in 15 mL of dichloromethane was added, drop-wise, freshly sublimed trimethylamine-N-oxide (TMNO) (4 mg, 0.53 mmol) in 10 mL of dichloromethane, over 10-15 min period, while employing a gentle argon purge with stirring. The resulting solution was stirred an additional 30 min whereupon the solvent was removed *in vacuo* to give an orange-red residue. The product was found to be extremely moisture-sensitive, and was also prone to further reaction in solution, at ambient temperature, resulting in the formation of unidentified products. Therefore compound **27** has been characterized via solution spectroscopy, only when prepared *in situ* at 0 °C, through comparison of its spectral parameters to those of its dppm analogue (**1**).

(g) ***trans*-$[Rh_2Cl_2(CO)_2(depm)_2]$ (28).** A solution of $[Rh_2Cl_2(COD)_2]$ (110 mg, 0.223 mmol) in 20 mL of acetone was placed under an atmosphere of CO and stirred for 10 min. To this solution was added dropwise, over a 5 min period, 100 μL (0.441 mmol) of depm in 10 mL of acetone, causing the color to change from yellow to orange. The solution was then refluxed for ½ h whereupon it was cooled to room temperature and reduced to dryness *in vacuo*. The residue was redissolved into *ca.* 5 mL of THF, and Et_2O (20 mL) was added to precipitate an orange solid which was further washed with Et_2O (2 x 5 mL) and dried *in vacuo*

yielding 85 mg (53 % yield) of spectroscopically pure compound **28**. HRMS *m/z* calcd for $Rh_2P_4O_2C_{20}H_{44}Cl$: 681.0088. Found: 681.0090.

(h) **[$Rh_2(CO)_3(depm)_2$] (29).** [$Rh_2Cl_2(CO)_2(depm)_2$] (**28**) (65 mg, 0.091 mmol) was dissolved in 20 mL of THF and stirred under a static atmosphere of CO. 2 mL of aqueous 1M KOH was transferred dropwise, via a syringe, onto the stirred solution and the resulting mixture left to stir for 1 ½ h. At this point the solvent was removed *in vacuo* to give an oily brown residue, which was then extracted with benzene (20 mL). Filtration through celite gave a clear orange-brown solution, which when reduced to dryness *in vacuo* afforded 55 mg of the spectroscopically pure complex (**29**) as a viscous orange-brown oil (90 % yield). HRMS *m/z* calcd for $Rh_2P_4O_3C_{21}H_{44}$: 674.3091.

(i) **[$Rh_2(CO)_4(depm)_2$] (30).** [$Rh_2(CO)_3(depm)_2$] (**29**) (50 mg, 0.072 mmol) was dissolved in 7 mL of d_6-benzene and placed under an atmosphere of CO, causing the color of the solution to change from orange to yellow. The conversion of **29** to **30** was determined to be quantitative via NMR spectroscopy. However, removal of the CO atmosphere resulted in complete reversion back to the tricarbonyl starting material, thus compound **30** has been characterized *in situ* via NMR spectroscopy.

(j) **[$Rh_2(CH_3)(CO)_3(depm)_2$][CF_3SO_3] (31).** To a solution of [$Rh_2(CO)_3(depm)_2$] (**29**) (70 mg, 0.104 mmol) in 10 mL of benzene, cooled in an ice bath to 0 °C, was slowly added, over a 5 min period, 12 μL (0.108 mmol) of neat methyltrifluoromethanesulphonate (MeOTf), giving a reddened color to the solution. This mixture was stirred for ½ h

while maintaining the temperature at 0 °C, during which time a precipitate was formed. The product was isolated and further washed with pentane (2 x 10 mL) then dried *in vacuo* to give 60 mg of resinous red-orange solid (70 % yield). Attempts at recrystallization or redissolution of compound **31** into NMR solvents at room temperature showed the appearance of another new set of signals in the NMR spectra corresponding to compound **32**.

(k) **$[Rh_2(CH_3CO)(CO)_2(depm)_2][CF_3SO_3]$ (32).** Leaving compound **31** (50 mg, 0.060 mmol), in solution at ambient temperature, resulted in its conversion to compound **32**, over the course of hours, as established by NMR spectroscopy (see Results section). Isolation of this species has been hampered by its extreme moisture sensitivity, and its subsequent decomposition to unidentified products, thus characterization of this complex has been thus far limited to NMR spectroscopy.

(l) ***trans*-$[RhIrCl_2(CO)_2(depm)_2]$ (33).** $[Ir(CO)(depm)_2][Cl]$ (244mg, 0.382 mmol) was dissolved in 7mL of dichloromethane, with stirring. In a separate flask, $[Rh(Cl)(CO)_2]_2$ (75mg, 0.197 mmol) was also dissolved in 7mL of dichloromethane, with stirring. The $[IrCl(CO)(depm)_2]$ solution was then added to the $[Rh(Cl)(CO)_2]_2$ solution, over 5 min, and the resulting mixture was left closed under a static atmosphere of argon, without agitation for 2 h. The solvent was removed *in vacuo* and the residue redissolved in 7mL of THF, followed by the addition of pentane (30 mL) to precipitate a dark orange solid. The solid was further washed with pentane (2 x 10 mL) and dried *in vacuo* giving 200 mg (67 % yield). HRMS *m/z* calcd for $IrRhP_4O_2C_{20}H_{44}Cl$: 771.0659. Found: 771.0658.

(m) [RhIr(CO)$_3$(depm)$_2$] (34). Method a) [RhIrCl$_2$(CO)$_2$(depm)$_2$] (**33**) (275mg, 0.341 mmol) was dissolved in 20 mL of THF and stirred under a dynamic atmosphere of CO. 8 mL of aqueous 1M KOH was transferred dropwise, via syringe, to the stirred solution and the resulting mixture was stirred for 1 ½ h. The solvent was removed under vacuum and the product extracted (3x) with 20 mL of benzene. Filtration through celite gave a clear orange-brown solution, which was purged with CO for 5 min followed by argon for 10 min. The solvent was reduced to dryness *in vacuo* affording the complex as a spectroscopically pure viscous orange-brown oil (198 mg, 76 % yield). HRMS *m/z* calcd for IrRhP$_4$O$_2$C$_{20}$H$_{45}$ [M+H$^+$-CO]: 737.1054. Found: 737.1049.

Method b) [RhIrCl$_2$(CO)$_2$(depm)$_2$] (37mg, 0.046 mmol) was dissolved in 10 mL of acetone. Excess NaBH$_4$ (0.200 mmol) was added directly to the solution which was allowed to stir for 1 h. The solvent was removed *in vacuo* and the product redissolved in 10 mL of benzene or THF. Filtration through celite gave a clear orange-brown solution, which was purged with CO for 5 min followed by argon for 10 min. The solvent was reduced to dryness *in vacuo* affording the complex as a viscous orange-brown oil. However, samples obtained via this method were always less pure, spectroscopically, and were generally obtained in poorer yields compared to the first method.

(n) [RhIr(CO)$_4$(depm)$_2$] (35). [RhIr(CO)$_3$(depm)$_2$] (**34**) (50 mg, 0.066 mmol) was dissolved in 0.7 mL of d_6-benzene and placed under an atmosphere of CO, causing the color to change from orange to yellow. NMR spectroscopy showed complete conversion of compound **34** to compound **35**. However, subsequent removal of the solvent, *in vacuo*, resulted in the loss of a CO, with quantitative reversion back to the

starting compound, thus the characterization of compound **35** has been limited to solution NMR spectroscopy.

(o) **$[RhIr(CH_3)(CO)_3(depm)_2][CF_3SO_3]$ (36).** To a solution of 75 mg (0.098 mmol) of $[RhIr(CO)_3(depm)_2]$ (**34**) in 10 mL of benzene was slowly added drop-wise, over a 5 min period, 11 μL (0.098 mmol) of neat MeOTf. The resulting mixture was stirred for 1 h whereupon it was reduced *in vacuo* to dryness and the residue redissolved in a minimum volume of THF (2 mL). Pentane (10 mL) was added to precipitate a dark yellow-brown solid which was isolated and further washed with pentane (2 x 10 mL) then dried *in vacuo* giving 60 mg of spectroscopically pure compound **36** (79 % yield).

(p) **$[RhIr(CH_3)(CO)_2(depm)_2][CF_3SO_3]$ (37).** To a solution of 90 mg (0.097 mmol) of $[RhIr(CH_3)(CO)_3(depm)_2][CF_3SO_3]$ (**36**) in 15 mL of CH_2Cl_2 was slowly added freshly sublimed TMNO (7 mg, 0.530 mmol) in 10 mL of CH_2Cl_2. The solvent was immediately removed *in vacuo* resulting in a dark brown-red residue. Much like its homobinuclear congeners, the product was unstable and was also extremely moisture-sensitive and subsequent recrystallization from various dried solvents resulted only in decomposition or hydrolysis products, thus compound **37** has been characterized via NMR spectroscopy.

X-Ray Data Collection. Data collection and structure solution (*vide infra*) were carried out by R. McDonald and M. J. Ferguson. Red crystals of $[Ir_2Cl_2(CO)_2(depm)_2]$ (**23**) were obtained *via* slow diffusion of *n*-pentane into a

THF solution of the complex. Red crystals of $[Rh_2Cl_2(CO)_2(depm)_2]$ (**28**) were obtained *via* slow diffusion of *n*-pentane into a THF solution of the complex. Red crystals $[RhIrCl_2(CO)_2(depm)_2]$ (**33**) were obtained *via* slow diffusion of diethyl ether into a dichloromethane solution of the compound. In all cases the *trans*-complexes showed disorder amongst the chloro- and carbonyl ligands, with varying degrees of occupancy for each in the respective sites, designated 'A' and 'B' (Ir_2; 0.6A:0.4B, Rh_2; 0.75A:0.25B, RhIr; 0.45A:0.55B). In addition the mixed-metal complex also showed 50% disorder between the two metal centers. See Table 4.4 for a complete summary of crystal data and X-ray data collection information for the three *trans*-complexes.

Colorless crystals of $[Ir_2(H)(CO)_3(\mu\text{–}CH_2)(depm)_2][CF_3SO_3]$ (**26**) were obtained *via* slow diffusion of diethyl ether into a dichloromethane solution of the compound. The structure solution shows some disorder in the position of the carbonyl ligand adjacent to the hydride, along with the component ethyl groups of one end of the associated phosphine. The C-C bond distance in the latter was restrained to be 1.53(1) Å during refinement, along with the Ir-H distance, of the hydride, which was restrained at 1.65(1) Å and whose placement was idealized. See Table 4.5 for a summary of crystal data and X-ray data collection information for compound **26**.

Pale orange crystals of $[RhIr(CH_3(CO)_3(depm)_2][CF_3SO_3]$ (**36**) were obtained *via* slow diffusion of pentane into a dichloromethane solution of the compound. The mixed-metal complex showed disorder in the occupancy of metals in each of the respective sites, designated 'A' and 'B' (0.6A:0.4B), along with the associated bridging carbonyls. The structure solution also shows disorder in the position of one of the ethyl groups of one of bridging bisphosphine ligands (0.67A:0.33B). See Table 4.6 for a summary of crystal data and X-ray data collection information for compound **36**.

Table 4.4. Crystallographic Experimental Details for Compounds **23, 28** and **33**, the 'trans-depm' series

A. Crystal Data

formula	$C_{20}H_{44}Cl_2Ir_2O_2P_4$	$C_{20}H_{44}Cl_2O_2P_2Rh_2$	$C_{20}H_{44}Cl_2IrO_2P_4Rh$
formula weight	895.73	717.15	806.44
crystal dimensions (mm)	0.54 × 0.52 × 0.43	0.37 × 0.32 × 0.28	0.19 × 0.18 × 0.12
crystal system	monoclinic	monoclinic	monoclinic
space group	$P2_1/n$ (an alternate setting of $P2_1/c$ [No. 14])	$P2_1/n$ (an alternate setting of $P2_1/c$ [No. 14])	$P2_1/n$ (an alternate setting of $P2_1/c$ [No. 14])
unit cell parameters[a]			
a (Å)	10.5127 (5)	10.4972 (6)	10.5146 (7)
b (Å)	11.6941 (6)	11.6908 (6)	11.6828 (7)
c (Å)	11.9926 (6)	12.0101 (7)	12.0077 (8)
β (deg)	103.8544 (9)	103.795 (1)	103.794 (1)
V (Å^3)	1431.4 (1)	1431.4 (1)	1432.5 (2)
Z	2	2	2
ρ_{calcd} (g cm^{-3})	2.078	1.664	1.870
μ (mm^{-1})	9.713	1.579	5.642

B. Data Collection and Refinement Conditions

diffractometer	Bruker PLATFORM/ SMART 1000 CCD	Bruker PLATFORM/ SMART 1000 CCD	Bruker PLATFORM/ SMART 1000 CCD
radiation (λ [Å])	graphite-monochromated Mo Kα (0.71073)	graphite-monochromated Mo Kα (0.71073)	graphite-monochromated Mo Kα (0.71073)

(continued)

Table 4.4. (continued)

Formula	$C_{20}H_{44}Cl_2Ir_2O_2P_4$	$C_{20}H_{44}Cl_2O_2P_2Rh_2$	$C_{20}H_{44}Cl_2IrO_2P_4Rh$
temperature (°C)	–80	–80	–80
scan type	ω scans (0.2°) (20 s exposures)	ω scans (0.2°) (25 s exposures)	ω scans (0.2°) (25 s exposures)
data collection 2θ limit (deg)	52.80	52.78	52.72
total data collected	7929 ($-12 \le h \le 13$, $-14 \le k \le 14$, $-14 \le l \le 14$)	6899 (-13<=h<=13, -14<=k<=13, -12<=l<=15)	8230 ($-13 \le h \le 13$, $-10 \le k \le 14$, $-14 \le l \le 13$)
independent reflections	2908 (R_{int} = 0.0248)	2912 (R_{int} = 0.0264)	2919 (R_{int} = 0.0272)
number of observed reflections (*NO*)	2836 [$F_o^2 \ge 2\sigma(F_o^2)$]	2749 [$F_o^2 \ge 2\sigma(F_o^2)$]	2713 [$F_o^2 \ge 2\sigma(F_o^2)$]
structure solution method	direct methods (*SHELXS–86*[c])	direct methods (*SHELXS–86*[c])	direct methods (*SHELXS–86*[c])
Refinement method[b]	full-matrix least-squares on F^2 (*SHELXL–93*[d])	full-matrix least-squares on F^2 (*SHELXL–93*[d])	full-matrix least-squares on F^2 (*SHELXL–93*[d])
absorption correction method	empirical (*SADABS*)	empirical (*SADABS*)	empirical (*SADABS*)
range of transmission factors	0.1027–0.0773	0.6662–0.5927	0.5509–0.4137
data/restraints/ parameters	2908 [$F_o^2 \ge -3\sigma(F_o^2)$] / 0 / 139	2912 [$F_o^2 \ge -3\sigma(F_o^2)$] / 0 / 163	2919 [$F_o^2 \ge -3\sigma(F_o^2)$] / 0 / 163
goodness-of-fit (*S*)[e]	1.226 [$F_o^2 \ge -3\sigma(F_o^2)$]	1.139 [$F_o^2 \ge -3\sigma(F_o^2)$]	1.111 [$F_o^2 \ge -3\sigma(F_o^2)$]

(continued)

Table 4.4. (continued)

Formula	$C_{20}H_{44}Cl_2Ir_2O_2P_4$	$C_{20}H_{44}Cl_2O_2P_2Rh_2$	$C_{20}H_{44}Cl_2IrO_2P_4Rh$
final *R* indices[f]			
R_1 [$F_o^2 \geq 2\sigma(F_o^2)$]	0.0265	0.0231	0.0202
wR_2 [$F_o^2 \geq -3\sigma(F_o^2)$]	0.0725	0.0608	0.0493
largest difference peak and hole	2.075 and –3.059 e Å^{-3}	0.641 and –0.303 e Å^{-3}	0.857 and –0.599 e Å^{-3}
Reflections	8106	6740	6982
2θ	$4.63° < 2\theta < 52.75°$	$4.64° < 2\theta < 52.75°$	$4.63° < 2\theta < 52.71°$

[a]Obtained from least-squares refinement

[b]Programs for diffractometer operation, data collection, data reduction and absorption correction were those supplied by Bruker.

[c]Sheldrick, G. M. *Acta Crystallogr.* **1990**, *A46*, 467–473.

[d]Sheldrick, G. M. *SHELXL-93*. Program for crystal structure determination. University of Göttingen, Germany, 1993. Refinement on F_o^2 for all reflections (all of these having $F_o^2 \geq -3\sigma(F_o^2)$). Weighted *R*-factors wR_2 and all goodnesses of fit *S* are based on F_o^2; conventional *R*-factors R_1 are based on F_o, with F_o set to zero for negative F_o^2. The observed criterion $F_o^2 > 2\sigma(F_o^2)$ is used only for calculating R_1, and is not relevant to the choice of reflections for refinement. *R*-factors based on F_o^2 are statistically about twice as large as those based on F_o, and *R*-factors based on ALL data will be even larger.

[e]$S = [\Sigma w(F_o^2 - F_c^2)^2/(n-p)]^{1/2}$ (n = number of data; p = number of parameters varied; $w = [\sigma^2(F_o^2) + (0.0229P)^2 + 0.9846P]^{-1}$ where $P = [\text{Max}(F_o^2, 0) + 2F_c^2]/3$). [f]$R_1 = \Sigma||F_o| - |F_c||/\Sigma|F_o|$; $wR_2 = [\Sigma w(F_o^2 - F_c^2)^2/\Sigma w(F_o^4)]^{1/2}$.

Table 4.5. Crystallographic Experimental Details for $[Ir_2(H)(CO)_3(\mu\text{-}CH_2)(depm)_2][CF_3SO_3]$ (**26**)

A. Crystal Data	
formula	$C_{23}H_{47}F_3Ir_2O_6P_4S$
formula weight	1016.95
crystal dimensions (mm)	0.32 × 0.23 × 0.19
crystal system	triclinic
space group	$P\bar{1}$ (No. 2)
unit cell parameters[a]	
a (Å)	10.6784 (7)
b (Å)	12.5837 (9)
c (Å)	14.917 (1)
α (deg)	111.404 (1)
β (deg)	96.287 (1)
γ (deg)	107.840 (1)
V (Å^3)	1720.2 (2)
Z	2
ρ_{calcd} (g cm^{-3})	1.963
μ (mm^{-1})	8.024
B. Data Collection and Refinement Conditions	
diffractometer	Bruker PLATFORM/SMART 1000 CCD[b]
radiation (λ [Å])	graphite-monochromated Mo Kα (0.71073)
temperature (°C)	–80
scan type	ω scans (0.3°) (20 s exposures)
data collection 2θ limit (deg)	52.78
total data collected	13362 ($-13 \le h \le 13$, $-15 \le k \le 15$, $-18 \le l \le 18$)
independent reflections	6992 (R_{int} = 0.0224)
number of observed reflections (*NO*)	6039 [$F_o^2 \ge 2\sigma(F_o^2)$]
structure solution method	direct methods (*SHELXS–86*[c])
refinement method	full-matrix least-squares on F^2 (*SHELXL-93*[d])
absorption correction method	Gaussian integration (face-indexed)
range of transmission factors	0.3109–0.1833
data/restraints/parameters	6992 [$F_o^2 \ge -3\sigma(F_o^2)$] / 3[e] / 354
goodness-of-fit (S)[f]	1.050 [$F_o^2 \ge -3\sigma(F_o^2)$]
final R indices[g]	
R_1 [$F_o^2 \ge 2\sigma(F_o^2)$]	0.0308
wR_2 [$F_o^2 \ge -3\sigma(F_o^2)$]	0.0811
largest difference peak and hole	2.273 and –0.746 e Å^{-3}

[a]Obtained from least-squares refinement of 4949 reflections with $4.48° < 2\theta < 52.79°$.

Table 4.5. Crystallographic Experimental Details (continued)

[b]Programs for diffractometer operation, data collection, data reduction and absorption correction were those supplied by Bruker.

[c]Sheldrick, G. M. *Acta Crystallogr.* **1990**, *A46*, 467–473.

[d]Sheldrick, G. M. *SHELXL-93*. Program for crystal structure determination. University of Göttingen, Germany, 1993. Refinement on F_o^2 for all reflections (all of these having $F_o^2 \geq -3\sigma(F_o^2)$). Weighted R-factors wR_2 and all goodnesses of fit S are based on F_o^2; conventional R-factors R_1 are based on F_o, with F_o set to zero for negative F_o^2. The observed criterion of $F_o^2 > 2\sigma(F_o^2)$ is used only for calculating R_1, and is not relevant to the choice of reflections for refinement. R-factors based on F_o^2 are statistically about twice as large as those based on F_o, and R-factors based on ALL data will be even larger.

[e]The Ir(2)–H(2) distance was restrained to be 1.65(1) Å. The C(25)–C(26A) and C(25)–C(26B) distances were restrained to be 1.53(1) Å.

[f]$S = [\Sigma w(F_o^2 - F_c^2)^2/(n-p)]^{1/2}$ (n = number of data; p = number of parameters varied; $w = [\sigma^2(F_o^2) + (0.0399P)^2 + 3.1190P]^{-1}$ where $P = [\text{Max}(F_o^2, 0) + 2F_c^2]/3$).
[g]$R_1 = \Sigma||F_o| - |F_c||/\Sigma|F_o|$; $wR_2 = [\Sigma w(F_o^2 - F_c^2)^2/\Sigma w(F_o^4)]^{1/2}$.

Table 4.6. Crystallographic Experimental Details for $[Ir_2(CH_3)(CO)_3(depm)_2][CF_3SO_3]$ (**36**)

A. Crystal Data	
formula	$C_{23}H_{47}F_3IrO_6P_4RhS$
formula weight	927.66
crystal dimensions (mm)	0.54 × 0.16 × 0.15
crystal system	monoclinic
space group	$P2_1/c$ (No. 14)
unit cell parameters[a]	
a (Å)	8.0072 (12)
b (Å)	18.318 (3)
c (Å)	23.367 (4)
β (deg)	90.877 (2)
V (Å^3)	3426.9 (9)
Z	4
ρ_{calcd} (g cm^{-3})	1.798
μ (mm^{-1})	4.658

Table 4.6. Crystallographic Experimental Details (continued)

B. Data Collection and Refinement Conditions

diffractometer	Bruker PLATFORM/SMART 1000 CCD[b]
radiation (λ [Å])	graphite-monochromated Mo Kα (0.71073)
temperature (°C)	–80
scan type	ω scans (0.3°) (20 s exposures)
data collection 2θ limit (deg)	52.86
total data collected	25673 ($-9 \le h \le 10$, $-22 \le k \le 22$, $-29 \le l \le 29$)
independent reflections	6971 (R_{int} = 0.0346)
number of observed reflections (*NO*)	6224 [$F_o^2 \ge 2\sigma(F_o^2)$]
structure solution method	direct methods (*SHELXS–97*[c])
refinement method	full-matrix least-squares on F^2 (*SHELXL–97*[d])
absorption correction method	multi-scan (*SADABS*)
range of transmission factors	0.5417–0.1876
data/restraints/parameters	6971 [$F_o^2 \ge -3\sigma(F_o^2)$] / 18[e] / 384
goodness-of-fit (*S*)[f]	1.182 [$F_o^2 \ge -3\sigma(F_o^2)$]
final *R* indices[g]	
R_1 [$F_o^2 \ge 2\sigma(F_o^2)$]	0.0526
wR_2 [$F_o^2 \ge -3\sigma(F_o^2)$]	0.1334
largest difference peak and hole	3.100 and –1.649 e Å^{-3}

[a]Obtained from least-squares refinement of 6215 reflections with $5.56° < 2\theta < 52.86°$.

[b]Programs for diffractometer operation, data collection, data reduction and absorption correction were those supplied by Bruker.

[c]Sheldrick, G. M. *Acta Crystallogr.* **1990**, *A46*, 467–473.

[d]Sheldrick, G. M. *SHELXL-97*. Program for crystal structure determination. University of Göttingen, Germany, 1997.

[e]The minor (40%) component of the disordered $RhIr(CO)_3(CH_3)$ fragment (IrB, RhB, O1B, O2B, O3B, C1B, C2B, C3B, C4B) was restrained to have the same bond lengths and angles as the major orientation.

[f]$S = [\Sigma w(F_o^2 - F_c^2)^2/(n-p)]^{1/2}$ (n = number of data; p = number of parameters varied; $w = [\sigma^2(F_o^2) + (0.0304P)^2 + 46.1634P]^{-1}$ where $P = [\text{Max}(F_o^2, 0) + 2F_c^2]/3$).

[g]$R_1 = \Sigma||F_o| - |F_c||/\Sigma|F_o|$; $wR_2 = [\Sigma w(F_o^2 - F_c^2)^2/\Sigma w(F_o^4)]^{1/2}$.

4.3. Results and Compound Characterization

The preparations of the depm analogues of **1** and its precursors, have been achieved via similar synthetic methods to those involved in the preparation of the dppm and (where possible) dmpm complexes. Data for the depm ethyl protons are not discussed in this section since they are not diagnostic in structural discussions, however they are summarized in the respective Tables (4.1 - 4.3). In all cases, disscussion of the depm methylene resonances refers to the methylene group bridging the two phosphine nuclei and not to the methylenes of the ethyl substituents.

4.3.1. Diiridium Complexes

4.3.1.1. *trans*-$[Ir_2Cl_2(CO)_2(depm)_2]$ (23)

The reaction of $[IrCl(COD)]_2$ with two equivalents of depm, followed by the addition of CO is initially carried out in CH_2Cl_2, giving an orange-red solution. Subsequent solvent removal and extraction of this mixture into a THF solution, followed by refluxing under an argon purge, results in a distinct color change to violet, and subsequent isolation yields $[Ir_2Cl_2(CO)_2(depm)_2]$ (**23**), as shown in the representation below, as a dark red-purple solid in modest yields.

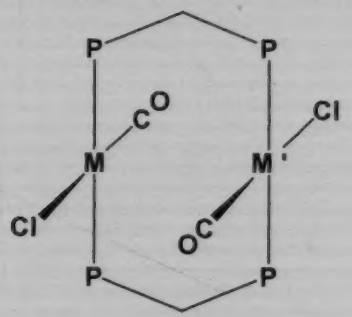

23

Figure 4.2. *General structure of trans-$[MM'_2Cl_2(CO)_2(depm)_2]$ (M, M' = Rh, Ir)*

It should be noted that insufficient purging and/or reflux times in the last synthetic step results in the formation of the related polycarbonyl complexes $[Ir_2Cl_2(CO)_x(depm)_2]$ (x = 3, 4), as has been observed previously in the analogous dppm system.[12] Characterization of these higher carbonyl complexes has not been carried out since **23** was our targeted precursor for subsequent reactions, and, in any case, all such complexes present in the isolated mixture proved to be equally transformable to the same formally Ir(0)/Ir(0) carbonyl species under reducing conditions (*vide infra*).

The $^{31}P\{^1H\}$ NMR spectrum of compound **23** appears as a singlet at 8.28 ppm, indicative that all of the ^{31}P nuclei are chemically equivalent. In the ^1H NMR spectrum, all four methylene protons are displayed as a broad multiplet at 2.52 ppm, which is consistent with the proposed symmetrical '*trans*' geometry, in which the carbonyl, and chloro ligands on one metal are inversion related to those on the adjacent metal. Further evidence for the neutral formulation of compound **23** is supported by its infrared spectrum, which shows only a single carbonyl stretch at 1937 cm^{-1}. In the cationic dicarbonyl, $[Ir_2(CO)_2(\mu\text{-}Cl)(depm)_2][Cl]$, two carbonyl stretches would be expected, which should also be at somewhat higher frequency. The solid-state geometry in compound **23** has been confirmed crystallographically, through a single crystal X-ray diffraction study. The resulting structure, the ORTEP representation of which is shown in Figure 4.2, is consistent with that of the previously characterized dirhodium dppm analogue[13] and the analogous $[RhMCl_2(CO)_2(depm)_2]$ (M=Rh, Ir) complexes investigated herein (*vide infra*). The structure clearly shows the *trans* di-bridged arrangement of the diphosphine ligands about the two Ir centers. Although there was a slight disorder in the occupancy of the chloro and carbonyl ligands, between the two sites designated 'A' and 'B', these groups are also found in an approximate *trans* relationship; both sharing one metal, and related to those on the adjacent metal by inversion symmetry, so that both chlorines are on opposite sides of the Ir_2P_4 plane, as are the carbonyls. These equatorial ligands show a slight bending away from the inversion center, giving a Cl-Ir-CO angle of

173.3(3)°. Presumably, this bending occurs to minimize the repulsive interactions between the adjacent Cl and CO ligands on the adjacent metals.

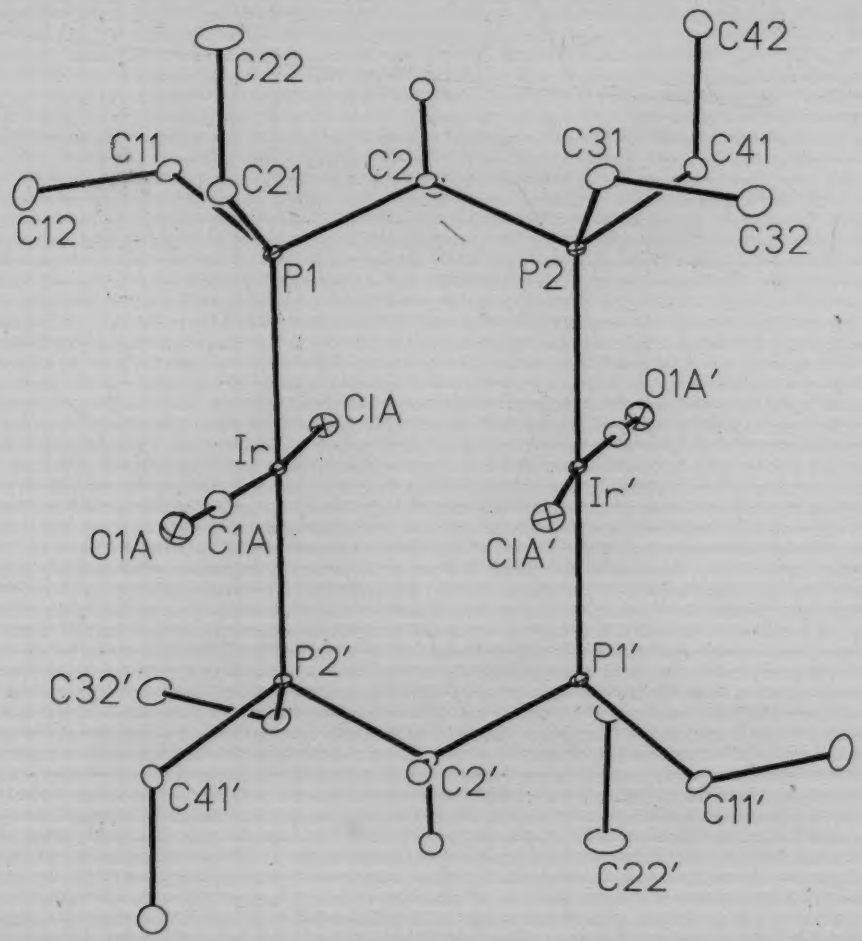

Figure 4.3. *Perspective view of one disordered molecule of trans-*$[Ir_2Cl_2(CO)_2(depm)_2]$ **(23)** *molecule showing the atom labelling scheme. Non-hydrogen atoms are represented by Gaussian ellipsoids at the 20% probability level. Hydrogen atoms are shown with arbitrarily small thermal parameters except for ethyl hydrogens, which are not shown. Primed atoms are related to unprimed ones via the crystallographic inversion center at the midpoint between the metals.*

Consistent with this idea the non-bonded contacts between Cl_A and $C_{1A'}$ (3.354(9) Å) is less than the normal van der Waals separation expected of 3.5 Å.[14] The metal-metal distance is the same as the non-bonded P-P separation within the bridging diphosphines showing no mutual attraction of the metals. The ethyl substituents display an alternating (axial/equatorial) arrangement which appears to be quite characteristic of these species (*vide infra*). All bond lengths are normal for such species; selected bond lengths and angles are included in Tables 4.7 and 4.8, respectively.

Table 4.7. Selected Interatomic Distances (Å) for *trans*-$[Ir_2Cl_2(CO)_2(depm)_2]$ (**23**)

Atom1	Atom2	Distance	Atom1	Atom2	Distance
Ir	Ir'	3.1274(3)†	P(1)	C(21)	1.821(5)
Ir	Cl(A)[a]	2.393(3)	P(2)	C(2)	1.837(4)
Ir	Cl(B)[b]	2.383(5)	P(2)	C(31)	1.836(5)
Ir	P(1)	2.315(1)	P(2)	C(41)	1.836(5)
Ir	P(2')	2.315(1)	O(1A)	C(1A)	1.12(1)
Ir	C(1A)	1.79(1)	O(1B)	C(1B)	1.22(2)
Ir	C(1B)	1.75(2)	C(11)	C(12)	1.530(7)
P(1)	P(2)	3.125(1)†	C(21)	C(22)	1.529(7)
P(1)	C(2)	1.828(4)	C(31)	C(32)	1.524(7)
P(1)	C(11)	1.826(5)	C(41)	C(42)	1.542(7)

Primed atoms are related to unprimed ones via the crystallographic inversion centre (0, 0, 0). [a]Refined with an occupancy factor of 0.6. [b]Refined with an occupancy factor of 0.4. †Nonbonded distance.

Table 4.8. Selected Interatomic Angles (deg) for *trans*-$[Ir_2Cl_2(CO)_2(depm)_2]$ (**23**)

Atom1	Atom2	Atom3	Angle	Atom1	Atom2	Atom3	Angle
Cl(A)	Ir	P(1)	88.00(5)	Ir'	P(2)	C(2)	111.7(1)
Cl(A)	Ir	P(2')	93.27(5)	Ir'	P(2)	C(31)	117.0(2)
Cl(A)	Ir	C(1A)	173.3(3)	Ir'	P(2)	C(41)	114.9(2)
Cl(B)	Ir	P(1)	91.94(7)	C(2)	P(2)	C(31)	106.8(2)
Cl(B)	Ir	P(2')	86.78(7)	C(2)	P(2)	C(41)	100.8(2)
Cl(B)	Ir	C(1B)	173.8(4)	C(31)	P(2)	C(41)	104.1(2)
P(1)	Ir	P(2')	178.72(4)	Ir	C(1A)	O(1A)	179.5(9)
P(2)	C(41)	C(42)	116.5(3)	Ir	C(1B)	O(1B)	180(1)
C(2)	P(1)	C(11)	100.8(2)	P(1)	C(2)	P(2)	117.0(2)
C(2)	P(1)	C(21)	106.1(2)	P(1)	C(11)	C(12)	113.1(4)
C(11)	P(1)	C(21)	104.3(2)	P(1)	C(21)	C(22)	117.2(4)
				P(2)	C(31)	C(32)	110.8(4)

4.3.1.2. $[Ir_2(CO)_3(depm)_2]$ (24)

The reduction of compound **23** has been carried out under an atmosphere of CO, in the presence of a 1M solution of KOH/H_2O to yield the neutral tricarbonyl compound $[Ir_2(CO)_3(depm)_2]$ (**24**), which is isolable in moderate yields as an air-sensitive orange-brown oil. While the reduction is achievable via other routes (e.g. using $NaBH_4$ under a CO atmosphere), impurities formed in these other methods make the former method preferable.

The $^{31}P\{^1H\}$ NMR spectrum of **24** at ambient temperature shows a broad singlet at -11.0 ppm, while the ^1H NMR spectrum, at this temperature, displays only one signal for the methylene protons of the depm ligands, which appears as a broad multiplet at 3.13 ppm, integrating for all four protons. A ^{13}CO-enriched sample of **24** shows only one broad singlet carbonyl resonance at 185 ppm in the room temperature ^{13}C NMR spectrum.

Upon cooling to -75 °C, the $^{31}P\{^1H\}$ NMR spectrum of **24** exhibits a pattern more typical of an AA'BB' spin system, with two chemically inequivalent phosphorus environments, displaying broad signals at 8.9 ppm and -28.0 ppm. No resolution is observed in the methylene proton signals in the ^1H NMR spectrum, at this

temperature, suggesting a process is at work, even at low temperatures, that equilibrates these moieties. At this temperature three carbonyl resonances are now observed in the ^{13}C NMR spectrum of a ^{13}CO-enriched sample of **24**, at -75 °C, appearing as singlets at 180 ppm, 189, ppm and 194 ppm, integrating for one carbon each; however, these resonances are broad and offer no observable change under ^{31}P decoupling conditions.

These results suggest that compound **24** does not have a static, symmetrical A-frame structure, but instead is a highly-fluxional species, even at low temperature. A similar fluxionality has been observed for the $[MM'(CO)_3(dppm)_2]$ (MM' = Rh_2 [15], Ir_2 [16], RhIr [17]) and $[MM'(CO)_3(dmpm)_2]$ (MM' = Rh_2 [18], Ir_2 [19]) analogues (Scheme 4.1), and the X-ray structure of the Rh_2 and RhIr species established the unsymmetrical structure wherein one set of the ends of the diphosphine ligands are held in *trans* orientration, while the other two are in a *cis* arrangement with one another.

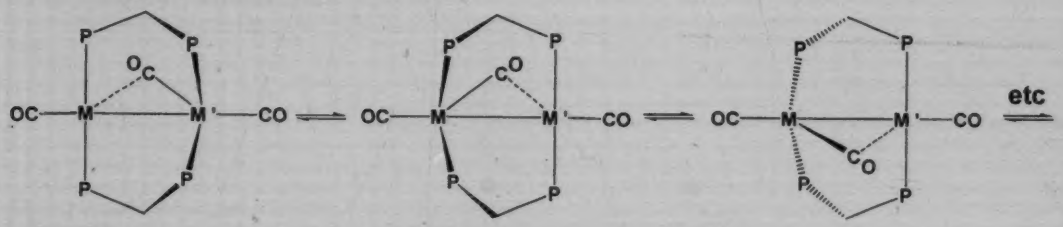

Scheme 4.1. *Fluxionality of tricarbonyl complexes*

In this case, the carbonyl ligands are presumably undergoing a "merry-go-round" migration around the equatorial plane of the complex, in conjunction with a change in the *cis-trans* arrangement of the bridging diphosphines ligands, which are found mutually *trans* on one metal and mutually *cis* on the other. The alternating coordination sphere about each metal is then different, with one being coordinated to five atoms (including the adjacent metal), in a distorted trigonal bypyramidal orientation, and the other, coordinated to four atoms in a distorted square planar arrangement.

The room temperature IR spectrum of compound **24** shows multiple peaks at 1983 cm^{-1}, 1964 cm^{-1}, 1952 cm^{-1} and 1758 cm^{-1}, supporting the assertion that, at this temperature, all three carbonyls are exchanging, generating at least two unique structural arrangements, at a rate detectable on the IR timescale, yet faster than is discernible on the NMR timescale.[20]

4.3.1.3 $[Ir_2(CO)_4(depm)_2]$ (25)

Addition of CO to samples of **24** yields the tetracarbonyl complex $[Ir_2(CO)_4(depm)_2]$ (**25**). Unlike its dppm analogue,[15] which must be stored under CO to prevent reversion to the tricarbonyl species, compound **25** is only modestly susceptible to CO loss and may be isolated as a dark yellow oil, containing a mixture of itself along with the tricarbonyl precursor.

Analogous to the related dmpm and dppm complexes, both the $^{31}P\{^1H\}$ NMR and $^{13}C\{^1H\}$ NMR spectra each display only a single resonance at ambient temperature, both appearing as singlets at -31.4 ppm and 190 ppm, respectively, while the ^1H NMR spectrum at this temperature shows the bridging methylene protons of the depm ligands at 2.71 ppm as single multiplet signal, integrating for four protons. With the molecular formula given, it is not difficult to propose a symmetric structure that is consistent with the NMR data, in which all carbonyls are chemically equivalent and terminally bound. However, the IR data at the same temperature are not consistent with such a structure, displaying four carbonyl stretches at 2013 cm^{-1}, 1997 cm^{-1}, 1937 cm^{-1} and 1780 cm^{-1}; the last low-frequency stretch is consistent with a bridging carbonyl. This suggests that the NMR data are simplified by some fluxional process(es) that gives rise to an average symmetric structure on the NMR timescale. Such a notion is supported by the NMR data at lower temperature.

At -75 °C, the $^{31}P\{^1H\}$ NMR spectrum shows two chemically inequivalent phosphorus environments, displaying resolved triplets at -19.6 ppm and -41.1

ppm ($^2J_{PP}$ = 53.7 Hz). In addition, at this temperature, four independent carbonyl resonances are observed in the ^{13}C NMR spectrum of a ^{13}CO-enriched sample of **25**, displaying broad singlets at 181 ppm, 192 ppm, 194 ppm and 195 ppm. Although ^{31}P decoupling experiments were not carried out, all NMR data at low temperature are consistent with an unsymmetrical species that is undergoing rapid fluxionality at ambient temperatures. Compound **25** is reminiscient of the dmpm analogue,[21] $[Ir_2(CO)_4(dmpm)_2]$ (dmpm = $Me_2PCH_2PMe_2$), the structure of which has been established by X-ray crystallography, the spectral structural parameters of which, over the temperature range noted above, are very similar to those of **25**. We therefore assign **25** a similar structure, as diagrammed in Scheme 4.2. This structure is also consistent with that expected from CO addition to the coordinatively unsaturated Ir center in compound **24**. Although the dmpm analogue of **25** was not shown in the publication as having a semi-bridging carbonyl, we show it that way in Scheme 4.2 owing to the low frequency carbonyl stretch in the IR spectrum. Schemes 4.1 and 4.2 are highly abbreviated, with a number of potential species omitted, but are meant to represent that the fluxionality is proposed to occur via a "merry-go-round" carbonyl motion accompanied by a "wagging" of each end of the diphosphine framework from front to back.

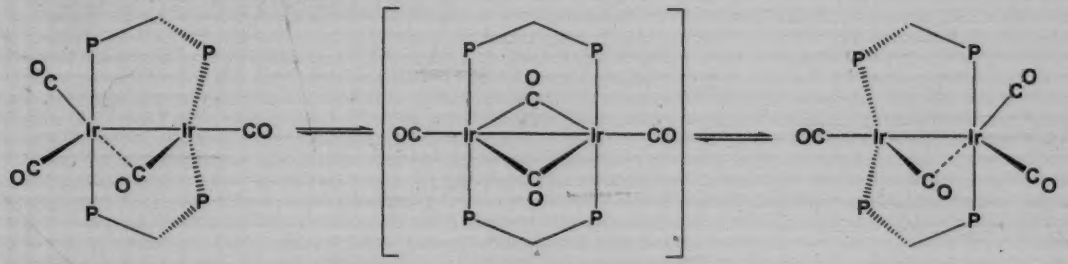

Scheme 4.2. *Fluxionality of tetracarbonyl complexes*

4.3.1.4. $[Ir_2(H)(CO)_3(\mu\text{-}CH_2)(depm)_2][CF_3SO_3]$ (26)

Addition of MeOTf to compound **24** at ambient temperature yields the methylene-bridged hydride complex $[Ir_2(H)(CO)_3(\mu\text{-}CH_2)(depm)_2][CF_3SO_3]$ (**26**), in good yield as an red-orange oil.

The $^{31}P\{^1H\}$ NMR spectrum of compound **26** appears as expected, displaying an AA'BB' spin pattern of broad multiplet signals at -8.9 ppm and -19.5 ppm. Interestingly, only a single broad resonance, integrating for four protons, attributable to the depm methylene protons is displayed at 2.75 ppm in the ^1H NMR spectrum. Activation of the incoming methyl ligand has been confirmed by the presence of both a bridging methylene resonance at 3.95 ppm, integrating for two protons, along with a new hydride resonance appearing at -12.4 ppm in the ^1H NMR spectrum. While both signals are relatively broad, the high-field hydride signal does show 16 Hz ($^2J_{PH}$) coupling to the set of adjacent phosphines at -8.9 ppm, confirming its terminal orientation as shown in Scheme 4.3.

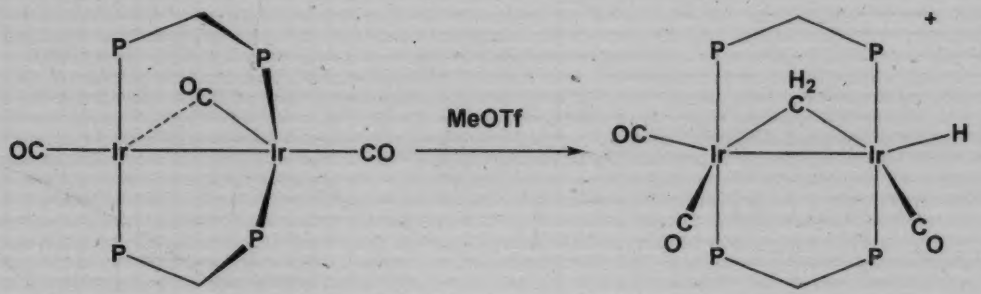

24 **26**

Scheme 4.3. *Reaction of* **24** *with MeOTf to generate* $[Ir_2(H)(CO)_3(\mu\text{-}CH_2)(depm)_2]^+$ (**26**)

At ambient temperature, the $^{13}C\{^1H\}$ NMR spectrum shows only a single resonance attributable to the carbonyl carbons at 177.1 ppm, while the room

temperature IR spectrum shows three peaks at 1990 cm^{-1}, 1965 cm^{-1}, and 1932 cm^{-1}, suggesting terminal arrangements for all three carbonyls.

Upon cooling, at -75 °C, the $^{31}P\{^{1}H\}$ NMR spectrum shows sharpening of the spectrum, allowing the mutual coupling between the ^{31}P centers to be resolved ($^{2}J_{PP}$ = 32 Hz), with the signals appearing as pseudo-triplets at -7.5 ppm and -18.9 ppm. The three anticipated carbonyl resonances are also observed at this temperature in the $^{13}C\{^{1}H\}$ NMR spectrum of a ^{13}CO-labelled sample, showing doublets ($^{2}J_{CC}$) of triplets ($^{2}J_{CP}$ = 12 hz and 19 Hz respectively) at 166.3 ppm and 178.7 ppm along with a multiplet at 180.2 ppm, integrating for one carbon each. The two higher-field signals are coupled to different sides of the diphosphine framework, as shown by selective ^{31}P decoupling of the ^{13}C NMR spectrum, with the intermediate signal showing coupling to the phosphines attached to the same metal as that of the hydride (-8.9 ppm). The lower-field multiplet is attributed to the carbonyl found in a position between the other two, and hence gives a more complicated signal in the ^{13}CO/ $^{13}CH_3$-enriched sample. The methylene carbon is displayed as a multiplet at 47 ppm in the ^{13}C NMR spectrum, the shift of which is consistent with its bridging orientation.

The structure of **26** has been confirmed by X-ray crystallography and an ORTEP representation of the complex cation $[Ir_2(H)(CO)_3(\mu\text{-}CH_2)(depm)_2]^+$ is presented in Figure 4.4. Selected bond lengths and angles are also included in Tables 4.9 and 4.10, respectively.

While the room temperature NMR data suggest some type of fluxional process, whereby the methyl group is reformed and subsequently cleaved, as has been observed with the dppm analogue,[22] the solid-state structure of **26** is clearly consistent with the low temperature data acquired for this compound. The bridging diphosphines are arranged in a trans orientation, giving a distorted pseudo-octahedral environment around each metal center. Both metals have similar geometries, differing mainly by the replacement of the carbonyl opposite the metal-metal bond on one metal by a hydride on the other. The presence of a

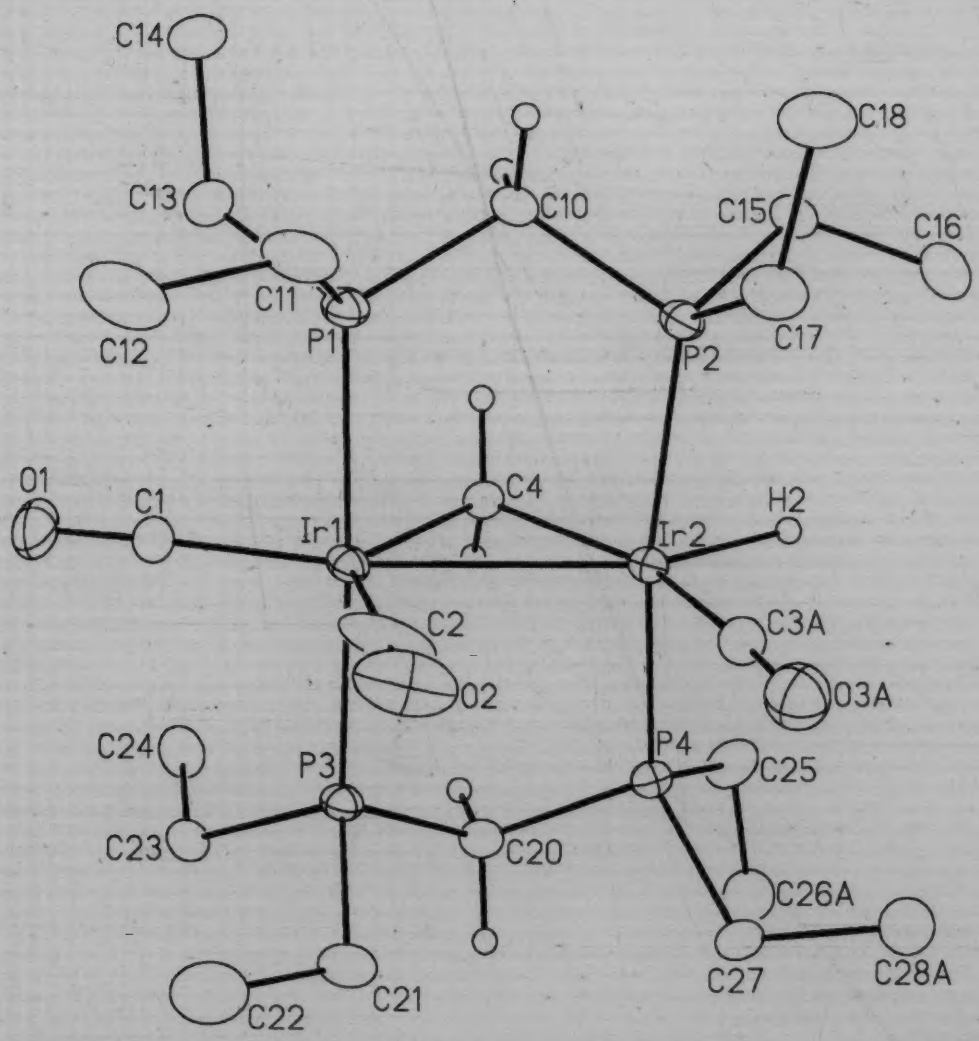

Figure 4.4. *Perspective view of the* $[Ir_2(H)(CO)_3(\mu\text{-}CH_2)(depm)_2]^+$ **(26)** *cation showing the atom labelling scheme. Non-hydrogen atoms are represented by Gaussian ellipsoids at the 20% probability level. Hydrogen atoms are shown with arbitrarily small thermal parameters for the hydride, bridging methylene, and depm methylene groups and are not shown for the depm ethyl groups.*

Table 4.9. Selected Interatomic Distances (Å) for $[Ir_2(H)(CO)_3(\mu\text{-}CH_2)(depm)_2]^+$ (**26**)

Atom1	Atom2	Distance	Atom1	Atom2	Distance
Ir(1)	Ir(2)	2.7887(3)	Ir(2)	C(4)	2.075(5)
Ir(1)	P(1)	2.354(1)	Ir(2)	H(2)	1.65(1)[a]
Ir(1)	P(3)	2.354(1)	P(1)	P(2)	3.049(2)[b]
Ir(1)	C(1)	1.877(6)	P(3)	P(4)	3.015(2)[b]
Ir(1)	C(2)	1.932(7)	O(1)	C(1)	1.145(7)
Ir(1)	C(4)	2.163(5)	O(2)	C(2)	1.104(8)
Ir(2)	P(2)	2.311(1)	O(3A)	C(3A)	1.18(2)
Ir(2)	P(4)	2.307(1)	O(3B)	C(3B)	1.17(2)
Ir(2)	C(3A)	1.95(1)			
Ir(2)	C(3B)	1.81(1)			

[a]Distance restrained during refinement. [b]Nonbonded distance.

Table 4.10. Selected Interatomic Angles (deg) for $[Ir_2(H)(CO)_3(\mu\text{-}CH_2)(depm)_2]^+$ (**26**)

Atom1	Atom2	Atom3	Angle	Atom1	Atom2	Atom3	Angle
Ir(2)	Ir(1)	P(1)	92.11(4)	P(2)	Ir(2)	C(3A)	90.1(3)
Ir(2)	Ir(1)	P(3)	89.29(3)	P(2)	Ir(2)	C(3B)	95.3(4)
Ir(2)	Ir(1)	C(1)	157.0(2)	P(2)	Ir(2)	C(4)	89.9(2)
Ir(2)	Ir(1)	C(2)	85.5(3)	P(2)	Ir(2)	H(2)	83(2)
Ir(2)	Ir(1)	C(4)	47.5(1)	P(4)	Ir(2)	C(3A)	96.6(4)
P(1)	Ir(1)	P(3)	174.89(5)	P(4)	Ir(2)	C(3B)	87.4(4)
P(1)	Ir(1)	C(1)	87.8(2)	P(4)	Ir(2)	C(4)	89.3(1)
P(1)	Ir(1)	C(2)	92.8(2)	P(4)	Ir(2)	H(2)	84(2)
P(1)	Ir(1)	C(4)	86.9(1)	C(3A)	Ir(2)	C(3B)	18.9(4)
P(3)	Ir(1)	C(1)	89.0(2)	C(3A)	Ir(2)	C(4)	154.4(4)
P(3)	Ir(1)	C(2)	92.2(2)	C(3A)	Ir(2)	H(2)	102(2)
P(3)	Ir(1)	C(4)	90.4(1)	C(3B)	Ir(2)	C(4)	170.9(4)
C(1)	Ir(1)	C(2)	117.5(4)	C(3B)	Ir(2)	H(2)	85(2)
C(1)	Ir(1)	C(4)	109.6(3)	C(4)	Ir(2)	H(2)	103(2)
C(2)	Ir(1)	C(4)	132.9(3)	Ir(1)	C(1)	O(1)	176.5(8)
Ir(1)	Ir(2)	P(2)	94.25(4)	Ir(1)	C(2)	O(2)	177(1)
Ir(1)	Ir(2)	P(4)	95.99(4)	Ir(2)	C(3A)	O(3A)	177(1)
Ir(1)	Ir(2)	C(3A)	104.3(4)	Ir(2)	C(3B)	O(3B)	172(1)
Ir(1)	Ir(2)	C(3B)	121.8(4)	Ir(1)	C(4)	Ir(2)	82.3(2)
Ir(1)	Ir(2)	C(4)	50.2(1)	P(1)	C(10)	P(2)	113.5(3)
Ir(1)	Ir(2)	H(2)	153.3	P(3)	C(20)	P(4)	112.1(3)
P(2)	Ir(2)	P(4)	165.99(6)				

metal-metal bond may be inferred from the shorter distance between the two metal centers (2.7887(3) Å), compared to the P-P separation within each diphosphine ligand (3.049(2) Å, 3.015(2) Å), showing compression of the metal-metal vector. It is also noteworthy that this distance is almost 0.34 Å shorter than in compound **23**, for which there is no Ir-Ir bond. Placement of the bridging methylene and hydride groups in adjacent positions is consistent with their origin from C-H activation of the methyl ligand that of the non-bonded phosphines. Although the hydride was not located in the X-ray study, its idealized placement was chosen based on spectral evidence and the conspicuously vacant coordination site in the structure. The solid-state structure of compound **26** was found to have a disorder of the carbonyl group on Ir(2) such that two closely spaced carbonyl positions $C_{3A}O_{3A}$ and $C_{3B}O_{3B}$ in an approximate ratio 1:1 were resolved. Although no such disorder was resolved for the adjacent carbonyl C_2O_2, the elongated thermal ellipsoids may disguise a similar, but unresolved, disorder.

4.3.1.5. $[Ir_2(CH_3)(CO)_2(depm)_2][CF_3SO_3]$ (27)

Removal of a carbonyl from the tricarbonyl methylene-hydride complex (**26**) is achieved through the addition of trimethylamine-N-oxide (TMNO), resulting in the generation of the targeted methyl dicarbonyl complex $[Ir_2(CH_3)(CO)_2(depm)_2][CF_3SO_3]$ (**27**).

This species is again very similar to its dppm analogue, which has been characterized crystallographically.[21] However the highly reactive nature of the new depm complex with trace amounts of water and some solvents, at temperatures above 0 °C, has to date limited our characterization of this product to solution NMR techniques.

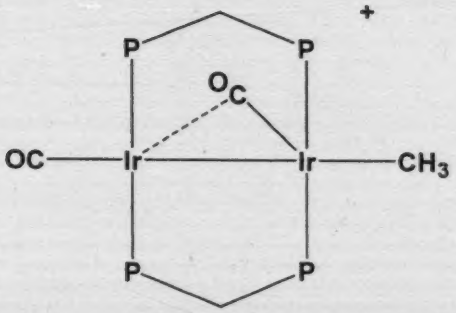

Figure 4.5. *Proposed structure of compound **27**; the depm analogue of compound **1**,* $[Ir_2(CH_3)(CO)_2(depm)_2][CF_3SO_3]$

In the $^{31}P\{^1H\}$ NMR spectrum, at 0 °C, a broad singlet is apparent at 23.2 ppm, corresponding to compound **27**. The ^1H NMR spectrum shows the depm methylene protons, that bridge the pair of ^{31}P nuclei, as a pair of doublets of multiplets, integrating for two protons each, at 2.3 ppm and 2.8 ppm, displaying the characteristic coupling to phosphorus, while the iridium-bound methyl group appears as a quintet at 0.57 ppm ($^3J_{HP}$ = 4 Hz), confirming the reformation of the methyl moiety from the methylene and hydride fragments of the precursor. The equal coupling to all four ^{31}P nuclei in this resonance may suggest that the methyl group in this species occupies a bridging position, similar to the conformation reported for the diiridium dmpm complex.[3] However, this coupling may also arise from a fluxional process that exchanges the terminally-bound methyl group from metal to metal, as has been observed for the dppm analogue. At -80 °C, in the $^{13}C\{^1H\}$ NMR spectrum of a ^{13}CO-enriched sample of **27** the carbonyls appear as two broad multiplet resonances at 168 ppm and 180 ppm. The lower-field shift of the latter suggests that this carbonyl approaches the second metal, possibly even interacting with it weakly in a semi-bridging arrangement, as has been seen in the dppm analogue, and described in preceding chapters. The presence of two different carbonyl resonances certainly supports the notion that the molecule does not have a 'fixed' symmetrical conformation, as would be the case if the aforementioned methyl moiety was being shared equally by both metals. The $^{13}CH_3$-enriched methyl group also

displays a broad high-field signal at 19.5 ppm the chemical shift of which is consistent with its reformation from the methylene and hydride fragments. The chemical shifts of the ^{31}P resonances are somewhat resolved into two broad resonances at -80 °C, appearing at 20 ppm and 26 ppm, supporting the unsymmetrical structure shown in Figure 4.8. Even at this temperature, however, the methyl resonance remains a broad quintet, in the ^{1}H NMR spectrum, whereupon selective irradiation of both closely spaced ^{31}P resonances results equally in a broad singlet, the breadth of which may mask unresolved coupling to the adjacent set of ^{31}P nuclei. The combination of room temperature and low temperature NMR data suggests that **27** undergoes a fluxional process in which the methyl group is shuffled back and forth on one side of the binuclear face, in a "windshield-wiper" like motion. Such a motion results in equal coupling of the methyl protons to all four ^{31}P nuclei, and is accompanied by movement of the carbonyl ligands from terminal to bridging and back again, thereby resulting in the two broad ^{13}C resonances observed.

Complex **27** is unstable at temperatures above 0 °C, reacting with chlorinated solvents to produce uncharacterized species, or similarily with trace water to form a hydroxide-bridged dicarbonyl species (**38**), which is stable and isolable at room temperature, and will be discussed in the next chapter. The latter reaction with water is accompanied by the liberation of methane which is observed in the ^{1}H NMR spectrum.

4.3.2. Dirhodium Complexes

4.3.2.1. *trans*-$[Rh_2Cl_2(CO)_2(depm)_2]$ (28)

The reaction of $[RhCl(COD)]_2$ with two equivalents of depm, followed by the addition of CO is carried out in a refluxing solution of acetone, giving a clear orange solution, from which subsequent isolation yields $[Rh_2Cl_2(CO)_2(depm)_2]$ (**28**) as a dark orange, microcrystalline solid.

The $^{31}P\{^{1}H\}$ NMR spectrum of compound **28** (Figure 4.6) appears as a second order pattern at 17.9 ppm displaying a separation of 117 Hz between the two major peaks.

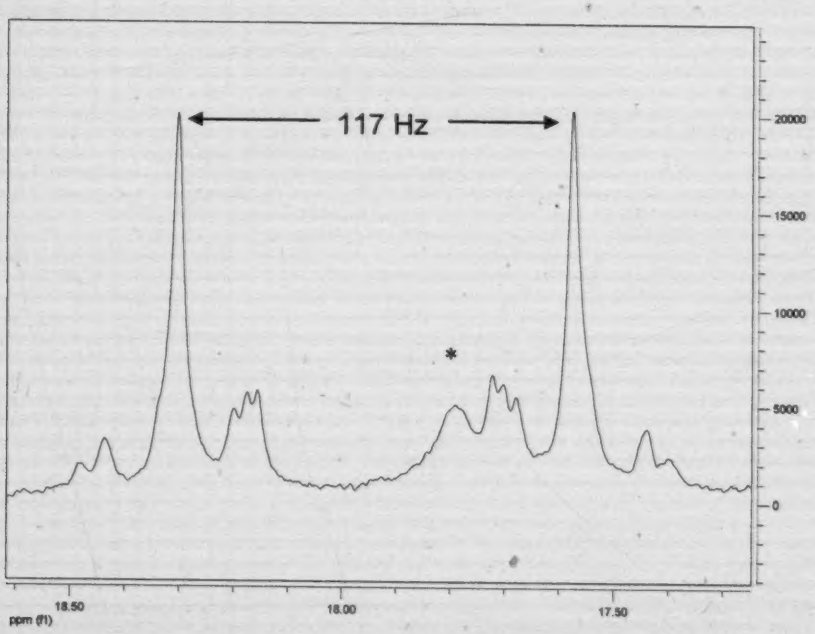

Figure 4.6. *$^{31}P\{^{1}H\}$ NMR spectrum of compound* **28**, $[Rh_2Cl_2(CO)_2(depm)_2]$. *The peak marked (*) is an unidentified impurity.*

This type of pattern is typical for such diphosphine-bridged dirhodium species,[23] and is indicative of a highly symmetric arrangement within the molecule. Unfortunately, a comparison of the spectroscopic data with the dppm analogue, *trans*-$[Rh_2Cl_2(CO)_2(dppm)_2]$,[24] was not possible owing to the insolubility of the latter. However, the dmpm complex has been prepared, and displays a very similar ^{31}P NMR spectrum[25] to that shown above.

Only the depm methylene protons, in addition to those of the depm ethyl groups, are apparent in the ^{1}H NMR spectrum, with the former appearing as a multiplet at 2.37 ppm, integrating for four protons. The $^{13}C\{^{1}H\}$ NMR spectrum of a ^{13}CO-enriched sample of **28** shows one broad doublet carbonyl resonances at 189.1 ppm, with a $^{1}J_{CRh}$ coupling value of 75 Hz. The single carbonyl stretch in the

infrared spectrum of **28**, at 1950 cm^{-1}, is further suggestive of the 'trans' symmetry, while the lower frequency of this stretch, compared to that of the dppm counterpart (ν(CO) = 1968 cm^{-1})[24] is presumably due to the greater basicity of the depm ligand; a similar decrease was observed for the analogous dmpm compound (ν(CO) = 1956 cm^{-1}).

The structure of **28** has been determined crystallographically, with an ORTEP view of the complex shown in Figure 4.7. The structure is analogous to that of the previously obtained dppm analogue,[24b] and, as noted, is essentially identical with the solid state structure of the diiridium depm congenor (*vide supra*) in which the inner coordination sphere about each metal atom is effectively square planar with a *trans* geometry at each metal, having the chloro and carbonyl ligands on adjacent metals mutually trans to one another, along with the framework diphosphines. The same disorder as that observed in the diiridium species, of the chloro- and carbonyl ligands, was encountered in the structure solution of the dirhodium complex, with an occupancy ratio of 45:55 between sites 'A' and 'B'.

The square planar geometry about the metals is not exactly perpendicular to the Rh-Rh vector, but is skewed slightly such that the chloro ligands on one metal approach the second metal, with both planes remaining parallel. This skewing was observed in the diiridium analogue (*vide supra*) and is proposed to help reduce the non-bonded contact between the chloro and carbonyl ligands on adjacent metals. A further indication of repulsive van der Waals contacts is the slight bending back of these ligands at each metal away from the ligands on adjacent the adjacent metal (Cl-Rh-CO = 174.9(2) °, 175.8(2) °: see Table 4.11). Otherwise, bond lengths and angles are closely comparable to the dppm analogue, with only a small notable difference in the Rh-Rh separation (3.2386(5) Å), which is slightly closer in the depm complex (3.1657(3) Å), yet remains consistent with no formal metal-metal bond.

Selected bond lengths and angles are also included in Tables 4.11 and 4.12, respectively.

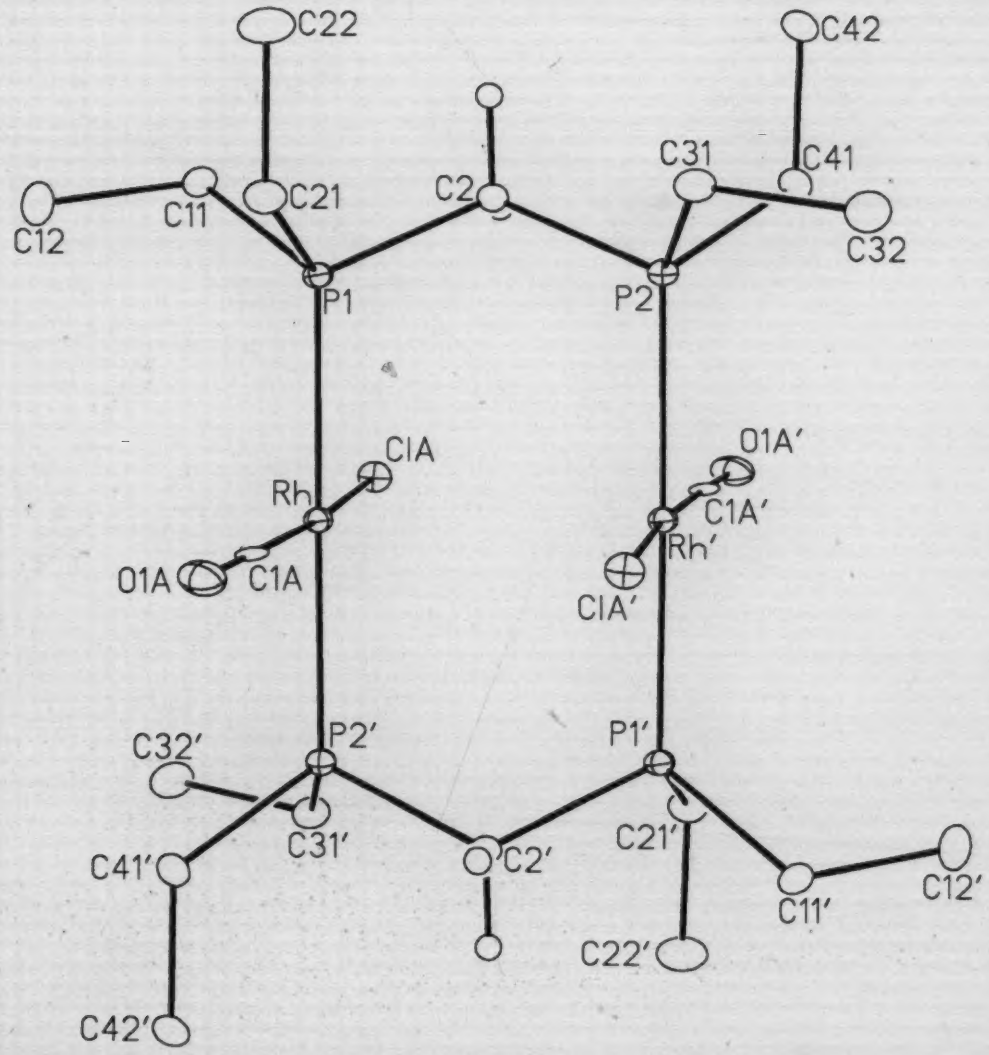

Figure 4.7. *Perspective view of one of the disordered molecules of* trans-$[Rh_2Cl_2(CO)_2(depm)_2]$ (**28**) *showing the atom labelling scheme. Non-hydrogen atoms are represented by Gaussian ellipsoids at the 20% probability level. Hydrogen atoms are shown with arbitrarily small thermal parameters except for the ethyl groups, which are not shown. Primed atoms are related to unprimed ones via the crystallographic inversion centre at the midpoint between the metals.*

Table 4.11. Selected Interatomic Distances (Å) for *trans*-$[Rh_2Cl_2(CO)_2(depm)_2]$ (**28**)

Atom1	Atom2	Distance
Rh	Rh'	3.1657(3)†
Rh	ClA	2.444(2)[a]
Rh	ClB	2.439(2)[b]
Rh	P1	2.3134(6)
Rh	P2'	2.3133(6)
Rh	C1A	1.820(8)
Rh	C1B	1.847(9)
P1	P2	3.1321(7)†
O1A	C1A	1.075(9)
O1B	C1B	1.028(11)

Primed atoms are related to unprimed ones via the crystallographic inversion centre (0, 0, 0).
[a]Refined with an occupancy factor of 0.45. [b]Refined with an occupancy factor of 0.55.
†Nonbonded distance.

Table 4.12. Selected Interatomic Angles (deg) for *trans*-$[Rh_2Cl_2(CO)_2(depm)_2]$ (**28**)

Atom1	Atom2	Atom3	Angle
ClA	Rh	P1	87.95(5)
ClA	Rh	P2'	93.26(5)
ClA	Rh	C1A	174.9(2)
ClB	Rh	P1	92.14(5)
ClB	Rh	P2'	86.62(5)
ClB	Rh	C1B	175.8(2)
P1	Rh	P2'	178.45(2)
P1	Rh	C1A	91.5(2)
P1	Rh	C1B	89.1(2)
P2'	Rh	C1A	87.4(2)
P2'	Rh	C1B	92.2(2)
Rh	P1	C2	112.85(7)
Rh	P1	C11	115.91(8)
Rh	P1	C21	116.16(8)
C2	P1	C11	100.6(1)
C2	P1	C21	105.8(1)
C11	P1	C21	103.8(1)
Rh'	P2	C2	111.53(7)
Rh'	P2	C31	117.38(8)
Rh'	P2	C41	115.53(8)
C2	P2	C31	106.4(1)
C2	P2	C41	100.6(1)
C31	P2	C41	103.7(1)
Rh	C1A	O1A	176.7(6)
Rh	C1B	O1B	177.0(6)
P1	C2	P2	117.5(1)
P1	C11	C12	112.7(2)
P1	C21	C22	117.1(2)
P2	C31	C32	110.9(2)
P2	C41	C42	117.0(2)

4.3.2.2. $[Rh_2(CO)_3(depm)_2]$ (29)

Reacting compound **28** with aqueous potassium hydroxide under an atmosphere of CO, yields the formally Rh(0)/Rh(0) dimer $[Rh_2(CO)_3(depm)_2]$ (**29**), which is isolable in moderate yields as a red-orange oil. As was the case for the diiridium analogue, this reduction is also achievable using other reagents (e.g. $NaBH_4$), although use of the aqueous KOH always gave cleaner, higher yields of compound **29**, thus is the preferred route. The NMR data are once again very similar to the dppm analogue and has allowed the spectroscopic characterization by comparison.

At ambient temperature the $^{31}P\{^1H\}$ NMR spectrum shows a broad second-order pattern reminiscent of an AA'A''A'''XX' spin system, at 15.1 ppm displaying a separation of 138 Hz between the two major peaks. The ^1H NMR spectrum at ambient temperature shows only one depm methylene signal as a broad quintet at 2.17 ppm (3.3 Hz). The ^{13}C NMR spectrum of a ^{13}CO-enriched sample of **29** at this temperature displays one broad singlet carbonyl resonance at 199 ppm. However, the room temperature IR spectrum shows three carbonyl stretches at 1952 cm^{-1}, 1934 cm^{-1}, and 1863 cm^{-1}, suggesting an arrangement having two distinctly terminal and perhaps one bridging carbonyl. These IR data are clearly inconsistent with the above NMR data, suggesting that the latter are simplified by some fluxional process which, among other things, exchanges the carbonyls.

At low temperatures, the NMR spectra appear quite different than at ambient temperature, consistent with the suggestion of fluxionality. At -110 °C, the $^{31}P\{^1H\}$ NMR spectrum of **29** appears as an AA'BB'XY spin system, having two chemically inequivalent phosphorus environments, displaying signals at 22.5 ppm and 8.5 ppm. Both are doublets of pseudo-triplets, with distinct rhodium coupling (117 Hz and 153 Hz, respectively), along with mutual phosphorus coupling of *ca.* 70 Hz. The higher-field phosphorus resonance also shows an additional coupling of 32 Hz to the low-field carbonyl in a ^{13}CO-enriched sample (*vide infra*). At -110 °C the three expected carbonyl resonances are observed as

two broad doublets at 183 ppm and 207 ppm, displaying typical $^{1}J_{RhC}$ coupling (71 Hz and 68 Hz, respectively) along with a doublet of triplets at 209 ppm, showing 77 Hz coupling to rhodium and 32 Hz of resolvable coupling to phosphorus (*vide supra*). Selective ^{31}P decoupling establishes that the high-field carbonyl is coupled to one end of the diphosphine framework at 22.5 ppm, while the two lower-field carbonyls are attached to the adjacent end at 8.5 ppm. This arrangement of carbonyl ligands is consistent with the proposed structure shown below (Figure 4.8), in which one rhodium center is in the preferred square planar geometry while the adjacent metal is in a pseudo-trigonal bypyramidal orientation, as has been established crystallographically for the dirhodium[14] and Rh/Ir[15] dppm analogues.

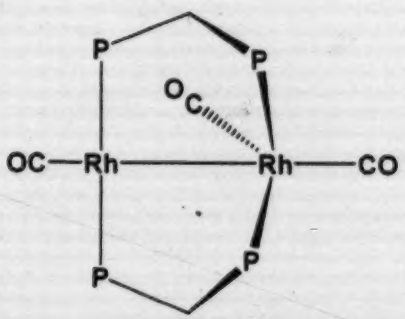

Figure 4.8. *Proposed structure of* $[Rh_2(CO)_3(depm)_2]$ **(29)**

Presumably, the fluxional process equilibrating the NMR data of compound **29** at room temperature is again the result of a "merry-go-round" migration of the carbonyl ligands, around the equatorial plane of the complex, along with interconversion of orientation of the bridging diphosphine, previously proposed in analogous systems of this type $[MM'(CO)_3(dppm)_2]$ (*vide supra*).

4.3.2.3. $[Rh_2(CO)_4(depm)_2]$ (30)

In solution, under excess CO, compound **29** is found in equilibrium with the tetracarbonyl species $[Rh_2(CO)_4(depm)_2]$ (**30**), which is highly susceptible to CO loss thus has only been characterized spectroscopically, in solution under a CO atmosphere. At ambient temperature the $^{31}P\{^1H\}$ NMR spectrum of **30** shows only a single second-order multiplet at 12.4 ppm, with a separation of 133 Hz between the two major peaks, while in the ^1H NMR spectrum, the methylene protons also appear as an averaged multiplet signal at 2.60 ppm.

Upon cooling to -80 °C, the $^{31}P\{^1H\}$ NMR spectrum of compound **30** is more typical of an AA'BB'XY spin system, giving sharpened multiplet signals at 24.3 ppm and -1.3 ppm. Two distinct sets of signals are apparent in the $^{13}C\{^1H\}$ NMR spectrum of a ^{13}CO-enriched sample, at this temperature: the first is a broad resonance integrating for for three carbons at 204 ppm, the breadth of which presumably masks the expected rhodium coupling; and the other is a lower-field resonance, integrating for one carbon, appearing as a doublet of triplets at 214 ppm. The coupling in the latter was determined to be due to coupling to rhodium ($^1J_{RhC}$ = 90 Hz), along with coupling to the adjacent set of diphosphines ($^2J_{CP}$ = 30 Hz). The structure suggested for compound **30** (Figure 4.9), which is analogous to that of the Ir_2 analogues of both dppm and dmpm, is expected to give four carbonyl resonances. The appearance of only two, in a 1:3 ratio, presumably results from accidental overlap of the signals for the three terminal carbonyl groups.

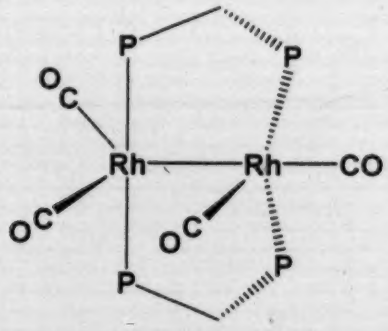

Figure 4.9. *Proposed structure of* $[Rh_2(CO)_4(depm)_2]$ (**30**)

Presumably the fluxionality of this species at room temperature, like that observed in other related analogues, is attributable to "merry-go-round" carbonyl motion accompanied by *cis/trans* phosphine interchange at the different metals, leading to an overall averaging of all of the equatorial carbonyl ligands, as described earlier.

4.3.2.4. $[Rh_2(CH_3)(CO)_3(depm)_2][CF_3SO_3]$ (31)

Upon addition of MeOTf to the tricarbonyl compound (**30**) at -20 °C, $[Rh_2(CH_3)(CO)_3(depm)_2]$ (**31**) is generated *in situ*, as evidenced by the appearance of a new signal in the $^{31}P\{^1H\}$ NMR spectrum, the resonance of which is shown as a rhodium-coupled (107 Hz) multiplet at 35.6 ppm. Instead of the AA'BB'XY spin pattern that might be expected for such a molecule, the simplicity and broadness of the $^{31}P\{^1H\}$ resonance of compound **31** suggests it too may be fluxional. This is further supported by the appearance of the ^1H spectrum, in which the depm methylene protons give only a single broad resonance at 2.35 ppm, along with a broad quintet, attributable to the methyl group protons, appearing at 0.63 ppm and displaying equal coupling (4 Hz) to all four phosphorus nuclei. Coupling in the latter has been confirmed through ^{31}P decoupling experiments which show that the multiplet collapses to a singlet upon broad-band ^{31}P irradiation. The $^{13}C\{^1H\}$ NMR spectrum shows two distinct carbonyl resonances in a ^{13}CO-labelled sample of compound **31**, the first appearing as a multiplet at 214 ppm, integrating for two carbons, and the next, another multiplet integrating for one carbon, at 199 ppm. The chemical shifts of these carbonyl resonances suggest there are two bridging and one terminal carbonyl, respectively, in the complex. In a $^{13}CH_3$-labelled sample of the compound, the methyl carbon appears as a multiplet at -0.3 ppm in the $^{13}C\{^1H\}$ NMR spectrum. The typical chemical shift and sp^3 coupling value ($^1J_{CH}$ = 130 Hz) suggests that the coordinated methyl group remains intact unlike that of the diiridium analogue (*vide supra*).

At -80 °C the NMR spectra of compound **31** are relatively unchanged, with a few notable exceptions. In the ^{31}P NMR spectrum the signals now show a slight broadening, perhaps suggestive of coincidentally overlapping resonances, while in the ^{13}C NMR spectrum further resolution is observed in the carbonyl signals. At this temperature the low field multiplet has been resolved into a triplet displaying 33 Hz coupling to rhodium, and still integrating in a 2:1 ratio with the higher-field resonance. The integration, splitting pattern, reduced $^{1}J_{CRh}$ coupling value and chemical shift of this signal all support the presence of two symmetrically bridging carbonyls in the complex. The higher-field resonance also resolves to a doublet, at -80 °C, displaying 75 Hz coupling to rhodium, consistent with a terminally-bound carbonyl. Surprisingly, the methyl proton resonance appears as a quintet in the ^{1}H NMR spectrum, even at -80 °C, even though it cannot occupy a bridging site. However, this approximately equal coupling to all four phosphorus nuclei can occur through the metal-metal bond such that adjacent $^{3}J_{PH}$ can be similar to $^{4}J_{PH}$. Such coupling to the phosphorus nuclei on the shared metal, along with a second interaction, through the metal-metal bond, to the phosphorus nuclei on the adjacent metal, is not common, but has been previously observed in dppm complexes.[26] Based on these data the proposed structure for compound **31** is shown in Figure 4.10.

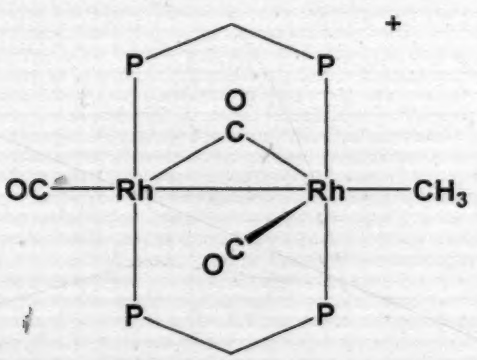

Figure 4.10. *Proposed structure of* $[Rh_2(CH_3)(CO)_3(depm)_2]^+$ **(31)**

Compound **31** may be isolated at 0 °C, among a mixture of products, as a red-orange powder. However, if left in solution, or if the solid is redissolved at temperatures higher than 0 °C, compound **31** undergoes a subsequent transformation wherein the methyl group migrates to a neighboring carbonyl to generate the acyl-dicarbonyl isomer, compound **32**, described below.

4.3.2.5. $[Rh_2(CO)_2(\mu\text{-}CH_3CO)(depm)_2][CF_3SO_3]$ (32)

Compound **32** $[Rh_2(CO)_2(\mu\text{-}CH_3CO)(depm)_2][CF_3SO_3]$ (**32**) is generated from compound **31**, as noted above, and is very prone to reaction with trace amounts of water and/or solvent, ultimately yielding the hydroxide-bridged and dicationic tricarbonyl products, $[Rh_2(CO)_2(\mu\text{-}OH)(depm)_2]^+$ and $[Rh_2(CO)_3(depm)_2]^{+2}$, respectively (as described in Chapter 5). Due to its propensity towards such reactions, compound **32** has only been characterized *in situ*, via analysis of its NMR parameters.

The $^{31}P\{^1H\}$ NMR spectrum of compound **32** at room temperature shows two very broad resonances at 22.5 ppm and 17.2 ppm, indicative of two chemically inequivalent ends of the diphosphine framework. The depm methylene protons display a single broad resonance at 2.55 ppm in the ^1H spectrum, which also shows a relatively broad singlet at 2.42 ppm, integrating for three protons, consistent with an acyl-methyl group. At low temperature (-80 °C) the depm methylene protons are slightly resolved into two distinct, yet still overlapping, broad signals at 2.52 ppm and 2.75 ppm, while the acyl resonance sharpens. Upon ^{13}C labelling of the methyl and carbonyl groups, the acyl methyl in the ^1H NMR spectrum is split into a doublet of doublets, showing coupling to the methyl group carbon (140 Hz) and to the adjacent carbonyl (5 Hz). The $^{31}P\{^1H\}$ NMR spectrum of compound **32** is also resolved at low temperature, showing an AA'BB'XY spin pattern, displaying a doublet of pseudo-triplets at 21.5 ppm ($^1J_{RhP}$ = 120 Hz), and the second mutually coupled ($^2J_{PP}$ = 19 Hz)) doublet of pseudo-triplets at 15.6 ppm ($^1J_{RhP}$ = 139 Hz). Compound **32** shows three distinct

carbonyl resonances in the $^{13}C\{^1H\}$ NMR spectrum; the first two represent terminal carbonyls appearing as a broad multiplet at 200 ppm, whose breadth presumably masks the expected rhodium coupling, along with a broad doublet at 194 ppm, displaying 76 Hz coupling to rhodium. The third resonance, appearing as a broad low-field multiplet at 320 ppm, is proposed to be the acyl carbonyl carbon, the low-field shift of which is suggestive of the bridging arrangement of this group (Figure 4.11), as has been previously proposed for the dppm analogue.[27] In a $^{13}CH_3$ and ^{13}CO-labelled sample, this low-field signal also shows $^1J_{CC}$ coupling of 22 Hz to the adjacent acyl methyl carbon, as observed in its resonance which appears at 44 ppm.

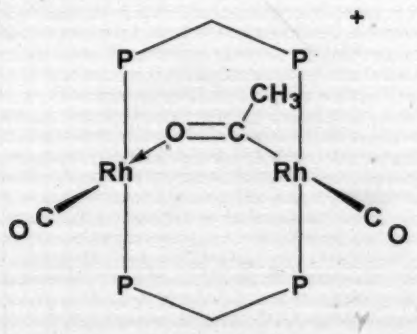

Figure 4.11. *Proposed structure of* $[Rh_2(CO)_2(\mu\text{-}CH_3CO)(depm)_2]^+$ **(32)**

Attempts to generate the targeted methyl dicarbonyl complex by carbonyl extraction via deinsertion from the acyl group have failed, due the propensity for compound **32** to transform in solution, at ambient temperatures and above, into uncharacterized metal-containing products, along with various, unidentified (apart from methane) organic byproducts.

4.3.3. Mixed Rhodium-Iridium Complexes

4.3.3.1. *trans*-$[RhIrCl_2(CO)_2(depm)_2]$ (33)

Addition of $[IrCl(CO)(depm)_2]$ to $[RhCl(CO)_2]_2$ affords the heterobinuclear, mixed-metal complex *trans*-$[RhIrCl_2(CO)_2(depm)_2]$ (**33**), as a dark red-orange solid. The $^{31}P\{^1H\}$ NMR spectrum of compound **33** appears as expected for a mixed-metal complex, with one end of the diphosphine framework, connected to rhodium metal, displaying a doublet of pseudo-triplets at 18.0 ppm, with resolvable $^1J_{RhP}$ coupling of 118 Hz, typical for this type of species, along with a mutually coupled pseudo-triplet ($^2J_{PP}$ = 64 Hz) at 9.6 ppm, corresponding to the iridium-bound ends of the diphosphines. Notably, both chemical shifts are very close to those of their respective homobinuclear depm complexes, as is the $^1J_{RhP}$ coupling value, indicating a very similar chemical environment around each corresponding metal center in the mixed metal complex to that of an individual metal in the homobinuclear analogue.

In the same conformation as observed in the Ir_2 and Rh_2 analogues, the chemical environments on each side of the $RhIrP_4$ plane are indentical, resulting in the observation of a single resonance for the depm methylene protons at 2.42 ppm in the ^1H NMR spectrum, integrating for four protons. Again, this chemical shift lies between that of the respective homobinuclear complexes, suggesting that the mixed-metal compound may be viewed as a hybrid of the two homobinuclear complexes. The IR spectrum of **33** shows two closely spaced carbonyl stretches in the solid state at 1934 cm^{-1} and 1943 cm^{-1}, with the carbonyl on iridium presumably displaying a lower stretching frequency than one in an analogous environment on rhodium (*cf.* $[IrCl(CO)(PPh_3)_2]$ (ν(CO) = 1967 cm^{-1})[28] *vs.* $[RhCl(CO)(PPh_3)_2]$ (ν(CO) = 1979 cm^{-1})[29]).

The structure of **33** has been confirmed by X-ray crystallography which shows a structure essentially superimposable on the Rh_2 and Ir_2 species, as shown earlier, so an ORTEP of this species is not shown here. Furthermore, the structure solution was found to be disordered about an inversion center which results in each metal site having a 50% occupancy each of Rh and Ir, so subtle diffrences about each metal are masked. A similar disorder of the chloro- and carbonyl ligands was also encountered between sites 'A' and 'B', as was

observed in the homobinuclear congeners (*vide supra*). Selected bond lengths and angles are given in Tables 4.13 and 4.14, respectively.

Table 4.13. Selected Interatomic Distances (Å) for *trans*-$[RhIrCl_2(CO)_2(depm)_2]$ (**33**)

Atom1	Atom2	Distance	Atom1	Atom2	Distance
Ir	Rh'	3.1595(3)†	Ir	C1B	1.794(8)
Ir	ClA	2.413(3)[a]	Rh'	P2	2.3147(7)
Ir	ClB	2.415(2)[b]	P1	P2	3.1305(9)†
Ir	P1	2.3148(7)	O1A	C1A	1.10(1)
Ir	P2'	2.3147(7)	O1B	C1B	1.137(9)
Ir	C1A	1.83(1)			

Primed atoms are related to unprimed atoms via the crystallographic inversion center (0, 0, 0). [a]Refined with an occupancy factor of 0.45. [b]Refined with an occupancy factor of 0.55. †Nonbonded distance.

Table 4.14. Selected Interatomic Angles (deg) for *trans*-$[RhIrCl_2(CO)_2(depm)_2]$ (**33**)

Atom1	Atom2	Atom3	Angle	Atom1	Atom2	Atom3	Angle
C1A	Ir	P1	91.91(6)	P1	Ir	C1B	91.6(2)
ClA	Ir	P2'	86.82(6)	P2'	Ir	C1A	92.1(3)
ClA	Ir	C1A	175.3(3)	P2'	Ir	C1B	87.2(2)
ClB	Ir	P1	88.00(6)	Ir	P1	C2	112.86(9)
ClB	Ir	P2'	93.25(6)	Ir	C1A	O1A	177.5(8)
ClB	Ir	C1B	174.3(2)	Ir	C1B	O1B	177.5(6)
P1	Ir	P2'	178.50(2)	P1	C2	P2	117.4(1)
P1	Ir	C1A	89.2(3)				

4.3.3.2. $[RhIr(CO)_3(depm)_2]$ (34)

As with the homobinuclear complexes, compound **33** is reduced to the Rh(0)/Ir(0) species under an atmosphere of CO, in the presence of a 1M solution of KOH/H_2O, yielding $[RhIr(CO)_3(depm)_2]$ (**34**), which is isolable in moderate yields as an red-orange oil. The NMR data are once again very similar to both the

dppm and homobinuclear depm analogues, thereby allowing its spectroscopic characterization via comparison.

The $^{31}P\{^{1}H\}$ NMR spectrum of compound **34** at ambient temperature shows the typical multiplet pattern; a doublet of pseudo-triplets for the rhodium-coupled end, appearing at 17.4 ppm, displaying a Rh-P coupling constant of 124 Hz and a P-P coupling within the pseudo-triplet of 64 Hz, along with its coupled partner due to the iridium bound end of the diphosphines at -28.8 ppm (Figure 4.12).

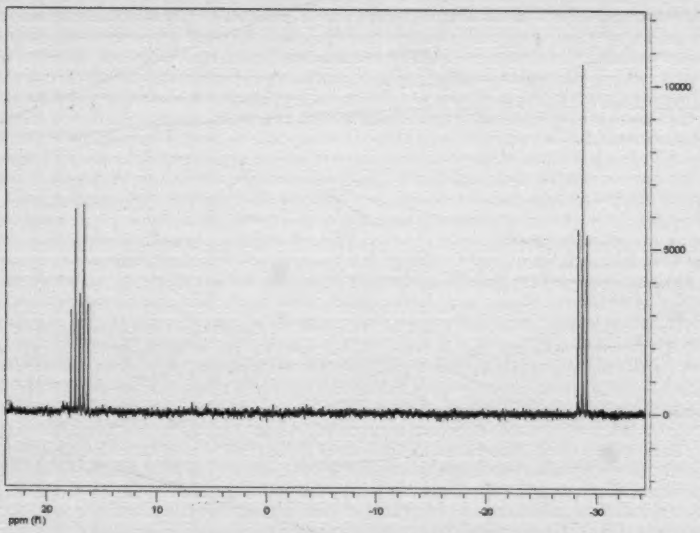

Figure 4.12. *$^{31}P\{^{1}H\}$ NMR spectrum of* $[RhIr(CO)_3(depm)_2]$ (**34**)

Consistent with the fluxional process observed in this class of compounds ($MM'(CO)_3(depm)_2$ (*vide supra*)), the ^{1}H NMR spectrum shows only the averaged depm methylene protons as a broad multiplet at 3.00 ppm, integrating for all four protons, while the ^{13}C NMR spectrum of a ^{13}CO-enriched sample of **34**, at ambient temperature, shows only two carbonyl resonances; the first is a broad singlet at 189 ppm, which integrates for two carbonyls relative to the second signal, which is a rhodium-coupled doublet appearing at 186 ppm ($^{1}J_{CRh}$ = 70 Hz).

Upon cooling, at -75 °C, the $^{31}P\{^1H\}$ NMR spectrum of compound **34** changes very little from that at room temperature, apart from slight changes in chemical shifts to 18.8 ppm and -30.5 ppm. The three expected carbonyl resonances are now observed at this temperature, appearing as relatively broad resonances; two as singlets at 191 ppm and 188 ppm, along with the final rhodium-bound carbonyl at 186 ppm, displaying typical $^1J_{RhC}$ coupling of 69 Hz. Since coupling to rhodium is only evident in one of the carbonyls, it appears the coordination sphere around each metal is considerably different than the other. The Rh atom is presumed to remain in its preferred square planar geometry, while the iridium atom takes on a distorted trigonal bipyramidal orientation to accommodate its coordination number of five. We propose that **34** has a structure like that of the Ir_2 and Rh_2 analogues (**24** and **29**) and also like that of the Rh/Ir(dppm)$_2$ analogue which has been characterized crystallographically.[17] The resulting non-A-frame configuration has the phosphorus atoms mutually *trans* on one metal (rhodium), and mutually *cis* on the other (iridium), as shown in Figure 4.13.

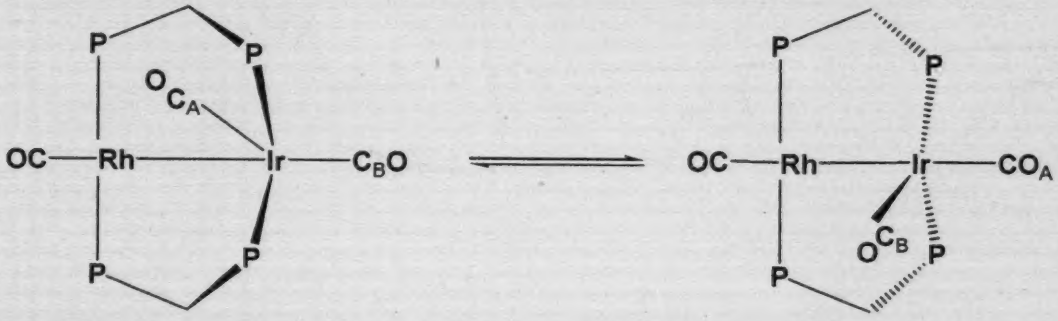

Figure 4.13. *Proposed structure of* [RhIr(CO)$_3$(depm)$_2$] (**34**) *together with its proposed fluxionality*

Notably, the high-field carbonyl resonance of **34** is unchanged at lower temperature, showing no exchange or coalescence with the Ir bound carbonyls, suggesting that it is not involved in the fluxional process. It appears that the Ir-bound carbonyls remain on that metal with the observed fluxionality due only to interconversion of the *cis*-oriented ends of the diphosphines, as has been

speculated in the dppm analogue.[17] The similarity in chemical shifts of the two Ir-bound carbonyls and the lack of rhodium coupling in either, suggests that these two carbonyls are in similar environments. In this case we show both terminally bound.

4.3.3.3. [RhIr(CO)$_4$(depm)$_2$] (35)

In solution, under excess CO, compound **34** is observed in equilibrium with its tetracarbonyl analogue [RhIr(CO)$_4$(depm)$_2$] (**35**). Much like the dppm analogue, and the previously noted Ir_2 and Rh_2 depm analogues (**25** and **30**), compound **35** is highly susceptible to CO loss thus has only been characterized spectroscopically in solution. The $^{31}P\{^1H\}$ NMR spectrum shows the typical second-order pattern for the rhodium-bound end appearing at 31.5 ppm (110 Hz), with the iridium bound end of the diphosphines displaying a triplet ($^2J_{PP}$ = 54 Hz) at -3.3 ppm. The methylene protons appear as an averaged multiplet signal at 2.42 ppm, at ambient temperature, in the ^1H NMR spectrum. Although $^{13}C\{^1H\}$ NMR data of compound **35** were not acquired, it is presumed to have a structure that is similar to that proposed for the homobinuclear dirhodium depm analogue, on the basis of that reported for [Ir_2(CO)$_4$(dmpm)$_2$],[21] wherein both metals display an unsymmetrical distorted trigonal bypyramidal-like geometry. However another structure of **35** is feasible wherein the Rh center remains in a square planar geometry and the additional carbonyl is coordinated at the Ir center, giving it an octahedral geometry, in an arrangement like that of the methyl dicarbonyl compound [RhIr(CH$_3$)(CO)$_3$(depm)$_2$][CF_3SO_3] (**36**) (*vide infra*). Complete characterization of this species should be carried out at low temperature.

4.3.3.4. [RhIr(CH$_3$)(CO)$_3$(depm)$_2$][CF_3SO_3] (36)

Addition of MeOTf to the mixed-metal tricarbonyl compound (**34**), at ambient temperature, generates $[RhIr(CH_3)(CO)_3(depm)_2][CF_3SO_3]$ (**36**) which may be isolated as an red-orange oil. The $^{31}P\{^1H\}$ NMR spectrum of compound **36** shows a pattern typical of an AA'BB'X spin system, displaying a rhodium-coupled multiplet at 33.0 ppm (110 Hz), along with a mutually coupled pseudo-triplet ($^2J_{PP}$ = 42 Hz) at -10.5 ppm. The ^1H NMR spectrum shows only a single broad resonance for the depm methylene protons at 3.00 ppm, along with a new triplet at 0.2 ppm ($^2J_{Hp}$ = 6 Hz) attributable to the methyl group, the protons of which show coupling to the two Ir-bound ^{31}P phosphorus nuclei at -10.5 ppm. The $^{13}C\{^1H\}$ NMR spectrum shows two distinct sets of carbonyl resonances in a ^{13}CO-labelled sample of compound **36**; the first of which is a broad singlet at 185 ppm having twice the intensity of the other, which appears as a doublet of triplets at 183.6 ppm, showing 71 Hz coupling to rhodium, along with 22 Hz coupling to phosphorus. The absence of coupling to Rh in the first signal clearly establishes that this pair of carbonyls are bound to iridium, and the relatively low-field chemical shift (an Ir-bound CO is generally upfield from an equivalent one on Rh) suggests an orientation towards the adjacent metal, possibly even slightly semi-bridging, although no rhodium coupling was resolved, indicating that any semi-bridging interaction must be weak. The methyl carbon appears as a singlet at -35.0 ppm, in a $^{13}CH_3$-labelled sample of compound **36**, the chemical shift of which supports the assertion of the intact nature of this moiety, and the lack of resolvable rhodium coupling suggests its attachment to iridium, as shown in Figure 4.14, in the same arrangement as that as the crystallographically characterized dppm complex.[30]

This proposed orientation was supported by an X-ray crystal structure of **36**. This structure shows a disorder in which a 60 % $Ir(CH_3)(CO)_2$ moiety is superimposed on a 40 % Rh(CO) group and vice versa. Figure 4.15A shows the ligand equatorial plane with the two disordered molecules superimposed, while figure 4.15B shows the major species (depm ligands omitted for clarity).

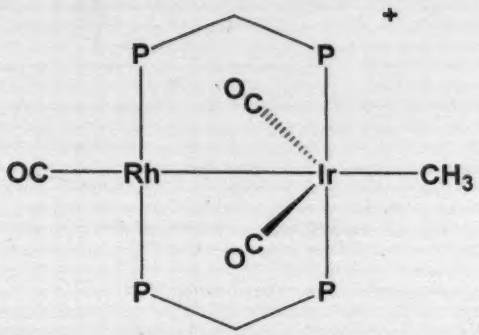

Figure 4.14. *Proposed structure of* $[RhIr(CH_3)(CO)_3(depm)_2]^+$ (**36**)

Since the minor occupant was constrained to have the same bond lengths and angles as the major occupant, only the latter are shown in Tables 4.15 and 4.16. An ORTEP diagram of the full structure of the major disordered form is shown in Figure 4.16.

It is interesting that this is the only A-frame-like complex of depm in which an alternating axial/equatorial arrangement of ethyl substituents is not observed.

The almost superimposed methyl and carbonyl groups mean that these positions will not be well refined, so any bonding parameters associated with the averaging atoms will be uncertain. In spite of the disorder the structure refined well and clearly supports the structure proposed on the basis of spectral studies.

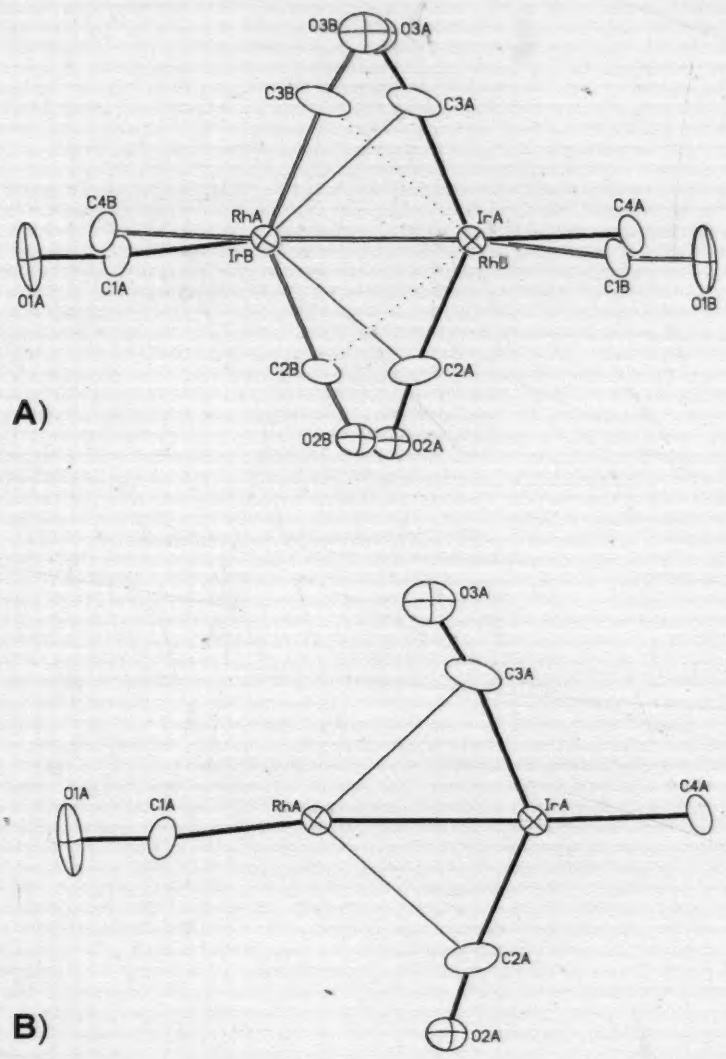

Figure 4.15. *Equatorial-plane view of* $[RhIr(CH_3)(CO)_3(depm)_2]^+$ *with depm ligands omitted* **A)** *the two dispordered molecules superimposed* **B)** *the major occupancy molecule*

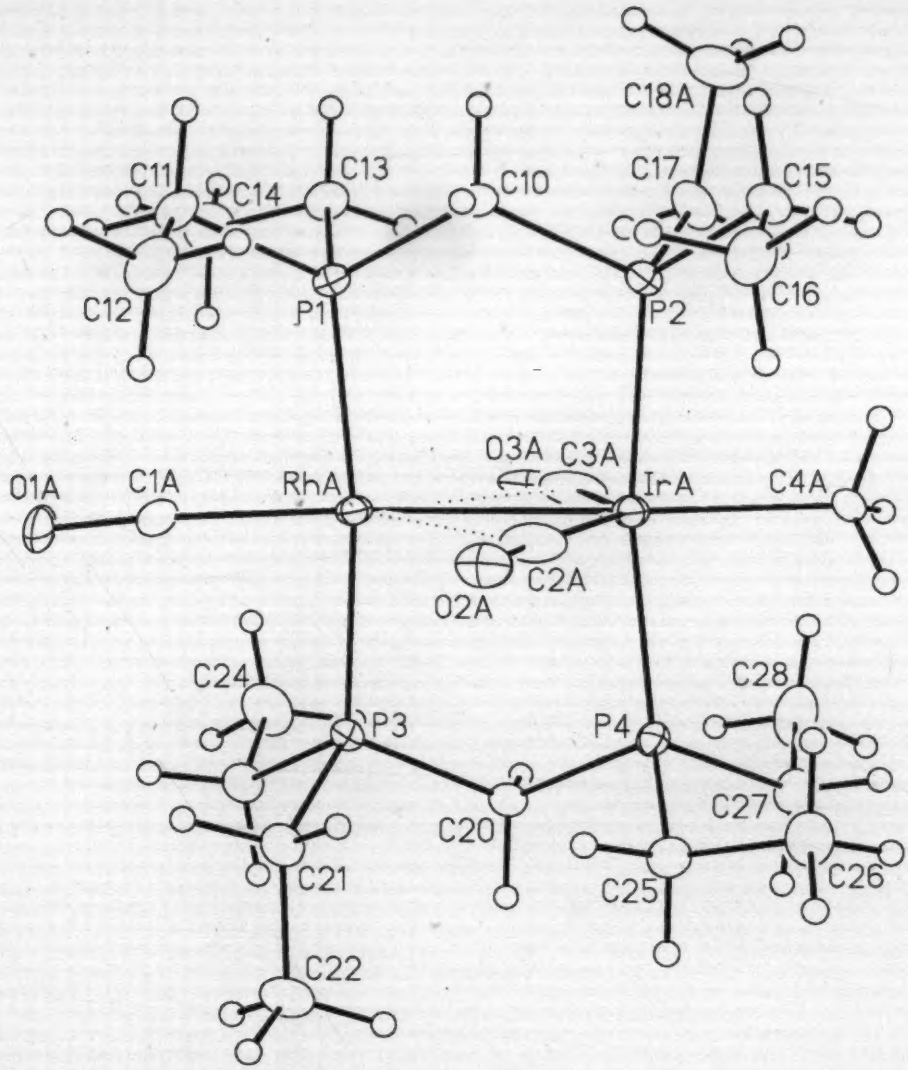

Figure 4.16. *Perspective view of the $[RhIrMe(CO)_3(depm)_2]^+$ (**36**) cation showing the atom labelling scheme. Only the major orientation of the disordered $RhIr(CO)_3(CH_3)$ fragment (IrA, RhA, O1A, O2A, O3A, C1A, C2A, C3A, C4A) is shown. Non-hydrogen atoms are represented by Gaussian ellipsoids at the 20% probability level. Hydrogen atoms are shown with arbitrarily small thermal parameters.*

Table 4.15. Selected Interatomic Distances (Å) for $[RhIr(CH_3)(CO)_3(depm)_2]$ (**36**)

Atom1	Atom2	Distance	Atom1	Atom2	Distance
IrA	C2A	1.96(1)	O1A	C1A	1.16(2)
IrA	C3A	2.02(2)	O2A	C2A	1.07(2)
IrA	C4A	2.11(2)	O3A	C3A	1.07(7)
IrA	RhA	2.7281(7)	RhA	C2A	2.688
RhA	C1A	1.94(2)	RhA	C3A	2.704

Table 4.16. Selected Interatomic Angles (deg) for $[RhIr(CH_3)(CO)_3(depm)_2]$ (**36**)

Atom1	Atom2	Atom3	Angle	Atom1	Atom2	Atom3	Angle
C2A	IrA	C3A	135.3(6)	C4A	IrA	RhA	178(1)
C2A	IrA	C4A	114.6(9)	C1A	RhA	IrA	172.56(8)
C3A	IrA	C4A	110.1(9)	O1A	C1A	RhA	174(3)
C2A	IrA	RhA	67.7(4)	O2A	C2A	IrA	175(1)
C3A	IrA	RhA	67.6(5)	O3A	C3A	IrA	171(5)

4.3.3.5. $[RhIr(CH_3)(CO)_2(depm)_2][CF_3SO_3]$ (37)

Removal of a carbonyl ligand from the tricarbonyl methyl complex (**36**) is effected through the addition of TMNO, resulting in the production of the methyl dicarbonyl complex $[RhIr(CH_3)(CO)_2(depm)_2][CF_3SO_3]$ (**37**). This species is again very similar to the homobinuclear depm analogues, and again the reactive nature of the new species, particularly with trace amounts of water, at temperatures above 0 °C, has limited our characterization of this product, to date, to solution NMR.

The $^{31}P\{^1H\}$ NMR spectrum of compound **37** shows the expected doublet of pseudo-triplets at 22.5 ppm ($^1J_{RhP}$ = 111 Hz), along with a complementary pseudo-triplet ($^2J_{PP}$ = 47 Hz) at 19.8 ppm. The ^1H NMR spectrum reveals the depm methylene protons as a pair of doublets of multiplets, integrating for two protons each, at 2.7 ppm and 2.4 ppm, displaying the characteristic 14 Hz coupling to phosphorus. The methyl group protons appear as a triplet at 0.58

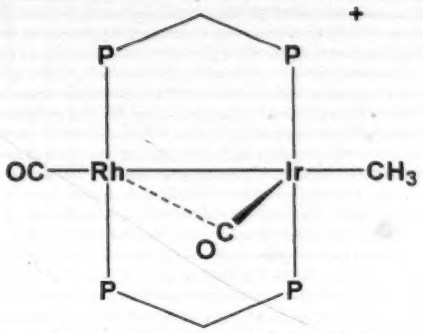

Figure 4.17. *Proposed structure of compound **37**; the mixed-metal (Rh/Ir) depm analogue of compound **1***

ppm ($^3J_{HP}$ = 9.0 Hz), in the ^{1}H NMR spectrum, that collapses to a singlet upon selective ^{31}P decoupling of the iridium-bound phosphorus nuclei. The $^{13}C\{^1H\}$ NMR spectrum of a ^{13}CO-enriched sample shows the two expected carbonyl resonances, a triplet at 182.7 ppm ($^2J_{PC}$ = 7 Hz), and a doublet of triplets at 176.6 ppm ($^2J_{PC}$ = 17 Hz, $^1J_{RhC}$ = 73 Hz), while the $^{13}CH_3$-enriched methyl group displays a singlet at 9.9 ppm. Although the coupling between the lower-field, iridium-bound carbonyl and rhodium was observed in the resolution-enhanced $^{13}C\{^1H\}$ NMR spectrum of the dppm analogue (7 Hz), it was not observed in compound **37**, nonetheless, the structure is presumed to be as shown in Figure 4.17.

Complex **37** is unstable at temperatures above 0 °C, reacting with trace amounts of water to yield the bridging-hydroxide dicarbonyl species (**47**), which is stable and isolable at room temperature, and will be discussed in the next chapter.

4.4. Discussion

The chemistry reported in this chapter, involving the depm ligand, demonstrates that this ligand system offers a very similar environment for bimetallic complexes relative to that observed for the closely related dppm and dmpm ligand systems,

apart from the differences in steric demands of the diphosphine substituents. The methods of preparation employed, along with the subsequent characteristics of the depm compounds, appear to lie somewhere between those containing the sterically smaller, dmpm phosphines, which can often be described as capricious, and those involving the larger dppm ligand system, which have in our experience been straight forward. The difference in reactivity between these two extremes (dppm vs. dmpm) is a result of the extreme differences in both their steric and electronic properties, which has been previously demonstrated by other workers in our group.[4,18] For example, in the dmpm chemistry, attempts to prepare bis-phosphine complexes often led to the formation of tris-phosphine-bridged species, presumably due to the lower steric demands of the ligands. Such complexes have rarely been observed in compounds employing the dppm system. Furthermore, in dmpm complexes the electron donating characteristics of the ligand system allow for stabilization of higher order carbonyl complexes, relative to their dppm congeners, in which the phenyl substituents not only crowd the metal centers, but are also less electron donating, therefore less capable of supporting the additional π-acceptor carbonyls. Furthermore, the addition of only one "CH_3^+" unit to the $[Ir(CO)_4(dmpm)_2]$ species was never possible; the reaction always yielded the dicationic dimethyl species, while single methyl group addition to the dppm or depm analogues was relatively straightforward.

For all species (dppm, dmpm, and depm) the initial compounds, from neutral *'trans'* dichloro complexes to the formally M(0)/M'(0) complexes $[MM'(CO)_3(diphosphine)_2]$, show many parallels, as is described in what follows.

In both the homo- and heterobinuclear *trans*-depm complexes $[MM'Cl_2(CO)_2(depm)_2]$ (M,M' = Rh, Ir), the solid-state structure has the chloro ligands, along with the carbonyls, in a mutually *trans* arrangement on adjacent metals, as illustrated in Figure 4.18, as confirmed by X-ray crystallography.

In all cases, the solid-state IR stretches in the *trans*-depm compounds are lower in frequency compared to their dppm counterparts, offering support to the

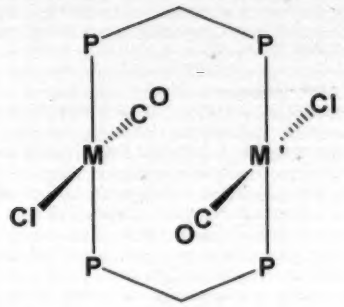

Figure 4.18. *General structure for trans-depm complexes;* MM' = Rh_2, Ir_2, RhIr

proposal that the more electron-donating depm ligand is enhancing the electron richness of the metal, thereby increasing back-bonding to the carbonyl.

Upon reduction, under CO, the above precursor dichloro-complexes are readily converted to the tricarbonyl complexes $[MM'(CO)_3(depm)_2]$ (M,M' = Rh, Ir). Initially the rhodium-iridium and diiridium depm compounds are generated as mixtures of tri- and tetracarbonyl complexes, attributable to the increased strength of the metal-carbonyl bond, however both systems may be induced to liberate the fourth carbonyl under different conditions (*vide infra*). Infrared and variable temperature NMR data, which are very comparable to that known for the dppm and dmpm analogues, have suggested that the structure of the tricarbonyl complexes is as illustrated in the following Figure 4.19.

Formally the metal atoms can be considered as neutral M(0) centers, with a single metal-metal bond, however it has been suggested[30] that different coordination spheres at each metal may lead to a mixed-valence M(+1)/M(-1) species in which the $M(CO)_2P_2^-$ moiety, donates a pair of electrons to the (otherwise $14e^-$) M(+1) metal center. Either configuration leads to a distorted square planar geometry at one metal, in which the phosphines are mutually trans, and a distorted 5-coordinate geometry arrangement at the adjacent metal, in which the phosphines are mutually *cis* to one another. The geometry at the second metal is possibly best described as a distorted tetrahedral ($M'P_2(CO)_2^-$)

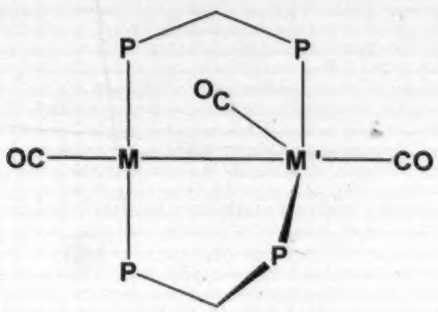

Figure 4.19. *General structure for tricarbonyl depm complexes;* MM' = Rh_2, Ir_2, RhIr

species in which electron-pair donation to the other metal (M) from a filled d-orbital results in some distortion of this metal. The carbonyl ligands are arranged such that two are terminally coordinated to opposite metals, while the third may interact strongly with one metal, and more weakly with the other, in a weakly semi-bridging manner as has been reported for both the homo- and heterobimetallic dppm complexes.[15, 16, 17] The proposed mechanism of fluxionality within these species, all of which display this phenomenon at room temperature, differs slightly between the homo- and heterobinuclear complexes. In the homobinuclear dirhodium and diirdiium complexes the process involves an alternating *cis/trans* arrangement of the diphosphine framework along with a concomitant "merry-go-round" migration of the carbonyl ligands, whereas in the mixed-metal complex only the carbonyls at the iridium center are exchanged by a dynamic process accompanied by "wagging" of the phosphines attached to that metal center. Whereas there is no difference in M-CO bond strengths at each metal when the metals are the same, the stronger Ir-CO bond compared to Rh-CO in the mixed Rh/Ir species is apparently enough to disfavor carbonyl transfer from iridium to rhodium. This difference has previously been noted in the dppm complexes of Rh/Ir.

Addition of CO to the tricarbonyl complexes is readily accomplished, and as mentioned, results in isolable tetracarbonyl complexes for both the iridium-

containing bimetallic compounds. Whereas the fourth carbonyl is extremely labile in the dirhodium complex, much like that of its dmpm and dppm counterpart, it is found to be relatively inert to CO loss in the diiridium depm compound, even more so than its dppm congenor, presumably due to the increased electron donation from the ligand system, and perhaps, additionally, due to a slight decrease in the steric bulk surrounding the bimetallic core. This is consistent with the findings in the dmpm system, wherein formation of the tetracarbonyl analogue is favored over the tricarbonyl under the same reaction conditions. The structures of the depm tetracarbonyl complexes investigated were established via NMR spectroscopy, and are presumed to have the same orientation as that of the crystallographically characterized dmpm analogue,[20] as shown in Figure 4.20.

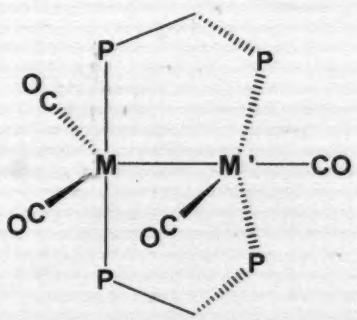

Figure 4.20. *General structure for tetracarbonyl depm complexes;* MM' = Ir_2, Rh_2, RhIr

Whereas all of the preceding neutral depm compounds shared many similarities, significant differences are observed in the series of cationic methyl complexes. As was the case with the dppm analogues, addition of methyl triflate to the precursor tricarbonyl depm complexes yields three subtly different types of species. The diiridium species undergoes C-H bond activation of the iridium-bound methyl group, to form a methylene-hydride complex, in which coordination of the substrate at one metal results in C-H bond activation of the methyl group at the adjacent metal (see Chapter 1). The facile C-H activation in

this species is consistent with the greater basicity of iridium, compared to rhodium, and the greater bond strength of the resulting metal-H and metal-C bonds generated. The structure of **26** is as shown in Figure 4.21 and has been confirmed crystallographically.

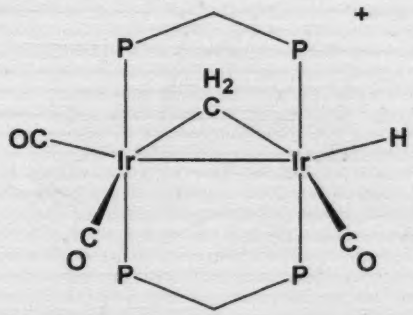

Figure 4.21. *C-H activation of methyl ligand in diiridium compound* **26**

In the mixed-metal system, the methyl ligand is terminally bound to one iridium. This has been previously observed in the dppm system,[22] and is presumably the result of the greater metal-carbon bond strength encountered with the third row metal, leading to the preferred bonding of the electrophilic "CH_3^+" group to the electron-rich center. Whereas, subsequent activation of the methyl moiety was achieved by the adjacent metal in the Ir_2 analogue (*vide supra*), the second row rhodium atom in the mixed-metal complex does not favor this transformation, maintaining its preferred square planar geometry. The iridium bound methyl group shares the metal with two carbonyls, and is *trans* to the carbonyl on the adjacent rhodium, in what presumably is a net stabilizing orientation, giving an overall symmetry to the complex as shown in Figure 4.22.

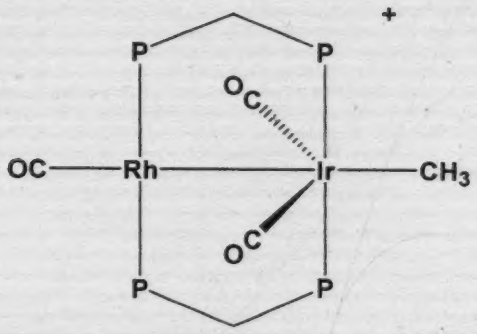

Figure 4.22. *Structure of methyl tricarbonyl mixed-metal complex* (**36**)

In the dirhodium system, addition of "CH_3^+" to the neutral tricarbonyl precursor at -20 °C initially leads to a terminally bound methyl species, very analogous to that of the Rh/Ir product. Notably, the clearly bridging nature of the carbonyls in the dirhodium species, compared to the mixed-metal analogue, is presumably a reflection of the greater tendency for the second row metal to support bridging carbonyls.

At higher temperatures, this product (**31**) transforms into the related bridging-acyl species (**32**).This transformation (Scheme 4.4) illustrates the greater tendency for rhodium alkyls to undergo migratory insertion, compared to their iridium analogues, a phenomenon that has been well established for mononuclear species,[31] as well as in analogous dppm complexes.[27] It does appear, however, that the substitution of depm for dppm in the diphosphine framework does indeed impart greater electron richness to the metals, as evidenced via the initial production and stabilization of the tricarbonyl methyl species, presumably due to the greater π back-donation. Greater π back-donation increases the electron density at the carbonyl carbon and lowers the tendency toward migratory insertion. Such a species was postulated, but not observed, in the dirhodium dppm system, which also gives rise to an analogous acyl-bridged dicarbonyl species.

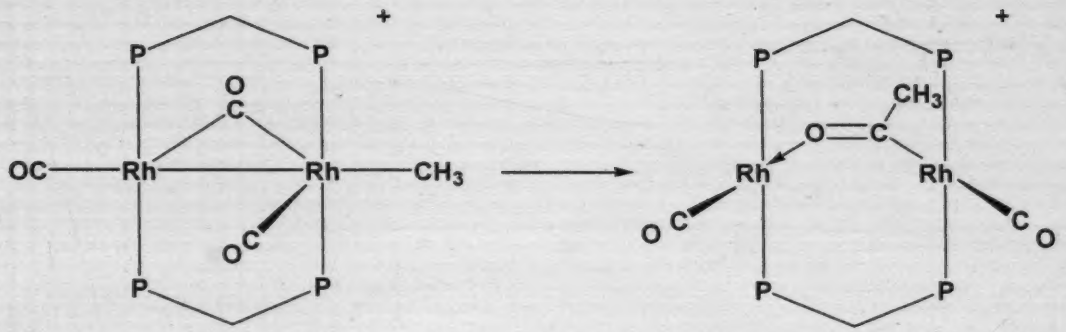

Scheme 4.4: *Transformation of methyl tricarbonyl* (**31**) *to acyl dicarbonyl* (**32**)

The final step in the production of depm analogues of **1** is the subsequent removal of a carbonyl group from the methylated tricarbonyl complexes. This step has proven the most difficult to achieve with the depm system, compared with the relative ease with which the analogous dppm complexes are prepared; a trend that is consistent with the difficulties encountered when using the dmpm ligand. Since the dirhodium depm species gave way to a migratory insertion product, generating an acyl-dicarbonyl complex that shows further transformations at room temperature, its reaction with TMNO, as a carbonyl removal reagent, has not yet been investigated. In the dirhodium dppm analogue, removal of a CO ligand from the acyl compound, to generate the targeted dicarbonyl methyl complex, was accomplished under refluxing conditions. However, the highly reactive nature of the depm acyl complex has precluded refluxing conditions as a method for carbonyl removal, and this system's subsequent reactivity is further explored in the next chapter.

In the iridium-containing systems, in which no subsequent transformation of the methyl tricarbonyl compounds is observed, preparation of the targeted methyl dicarbonyl complexes was attempted via reaction with TMNO, with limited success in both cases. While the dppm analogues have been isolated and characterized, both the diiridium and mixed-metal depm analogues of **1** have shown much higher propensity towards reactivity in solution, reacting with trace

water and/or even with solvents, making it difficult to capture and characterize these complexes. However both systems are very similar spectroscopically to their dppm analogues, so their formulation, at this stage, has been based upon analogies with the better defined dppm system.

Upon carbonyl removal from the diiridium compound $[Ir_2(H)(CO)_3(\mu\text{-}CH_2)(depm)_2]^+$ reformation of an intact methyl group occurs, yielding the target $[Ir_2(CH_3)(CO)_2(depm)_2]^+$ (**27**). Coupling to all four phosphines was observed, even at low temperatures, suggesting the possibility that this group undergoes a "windshield-wiper" type motion across one side of the binuclear face, as illustrated in the following scheme (Scheme 4.5).

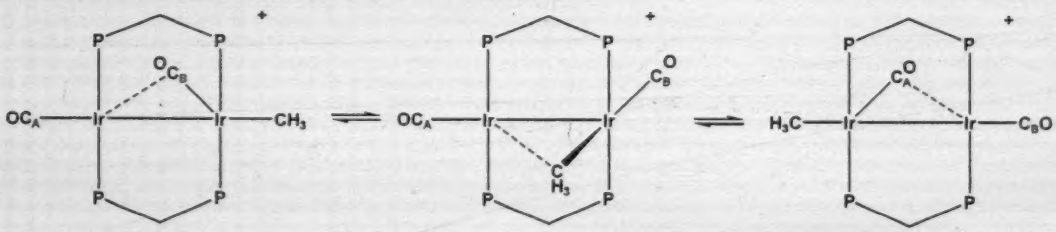

Scheme 4.5. *Fluxionality proposed for* $[Ir_2(CH_3)(CO)_2depm_2]^+$ *complex*

Such a mechanism has been proposed to explain the fluxional nature of the dppm analogue[32] and is consistent with the observed spectral data for both complexes. In the solid state structure of compound **1**, the methyl group was determined to be terminally bound to a single metal, while one carbonyl was found in a bridging position (Figure 4.23).

The mixed-metal methyl dicarbonyl compound (**37**) is proposed to have a similar conformation, however, the methyl group in this complex displays coupling to only a single side of the bridging diphosphine framework. Presumably due to the heterobinuclear nature, and weaker rhodium-carbon bond, this complex does not undergo a fluxional process at ambient temperature, and instead favors the structure in which the methyl group remains terminally bound to iridium. This is

consistent with that found for the dppm analogue, in both the solid-state and in solution.[33]

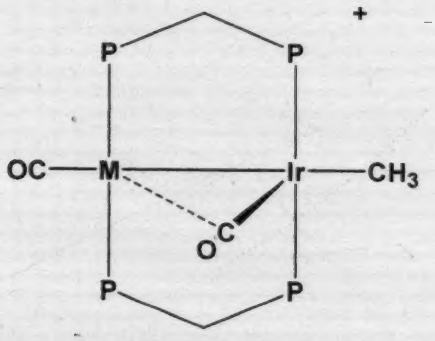

Figure 4.23. *General structure proposed for* $[MIr(CH_3)(CO)_2depm_2]^+$ (M = Ir, Rh) *complexes*

4.5. Conclusions

By and large, the reactivity of the depm complexes differs from that of the dppm species as predicted on the basis of both increased basicity and smaller steric bulk. This is encouraging from the perspective of the subsequent reactivity of these new species. The "down-side" of this increased reactivity are the difficulties associated with handling some of the complexes, although, as noted, these difficulties can be overcome. Although reactivity with some solvents presented aggravations during these preliminary studies, it also suggests exciting possibilities in substrate activation.

Within the series of Rh_2, Rh/Ir and Ir_2 complexes under study, the trends observed are largely, as we might expect, on the basis of the greater bond strengths and tendency for oxidative addition of Ir and the greater lability and migratory insertion tendencies for rhodium.

4.6. References

1. a) J.R. Torkelson, R. McDonald, M. Cowie, *J. Am. Chem. Soc.* **1998**, *120*, 4047. b) J.R. Torkelson, Ph. D. Thesis, University of Alberta, 1998. c) J.R.Torkelson, R. McDonald, M. Cowie, *J. Am. Chem. Soc.* **1998**, *120*, 4047-4048. d) D. Ristic-Petrovic, D.J. Anderson, J.R Torkelson, R. McDonald, M. Cowie, *Organometallics* **2005**, *24*, 3711-3724.
2. D. Ristic-Petrovic, J. R. Torkelson, R. W. Hilts, R. McDonald, M. Cowie, *Organometallics* **2000**, *19*, 4432.
3. M.K. Reinking, P.E. Fanwick, C.P. Kubiak, *Angew. Chem. Int. Ed.* **1989**, *10*, 1377-1379.
4. D. Ristic-Petrovic, Ph. D. Thesis, University of Alberta, 2002.
5. A.L. Fernandez, M.R. Wilson, A. Prock, W.P. Giering, *Organometallics* **2001**, *20*, 3429-3435.
6. a) K.A. Bunten, L. Chen, A.L. Fernandez, A.J. Poe, *Coord. Chem. Rev.* **2002**, *233-234*, 41-51. b) C.A. Tolman, *Chem. Rev.* **1977**, *77*, 313.
7. Z.S. Novikova, A.A. Prishchenko, I.F. Lutsenko, *J. Gen. Chem.* **1977**, *47*, 775.
8. K. Vrieze, J.P. Collman, C.T. Sears, *Inorg. Synth.* **1968**, *11*, 101.
9. L. Vaska, J.W. DiLuzio, *J. Am. Chem. Soc.* **1961**, *83*, 2784-2785.
10. G. Gordano, R.H. Crabtree, *Inorg. Synth.* **1979**, *19*, 218.
11. J.A. McCleverty, G. Wilkinson, *Inorg. Synth.* **1990**, *28*, 88.
12. B.R. Sutherland, M. Cowie, *Inorg. Chem.* **1984**, *23*, 2324.
13. J.T. Mague, J.P. Mitchener, *Inorg. Chem.* **1969**, *8*, 119.
14. J.E Huheey, E.A. Keiter, R.L Keiter, *Inorganic Chemistry, Principles of Structure and Reactivity*, fourth edition, Harper Collins,New York, 1993, 292.
15. a) C.P. Kubiak, C. Woodcock, R. Eisenberg, *Inorg. Chem.* **1982**, *21*, 2119. b) C. Woodcock, R. Eisenberg, *Inorg. Chem.* **1985**, *24*, 1285.
16. B.R. Sutherland, M. Cowie, *Organometallics* **1985**, *4*, 1637-1648.
17. R. McDonald, M. Cowie, *Inorg. Chem.* **1990**, *29*, 1564.

18. J. A. Jenkins, Ph. D. Thesis, University of Alberta, 1991. J. A. Jenkins, M. Cowie, *Organometallics* **1992**, *11*, 2767.
19. M.K. Reinking, J. Ni, P.E. Fanwick, C.P. Kubiak *J. Am. Chem. Soc.* **1989**, *111*, 6459-6461.
20. C.H. Londergan, C.P. Kubiak, *Chem. Eur. J.* **2003**, 9, 5962-5969.
21. M.K. Reinking, Ph. D. Thesis, Purdue University, 1989.
22. a) F.H. Antwi-Nsiah, Ph. D. Thesis, University of Alberta, 1994. b) J.R. Torkelson, F.H. Antwi-Nsiah, R. McDonald, M. Cowie, J.G. Prius, K.J. Jalkanen, R.L. DeKock, *J. Am. Chem. Soc.* **1999**, *121*, 3666-3683.
23. J.T. Mague, A.R. Sanger, *Inorg. Chem.* **1979**, *18*, 2060-2066.
24. a) J.T. Mague, J.P Mitchener, *Inorg. Chem.* **1969**, *8*, 119. b) S. Dwight, M. Cowie, *Inorg. Chem.* **1980**, *19*, 2500-2507.
25. J.A. Jenkins, J.P. Ennett, M. Cowie, *Organometallics* **1988**, *7*, 1845-1853.
26. a) B.D. Rowsell, S.J. Trepanier, R. Lam, R. McDonald, M. Cowie, *Organometallics*, **2002**, *21*, 3228-3237. b) O. Oke, R. McDonald, M. Cowie, *Organometallics* **1999**, *18*, 1629. c) M.M. Dell'Anna, S.J. Trepanier, R. McDonald, M. Cowie, *Organometallics*, **2001**, *20*, 88.
27. F. Shafiq, K.W. Kramarz, R. Eisenberg, *Inorg. Chim. Acta.* **1993**, *213*, 111-119.
28. L. Vaska, J.W. Di Luzio, *J. Am. Chem. Soc.* **1961**, *83*, 2784.
29. A. Roodt, S. Otto, G. Steyl, *Coord. Chem. Rev.* **2003**, *245*, 121-137.
30. R. McDonald, Ph. D. Thesis, University of Alberta, 1991.
31. R.S. Dickson, *Organometallic Chemistry of Rhodium and Iridium*, Academic Press, London, 1983.
32. F.H Antwi-Nsiah, O. Oke, M. Cowie, *Organometallics* **1996**, *15*, 1042-1054.
33. O. E. Oke, Ph. D. Thesis, University of Alberta, 1999.

Chapter 5

Peripheral Reactivity Related to the DEPM Methyl Complexes of Iridium, Rhodium, and Rhodium/Iridium

5.1. Introduction

In the last chapter, it was shown that the different depm analogues of the diiridium compound $[Ir_2(CH_3)(CO)_2(dppm)_2][CF_3SO_3]$ (**1**), namely, $[MM'(CH_3)(CO)_2(depm)_2]^+$ (MM' = Ir_2, RhIr), were highly reactive in solution, often reacting with water and/or solvent, resulting in their transformation to undesired byproducts. Although these products were peripheral to our targeted study, at the time they required characterization, nonetheless, in order to obtain information on the reactivity of the targeted precursor complex.

In this chapter are described some of these reactions and our efforts at characterization of the products. Due to lack of time, the reactions with solvent, which are intriguing, have not been pursued, but clearly this should be followed up. Characterization of products is sometimes incomplete, from a publication perspective, but is viewed as adequate to establish the formulae, if not the detailed stereochemistry or dynamics of the complexes.

5.2. Experimental

5.2.1. General Comments. All solvents were dried (using appropriate drying agents), distilled before use and stored under dinitrogen. Deuterated solvents used for NMR experiments were freeze-pump-thaw degassed (three cycles) and stored under nitrogen or argon over molecular sieves. Reactions were carried out under argon using standard Schlenk techniques, and compounds that were used as solids were purified by recrystallization. Prepurified argon and nitrogen

were purchased from Linde, carbon-13 enriched CO (99%) was supplied by Isotec Inc. All purchased gases were used as received. All other reagents were obtained from Aldrich and were used as received (unless otherwise stated).

Proton NMR spectra were recorded on Varian Unity 400, 500 or 600 spectrometers, or on a Bruker AM400 spectrometer. Carbon-13 NMR spectra were recorded on Varian Unity 400 or Bruker AM300 spectrometers. Phosphorus-31 and fluorine-19 NMR spectra were recorded on Varian Unity 400 or Bruker AM400 spectrometers. Two-dimensional NMR experiments (COSY, ROESY, TOCSY and ^{13}C-^{1}H HMQC) were obtained on Varian Unity 400 or 500 spectrometers.

Because the compounds appearing in this chapter were peripheral to our original targeted molecules, their complete analysis has not been meticulously pursued, and only spectroscopic data are presented towards their characterization (Table 5.1).

Table 5.1. Spectroscopic data for the compounds

compound	$\delta(^{31}P\{^1H\})^c$	$\delta(^1H)^d$	$\delta(^{13}C\{^1H\})^{e,f}$
$[Ir_2(CO)_2(\mu\text{-}OH)(depm)_2][CF_3SO_3]$ (**38**)	16.5 (s)	3.6 (b, 1H), 2.85 (m, 4H), 2.15 (m, 16H), 1.15 (m, 24H),	185 (s, br)
$[Ir_2(CO)_3(\mu\text{-}H)(depm)_2][CF_3SO_3]$ (**39**)	15.8 (s)	2.45 (q, 4H), 2.15 (m, 16H), 1.15 (m, 24H), -10.4 (q, 1H, $^2J_{HP}$ = 9.8 Hz)	184 (s, br) (186 (s, br, 2C), 184 (s, br))^k
$[Ir_2(H)(CO)_4(depm)_2][CF_3SO_3]$ (**40**)	-9.5 (t, $^2J_{PP}$ = 30 Hz, 2P), -11.2 (t, $^2J_{PP}$ = 30 Hz)	3.4 (m, 4H), 2.20 (m, 16H), 1.15 (m, 24H) -8.8 (t, $^2J_{HP}$ = 14 Hz, 1H)	192 (t, $^2J_{CP}$ = 10 Hz), 187 (t, $^2J_{CP}$ = 13 Hz)
$[Ir_2(CH_3)(CO)_4(depm)_2][CF_3SO_3]$ (**41**)	-14.9 (m), -18.6 (m)	2.75 (q, 4H), 2.20 (m, 16H), 1.20 (m, 24H), 0.68 (t, 3H, $^3J_{PH}$ = 5 Hz)	191.1 (t, $^2J_{CP}$ = 11 Hz), 187.3 (t, $^2J_{CP}$ = 13 Hz), -40.1 (t, $^2J_{CP}$ = 6 Hz)
$[Ir_2(CH_3CO)(CO)_4(depm)_2][CF_3SO_3]$ (**42**)	-15.7 (m), -20.9 (m)	3.35 (q, 4H), 2.60 (s, 3H), 2.20 (m, 16H), 1.15 (m, 24H)	195.2 (t, $^2J_{CP}$ = 10 Hz), 188.2 (t, $^2J_{CP}$ = 13 Hz), 220.5 (dt, 1C), 53 (b, m)

Notes: [a] NMR abbreviations: s = singlet, d = doublet, t = triplet, q = quintet, m = multiplet, br = broad. [b] NMR data in CD_2Cl_2 unless otherwise stated. [c] $^{31}P\{^1H\}$ chemical shifts are referenced vs. external 85% H_3PO_4 [d] ^1H and ^{13}C chemical shifts are referenced vs. external TMS [e] ν(CO) [f] Nujol. [g] CH_2Cl_2 [h] C_6H_6 [i] C_6D_6 [j] IR abbreviations: s = strong, m = medium, w = weak [k] indicates low temperature data

Table 5.1. (con't) Spectroscopic data for the compounds

Compound	$\delta(^{31}P\{^1H\})^c$	$\delta(^1H)^d$	$\delta(^{13}C\{^1H\})^{e,f}$
$[Rh_2(CO)_3(depm)_2][CF_3SO_3]_2$ (**43**)	29.0 (b, d, $^1J_{PRh}$ = 93 Hz)	2.7 (m, 4H), 2.05 (m, 16H), 1.25 (m, 24H)	189 (b)
$[Rh_2(CO)_5(depm)_2][CF_3SO_3]_2$ (**44**)	32 (b)	3.0 (q, 4H), 2.20 (m, 16H), 1.2 (m, 24H)	192 (b)
$[Rh_2(\mu\text{-}OH)(CO)_2(depm)_2][CF_3SO_3]$ (**45**)	21.7 (dm, $^1J_{PRh}$ = 120 Hz)	2.65 (m, 4H), 2.15 (m, 16H), 1.15 (m, 24H), 0.78 (q, 1H, $^3J_{HP}$ = 2.5 Hz)	191.6 (dt, $^1J_{CRh}$ = 70 Hz, $^2J_{CP}$ = 16 Hz)
$[Rh_2(H)(CO)_3(depm)_2][CF_3SO_3]$ (**46**)	35.2 (dm, $^1J_{PRh}$ = 97 Hz)	2.23 (m, 4H), 2.00 (m, 16H), 1.22 (m, 24H), -10.3 (m, 1H, $^1J_{HRh}$ = 24 Hz, $^2J_{HP}$ = 12 Hz)	194 (m, br)
$[RhIr(\mu\text{-}OH)(CO)_2(depm)_2][CF_3SO_3]$ (**47**)	20.6 (dt, $^1J_{PRh}$ = 117 Hz), 17.2 (t, $^2J_{PP}$ = 14 Hz)	3.33 (s, 1H), 2.7 (m, 2H), 2.3 (m, 2H), 2.05 (m, 16H), 1.20 (m, 24H)	190.7 (dt, $^1J_{CRh}$ = 71.5 Hz, $^2J_{CP}$ = 16.5 Hz), 174.8 (t, $^2J_{CP}$ = 10.5 Hz)
$[RhIr(CO)_3(\mu\text{-}H)(depm)_2][CF_3SO_3]$ (**48**)	27.7 (dt, $^1J_{PRh}$ = 107 Hz), -5.5 (t, $^2J_{PP}$ = 46 Hz)	2.85 (q, 4H), 1.95 (m, 16H), 1.20 (m, 24H), -11.3 (m, 1H, $^1J_{HRh}$ = 20.8 Hz, $^2J_{HP}$ = 9.7 Hz)	180.3 (t, $^2J_{CP}$ = 9.3 Hz) 187.2. (dt, $^1J_{CRh}$ = 75 Hz, $^2J_{CP}$ = 16 Hz

Notes: [a] NMR abbreviations: s = singlet, d = doublet, t = triplet, q = quintet, m = multiplet, br = broad. [b] NMR data in CD_2Cl_2 unless otherwise stated. [c] $^{31}P\{^1H\}$ chemical shifts are referenced vs. external 85% H_3PO_4 [d] ^1H and ^{13}C chemical shifts are referenced vs. external TMS [e] $\nu(CO)$ [f] Nujol. [g] CH_2Cl_2 [h] C_6H_6 [i] C_6D_6 [j] IR abbreviations: s = strong, m = medium, w = weak [k] indicates low temperature data

5.2.2. Preparation of Compounds

(a) **$[Ir_2(CO)_2(\mu\text{-}OH)(depm)_2][CF_3SO_3]$ (38).** To a solution of $[Ir_2(CH_3)(CO)_2(depm)_2][CF_3SO_3]$ (**27**) (50 mg, 0.050 mmol), generated *in situ* at -20 °C in 5 mL of dichloromethane, was added 5 μL (0.277 mmol) of water and the resultant mixture stirred while warming to room temperature over the course of ½ h. The solvent was removed *in vacuo* and the product recrystallized from dichloromethane and pentane affording 35 mg of compound **38** as bright yellow powder (70 % yield).

(b) **$[Ir_2(CO)_3(\mu\text{-}H)(depm)_2][CF_3SO_3]$ (39).** **Method i)** A solution of $[Ir_2(CO)_2(\mu\text{-}OH)(depm)_2][CF_3SO_3]$ (**38**) dissolved in 0.7 mL of d_2-dichloromethane was purged with CO for 2 min, resulting in the formation of compound **40** (*vide infra*), as determined spectroscopically. Attempts to isolate the complex as a solid in the absence of CO resulted in the conversion to compound **39**. **Method ii)** To a solution of $[Ir_2(CO)_3(depm)_2]$ (**31**) (125 mg, 0.147 mmol) in 30 mL of benzene was slowly added drop-wise 15 μL (0.170 mmol) of neat triflic acid (HOTf). The resulting mixture was stirred for 1 h whereupon it was reduced *in vacuo* to *ca.* 2 mL. Pentane (10 mL) was added to precipitate a dark red solid which was isolated, further washed with pentane (2 x 10 mL) and dried *in vacuo* giving 115 mg of compound **39** (78 % yield).

(c) **$[Ir_2(H)(CO)_4(depm)_2][CF_3SO_3]$ (40).** A solution of $[Ir_2(CO)_3(\mu\text{-}H)(depm)_2][CF_3SO_3]$ (**39**) dissolved in 0.7 mL of d_2-dichloromethane was put under an atmosphere of CO resulting in the generation of compound **40**, as determined spectroscopically. This species has only been characterized in solution, as removal of the CO atmosphere resulted in

quantitative conversion to compound **39** (*vide supra*). This species was also prepared from compound **38**, as described in section (b).

(d) **$[Ir_2(CH_3)(CO)_4(depm)_2][CF_3SO_3]$ (41) and $[Ir_2(CH_3CO)(CO)_4(depm)_2][CF_3SO_3]$ (42).** Excess carbon monoxide was transferred via gas-tight syringe onto a solution of 50 mg (0.037 mmol) of $[Ir_2(\mu\text{-}CH_2)(H)(CO)_3(depm)_2][CF_3SO_3]$ (**26**) in 0.7 mL of d_2-dichloromethane. Under these conditions both complexes (**41** and **42**) could be sequentially identified spectroscopically through NMR studies. However, removal of the CO atmosphere resulted only in regeneration of the starting compound (**26**).

(e) **$[Rh_2(CO)_3(depm)_2][CF_3SO_3]_2$ (43).** To a solution of $[Rh_2(CO)_3(depm)_2]$ (**29**) (95 mg, 0.089 mmol), in 10 mL of acetone at 0 °C, was added 85 μL (0.960 mmol) of neat triflic acid and the solution stirred for 3 h, while warming to ambient temperature. The solvent was subsequently removed *in vacuo*, and the isolated orange solid was recrystallized from acetone and pentane, affording 75 mg (62 % yield) of compound **43**. Notably, this compound was also generated upon addition of excess methyl triflate to the neutral precursor tricarbonyl complex, under the same conditions (see Chapter 4), however this route was not as clean, producing a number of other uncharacterized species.

(f) **$[Rh_2(CO)_5(depm)_2][CF_3SO_3]_2$ (44).** To an NMR-scale solution (50 mg, 0.037 mmol, in 0.7 mL of acetone) of compound **43** was added excess CO, producing a clear yellow solution. The sample was subsequently investigated via multinuclear NMR spectroscopy. Stepwise

addition of CO first produced a tetracarbonyl species, which, under under CO continued to give the pentacarbonyl compound (**44**). Although X-ray quality crystals of **44** were obtained in the solid state (*vide infra*), removal of the CO atmosphere from a solution of **44** resulted in reversion to starting material, thus this compound has been primarily characterized spectroscopically and crystallographically.

(g) **$[Rh_2(CO)_2(\mu\text{-}OH)(depm)_2][CF_3SO_3]$ (45).** To a solution of $[Rh_2(CO)_3(depm)_2][CF_3SO_3]_2$ (**43**) (75 mg, 0.089 mmol), generated in 10 mL of acetone at ambient temperature, was added 5 μL (0.277 mmol) of water, causing the solution to lighten in color. Maintaining this temperature for ½ h, while stirring, caused the color to become bright yellow. The solvent was subsequently removed *in vacuo* and the residue extracted 3 times into 5mL of ether. The extraction solvent was removed *in vacuo* and and the isolated yellow solid further dried giving 50 mg of compound **45** (70 % yield).

(h) **$[Rh_2(CO)_3(\mu\text{-}H)(depm)_2][CF_3SO_3]$ (46). Method i)** A solution of $[Rh_2(CO)_2(\mu\text{-}OH)(depm)_2][CF_3SO_3]$ (**40**) (37mg, 0.046 mmol) dissolved in 0.7 mL of d_2-dichloromethane was purged with CO for 2 min. Spectroscopic parameters of the resultant complex were identical to those from method ii. **Method ii)** To a solution of 100 mg (0.148 mmol) of $[Rh_2(CO)_3(depm)_2]$ (**29**) in 30 mL of benzene was slowly added drop-wise 15 μL (0.170 mmol) of neat triflic acid (HOTf). The resulting mixture was stirred for 1 h whereupon it was reduced *in vacuo* to *ca.* 2 mL. Pentane (10 mL) was added to precipitate a dark orange-red solid which was isolated, and further washed with pentane (2 x 10 mL), then dried *in vacuo* giving 90 mg of spectroscopically pure compound **46** (75 % yield).

HRMS *m/z* calcd for $Rh_2P_4O_2C_{20}H_{45}$ [M^+-CO]: 647.0473. Found: 647.0475.

(i) **[RhIr(CO)$_2$(μ-OH)(depm)$_2$][CF$_3$SO$_3$] (47).** To a solution of [RhIr(CH$_3$)(CO)$_2$(depm)$_2$][CF$_3$SO$_3$] (**37**) (90mg, 0.097 mmol), prepared *in situ* in 7ml CH_2Cl_2, was added 5 μL (0.277 mmol) of water. The solution was stirred at room temperature for ½ h, during which time the color lightened to a pale orange. The solvent was then removed *in vacuo* and the product recrystallized from dichloromethane and pentane affording 67 mg of an orange powder (77 % yield).

(j) **[RhIr(CO)$_3$(μ-H)(depm)$_2$][CF$_3$SO$_3$] (48). Method i)** A solution of [RhIr(CO)$_2$(μ-OH)(depm)$_2$][CF$_3$SO$_3$] (**40**) (37mg, 0.046 mmol) dissolved in 0.7 mL of d_2-dichloromethane was purged with CO for 2 min. Spectroscopic parameters of the resultant complex were identical to those from method ii. **Method ii)** To a solution of [RhIr(CO)$_3$(depm)$_2$] (**31**) (100 mg, 0.131 mmol) in 30 mL of benzene was slowly added drop-wise 15 μL (0.170 mmol) of neat triflic acid (HOTf). The resulting mixture was stirred for 1 h whereupon it was reduced to dryness *in vacuo*. The solid was recrystallized from dichloromethane and pentane affording a dark red-orange solid, which, after isolation and further washing with pentane (2 x 10 mL), was dried *in vacuo* giving 90 mg of compound **48** (75 % yield). HRMS *m/z* calcd for $RhIrP_4O_3C_{21}H_{45}$: 913.6678. Found: 913.6676.

X-Ray Data Collection. Data collection and structure solution (*vide infra*) were carried out by R. McDonald and M. J. Ferguson.

Bright yellow crystals of $[Rh_2(CO)_5(depm)_2][CF_3SO_3]_2$ (**44**), suitable for X-ray diffraction, were obtained *via* slow diffusion of *n*-pentane into a saturated acetone solution of the complex prepared under CO. The structure solution showed no disorder amongst the atoms and was refined very well. See Table 5.2 for a summary of crystal data and X-ray data collection information.

Table 5.2. Crystallographic Experimental Details for $[Rh_2(CO)_5(depm)_2]^{2+}$ (**44**)

A. Crystal Data	
formula	$C_{25}H_{44}F_6O_{11}P_4Rh_2S_2$
formula weight	1028.42
crystal dimensions (mm)	0.49 × 0.40 × 0.16
crystal system	monoclinic
space group	$P2_1/m$ (No. 11)
unit cell parameters[a]	
a (Å)	9.5764 (6)
b (Å)	21.346 (1)
c (Å)	10.0396 (6)
β (deg)	108.081 (1)
V (Å^3)	1950.9 (2)
Z	2
ρ_{calcd} (g cm^{-3})	1.751
μ (mm^{-1})	1.196
B. Data Collection and Refinement Conditions	
diffractometer	Bruker PLATFORM/SMART 1000 CCD[b]
radiation (λ [Å])	graphite-monochromated Mo Kα (0.71073)
temperature (°C)	–80
scan type	ω scans (0.2°) (20 s exposures)
data collection 2θ limit (deg)	52.72
total data collected	11122 ($-8 \le h \le 11, -26 \le k \le 26, -12 \le l \le 12$)
independent reflections	4079 (R_{int} = 0.0200)
number of observed reflections (*NO*)	3810 [$F_o^2 \ge 2\sigma(F_o^2)$]
structure solution method	direct methods (*SHELXS–86*[c])
refinement method	full-matrix least-squares on F^2 (*SHELXL–93*[d])
absorption correction method	multi-scan (*SADABS*)
range of transmission factors	0.8317–0.5918
data/restraints/parameters	4079 [$F_o^2 \ge -3\sigma(F_o^2)$] / 0 / 244
goodness-of-fit (S)[e]	1.040 [$F_o^2 \ge -3\sigma(F_o^2)$]

Table 5.2. Crystallographic Experimental Details (continued)

final *R* indices[f]	
R_1 [$F_o^2 \geq 2\sigma(F_o^2)$]	0.0225
wR_2 [$F_o^2 \geq -3\sigma(F_o^2)$]	0.0625
largest difference peak and hole	0.694 and –0.526 e Å^{-3}

[a]Obtained from least-squares refinement of 5433 reflections with $4.86° < 2\theta < 52.72°$.

[b]Programs for diffractometer operation, data collection, data reduction and absorption correction were those supplied by Bruker.

[c]Sheldrick, G. M. *Acta Crystallogr.* **1990**, *A46*, 467–473.

[d]Sheldrick, G. M. *SHELXL-93*. Program for crystal structure determination. University of Göttingen, Germany, 1993. Refinement on F_o^2 for all reflections (all of these having $F_o^2 \geq -3\sigma(F_o^2)$). Weighted *R*-factors wR_2 and all goodnesses of fit *S* are based on F_o^2; conventional *R*-factors R_1 are based on F_o, with F_o set to zero for negative F_o^2. The observed criterion of $F_o^2 > 2\sigma(F_o^2)$ is used only for calculating R_1, and is not relevant to the choice of reflections for refinement. *R*-factors based on F_o^2 are statistically about twice as large as those based on F_o, and *R*-factors based on ALL data will be even larger.

[e]$S = [\Sigma w(F_o^2 - F_c^2)^2/(n-p)]^{1/2}$ (n = number of data; p = number of parameters varied; $w = [\sigma^2(F_o^2) + (0.0344P)^2 + 1.1794P]^{-1}$ where $P = [\text{Max}(F_o^2, 0) + 2F_c^2]/3$).

[f]$R_1 = \Sigma||F_o| - |F_c||/\Sigma|F_o|$; $wR_2 = [\Sigma w(F_o^2 - F_c^2)^2/\Sigma w(F_o^4)]^{1/2}$.

5.3. Results and Discussion

5.3.1. Diiridium Complexes

5.3.1.1. $[Ir_2(CO)_2(\mu\text{-}OH)(depm)_2][CF_3SO_3]$ (38)

As described in the previous chapter, the dicarbonyl methyl complex $[Ir_2(CH_3)(CO)_2(depm)_2][CF_3SO_3]$ (**27**) is susceptible, at temperatures above 0 °C, to reaction with water, yielding the hydroxide-bridged dicarbonyl complex, $[Ir_2(CO)_2(\mu\text{-}OH)(depm)_2][CF_3SO_3]$ (**38**) and methane, as detected in the ^{1}H NMR spectrum. The source of water in these reactions is presumed to come from use

of TMNO that had not been freshly sublimed, from insufficiently dried solvents or glassware, or from slow leakage of air into the septum-capped NMR tubes. Characterization of **38** by NMR spectroscopy showed a symmetrical species in which all four ^{31}P nuclei are chemically equivalent, displaying a singlet at 16.5 ppm in the $^{31}P\{^1H\}$ NMR spectrum, and for which only a single carbonyl resonance (singlet) was observed at 185 ppm in the $^{13}C\{^1H\}$ NMR spectrum. A broad resonance in the ^1H NMR spectrum, integrating as one proton, was observed at 3.6 ppm, and the accompanying signals indicating the formation of methane suggested that this resonance could correspond to a hydroxide ligand that had resulted from hydrolysis of **27**. The analogous dppm complex $[Ir_2(CO)_2(\mu\text{-}OH)(dppm)_2][CF_3SO_3]$ had previously been characterized[1] and displays very similar ^{31}P chemical shift data (singlet at 15.2 ppm), so on this basis we tentatively assigned the same A-frame structure to **38**, as diagrammed below (see Figure 5.1).

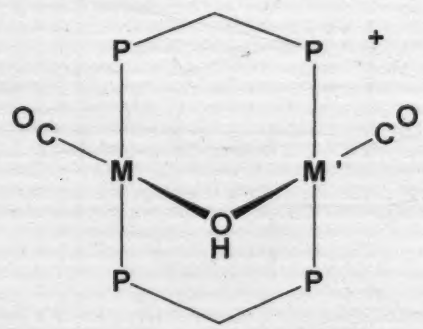

Figure 5.1. *A-frame structure in hydroxide-bridged dicarbonyl depm complexes*

Support for this formulation came from the introduction of D_2O to a sample of **38**, resulting in instantaneous loss of the OH signal in the ^1H NMR spectrum, via proton-deuteron exchange. Subsequent deliberate addition of water to samples of compound **27** resulted in quantitative and rapid conversion to **38**.

5.3.1.2. $[Ir_2(CO)_3(\mu\text{-}H)(depm)_2][CF_3SO_3]$ (39)

Further characterization of **38** was obtained in its reaction with CO, which initially yields the tetracarbonyl hydride complex $[Ir_2(H)(CO)_4(depm)_2][CF_3SO_3]$ (**40**) (*vide infra*), presumably with the concomitant generation of CO_2 in water-gas-shift related chemistry. Subsequent attempts to isolate the product of this reaction, led to the formation of the tricarbonyl hydride complex $[Ir_2(CO)_3(\mu\text{-}H)(depm)_2][CF_3SO_3]$ (**39**), via facile CO loss. This hydride species, diagrammed below, could also be obtained more directly via protonation of the neutral tricarbonyl compound (**24**) at ambient temperature. The $^{31}P\{^1H\}$ NMR spectrum of this product shows a singlet at 15.8 ppm, consistent with the symmetrical structure shown in Figure 5.2, which is analogous to that established crystallographically for the dppm compound.[2]

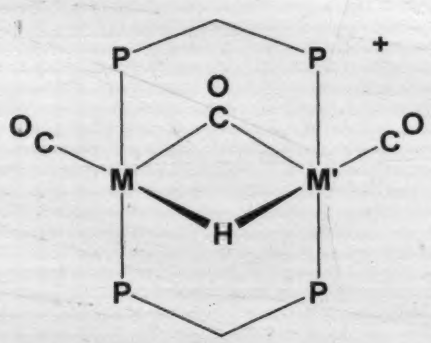

Figure 5.2. *Proposed structure of the homobinuclear hydride tricarbonyl depm complexes* (M = M' = Ir (**39**), M = M' = Rh (**46**))

Evidence in support of this proposed structure for compound **39** is apparent in the ^1H spectrum, in which an up-field quintet is apparent at -10.4 ppm, attributable to the bridging hydride ligand, that shows equal coupling ($^2J_{HP}$ = 9.8 Hz) to all four phosphorus nuclei. Although diagrammed as containing a bridging carbonyl ligand, on the basis of analogies with the dppm complexes, this aspect is not unambiguous in compound **39**. Although the IR spectrum shows two peaks at 1945 cm^{-1}, and 1890 cm^{-1}, suggesting the presence of terminal and

bridging carbonyls, the $^{13}C\{^1H\}$ NMR spectrum shows only a single broad signal at 184.4 ppm. Upon cooling to -78 °C, this resonance is only slightly resolved to two sets of broad signals, appearing in a 2:1 ratio, at 186 ppm and 184 ppm, respectively, suggesting that this species may be fluxional at higher temperatures, as outlined in the following scheme (Scheme 5.1).

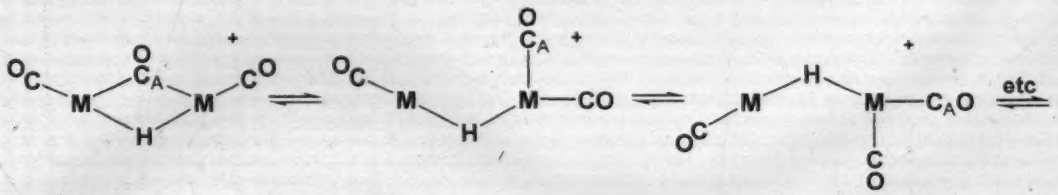

Scheme 5.1. *Mechanism proposed for fluxionality observed in the* $[MM'(CO)_3(\mu\text{-}H)(depm)_2][CF_3SO_3]$ (M, M' = Rh, Ir) *complexes*

The observation of only one ^{13}C resonance at room temperature must involve complete exchange of all carbonyls, which may occur by a "merry-go-round" motion of all ligands in the equatorial plane (the non-phosphine ligands) as is well known in such binuclear complexes. However, hydride ligands are also notoriously mobile and can "tunnel" between the pair of metals, a process that can only happen if the carbonyl moves out of the bridge, allowing the fluxional process, like that diagrammed in Scheme 5.1, to occur. Nevertheless, the proximity of the two ^{13}CO resonances remains puzzling on the basis of the proposed terminal and bridging modes.

5.3.1.3. $[Ir_2(H)(CO)_4(depm)_2][CF_3SO_3]$ (40)

As mentioned above, $[Ir_2(H)(CO)_4(depm)_2][CF_3SO_3]$ (**40**) may be generated through CO addition to the hydroxide-bridged complex **38**. However, this species is stable only under an atmosphere of CO, so has been exclusively characterized in solution by NMR spectroscopy. The $^{31}P\{^1H\}$ NMR spectrum of compound **40** shows a pair of mutually coupled pseudo-triplets ($^2J_{PP}$ = 30 Hz) at -9.5 ppm and

-11.2 ppm. Although the chemical shifts are similar to that of the dppm analogue, which appears as a singlet -9.6 ppm,[3] the depm complex displays an AA'BB' splitting pattern, indicating different chemical environments for each side of the diphosphines. Further evidence for the side-to-side asymmetry in compound **40** is also apparent upon examination of the hydride resonance in the ^{1}H NMR spectrum. Whereas in the dppm complex this signal is a quintet, showing equal coupling to all four phosphorus atoms, as also noted above for compound **39**, the hydride resonance in compound **40** appears as a triplet at -8.8 ppm, showing coupling to only one side of the diphosphine framework, suggesting it is terminally bound to the associated metal. The single resonance of the depm methylene protons, appearing at 3.4 ppm, may suggest an element of front/back symmetry exists in the molecule, which is supported by the presence of only two equal intensity resonances in the $^{13}C\{^{1}H\}$ NMR spectrum of a ^{13}CO-labelled sample of **40**. Both 'sets' of carbonyls are displayed as two distinct triplets, representing two carbonyls each, at 192 ppm ($^{2}J_{CP}$ = 10 Hz), and 187 ppm ($^{2}J_{CP}$ = 13 Hz), and based on the available spectral evidence, along with comparison to the analogous methyl (**41**) and acyl (**42**) complexes (*vide infra*), the proposed structure is as shown in Figure 5.3.

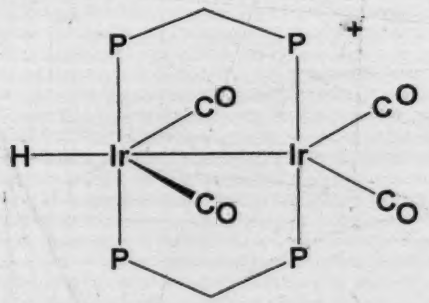

Figure 5.3. *Proposed structure of* $[Ir_2(H)(CO)_4(depm)_2][CF_3SO_3]$ (**40**)

5.3.1.4. $[Ir_2(CH_3)(CO)_4(depm)_2][CF_3SO_3]$ (41)

Addition of CO to the methylene-hydride tricarbonyl compound $[Ir_2(H)(CO)_3(\mu\text{-}CH_2)(depm)_2][CF_3SO_3]$ (**26**) leads to the formation of the methyl tetracarbonyl species $[Ir_2(CH_3)(CO)_4(depm)_2][CF_3SO_3]$ (**41**), in which the methyl moiety has reformed upon coordination of an additional CO ligand, resulting in the structure depicted in the following scheme (Scheme 5.2).

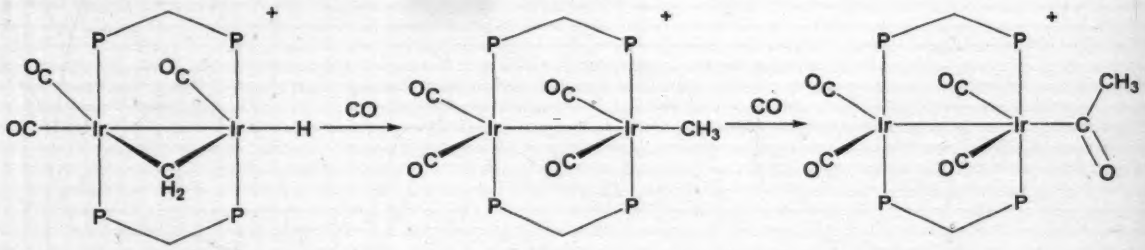

Scheme 5.2. *Reaction of CO with* $[Ir_2(H)(CO)_3(\mu\text{-}CH_2)(depm)_2][CF_3SO_3]$ (**26**)

The $^{31}P\{^1H\}$ NMR spectrum of compound **41** shows an AA'BB' spin system, displaying broad multiplet signals at -14.9 ppm and -18.6 ppm, similar to its dppm counterpart.[4] In the ^1H spectrum, the methyl signal appears as a triplet at 0.68 ppm ($^3J_{PH}$ = 5 Hz), while only a single broad resonance for all four of the depm methylene protons is apparent at 2.75 ppm, suggesting the presence of a plane of symmetry relating both sides of the metal-phosphorus plane, or a fluxional process. The $^{13}C\{^1H\}$ NMR spectrum, of a ^{13}CO-labelled sample, shows two distinct triplets, representing two carbonyls each, at 191.1 ppm ($^2J_{CP}$ = 11 Hz), and 187.3 ppm ($^2J_{CP}$ = 13 Hz), indicative of the symmetry of the complex creating two sets of terminal carbonyl ligands. In a $^{13}CH_3$-methyl labelled sample of the compound, the methyl carbon appears as a triplet at -40.1 ppm ($^2J_{CP}$ = 6 Hz), suggesting that the coordinated methyl group is intact and terminally metal bound. Compound **41** is only stable in solution, under a CO atmosphere, with removal of the CO resulting in regeneration of the starting complex (**26**).

5.3.1.5. $[Ir_2(CH_3CO)(CO)_4(depm)_2][CF_3SO_3]$ (42)

Upon continued exposure to CO, compound **41** is further transformed into an acyl complex $[Ir_2(CH_3CO)(CO)_4(depm)_2][CF_3SO_3]$ (**42**), in which migratory insertion of the methyl group to a carbonyl moiety has been accompanied by the coordination of an additional CO ligand (see Scheme 5.2).

Like that of its precursor, the $^{31}P\{^1H\}$ NMR spectrum of compound **42** also appears as an AA'BB' spin system displaying broad multiplet signals at -15.7 ppm and -20.9 ppm. In the ^1H spectrum, the methyl triplet at 0.68 ppm of the precursor (**41**) has been replaced by a singlet at 2.6 ppm, which integrates for three protons, corresponding to the new acyl methyl group, while only a single broad resonance for all four of the depm methylene protons is apparent at 3.35 ppm. The $^{13}C\{^1H\}$ NMR spectra, of a ^{13}CO-labelled sample, shows the acyl carbonyl resonance as a doublet of triplets at 220.5 ppm, integrating for one carbon, relative to the two other distinct triplets, representing two carbonyls each, at 195.2 ppm and 188.2 ppm. The latter two sets of signals are very reminiscent of the methyl precursor (**41**), suggesting similarities in their structure, and are also quite close to those of the dppm analogue,[4] in which two CO ligands have been assigned as terminally bound to each metal, while the acyl group is terminally bound to a single metal on one side of the diphosphine framework. The downfield shift in the methyl carbon (from -40 ppm to 53 ppm), in a $^{13}CH_3$-labelled sample of compound **42**, is also consistent with this type of geometry. Like the precursor, **42** is only stable in solution, with complete removal of the CO atmosphere resulting in regeneration of the starting complex (**26**).

5.3.2. Dirhodium Complexes

5.3.2.1. $[Rh_2(CO)_3(depm)_2][CF_3SO_3]_2$ (43)

When the methyl tricarbonyl precursor (**31**) is exposed in solution to excess methyl triflate, at ambient temperature, $[Rh_2(CO)_3(depm)_2][CF_3SO_3]_2$ (**43**) is generated. The spectral parameters of **43** are very similar in nature to their dirhodium dppm analogue,[5] reported by Eisenberg, and are consistent with the tricarbonyl formulation proposed (Figure 5.4). This species can also be generated by the addition of excess triflic acid to $[Rh_2(CO)_3(depm)_2]$ (**30**), presumably via successive protonation leading to the elimination of hydrogen along with the dicationic tricarbonyl compound (**43**).

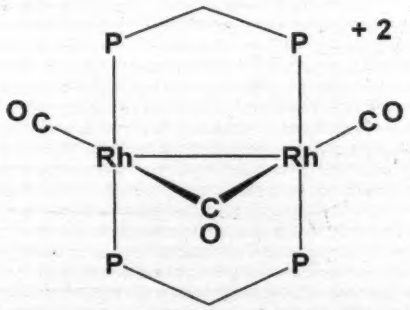

Figure 5.4. *Proposed structure of* $[Rh_2(CO)_3(depm)_2]^{+2}$ (**43**)

The $^{31}P\{^1H\}$ NMR spectrum of compound **43**, at ambient temperature, shows one broad multiplet at 29.0 ppm in which the splitting between the two major peaks is 93 Hz, indicative of two chemically equivalent ends of the diphosphine framework. Such a spectrum is typical of an AA'A''A'''XX' spin system in which the rhodium nuclei are represented by XX'. The structure is proposed to have an A-frame-type geometry with one terminal carbonyl on each metal, opposite the bridging carbonyl on the opposite face of the diphosphine framework. Upon ^{13}C labelling of the carbonyls only one broad resonance is apparent at 189 ppm in the ^{13}C NMR spectrum at ambient temperature, suggesting that this species may be fluxional on the NMR timescale, interconverting terminal and bridging carbonyl positions. Unfortunately, this species has not been characterized further, at this time, however, low temperature studies should be carried out.

5.3.2.2. $[Rh_2(CO)_5(depm)_2][CF_3SO_3]_2$ (44)

Reaction of the dicationic tricarbonyl complex (**43**) with CO, results in successive addition of carbonyl ligands, presumably proceeding through an uncharacterized tetracarbonyl species, leading ultimately to the dicationic pentacarbonyl complex $[Rh_2(CO)_5(depm)_2][CF_3SO_3]_2$ (**44**), as diagrammed in Figure 5.5.

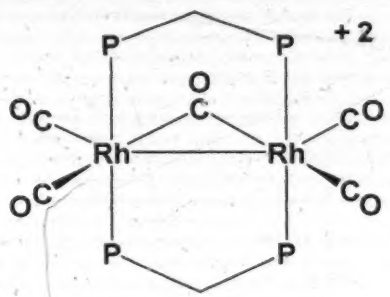

Figure 5.5. *Structure of* $[Rh_2(CO)_5(depm)_2]^{+2}$ (**44**)

The $^{31}P\{^1H\}$ NMR spectrum of **44**, at ambient temperature, shows a very broad second-order doublet at 32 ppm, with unresolved coupling. The breadth of this signal, suggests a fluxional process, previously observed in the analogous diiridium dppm system $[Ir(CO)_4(\mu\text{-}CO)(dppm)_2]^{+2}$.[6] Consistent with this assertion, the ^1H NMR spectrum at this temperature shows only the averaged depm methylene protons as a broad resonance at 3.0 ppm, while the ^{13}C NMR spectrum of a ^{13}CO-enriched sample of **44** at room temperature displays one broad singlet carbonyl resonance at 192 ppm.

The proposed structure of **44** has been confirmed crystallographically, as shown in the ORTEP representation for the complex cation $[Rh_2(CO)_5(depm)_2]^{+2}$ in Figure 5.6. As with the other depm complexes investigated cystallographically, the ethyl moieties on the phosphines alternate between axial and equatorial positions in the bridging depm ligands, which are oriented in a *trans* geometry at each metal. The structure shows a symmetrical arrangement of carbonyls in which both metals have essentially identical geometries. Interestingly, the

carbonyls opposite the Rh-Rh bond have significantly shorter Rh-C distances (1.904(3), 1.924(3) Å) than those that are essentially perpendicular to the Rh-Rh vector (1.992(3), 1.998(3) Å). The bridging carbonyl has slightly elongated Rh-C bond lengths (relative to the terminal ligands) and is bound unsymmetrically to both metals (Rh1-C3 = 2.195(3) Å; Rh2-C3 = 2.025(3) Å). Other selected bond lengths and angles are also included in Tables 5.3 and 5.4, respectively.

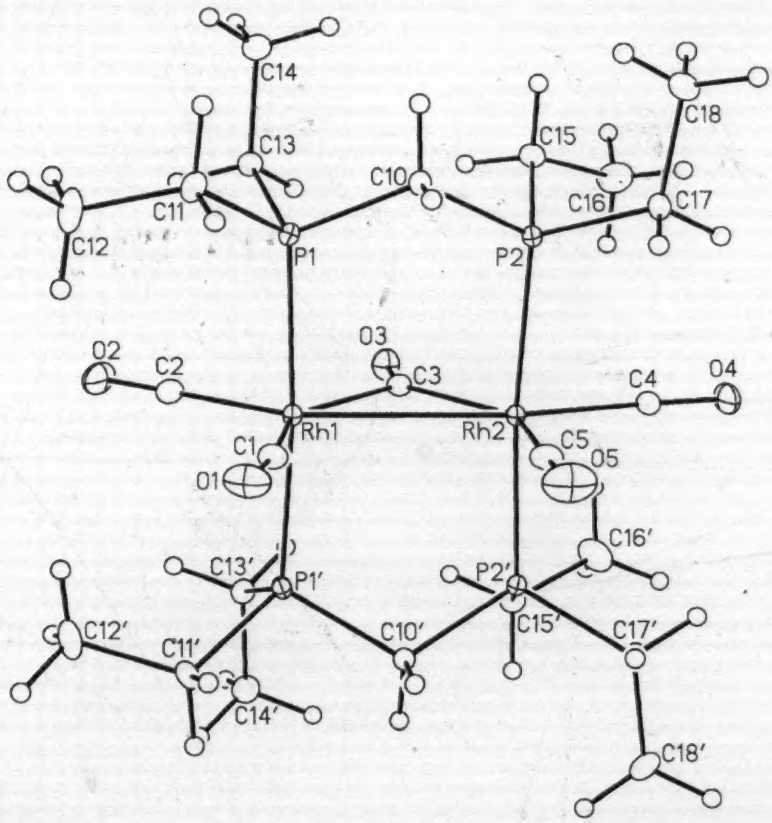

Figure 5.6. *Perspective view of the* $[Rh_2(CO)_5(depm)_2]^{+2}$ (**44**) *cation showing the atom labelling scheme. The primed atoms are related to the unprimed ones by a mirror plane in the equatorial plane of the complex. Non-hydrogen atoms are represented by Gaussian ellipsoids at the 20% probability level. Hydrogen atoms are shown with arbitrarily small thermal parameters.*

Table 5.3. Selected Interatomic Distances (Å) for $[Rh_2(CO)_5(depm)_2]^{+2}$ (**44**)

Atom1	Atom2	Distance	Atom1	Atom2	Distance
Rh1	Rh2	2.8373(3)	P2	C10	1.813(2)
Rh1	P1	2.3550(5)	P2	C15	1.822(2)
Rh1	C1	1.992(3)	P2	C17	1.826(2)
Rh1	C2	1.904(3)	O1	C1	1.123(3)
Rh1	C3	2.195(3)	O2	C2	1.130(4)
Rh2	P2	2.3539(5)	O3	C3	1.157(3)
Rh2	C3	2.025(3)	O4	C4	1.126(3)
Rh2	C4	1.924(3)	O5	C5	1.116(4)
Rh2	C5	1.998(3)	C11	C12	1.520(3)
P1	P2	3.0420(6)†	C13	C14	1.526(3)
P1	C10	1.821(2)	C15	C16	1.519(3)
P1	C11	1.822(2)	C17	C18	1.518(3)
P1	C13	1.826(2)			

†Nonbonded distance.

Table 5.4. Selected Interatomic Angles (deg) for $[Rh_2(CO)_5(depm)_2]^{+2}$ (**44**)

Atom1	Atom2	Atom3	Angle	Atom1	Atom2	Atom3	Angle
Rh2	Rh1	P1	92.08(1)	Rh1	Rh2	C5	91.24(9)
Rh2	Rh1	C1	101.55(8)	P2	Rh2	P2'	173.72(2)
Rh2	Rh1	C2	141.2(1)	P2	Rh2	C3	90.93(1)
Rh2	Rh1	C3	45.26(7)	P2	Rh2	C4	86.87(1)
P1	Rh1	P1'	175.65(2)	P2	Rh2	C5	91.14(1)
P1	Rh1	C1	90.21(1)	C3	Rh2	C4	111.1(1)
P1	Rh1	C2	87.98(1)	C3	Rh2	C5	141.6(1)
P1	Rh1	C3	91.01(1)	C4	Rh2	C5	107.3(1)
C1	Rh1	C2	117.2(1)	Rh1	C1	O1	171.9(3)
C1	Rh1	C3	146.8(1)	Rh1	C2	O2	179.1(3)
C2	Rh1	C3	96.0(1)	Rh1	C3	Rh2	84.4(1)
Rh1	Rh2	P2	92.90(1)	Rh1	C3	O3	133.2(2)
Rh1	Rh2	P2'	92.90(1)	Rh2	C3	O3	142.4(2)
Rh1	Rh2	C3	50.33(8)	Rh2	C4	O4	174.1(3)
Rh1	Rh2	C4	161.46(9)	Rh2	C5	O5	177.5(3)

5.3.2.3. $[Rh_2(CO)_2(\mu\text{-}OH)(depm)_2][CF_3SO_3]$ (45)

Much as observed in the diiridium depm system, the hydroxide-bridged dicarbonyl compound $[Rh_2(CO)_2(\mu\text{-}OH)(depm)_2][CF_3SO_3]$ (**45**) was initially encountered in the reaction of the methyl tricarbonyl precursor (**31**) with adventitious water. However, this compound can be more cleanly prepared upon exposure of compound **43** to water (Scheme 5.3). Presumably the third carbonyl group present in the unobserved intermediates in both of these transformations is labile and is subsequently liberated intact, as has been observed in the analogous dppm complex.[5] It is interesting that a hydride complex, resulting from nucleophilic attack of a hydroxide ligand at a carbonyl (with subsequent loss of CO_2), is not obtained.

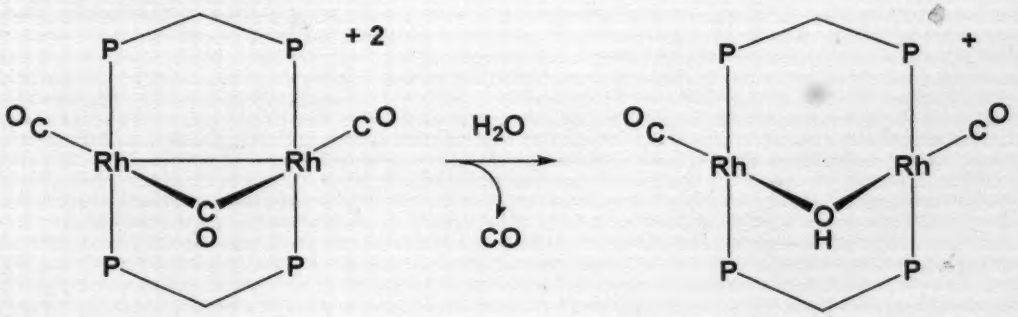

43 **45**

Scheme 5.3. *Generation of the hydroxide-bridged complex* (**45**) *via the addition of water to the dicationic tricarbonyl species* (**43**)

The spectral parameters of **45** are very similar to those of their diiridium counterpart (**38**), and also to that of the associated dppm analogue, thus are consistent with the symmetrical dicarbonyl formulation proposed. The $^{31}P\{^1H\}$ NMR spectrum of compound **45** at room temperature shows one rhodium-coupled multiplet with a separation of 120 Hz between the two major peaks, indicative that all four phosphorus atoms are in the same chemical environment. Much like the diiridum analogue, wherein two distinct environments would be

expected for the the depm methylene protons, all four coincidentally appear as a single resonance, at 2.65 ppm, in the ^{1}H NMR spectrum. The hydroxide proton appears as a quintet at 0.78 ppm in the ^{1}H spectrum, displaying equal coupling to all four phosphorus nuclei ($^3J_{HP}$ = 2.5 Hz), and this proton is readily exchanged by deuterium upon addition of D_2O, resulting in the immediate disappearance of the OH resonance. The structure is again proposed to be an A-frame geometry with one carbonyl group on each metal, both in a trans-like arrangement with the bridging hydroxide on the opposite face of the diphosphine framework. Upon ^{13}C-labelling of the carbonyls, only one resonance is apparent at 191.6 ppm in the ^{13}C NMR spectrum, showing 70 Hz coupling to rhodium along with 16 Hz coupling to the adjacent phosphorus nuclei. The presence of only one resonance in the ^{13}C NMR spectrum supports the assertion of only two equivalent carbonyls in the compound, as a third would most likely occupy the bridging position opposite the hydroxide group, and no evidence for such a moiety is apparent in either the NMR or IR spectra.

5.3.2.4. $[Rh_2(CO)_3(\mu\text{-}H)(depm)_2][CF_3SO_3]$ (46)

As in the Ir_2 analogue, reaction of **45** with CO generates the hydrido-bridged compound $[Rh_2(CO)_3(\mu\text{-}H)(depm)_2][CF_3SO_3]$ (**46**), which can also be obtained by protonation of the neutral tricarbonyl compound (**29**). This product displays a single rhodium-coupled multiplet at 35.2 ppm, with a separation of 97 Hz between the two major peaks, in the $^{31}P\{^1H\}$ NMR spectrum. The structure is proposed to be identical to that of the diiridium analogue (**39**) (Figure 5.2), and such an arrangement has been confirmed crystallographically for the dppm analogue.[7] Again, the depm methylene protons give only a single broad resonance at 2.23 ppm, integrating for four protons, while the bridging hydride appears at -10.3 ppm, showing equal coupling to all four phosphorus nuclei ($^2J_{HP}$ = 12 Hz), along with an additional coupling to rhodium ($^1J_{HRh}$ = 24 Hz). The carbonyls display only a single broad resonance in the $^{13}C\{^1H\}$ NMR spectrum at

194 ppm, while the room temperature IR spectrum shows three distinct stretches at 1990 cm^{-1}, 1967 cm^{-1}, and 1902 cm^{-1}. Although the IR data are consistent with the solid-state structure, they contrast the simplified NMR data obtained at ambient temperature, which may suggest that the molecule is undergoing a similar fluxional process to that proposed for the diiridium species.

5.3.3. Rhodium-Iridium Complexes

5.3.3.1. $[RhIr(CO)_2(\mu\text{-}OH)(depm)_2][CF_3SO_3]$ (47)

As with the homobinuclear analogues, the mixed-metal species, $[RhIr(CO)_2(\mu\text{-}OH)(depm)_2][CF_3SO_3]$ (**47**), is also generated through the exposure of the methyl dicarbonyl precursor $[RhIr(CH_3)(CO)_2(depm)_2][CF_3SO_3]$ (**37**) to water.

Compound **47** is very similar spectroscopically to the homobinuclear depm complexes, with both respective metal ends showing almost identical spectral parameters to the homobinuclear analogues (**38, 45**). The $^{31}P\{^1H\}$ NMR spectrum of compound **47** at room temperature shows one rhodium-coupled multiplet at 20.6 ppm ($^1J_{RhP}$ = 117 Hz, $^2J_{PP}$ = 14 Hz), along with another pseudo-triplet displaying the same J_{PP} coupling at 17.2 ppm, corresponding to the end of the diphosphine connected to the iridium. Unlike the homobinuclear analogues, the depm methylene protons appear in the ^1H NMR spectrum as independent multiplets, integrating for two protons each, at 2.3 ppm and 2.7 ppm. The resonance for the bridging hydroxide group appears as a broad singlet at 3.33 ppm, which again disappears upon addition of D_2O. The proposed A-frame structure is identical to the homobinuclear analogues, with one carbonyl group attached to each metal, along with a bridging hydroxide moiety on the opposite face of the diphosphine framework. Upon ^{13}C labelling of the carbonyls, two distinct resonance are apparent in the $^{13}C\{^1H\}$ NMR spectrum; the first is doublet of triplets at 190.7 ppm showing 71.5 Hz coupling to rhodium, along with 16.5 Hz coupling to the pair of adjacent phosphorus nuclei, and the second is a triplet at

174.8 ppm, also displaying coupling to the set of phosphines on iridium($^2J_{CP}$ = 10.5 Hz).

5.3.3.2. $[RhIr(CO)_3(\mu\text{-}H)(depm)_2][CF_3SO_3]$ (48)

To further aide in its characterization, compound **47** was reacted with CO resulting in the formation of the hydride-bridged product $[RhIr(CO)_3(\mu\text{-}H)(depm)_2][CF_3SO_3]$ (**48**). Although the compound has an iridium center, no higher order carbonyl complexes were observed, as they were with the diiridium compound (**40**), and the product is spectroscopically identical to that obtained upon addition of HOTf to the mixed-metal tricarbonyl compound **34**. The $^{31}P\{^1H\}$ NMR spectrum of this species shows the expected AA'BB'X spin pattern, giving a multiplet at 27.7 ppm ($^1J_{RhP}$ = 107 Hz, $^2J_{PP}$ = 46 Hz), along with the related triplet at -5.5 ppm, which is very similar to the previously characterized dppm analogue.[8] Like its dppm counterpart, the ^1H NMR spectrum of **48** shows only a single broad multiplet at 2.85 ppm, integrating for four protons, attributable to the depm methylene protons, along with the multiplet hydride resonance appearing at -11.3 ppm that shows coupling to both sets of diphosphines ($^1J_{HRh}$ = 20.8 Hz, $^2J_{HP}$ = 9.7 Hz). Two carbonyl resonances are apparent in the room temperature $^{13}C\{^1H\}$ NMR spectrum of a ^{13}CO-labelled sample of compound **48**; the first appears as a triplet at 180.3 ppm ($^2J_{CP}$ = 9.3 Hz) and integrates for two carbons relative to the second resonance, which appears as a doublet of triplets at 187.2 ppm ($^2J_{RhC}$ = 75 Hz, $^2J_{CP}$ = 16 Hz). This data suggests that the mixed-metal compound has two iridium-bound carbonyls and one bound to rhodium in an arrangement illustrated in the following Figure 5.7.

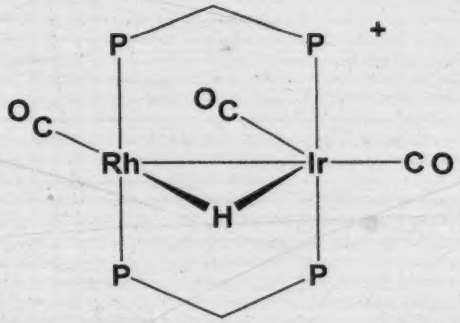

Figure 5.7. *Proposed structure of* $[RhIr(CO)_3(\mu\text{-}H)(depm)_2][CF_3SO_3]$ (**48**)

The appearance of a single resonance for the former may be indicative of fluxionality, on the NMR timescale, wherein the hydride ligand may "tunnel" between the pair of metals (Scheme 5.1), a process which equilibrates to the two carbonyls between semi-bridging and terminal sites.[3] Consistent with this assertion, the IR spectrum at room temperature displays two distinct stretches at 1960 cm^{-1}, and 1797 cm^{-1}, which supports the proposed arrangement as having both terminal and bridging carbonyls.

5.4. Conclusions

All of the depm analogues of **1** investigated appear to be much more reactive than their dppm counterparts, reacting readily in solution with trace amounts of water. This increased reactivity has made isolation of the methylated dicarbonyl complexes difficult, resulting primarily in the preparation of isolable hydroxide bridged complexes (**38**, **45**, **47**), which have been characterized spectroscopically, and by investigation of their subsequent reactivity.

From the hydroxide bridged complexes the related hydride tricarbonyl complexes (**39**, **46**, **48**) are readily prepared via the addition of CO, in a WGS (water-gas-shift) type of reaction, or more directly through the addition of triflic acid to the neutral precursor tricarbonyl complex. Whereas the dirhodium and mixed-metal hydrides were found exclusively as tricarbonyl species, the diiridium analogue generated a tetracarbonyl hydride complex under CO. The structure of this species is proposed to be comparable with that of the methyl tetracarbonyl and acly tetracarbonyl analogues, wherein the hydride acyl or methyl group is terminally-bound at one metal.

Although some degree of fluxionality is apparent in all of the hydride tricarbonyl complexes, the mechanism of these processes is not entirely clear, and should be further investigated.

5.5 References

1. a) B.R. Sutherland, M. Cowie, *Organometallics* **1985**, *4*, 1637-1648. b) D. Ristic-Petrovic, unpublished results.
2. B.R. Sutherland, M. Cowie, *Can. J. Chem.* **1986**, *64*, 464-469.
3. R. McDonald, Ph. D. Thesis, University of Alberta, 1991.
4. a) J. R. Torkelson, R. McDonald, M. Cowie, *J. Am. Chem. Soc.* **1998**, *120*, 4047. b) F.H. Antwi-Nsiah, Ph. D. Thesis, University of Alberta, 1994.
5. F. Shafiq, R. Eisenberg, *J. Orgmet. Chem.* **1994**, 337-345.
6. B.R. Sutherland, M. Cowie, *Organometallics* **1985**, *4*, 1637-1648.
7. C.P. Kubiak, C. Woodcock, R. Eisenberg, *Inorg. Chem.* **1982**, *21*, 2119.

Chapter 6

Conclusions

The work contained within the body of this thesis, aimed at effecting the activation of carbon-fluorine bonds in fluoroolefins, is an extension of previous work, on which I was also involved, relating to the binding of a series of fluoroethylenes to the complex $[Ir(CH_3)(CO)_2(dppm)_2][CF_3SO_3]$ (**1**). The pivotal finding of this previous work, of relevance to this thesis, was that *only* fluoroethylenes having at least one pair of geminal fluorines (eg. 1,1,-difluoroethylene, trifluoroethylene, and tetrafluoroethylene) were found to bind in a position bridging the pair of metals. Furthermore, X-ray structural studies on tetrafluoroethylene adducts clearly showed that, in this binding mode, the olefin carbons were completely rehybridized to sp^3 and that the fluorocarbyl group was best viewed as a 1,2-dimetallafluoroalkane, having resulted from 1,2-dimetal addition across the olefinic bond. This binding mode very much resembled a pair of fluoroalkyl groups, for which the lability towards fluoride ion abstraction was well documented. On this basis, we proposed that facile fluoride ion abstraction from bridged fluoroolefins should also be possible.

These ideas appear to have been well founded since all three bridged fluoroolefins underwent facile regioselective fluoride ion abstraction (at temperatures down to -20 °C) of one of the geminal fluorines to yield the appropriate fluorovinyl group. In addition, in the case of 1,1-difluoroethylene two isomers, one containing the bridged olefin and the other containing an η^2-bound olefin, coexisted under certain conditions, so we were able, in competition experiments, to establish that only the bridged olefin was susceptible to fluoride ion abstraction while the terminal olefin remained unreactive. This gave clear evidence (perhaps the first such evidence) that the pair of metals could interact with a fluoroolefin in a cooperative manner to give reactivity not seen, under these mild conditions, at a single metal.

Although most of our fluoride-abstractions used the strong fluorophile, trimethylsilyl triflate, we also found that triflic acid worked well and, in the case of trifluoroethlyene and 1,1-difluoroethylene, even water effected C-F activation. Even more exciting, the product in the latter case was 2-fluoropropene, presumably resulting from reductive elimination of the 1-fluorovinyl group, a product of fluoride ion abstraction, and the methyl group originating in compound **1**. Following upon this idea, we were successful in generating 2-fluoropropene and *cis*-difluoropropene from the respective fluorovinyl complexes in reactions with carbon monoxide, although in the latter case, isomerization of the olefin product to 2,3-difluoropropene was also observed. As a result of this strategy we were able to convert trifluoroethylene to a mixture of *cis*-difluoropropene and 2,3-difluoropropene and 1,1-difluoroethylene to 2-fluoropropene.

Substitution of a fluorine by hydrogen was also possible via fluoride-ion abstraction to give the above fluorovinyl complexes followed by hydrogenolysis. This sequence yielded trifluoroethylene from tetrafluoroethylene, and *cis*-difluoroethylene from trifluoroethylene.

Having successfully brought about the regioselective substitution of a fluorine in the above fluoroethylenes by either hydrogen or a methyl group (in at least most of the examples investigated), we then sought to effect the double C-F activation of these fluoroolefins, and investigate their subsequent replacement by H or CH_3. The first part was achieved by fluoride-ion abstraction from the α-carbon of the fluorovinyl groups to yield the corresponding fluorovinylidene- or vinylidene-bridged products. Here again, we were able to demonstrate that this C-F activation *only* occurred for the bridging (μ-η^1:η^2) fluorovinyl groups. At this stage these (fluoro)vinylidenes have proven unreactive towards migratory insertion and hydrogenolysis, so conversion of these into *gem*-substituted olefins has not yet been achieved.

In general the C-F activation investigations have been very successful, in that we have been able to accomplish most of our targeted goals, and more. Most

notably, we have clearly established a role played by adjacent metals in facilitating the activation of fluoroolefins, along with the importance of a bridging coordination mode, in both these transformations, and the subsequent activation of the resulting fluorovinyl products. This has allowed a definitive statement to be made about the favorable effects of metal-metal cooperativity in these systems – a concept upon which our investigations into the chemistry of binuclear complexes are based.

All of the C-F activation achieved in our studies has relied on the addition of some external fluorophile (Me_3SiOTf, HOTf, H_2O). In considering how to bring about the transformation that we effected stoichiometrically, in a catalytic manner, we might incorporate the fluorophile directly into the precursor complex. On the basis that fluoride-ion abstraction, in the form of HF, is a viable strategy for C-F bond activation, we should clearly investigate the use of binuclear hydride complexes in these activation studies. It is plausible that a catalytic cycle may be achieved in such hydride-containing systems, through intramolecular activation of the coordinated fluoroolefin and subsequent elimination of HF. Subsequent addition of molecular hydrogen would then complete the catalytic cycle, inducing elimination of the hydrogen-substituted fluoroolefin and regeneration of the metal-hydride precursor. It is feasible that such a system could facilitate the descibed transformation of numerous fluorolefin substrates. By the same token, the strength of the Si-F bond could also be exploited through studies of the reactivity of fluoroolefins with silyl complexes of our depm-bridged species, in an attempt to follow the success Milstein has achieved with the rhodium complex $[Rh(SiPh_3)(PMe_3)_3]$ in his studies on C-F activation with perfluoroaromatic substrates (*Science*, **1994**, 265, 359).

To complement our C-F activation investigations with compound **1**, a second stream of study was undertaken in which we proposed to change the bulky phenyl substituents on the diphosphine (dppm) ligands by smaller, more basic alkyl substituents, such as ethyl groups, in the related depm ancillary ligand. This change was anticipated to alleviate some of the problems encountered with

the dppm system, wherein coordination of the substrate prior to activation was inhibited, presumably through repulsive interactions between itself and the bulky phenyl substituents of the dppm ligands. In these investigation we also sought to prepare the dirhodium and mixed-metal (Rh/Ir) analogues of **1**, in order to promote some of the elimination reactions, as for example in the hydrogenolysis reactions, that were found to be sluggish with the diiridium system.

Preparation of the precursors of the depm analogues of compound **1** were generally successful, showing almost a hybrid of reactivity between that of the analogous and well-behaved dppm and the capricious dmpm complexes. As anticipated, the more basic depm ligand system appears to impart a greater electron-richness to the metal centers, and the decreased steric bulk of depm appears to allow more facile rearrangements over the bimetallic core. Generally, the more basic depm ligand system seems to achieve the increased reactivity that we sought. As a consequence, the targeted methyl complexes $[MM'(CH_3)(CO)_2(depm)_2]^+$ (M, M' = Rh, Ir) were very difficult to handle. Thus far, this reactivity has limited our characterization of these compounds to spectroscopic methods, however further investigations into amenable conditions for their isolation appear promising. Certainly, rigorous attempts should be made to exclude moisture from these reactions (glove box, sealed NMR tubes, etc.), as, in all cases, the reaction of the targeted complex with adventitious water resulted in the facile production of the hydroxide-bridged complex along with methane. The hydroxide-bridged species were identified from their subsequent transformation, via water-gas-shift related chemistry, into the corresponding cationic hydride-bridged tricarbonyl complexes, which also may hold some interesting promise (*vide supra*). Preliminary investigations with butadiene suggest a similar reactivity of the diiridium depm congener, to that seen with **1**, wherein two geminal C-H bonds were activated.

Obviously the targeted reactions of the depm analogues of **1** with fluoroethylenes and larger fluoroolefins, along with other substrates, are still of great interest and remain to be investigated. Although some preliminary work has been done on

the reaction of ethylene with solutions of $[Ir_2(CH_3)(CO)_2(depm)_2]^+$ generated at lower temperatures, further development of this strategy is required. Other preliminary work has suggested that the targeted fluoroolefin-bridged complexes might also be accessible via addition of the fluoroolefin to the methyl tricarbonyl precursor, without having to generate the reactive dicarbonyl compounds. It may be that the fluoroolefin group substitutes a carbonyl ligand, yielding the targeted dicarbonyl species directly, or if it remains a tricarbonyl product, carbonyl removal from this olefin adduct may be readily effected. It is also probable that this third carbonyl need not be removed prior to C-F activation (as was also the case with the dppm system), eliminating the need to prepare the difficult-to-handle depm analogues of **1**.

In any case, as noted, more rigorous handling techniques will surely alleviate our problem isolating our original target complexes so that we might investigate and compare the C-F activation potential of the depm complexes to those reported herein for the dppm system. Such reactions are sure to lead to further interesting transformations of fluoroolefins, and correlation of these results with the different metals involved (in the series of depm complexes prepared) will certainly help to better establish the roles of the adjacent metals in these processes.

Appendix I

Solvent	**Drying Agent/Indicator**	**Method**
Dichloromethane	P_2O_5 / None	Distillation
CD_2Cl_2	Na / Benzophenone	Vacuum Transfer
THF	Na / Benzophenone	Distillation
d_8-THF	Na / Benzophenone	Vacuum Transfer
Acetone	Drierite™	Distillation
d_6-Acetone	Molecular Sieves	Freeze-Pump-Thaw
Benzene	Na / Benzophenone	Distillation
C_6D_6	Molecular Sieves	Freeze-Pump-Thaw
Pentane	Na	Distillation
Diethylether	Na / Benzophenone	Distillation